Conformational Studies of Synthetic and Biopolymers at Mineral Interfaces Using Fluorescence Spectroscopy

By
Elfateh S. A. Belkasem

A thesis submitted in part fulfilment of the condition of admittance to the degree of Doctor of Philosophy (Ph.D.) of the Department of Chemistry, University Of Sheffield, Sheffield, UK.

June, 2013

Declaration

This thesis is submitted to the University of Sheffield for the degree of Doctor of Philosophy, having not been submitted to any other University or Teaching Institution for obtaining any degree. I declare that all work presented in this thesis is my own work, excluding where acknowledged and referenced accordingly.

Elfateh Belkasem

June 2013

This thesis is dedicated to the memory of my wonderful father, Elsanussi Eltaboni (1947-2012). I miss him every day, but I am glad to know, before he passed away, he was a proud of me.

ACKNOWLEDGEMENTS

- First, my greatest thanks have to go to Dr. Linda Swanson for her support throughout my PhD study. Numerous discussions allowed me to build up myself as a physical chemist researcher. My thanks must go to Dr. Maria Romero-Gonzales for her supervision on the potentiometric titration and ICP-MS work at the Kroto Research Institute.

- I am thankful to Dr. Linda Swanson's research group, Katie, Tom, Amy and Ameerah for making me a good team player. In addition, I would like to thank all of my colleagues on F-floor for contributing to a comfortable work environment. My thanks must go to Dr. Peter Aspinall and Dr. Kathryn Swindells for their endless patience in guiding me to the chemistry and photophysics work. Thanks are saved to Dr. Prodip Sarker and Dr. Gabriella Kakonyi for passing some of their postgraduate experience to me.

- I would like to thank everybody, whom I met through different circumstances and who made my years as a postgraduate student unforgettable.

- The Libyan Ministry of Higher Education is gratefully acknowledged for providing support in the form of finance my PhD study.

- Finally, I would like to thank my family and my wife for their continuing support.

ABBREVIATIONS

- [η] Intrinsic viscosity
- $<\tau_D>$ The average lifetime of the ACE-PAA
- $<\tau_{ET}>$ The average lifetime of the ACE-AMMA-PAA
- $<\tau_F>$ The average excited state lifetime
- A Acceptor
- AA Acrylic acid
- ACE Acenaphthylene
- ACE-AMMA-PAA Acenaphthylene (9-Anthryl) methyl methacrylate labelled poly (acrylic acid)
- ACEN Acenaphthene
- ACE-PAA Acenaphthylene labelled-poly (acrylic acid)
- AIBN 2,2'-Azobisisobutyronitrile
- *a* The Mark–Houwink constant
- AMMA (9-Anthryl)methyl methacrylate
- AmNS 4-(amino) naphthalene-1-sulfonic acid
- AmNS-Alginate Amino naphthalene sulfonate-labelled alginate
- AmNS-LPS Amino naphthalene sulfonate-labelled lipopolysaccharide
- $CDCl_3$ Deuterated chloroform
- C-MI Cell-Mineral Interface
- *c* Velocity of light
- C_ρ Concentration (mass per volume)
- D Discriminator, Donor, or The particle diameter
- d Density (g/cm^3)
- d(t) Fluorescence intensities difference as function in time
- DCC N,N'-Dicyclohexyl carbodiimide
- DLS Dynamic light scattering
- DLVO Derjaguin, Landau, Verwey and Overbeek theory
- DMAP 4-(Dimethyl amino) pyridine
- *E* Efficiency of energy transfer
- E Energy
- e.m.f Electromotive force (mV)
- EDC N-(3-Dimethylaminopropyl)-N′-ethylcarbodiimide hydrochloride
- EPS Exopolymer
- *F* Steady-state intensity or fluorescence
- FRET Fluorescence resonance energy transfer
- FTIR Fourier transform infrared spectroscopy
- GPC Gel permeation chromatography
- *h* Plank's constant
- HPLC High performance liquid chromatography
- Hz Hertz
- I|| Fluorescence intensity in parallel plane
- I⊥ Fluorescence intensity in

perpendicular plane

- I_A The maximum fluorescence intensity peak of acceptor
- IC Internal conversion
- ICP-MS inductively coupled plasma mass spectrometry
- I_D The maximum fluorescence intensity peak of donor
- I_{max} The maximum fluorescent emission
- ISC Intersystem crossing
- J Coupling constant
- J Integrated overlap of the experimental excitation and emission spectra
- k A constant related to the physical properties of solvent
- k The Mark–Houwink constant
- k_D^O Rate constant of donor in the absence of acceptor
- k_{ET} Rate constant of energy transfer
- k_f First order rate constant for fluorescence process
- K_h The Henry or affinity constant
- k_{IC} First order rate constant for internal conversion process
- k_{ISC} First order rate constant for intersystem crossing process
- k_{nr} First order rate constant for non-radiative process
- kPa Kilopascals
- LPS Lipopolysaccharide
- M Molar concentration, Molecule, or Monomer
- M* Excited molecule
- M1 excitation monochromator
- M2 emission monochromator
- MCA Multi channel analyser
- M_n Number average molecular weight
- M_v Viscosity average molecular weight
- M_w weight average molecular weight
- n Rotational energy sublevel
- $NaHCO_3$ Sodium bicarbonate
- NHS N-hydroxysuccinimide
- nm Nanometre
- NMR Nuclear magnetic spectroscopy
- NRET Non-radiative energy transfer
- ns Nanosecond
- ^oC The degree Celsius
- OD Optical density
- PAA Poly (acrylic acid)
- PC Personal computer
- pHzpc The zero point of charge
- pKa Acid dissociation constant, negative logarithm
- PM Photomultiplier
- ppm Part per million
- Q Quantum yield
- r Anisotropy or Separation distance between donor and acceptor
- $r(t)$ Anisotropy decay
- r_0 Intrinsic (Time-zero) anisotropy
- r_∞ Long-time anisotropy in an

anisotropy decay

- R_o Critical separation (Förster)distance between donor and acceptor
- s Second
- s(t) Fluorescence intensities sum as function in time
- S_0 Ground singlet electronic state
- S_1 First singlet electronic state
- S_2 Second singlet electronic state
- SA The surface area (m^2/g)
- *T* Temperature
- t Time
- T_1 First triplet electronic state
- T_2 Second triplet electronic state
- TAC Time-to-amplitude converter
- TCSPC Time-correlated single photon counting
- THF Tetrahydrofuran
- TLC Thin layer chromatography
- TRAMS Fluorescence time-resolved anisotropy measurements
- t_p Efflux time of aqueous polymer solution
- t_r Relative efflux time
- t_s Efflux time of solvent
- UHQ Ultra high quality
- UV Ultraviolet spectroscopy
- v Vibrational energy sublevel
- VR Vibrational relaxation
- wt% Weight-volume percentage
- XPS X-Ray photoelectron spectroscopy
- α The degree of dissociation
- δ Chemical shift
- ε_A or ε Molar extinction coefficient for absorption
- η Viscosity
- η_{inh} Inherent viscosity
- η_r Relative viscosity
- η_{red} Reduced viscosity
- η_{sp} Specific viscosity
- κ Orientation transition of donor and acceptor dipoles
- λ Wavelength
- λ_{em} Emission wavelength
- λ_{ex} Excitation wavelength
- λ_{max} Emission maxima
- ν Frequency of light or Wave number
- ρ_p Density of aqueous polymer solution
- ρ_r Relative density
- ρ_s Density of solvent
- τ_c Correlation time
- τ_f Fluorescence lifetime
- τ_n Intrinsic fluorescence lifetime
- Ωcm^{-1} Ohm per centimetre
- Φ_f Quantum yield of fluorescence

TABLE OF CONTENTS

LIST OF FIGURES

LIST OF TABLES

ABSTRACT

Bacterial attachment and aggregation play a vital role in both the formation of biofilm and the removal of undesired biofilms from mineral surfaces. The binding forces involved in this process consist of weak interactions, such as Vander Waals's forces and electrostatic interactions. Although attachment of bacterial cells to mineral surfaces is mainly governed by exopolymer alginate, lipopolysaccharide chemistry seems to play a role in adherence and biofilm accumulation. The project aims to use the synthetic poly (acrylic acid) (PAA) as a model for more complicated biopolymers. Because macromolecules are non-fluorescent, they have been covalently attached with fluorophores, such as ACE, AMMA and AmNS.

In an effort to understand the Cell-Mineral Interface process more fully, spectroscopic techniques have been used to investigate conformation and dynamics for PAA, alginate, and lipopolysaccharide (LPS) in both, bulk solution and onto alumina and silica surfaces, which should act as model systems for bacterial growth.

Initial solution dynamics of these macromolecules show that the model polymer and biopolymers exhibit partially coiled conformations at low pH values, but adopt a relatively expanded shape from around pH more than their pKa. The addition of simple electrolytes like NaCl and $CaCl_2$ to either system encourages the coiling of the polymer chain at high pH values. Furthermore, adding calcium chloride causes a much tighter coil, and PAA is the most ionic strength responsive polyelectrolyte.

A combination of fluorescence and ICP-MS demonstrated that PAA had a strong adsorption affinity for $A1_2O_3$, in contrast to the alginate and LPS adsorb weakly to the surface. And all polymers attract feebly to the SiO_2. The adsorption process is pH dependent: strong adsorption was observed at low pH. The dependence of adsorption on the minerals ($A1_2O_3$ and SiO_2) concentration was also examined at different pH conditions: the adsorption amount was observed to increase by increasing the solid concentration. Adsorption isotherms obtained at low and high mineral concentrations were found to be Henry in type.

Chapter 1. INTRODUCTION

The aim of this chapter is to give a short review of the cell-mineral interface scope and concept, followed by the theory of bacterial adhesion mechanism. Adsorption isotherms and the model charged polymer are also introduced, and then focus on the conformation of adsorbed polyelectrolyte. Synthesis of water-soluble fluorescently labelled polymers is described as well as the background on photophysics. Fluorescence and potentiometry techniques that are used in this project are also reviewed, as these topics need to be integrated to provide better understanding of the conformational behaviour of polymer and biopolymers. The final sections present the hypothesis and thesis objectives.

1.1. **Cell-Mineral Interface(C-MI) Project Scope**

The physicochemical interaction of cell macromolecules with solid surfaces, such as soil, rock or metal is a key step vital to a wide range of processes in Environmental Engineering Science to those in Surface Chemistry, Biological Imaging, Molecular Biology and Nanotechnology. This Cell-Mineral Interface (C-MI) concept is also important to understand phenomena as intensification of reactor technology using biofilms, anchoring between prostheses and tissue, and biotransformation of environmental pollution by naturally occurring attached microbial communities. These phenomena are mainly affected by the conformations of the cell wall with solid particles.

1.2. **Interactions at the Cell-Mineral Interface**

Microbiologists have known that bacteria attach to surfaces, such as soil, rock or metal according to the steps shown in [1, 2], where in step 1 (from left to right) a reversible adsorption of the outer membrane of bacteria occurs within the matter of seconds. Lipopolysaccharide (LPS) is the main component of this membrane. In step 2, the initial attachment (step 1) facilities the arrival of the other cells and form irreversible attachment within the time scale of minutes. Growth and division of bacteria attached onto the surface is the third step, while in step 4 the bacteria produce a glue-like substance known as extra cellular polymeric substance (EPS). The main component of EPS is alginate polysaccharide and this step leads to biofilm formation within the period of hours to days. The final step (step 5) is attachment of other organisms and material to the biofilm. With the

development of thick biofilm layers, this cell-mineral interface can cause plugging of channels in substrates like soil or porous rock and lead to blocking the flow of ground water. At larger scales it can also lead to plugging of pipes in water distribution systems [1]. Thus, the thorough understanding of the cell-mineral interface dynamic is a key point for controlling biofilm formation on various surfaces.

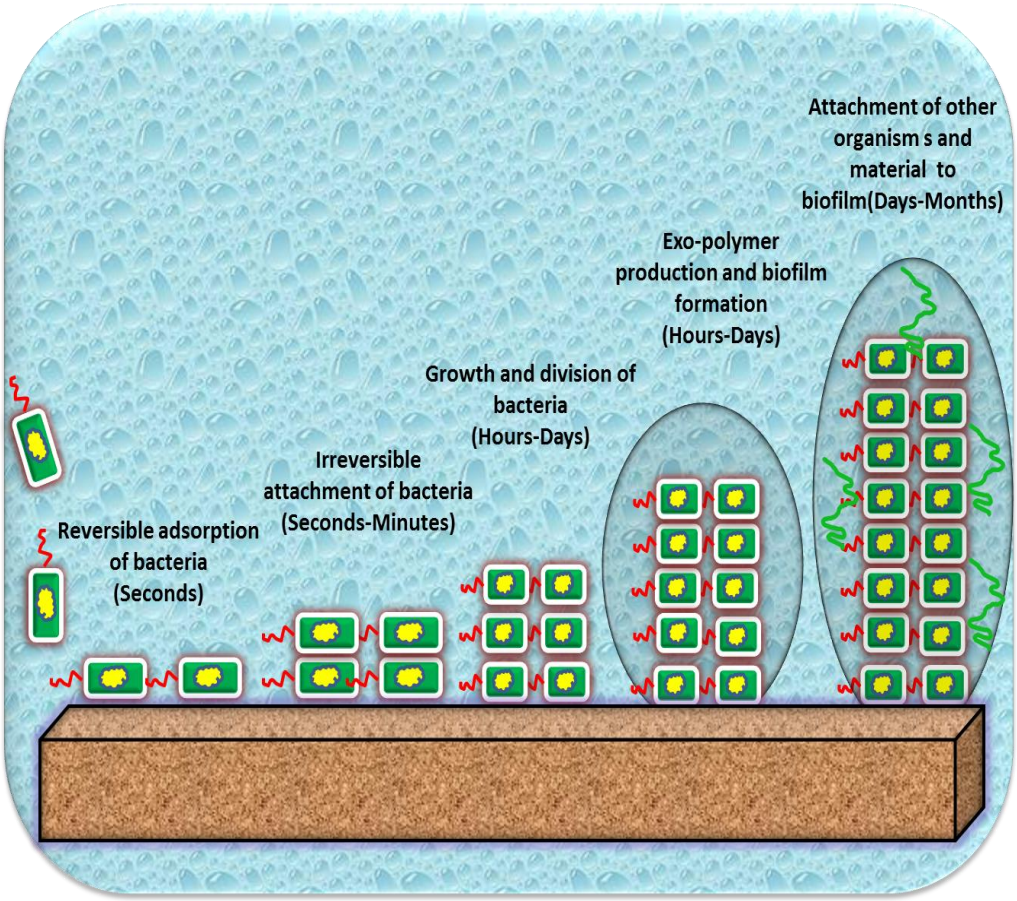

Figure 1.1 The typical steps of biofilm formation.

1.3. **Theory of Bacterial Adhesion Mechanism**

Many different types of bacteria interact with solid surfaces via initial attraction of the cells to the surface followed by adsorption and attachment. Research to clarify the mechanism of bacterial attachment to surfaces originated in the late 1930's by Zobell [3] and interest has recently increased with this field becoming a centre of attention for researchers across an extensive variety of fields [4-7]. Work in this area demands a better understanding of the factors controlling

the immobilization of microorganisms at solid-liquid interfaces. It is clear that the Cell-Mineral Interface still not clearly resolved [4, 7, 8].

There are several factors that influence the forces between a bacterium and a solid surface, which decide whether attachment will occur or not [9], (Figure 1.2). These forces differ in strength and in the separation distance at which they affect the interaction between the bacterium and the substrate surface. Only weakly attractive Van der Waals forces operate over relatively long separation distances, ca. >50nm, non-specific, macroscopic cell surface properties play the main dominating role in this step of attachment [9]. Whereas, at separation distances between 10 and 20 nm secondary interactions take place because of electrostatic interaction. In this situation the attachment is predicted to be reversible, however it changes to irreversible with time, due to a relocation on the bacterial cell surface, which in turn leads to specific and more complex interactions at these relatively short distances (10-20 nm) [9]. Accordingly, water layers have to be removed from in between the both interacting surfaces [9]. The main role of hydrophobicity and hydrophobic surface components in bacterial hold is its dehydration effect of this water layers, resulting in specific short range interactions [9]. Further specific interaction, as can be determined from short range polar forces may take place at separation distances less than 1.5 nm. This kind of interaction leads to irreversible bonding [9]. The ability of attached bacteria to increase surface hydrophobicity and to produce short range interactions depends mainly on the type of the strain, which in turn depends on the specific composition of both the surface and the cell thus resulting in unique interactions [9].

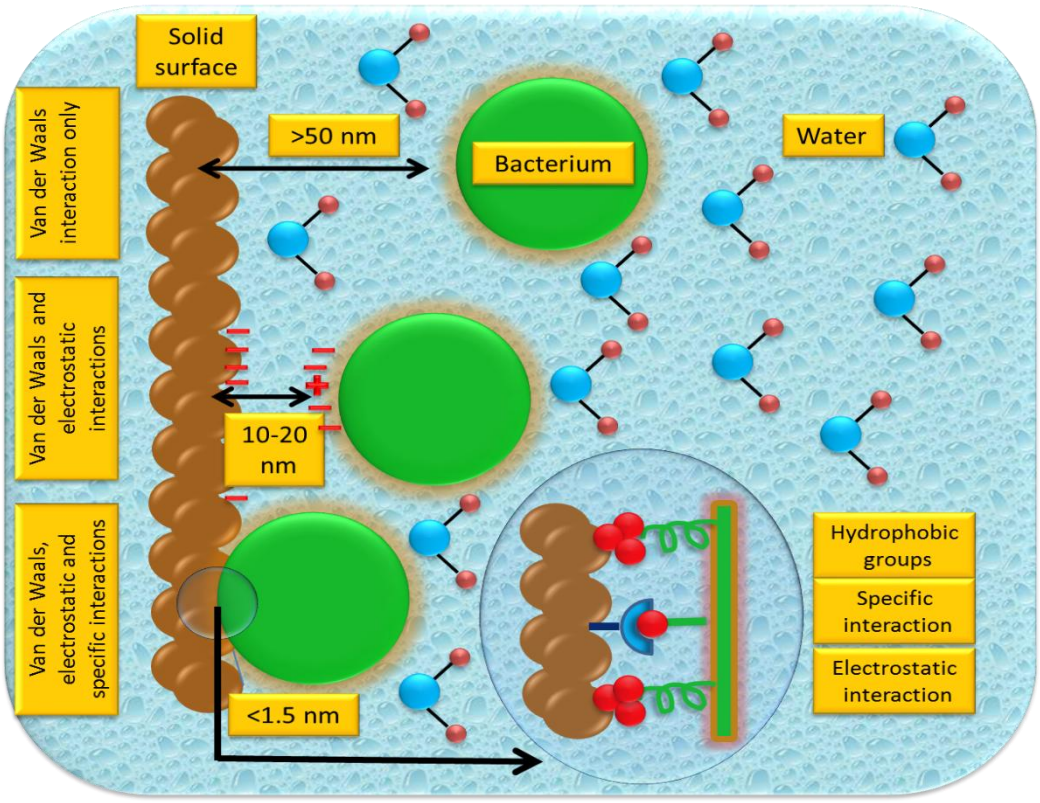

Figure 1.2 Schematic representation of interaction involved in bacterial attachment to solid surfaces, modified from Busscher and Weerkamp 1987 [9].

In this work, the type of interactions between biologically relevant macromolecules and mineral surfaces will be elucidated. These interactions are tackled by using poly (acrylic acid) as a model polymer system and builds up to study of biopolymers such as alginates and lipopolysaccharides. A fluorescence technique applied to fluorescently labelled samples will be utilized to give information concerning the conformational change of polymer in solution and at liquid-solid interface which is considered to play a vital role in the bacterial growth. The polymer-mineral systems will also be investigated using a range of surface sensitive techniques and spectroscopic methods.

1.3.1. **Complexity of bacterial attachment**

Attachment of bacteria is known as an enormously complex adhesion process [2], this complexity make bacterial adhesion mechanisms deviate from the model described by DLVO theory [2], named after Derjaguin, Landau, Verwey and Overbeek. The theory describes the total interaction of inert colloid particles

with charged surfaces as a summing up of their Coulomb and van der Waals interactions [2]. According to the separation distance between the colloid and surface, the interaction is divided into a long range Van der Waals interaction and a medium range electrostatic forces. Short range interactions are excluded in the DLVO theory [2, 9]. Unlike simple polyelectrolytes, the structure and chemical composition of a bacterial surface is widely heterogeneous. For instance, the outer membrane of Gram-negative bacteria is formed from a lipid layer consisted mainly of lipopolysaccharide (LPS) [2, 10, 11] (Figure 1.3).

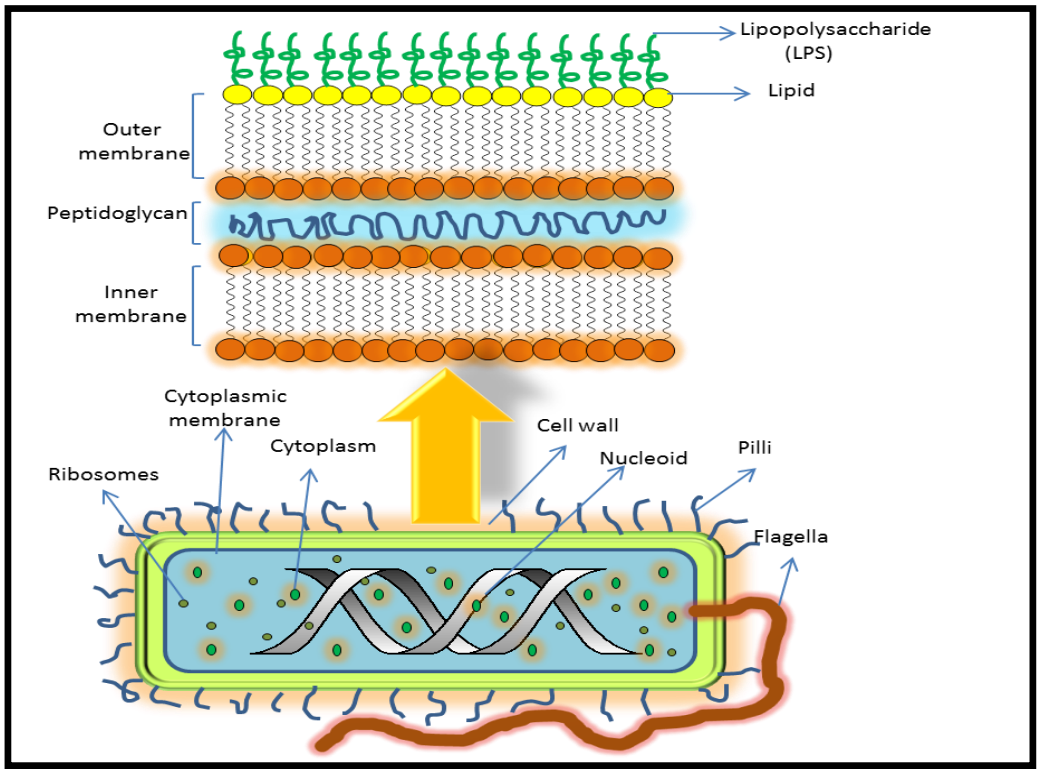

Figure 1.3 Structure of Gram-negative bacteria.

In addition, different types of outer membrane proteins are deposited in heterogeneous distribution at the outer membrane and many of these deposits stick out of cells forming cell appendages. Typical cell appendages are flagella and pilli, which produce hundred nanometres long fibrous structures. These bacterial nano-fibers cause deviation of bacterial cell attachment behaviour as of which expected by the DLVO theory. Additionally, although different structures on the same cell independently contribute to the net cell character, they are often described in terms of their combined contribution to the overall cellular behaviours. A hydrophobic portion localized at a bacterial nano-fiber against the hydrophilic main cell surface

specially orientates the cell at the interface [2, 12]. This complicity in natural biological system made a simple synthetic charged polymer, such as poly (acrylic acid) is as a typical model polymer for more complicated biopolymers when molecular interactions are investigated. Since the poly (acrylic acid) carrying only carboxyl groups at every second carbon of its aliphatic chain easily interact with any charged material exists in solution [13].

1.4. **Adsorption Isotherms**

Experimentally, polymer attachment to mineral particles can be quantified by studying the equilibrium distribution of a macromolecule between the solids and aqueous solution, which is usually referred to as an adsorption isotherm [14]. The name isotherm is applied to specify that adsorption process applies only when the temperature of the system is constant [14].

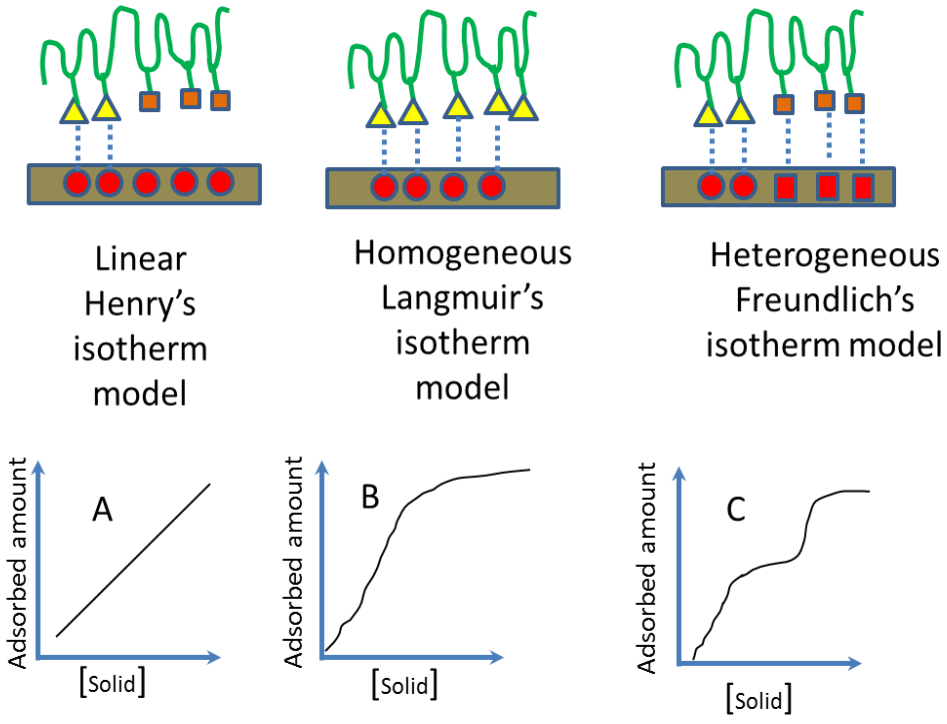

Figure 1.4 Adsorption isotherm models.

Since the adsorption of soluble macromolecules at solid/liquid interfaces is a complex phenomenon [15], different adsorption models – according to number and type of adsorption sites of adsorbates and adsorbents – have been developed and applied [14]. A linear relationship, also known as Henry's model is the

simplest kind of adsorption isotherm (Figure 1.4 A). In this model, the affinity of the adsorbate for the adsorbent remains constant over the investigated concentration range and time. It can be applied to very dilute solutions of the material, where the strongest adsorption sites are far away from being fully saturated [14, 15]. The second model known as the Langmuir isotherm (Figure 1.4 B) describes the condition in which relatively high concentrations of the adsorbate become more difficult to be adsorbed on the surface, i.e. the adsorption sites of the surface are completely saturated [14]. The third type is a sigmoidal isotherm model, also known as the Freundlich isotherm (Figure 1.4 C), which describes the sorption of heterogeneous material to a solid [14]. In general, depending on the composition of the adsorbent and the chemical properties of the adsorbate, multiple adsorption mechanisms can occur simultaneously and the resulting isotherms may have a variety of different shapes. When multiple adsorption occurs a particular adsorption mechanism may be difficult to prove [14].

In this project, adsorption isotherms of dilute aqueous solution for poly (acrylic acid) and biopolymers were studied as a function of pH, and at different alumina and silica concentrations. It is hypothesised that the alumina and silica particles mimic active sites existing on the surface of kaolin particles [16], which control the bacterial growth in natural water systems [17].

1.5. **Charged Model Polymer**

The study of macromolecules with ionisable functional groups attached onto a polymeric macromolecule's backbone was initially suggested by Herman Staudinger in 1932 [18]. Staundinger proposed the use of simple polymeric substances with one or few functional groups to provide basis for the study of more complicated biomacromolecules, which approach is similar to that which has been applied in the case of proteins. He selected poly(acrylic acid) (PAA) for the first such study as a model for biopolymer [18]. A model charged polymer can be defined as a polymer with ionisable repeat units, which can consequently show pH-dependent response when solubilised in aqueous medium [19]. As the term polyelectrolyte can also be extended to include natural biopolymers, which contain ionisable groups, such as alginic acid and biologically produced lipopolysaccharide [20], it is may be not surprising that synthetic polyelectrolytes are often used as typical models for more complex biomaterials [19]. The chosen-

pH responsive polymer for this study is poly (acrylic acid) (PAA), which has had its structure modified by fluorescents probes, such as acenaphthylene (ACE) and (9-anthryl) methyl methacrylate (AMMA) in order to study the polymer using fluorescent spectroscopy techniques.

1.5.1. **Conformational transition mechanism of poly (acrylic acid)**

Poly (acrylic acid) is classified as an amphiphilic weak acidic polyelectrolyte, which contains both hydrophilic (-COOH) and hydrophobic (-CH_2-) repeating units (Figure 1.5) [21, 22]. PAA might be charged and the local charge density varies with the pH of the environment [22, 23], Therefore, the presence of electrostatic charges along the polymer backbone influence the conformational change of PAA [22, 24]. PAA undergoes a switch from a collapsed coil to an expanded chain as the pH increases from acidic to neutral and basic [19, 25]. This behaviour is characterised by potentiometric titrations of the linear polymer [26] and can also be observed using optical density (OD) measurements as a function of pH [27]. Experimentally, a semi-dilute solution of PAA will turn cloudy as the polymer aggregates upon acidifying an aqueous solution and rapidly turns clear when adding base signifying the reversible nature of this interaction [28]. Consequently studying the behaviour of aqueous PAA solutions provides a starting point for the development of stimulus responsive polymers [29].

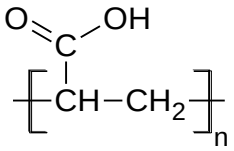

Figure 1.5 The repeat unit of linear PAA.

The conformational transition of synthetic polymers has become a subject of extensive interest in both experimental and theoretical studies for a number of years, because it provides a simple model for studying more complicated conformational transitions which occur in biopolymers [22]. It is well known that [22, 25] when the solution pH is lower than the pKa value of a given polymer, the polymer is regarded to be in a protonated state, and it becomes deprotonated when it is above its pKa value according to the following equation:

$$RCOOH \rightleftharpoons RCOO^- + H^+ \qquad \text{Equation 1.1}$$

Where, *R* indicates the backbone of a carboxylic functional group-containing polymer (e.g. poly (acrylic acid)). The relationship between *pKa* and *pH* is given by the extended Henderson-Hasselbalch equation [30];

$$\mathrm{pH} = \mathrm{pKa} - \mathrm{nlog}\frac{(1-\alpha)}{(\alpha)} \qquad \text{Equation 1.2}$$

Where, *pH* = *-log* of hydrogen ion concentration, *pKa* = *-log* of dissociation constant of PAA (Ka), *n* is an empirical parameter (*n* = 1 for low molecular weight polymer and *n* > 1 for high molecular weight polymer), and α is the degree of ionization or fraction dissociated.

Experimental studies have shown that PAA can exist in different conformations depending on the pH of solution [25]. Above the *pKa* of PAA, favourable interactions between water and the hydrophilic groups on PAA allow the polymer to stay soluble in water. An electrostatic repulsion in the chain occurs due to the deprotonation process, and as a result, the PAA chains stretch and adopt an expanded form. As the *pKa* is lowered (e.g. by adding acid), hydrophobic effects start to dominate, breaking down hydrogen bonds between PAA and water, causing the coil to collapse and thus minimising unfavourable interactions [22, 25, 31]. The conformational change of PAA chain with pH is schematically depicted in Figure 1.6.

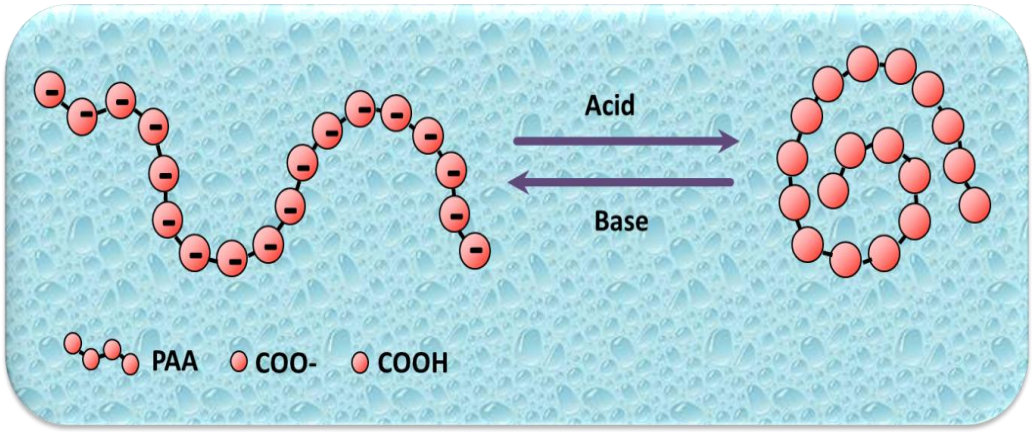

Figure 1.6 The pH response of linear PAA.

1.6. **Conformations of Adsorbed Polyelectrolyte**

Despite the fact that the conformation of adsorbed polyelectrolyte theory has not yet been well described [32], it has been agreed that the linear charged macromolecules can adopt diverse conformations at the solid surface, with variable degrees of attachment [33]. When oppositely charged polyelectrolyte chains attach to a mineral surface, a conformation that allows for maximum segment surface contact is preferred. Since the adsorption of one segment enhances the attachment chance of adjacent segments. In addition, an increase on the number of hydrophilic functional groups leads to increased binding between the polymer chain and the surface. The result is different conformations of adsorbed polyelectrolyte: some parts of the polyelectrolyte chain are in contact with surface as train, other parts are bound more loosely (as loops) or unattached (as a tail) [33] (Figure 1.7). Saoutar, *et al* studied the adsorption of poly (dimethyl acrylamide) on to colloidal silica from dilute aqueous solution and found that the chain lie flat on the particle surface [34].

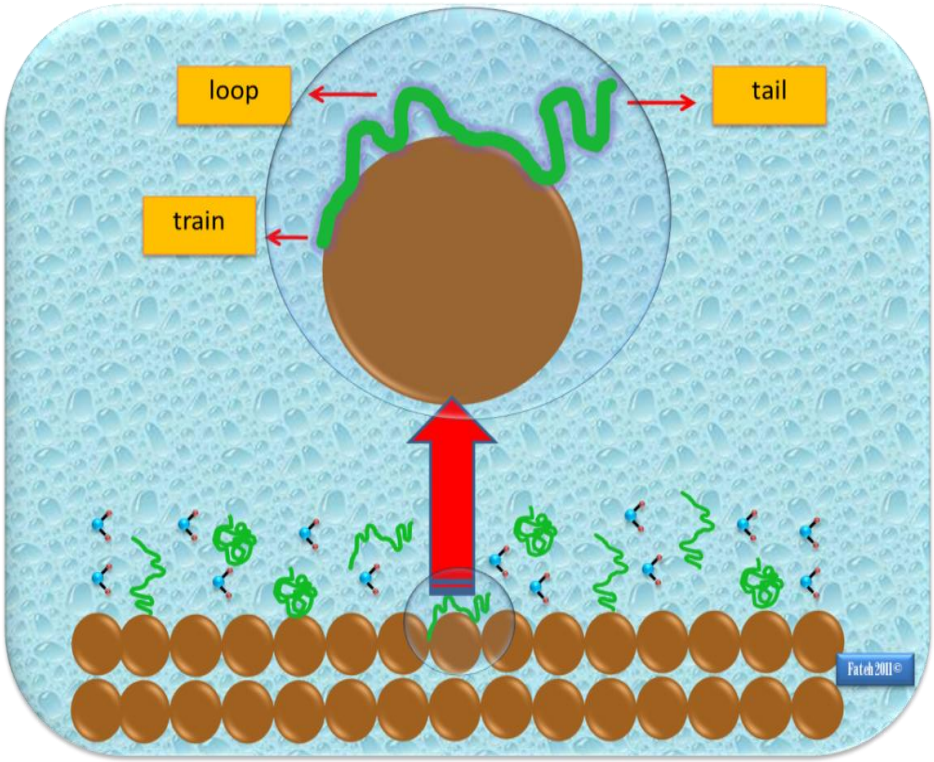

Figure 1.7 Predicted conformations of adsorbed polyelectrolyte.

Because polyelectrolytes are charged macromolecules, their conformation at the liquid/solid interface is expected to be pH and ionic strength dependant. At

low ionic strength, the strong adsorption of a charged polymer results in an adsorbed flat conformation. This expanded form is enough to neutralize the surface charge. This is due primarily to the screening of charges on the polyelectrolyte allowing closer contact between chains. At high ionic strength, the charge repulsion is screened, hence the polyelectrolyte chain lie in a collapsed form onto the solid surface [35]. In this project the conformation of adsorbed macromolecules on silica and alumina surfaces, will be characterised under different conditions, such as mineral concentration and pH values.

1.7. **Synthesis of Water-soluble Fluorescently Labelled Polymers**

In the past two decades, the study of fluorescently labelled polymers has become an attractive research area due to their versatile applications as fluorescent probes in different fields. Examples of these fields are signal intensification in biological diagnostics, optical imaging, light-harvesting and photo-chromic materials, fluorescence analysis of inter and intra-molecular polymer chain aggregations, and conformational changes of polymer chains [36-40]. This makes water-soluble fluorescent polymers useful tracers to perform as analogues in understanding the complex behaviour of biopolymers [36-40]. As most polymers are non-fluorescent [19] two general synthetic routes have been used to prepare such fluorescent-labelled polymers. The first protocol is the copolymerization of aromatic hydrocarbon monomers with a number of familiar monomers like acrylic acid and methacrylic acid [36-38, 41], while the other route is the chemical modification of polymers by amino fluorescent probes [42-44].

In this work a water soluble fluorescent PAA was synthesized through random copolymerization of acrylic acid in the presence of acenaphthylene (ACE) and/or (9-anthryl) methyl methacrylate (AMMA), based on the following free radical mechanism [45]:

Initiation:

$$\mathrm{I} \rightarrow 2R^{\bullet} \qquad \text{Equation 1.3}$$

$$R^{\bullet} + \mathrm{M} \rightarrow P_n^{\bullet} \qquad \text{Equation 1.4}$$

Propagation:

$$P_n^{\bullet} + \mathrm{M} \rightarrow P_{n+1}^{\bullet} \qquad \text{Equation 1.5}$$

Termination:

$$P_n^{\bullet} + R^{\bullet} \rightarrow P_n - R \qquad \text{Equation 1.6}$$

Where *I* represents the initiator, $R^{\bullet}$ is the initiating radical, *M* is the monomer, $P^{\bullet}_n$ is the growing macroradical with *n* monomer units and P_n -*R* is a terminated polymer produced from combination of an active chain end with an initiator radical.

Since it is not easy to label a biopolymer covalently by free radical reaction [46], the biopolymer containing pendant acenaphthylene analogous amino fluorophore was prepared using an EDC-mediated polymer coupling technique [44], EDC refers to N-ethyl-N′-(3-(dimethylamino) propyl) carbodiimide. A conjugation reaction between the carboxyl group of the biopolymer and the amino group of the fluorescent label takes place as shown in Figure 1.8. In the presence of an amine, carbodiimides encourage the production of an amide bond in two stages. First, the carbodiimide binds to the carboxyl group to form a highly reactive o-acylisourea intermediate, then the attack of the amine nucleophile on the carbonyl group of this ester results in the formation of a fluorescently labelled biopolymer via an amide bond [47].

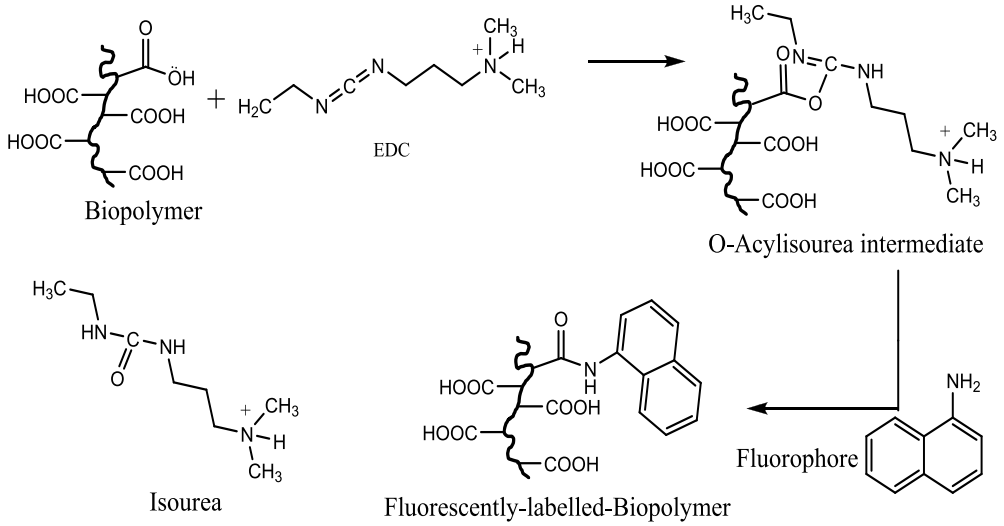

Figure 1.8 Schematics of EDC-mediated biopolymer coupling technique.

1.8. **Background on Photophysics**

Photophysics is a natural phenomenon that deals with the absorption of light by a molecule. During this process, a molecule absorbs a single quantum of light in such a way as to form electronically excited species. This constitutes the first step of any photophysical process, Equation 1.7 [48].

$$M + h\nu \rightarrow M^* \qquad \text{Equation 1.7}$$

According to Stark and Einstein, a molecule can absorb a photon if the energy E is equal to the difference between the ground and excited state, and the energy of the photon is given by the following equation:

$$E = h\nu \qquad \text{Equation 1.8}$$

where h is the Plank's constant equalling to 6.27 x 10^{-27} *erg s* and ν is the frequency of the absorbed light, $\nu = c/\lambda$, where c is the velocity of the light and λ is the wavelength of the absorbed light [49].

As shown in Figure 1.9, deactivation of an excited state can occur through several processes, such as a *photochemical process* (by formation of a new product), *quenching process* (interaction with a foreign species present in the bulk solution), *non-radiative deactivation* (release of excess energy as a heat), or *luminescence* (by emission of light) [48].

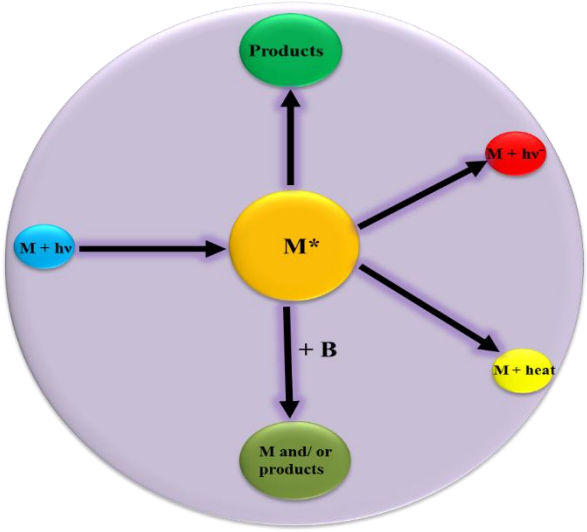

Figure 1.9 Light excitation of a molecule and deactivation of the electronically excited state.

1.8.1. **Unimolecular deactivation process**

A good starting point for a discussion of luminescence (*fluorescence* or *phosphorescence*) principle is a simplified Jablonski diagram, as illustrated in Figure 1.10. The Jablonski diagram is employed to represent the energy levels of a molecule. As depicted in Figure 1.10, $S_{0,}$ S_1 and S_2 represent ground, first and second singlet electronic states, respectively, whereas T_1 and T_2 describe first and second triplet electronic states, respectively. Each electronic energy level of a molecule also has numerous vibrational (*v*) and rotational (*n*) energy sublevels. In most organic molecules the ground state is a singlet, whereas the first triplet is the lowest excited state which can be obtained from the deactivation of higher excited states [38]. In Figure 1.10, transitions, shown by solid arrows, occur within about 10^{-15} *s* from the ground state to a higher energy level. This happens due to the *absorption* of light, which occurs immediately relative to nuclear motion, this is known as the Frank-Candon principle [38]. A molecule becomes excited when it absorbs light of a suitable wavelength, to a vibrationally excited energy level of a higher excited singlet state $S_{1,}$ S_2 etc. Whereas, the triplet excited state cannot be directly populated by light absorption but can be obtained from the deactivation of higher excited states [48]. However, *thermal relaxation or non-radiative process*, like *vibrational relaxation* (*VR*) generally occurs within 10^{-11}*s* or more, *rotational relaxation* (nearly 10^{-11} *s*) and *collisional relaxation* (nearly 10^{-10} s) carry the molecule to the lowest vibrational level of the first excited state (S_1) [50].

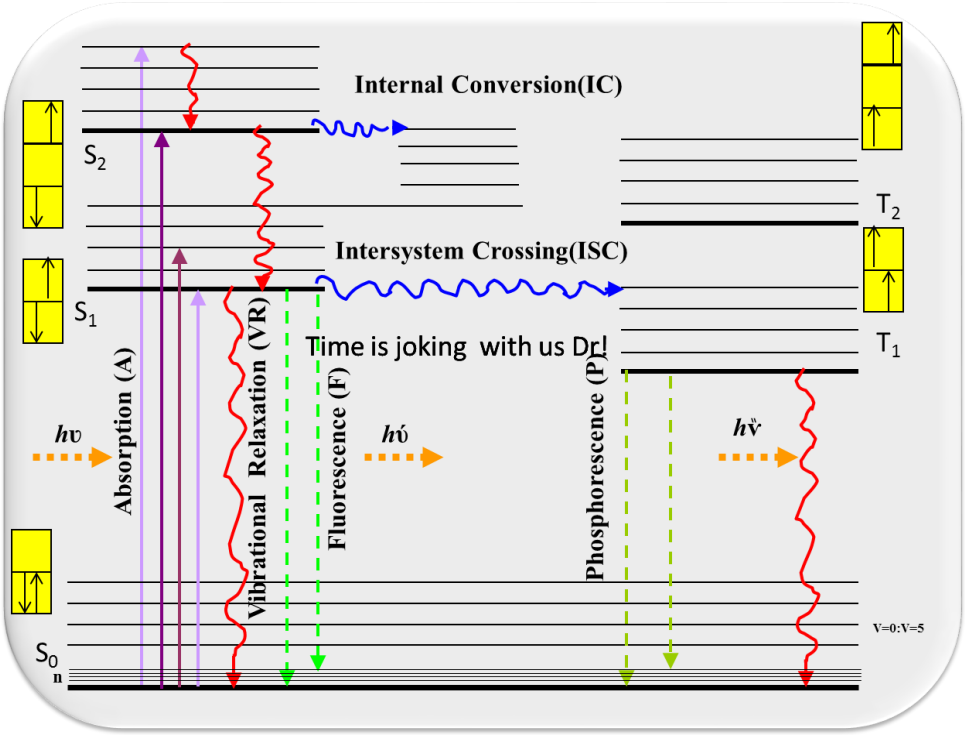

Figure 1.10 Simplified Jablonski (energy level) diagram.

Emission from the lowest vibrational state of S_1 to the electronic ground state (with spin-paired electrons) is termed as *fluorescence*, the decay time of fluorescence is usually from 10^{-9} to $10^{-7}s$ [46]. In contrary, *phosphorescence* occurs when the excited electron come back from the lowest excited triplet state to the singlet ground state. Phosphorescence is a longer-lived emission (approximately 10^{-5} to 10 *s*) compared to fluorescence. Furthermore, it occurs at longer wavelengths relative to that of fluorescence [46]. The relaxation may also happen by a non-radiative process such as *internal conversion* (*IC*) and *intersystem crossing* (*ISC*). *IC* is a thermal relaxation from a higher energy state to a lower energy state with no change in spin, whereas *ISC* involves a radiationless transition from S_1 to T_1 or from T_1 to S_0 [50]. Phosphorescence and *ISC* are *spin-forbidden* transitions. In contrast, fluorescence and *IC* are *spin-allowed* transitions [48].

1.8.2. **The fluorescence lifetime and the quantum yield**

The most important characteristics of an electronically excited molecule are the *fluorescence lifetime* and the *quantum yield*. The mean time the molecule spends in the excited state before relaxation to the ground state is termed the lifetime (τ_f), whereas as the quantum yield (Φ_f) is the ratio between the number of

emitted photons and the number of absorbed photons [38]. Each fluorescence or non-radiative process which causes relaxation of the excited stated is characterised by the lifetime:

$$\tau_f = \frac{1}{k_f + k_{IC} + k_{ISC}} = \frac{1}{k_f + k_{nr}} \qquad \text{Equation 1.9}$$

Where k_f, k_{IC}, k_{ISC} and k_{nr} are the first order rate constants for fluorescence, *IC*, *ISC* and non-radiative processes, respectively. The lifetime in the absence of the non-radiative process is termed as the intrinsic lifetime (τ_n) [38], and is given by:

$$\tau_n = \frac{1}{k_f} \qquad \text{Equation 1.10}$$

On the other hand, the quantum yield of fluorescence can be expressed by the following equation [38]:

$$\Phi_f = \frac{k_f}{k_f + k_{nr}} \qquad \text{Equation 1.11}$$

1.8.3. **Bimolecular deactivation process**

In addition to unimolecular processes, the excited molecule (*fluorophore*) may have a chance to interact with another chemical species when the fluorescence lifetime of the excited state is relatively long lived. This important interaction is known as *a bimolecular deactivation process* [48]. When this deactivation process includes the transfer of excitation energy from a donor molecule to another, the process is referred as *quenching* of the donor molecule. In contrast, the process is known as *fluorescence sensitization* if there is an increase in the fluorescence intensity of a fluorophore [51].

1.8.4. **Fluorescence resonance energy transfer (FRET)**

Energy transfer was observed for the first time by Cario and Frank during their work on sensitized fluorescence [52]. The energy transfer phenomenon can be defined as energy that transfers spontaneously from an excited fluorophore, called a donor (*D*) to another molecule called an acceptor (*A*). Energy transfer result from an overlap of the emission spectrum of the donor with the absorption spectrum of the acceptor [38]. The quenching of fluorescence of D^* and the

subsequent emission from A^* is the consequence of an energy transfer process [51].

$$D^* + A \rightarrow D + A^* \qquad \text{Equation 1.12}$$

According to the number of steps, energy transfer can be classified into two pathways. If the energy transfer is achieved in two-steps then the process is called *radiative* energy transfer (Equations 1.13 and 1.14), such a transfer does not require direct overlap between the donor and acceptor.

$$D^* \rightarrow D + h\nu \qquad \text{Equation 1.13}$$

$$A + h\nu \rightarrow A^* \qquad \text{Equation 1.14}$$

Non-radiative energy transfer (NRET) (Equation 1.12) occurs in single step from long or short range due to spectral overlap of the donor emission spectrum and the acceptor absorption spectrum. NRET occurs by two distinguishable mechanisms, the exchange and Coulomb mechanism [51, 52]. The Coulomb mechanism, is also termed as the Förster mechanism, and is dependent on the dipole-dipole interaction between the donor and the acceptor. Whereas, the exchange mechanism, is also known as the collision or overlap mechanism [38, 52].

Due to the degree of energy transfer dependence on the separation distance between *D* and *A*, the following equation was written by Förster [53];

$$k_{ET} = \left(\frac{k\ \kappa^2 k_D^o J(\varepsilon_A)}{r^6} \right) \qquad \text{Equation 1.15}$$

Where, k_{ET} represents the rate constant of energy transfer, r represents the separation distance between *D* and *A*, k is a constant related to the physical properties of solvent, ε_A is the excitation coefficient, k_D^O is the rate constant of donor in the absence of acceptor, κ is the orientation transition of *D* and *A* dipoles, and *J* is the integrated overlap of the experimental excitation and emission spectra and can be expressed as following [19];

$$J = \int_0^{\infty} I_D \varepsilon_A d\nu \qquad \text{Equation 1.16}$$

Where, I_D is the donor fluorescence spectra and ν is the wave number of the normalized fluorescence spectra. Experimentally, it is more suitable to determine the energy transfer efficiency (*ET*) instead of k_{ET}. As the *ET* efficiency can be defined as;

$$ET = \left(\frac{k_{ET}}{k_D^o + k_{ET}} \right) \qquad \text{Equation 1.17}$$

The *ET* efficiency can be experimentally quantified by estimation of critical separation distance (R_o). R_o represents Förster distance, is defined as the separation distance at which the ET efficiency is 50% [19, 53]. The R_o is mathematically related to k_{ET} as following;

$$k_{ET} = \left(\frac{k_D^o R_o^6}{r^6} \right) \qquad \text{Equation 1.18}$$

The *ET* efficiency can be related to R_o by combination of Equations 1.17 and 1.18, and this will give;

$$ET = \left(\frac{R_o^6}{r^6 + R_o^6} \right) \qquad \text{Equation 1.19}$$

If R_o is calculated for a desired *D* and *A* pair, practically it is possible to determine, the actual separation distance (r) in a defined polymer system, suggesting the applying of the Spectroscopic Ruler Technique term in order to explain such fluorescence measurements [19].

Consequently, incorporation of two fluorescent labels as a donor and an acceptor to a polymer (Figure 1.11) will let us investigate the conformational behaviour of macromolecule in both a bulk solution and at liquid-solid interface as a function of pH. An increase in energy transfer as the pH is decreased shows that the distance between the donor and acceptor has decreased representing a

collapse of the polymer chain. In terms of spectra, this manifests as a decrease in the intensity of the donor label and an increase in the intensity of the acceptor label.

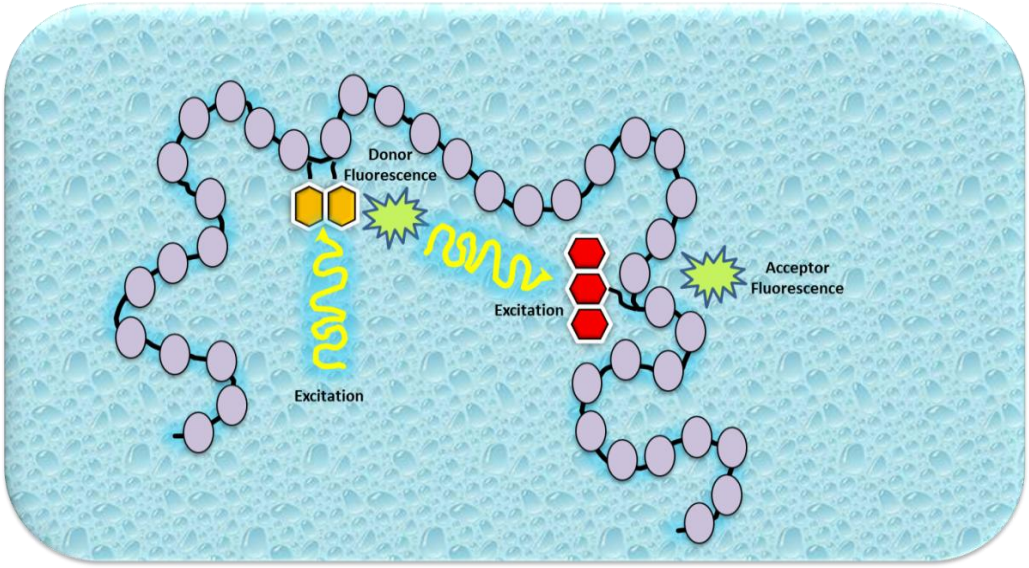

Figure 1.11 The principle behind fluorescence resonance energy transfer in a polymer chain.

1.8.5. **Fluorophores**

A fluorophore, also known as fluorescent probe, can be defined as a molecule, which absorbs energy of a specific wavelength and re-emits a photon at a different wavelength. The intensity and wavelength of the emitted photon depend on both the fluorophore and the surrounding environment of the fluorophore [49]. Since the model polymer and biopolymers are non-fluorescent, fluorescent probes will be introduced in order to monitor the behaviour of the polymers in solution and at liquid solid interface.

One main benefit of utilising fluorophores is that they can be covalently attached in suitably tiny quantities so that they do not disturb the conformational behaviour of polyelectrolyte [19]. The second advantage is that the fluorescence response of the covalently attached fluorescent label can be directly related back to the model polymer itself [54].

The fluorescent labels applied in this project are acenaphthylene (ACE), (9-anthryl) methyl methacrylate (AMMA), and 4-amino-1-naphthalene sulfonic acid (AmNS), respectively.

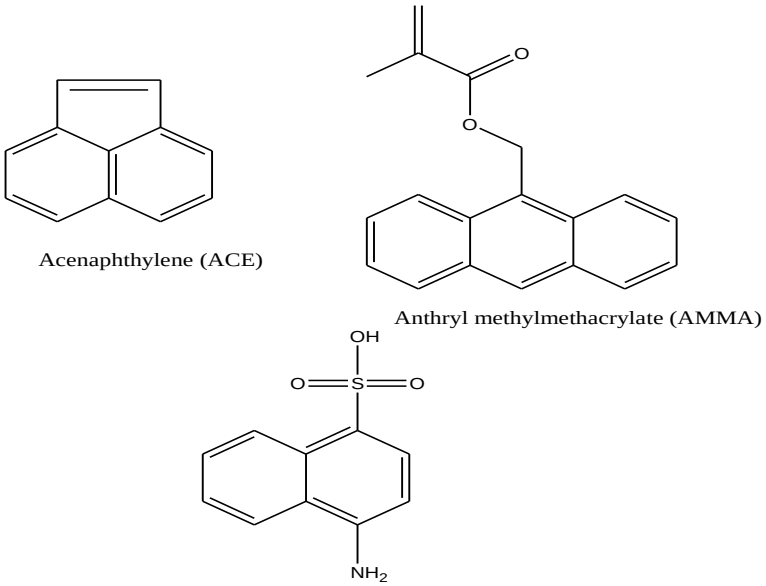

Figure 1.12 Fluorescent labels applied in this project.

ACE binds to the polymer backbone by formation of five membered ring [55]. This forms two covalent bonds meaning that ACE cannot rotate around its axis and therefore any motion of the label is directly related to that of the polymer. In contrast, AMMA attach to the polymer backbone by formation single bond, which rotate freely around its axis. The speed of rotation depends upon the viscosity of the surrounding environment. When the polymer is collapsed this will lead to a difficulty in the label dynamic of and this will change its fluorescence relative to if it can rotate freely [56].

ACE is a hydrophobic fluorophore [41], while the fluorescence spectra of AmNS in different solvents showed that apolar solvents decrease the solubility and reduce the quantum yield. This means that the fluorescence intensity of the probe enhances in a water-like surrounding [57].

1.9. **Fluorescence Instrumentation**

1.9.1. **Fluorescence steady state spectroscopy**

Fluorescence steady state spectroscopy is applied in order to generate a steady state spectra of a fluorophore. The steady state technique is performed with constant illumination and observation. The general schematic for a steady state spectrofluorometer is shown below:

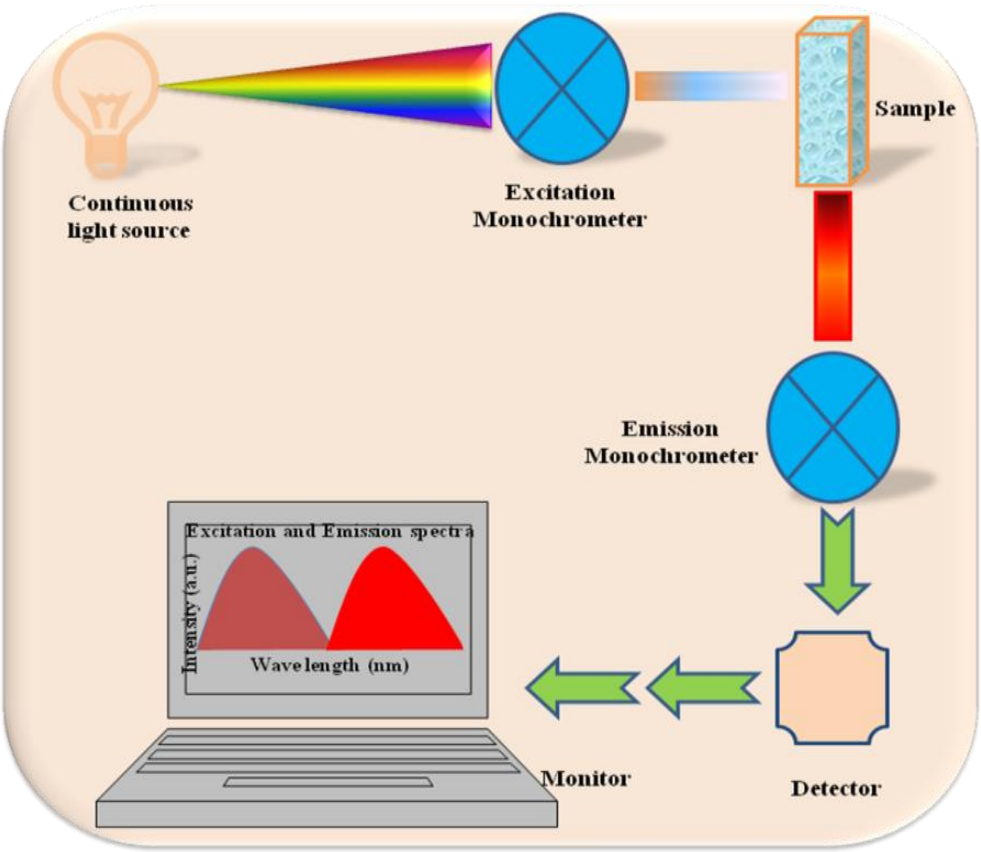

Figure 1.13 Schematic of a steady state spectrofluorometer.

In an ideal spectrofluorometer the light source is capable of producing a stable photon yield at all wavelengths. When the spectrofluorometer is run the fluorescence analysis begins in a systematic order. Firstly, light beam passes through the excitation monochromator, which in turn permit the selected excitation wavelength to pass. Then gratings remove any stray light and the particular wavelength passes through to the sample cuvette, where the sample is excited and emission happens. After that, fluorescence is observed at right angle to the excitation light in order to enhance the sensitivity of the fluorescence measurement. Then the emission monochromator select the desired emission wavelengths. According to what is being measured, photomultiplier tubes sense the fluorescence and let it to be quantified. Finally the quantified fluorescence passes through an amplifier to the computer where the output is represented spectrally [38].

Two kinds of spectra can be recorded on a steady state spectrofluorometer. The excitation spectrum represents the relative absorption of the sample at each individual excitation wavelength. In this case, the emission wavelength is fixed

and excitation wavelengths are scanned. When the excitation wavelength is fixed the emission wavelengths are scanned. The wavelength interval is determined by the slit widths [38].

Perkin Elmer LS50 luminescence spectrometer and fluoromax-4 spectrofluorometer

In the experiments decided in this thesis, fluorescence steady state excitation and emission spectra were recorded on a Perkin Elmer LS50 luminescence spectrometer (Figure 1.14) or fluoromax-4 spectrofluorometer (Figure 1.15).

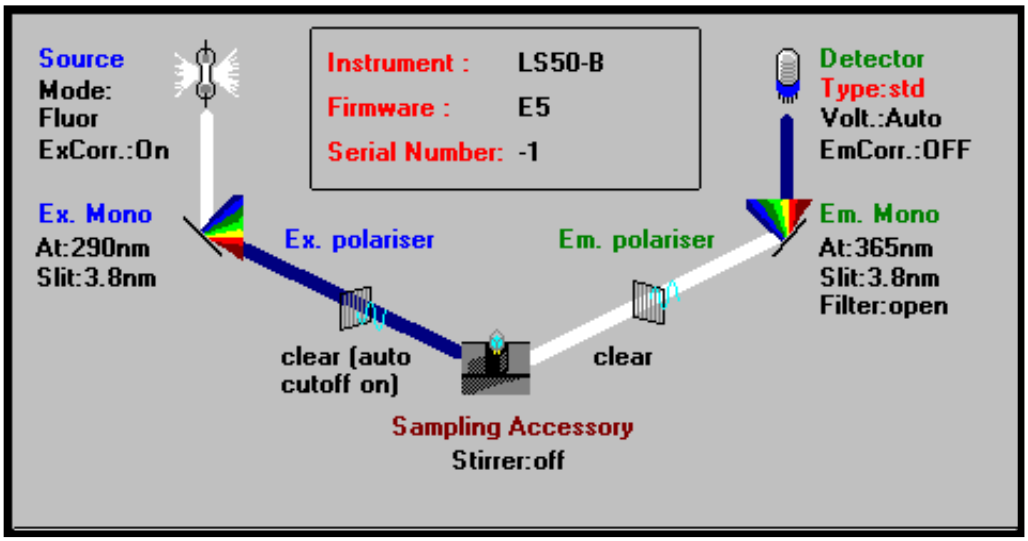

Figure 1.14 Schematic of Perkin Elmer LS50 luminescence spectrometer.

In both machines, a special Xenon flash tube is used as an excitation source which is triggered at line frequency (50 or 60Hz) to generate a strong, short period radiation pulse over the selected spectral range. The optical system consists of two excitation and emission reflection grating monochromators, a series of mirrors and the reference and sample photomultiplier detectors. The signals from the detectors are processed by the instrument electronics, and can be displayed on a PC monitor.

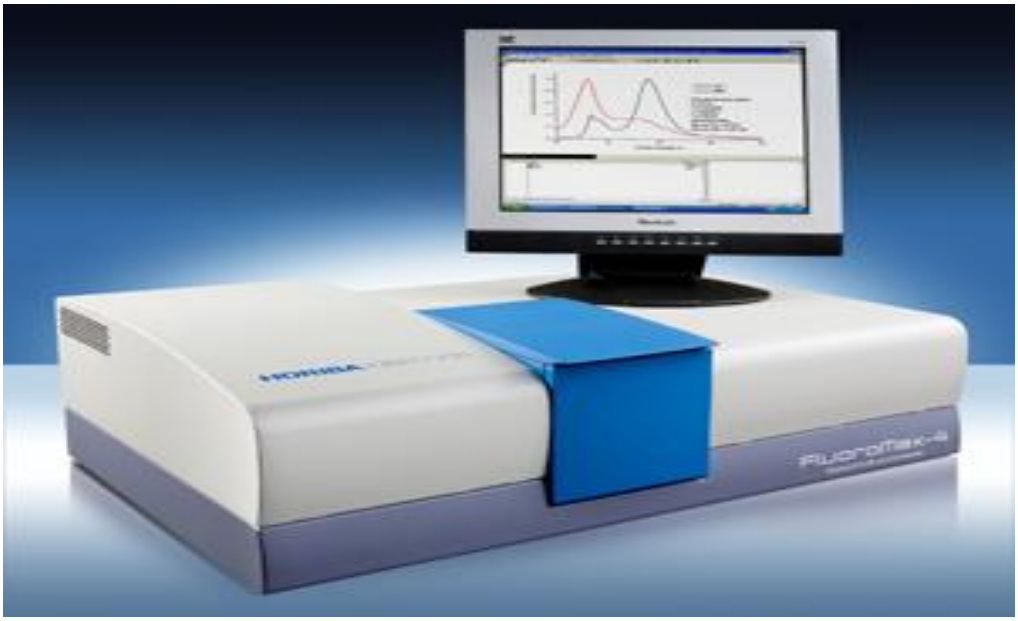

Figure 1.15 Picture of fluoromax-4 spectrofluorometer.

1.9.2. **Time resolve anisotropy measurements (TRAMS)**

Time-resolved fluorescence anisotropy measurements (TRAMS) are a powerful fluorescence technique that was employed in this project. TRAMS can be used to monitor polymer dynamics directly [41, 54, 58, 59]. When a fluorophore is covalently bound to the polymer backbone as a fluorescent label, the mobility of the fluorophore can be considered to reflect that of the polymer [41, 54, 58, 59].

Time resolved anisotropy measurements are described by the theory of photoselective absorption of fluorophores by polarized light [38, 58] (Figure 1.16). Photoselection of fluorophores, whose transition vectors are aligned parallel to that of the incident absorption, can be generated by applying a vertically polarised light [58]. During absorption processes fluorophore molecules which have the proper alignment and fluoresce generating a degree of anisotropy (r) or optical order within an otherwise isotropic population [58]. This anisotropy will decay if molecular motion take places simultaneously with the excited state fluorescence lifetime (τ_f) of fluorophore [58].

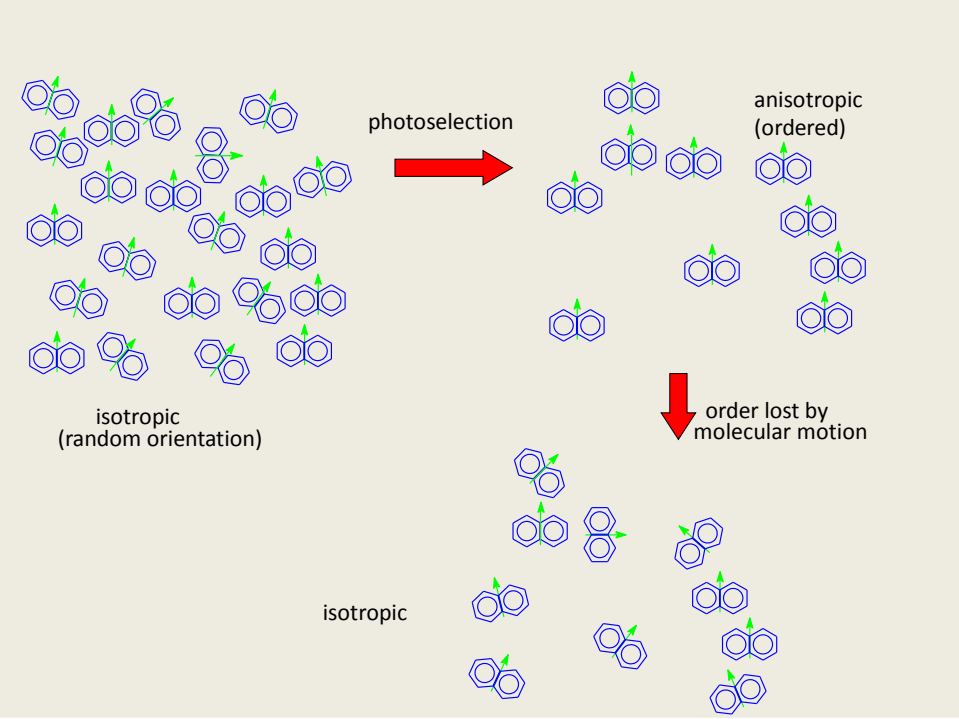

Figure 1.16 Photoselection of fluorophores modified from Swanson 2004 [60].

Information related with the molecular motion of fluorophore distribution can be provided by monitoring the loss of anisotropy as a function of time, $r(t)$ [58]. The anisotropy decay can be monitored by measuring the time-dependent intensity of fluorescence in the perpendicular, $I\perp(t)$ and parallel, $I||(t)$ planes. $r(t)$ can be estimated by use of the following equation [38, 58]:

$$r(t) = \frac{I_{\parallel}(t) - I_{\perp}(t)}{I_{\parallel}(t) + 2I_{\perp}(t)} = d(t)/s(t) \qquad \text{Equation 1.20}$$

Where, $d(t)$ and $s(t)$ are the difference and the sum functions, respectively. An exponential function (single exponential kinetic model such Equation 1.21) as below equation can be used to model $r(t)$

$$r(t) = B + A\,exp^{-t/\tau_c} \qquad \text{Equation 1.21}$$

Where, τ_c is the correlation time, which measures the molecular motion within the fluorophore population, B is a constant, which represents the anisotropy at $t = \infty$ and A is a constant, which represents the anisotropy at $t = 0$. Figure 1.17 illustrates a plot of the loss of anisotropy with time.

In very complex systems, where the fluorophore is existing in two or more different environments, a double exponential model is applied:

$$r(t) = B_1 + A_1 exp^{-t/\tau_{c1}} + B_2 + A_2 exp^{-t/\tau_{c2}} \quad \text{Equation 1.22}$$

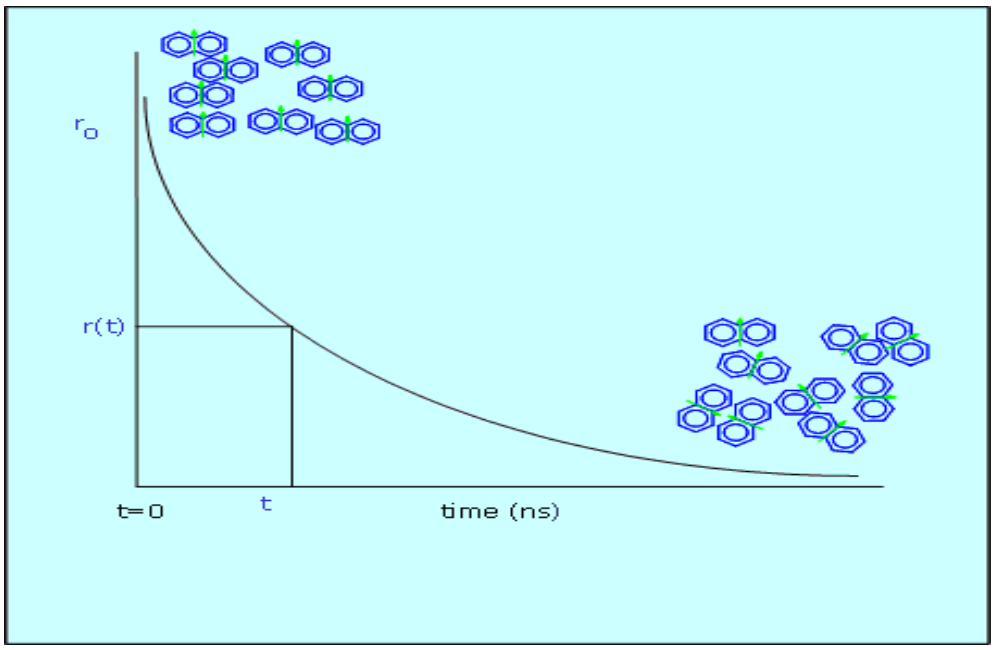

Figure 1.17 Schematic of the time resolved anisotropy process [60]. The fluorophores are excited by a polarised light source at t=0 and the anisotropy decrease is measured against time. When the fluorophore is covalently attached to a polymer backbone the faster the decay the more freedom the segment of the polymer chain has.

In this project an Edinburgh instruments 199 fluorescence spectrophotometer was used to measure the fluorescence anisotropy of fluorescent samples. A schematic illustration of this spectrometer is presented in Figure 1.18. An IBH nano LED pulsed diode was used as an excitation source in the Edinburgh instruments 199 fluorescence spectrophotometer. The analysis begins when the light generated by the excitation source is passed through an excitation monochromator (*M1*), where a specific wavelength is picked out to excite the sample. Then the fluorescence generated passes through the emission monochromator (*M2*), where the desired wavelength is selected, and is incident on the stop photomultiplier (*PM2*). This signal, following discrimination by (*D2*), stops the generation of voltage in the time-to-amplitude converter (*TAC*). The time

difference between the start and the stop pulses can be determined from this voltage.

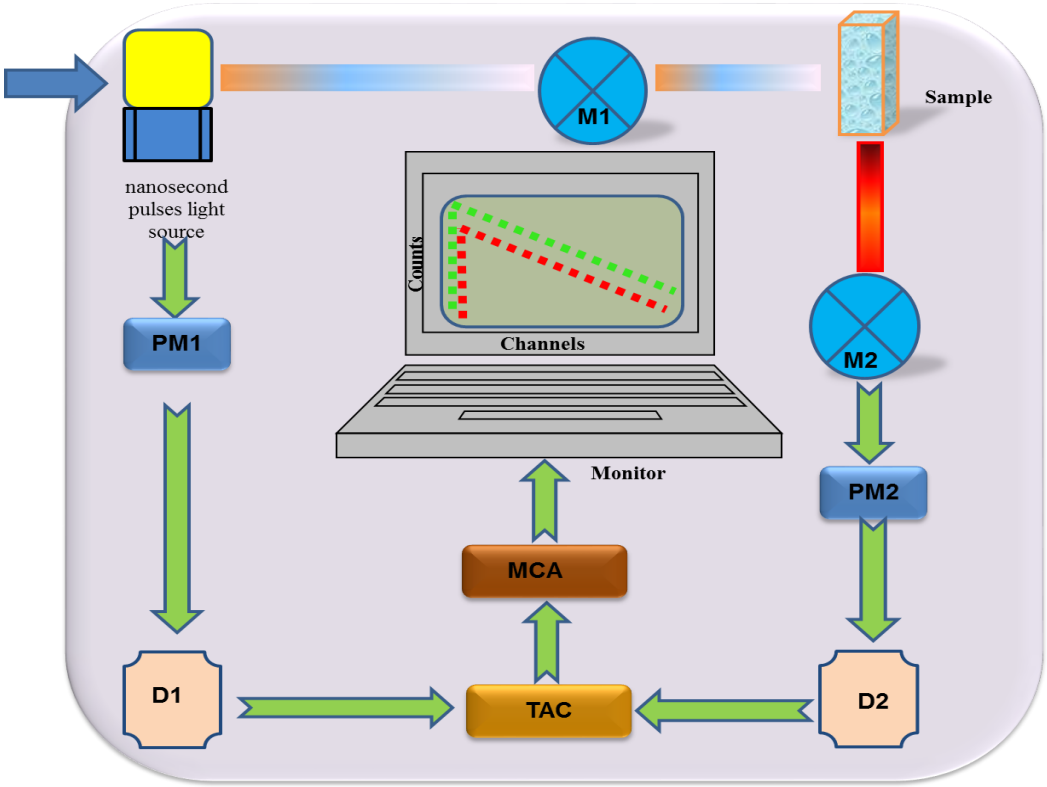

Figure 1.18 Schematic diagram of the Edinburgh Instruments 199 fluorescence spectrometer.

The output from the *TAC* is deposited in a multi-channel analyser (*MCA*). This process is repeated several times and the collection of data produces a curve of fluorescence counts against time in channels (Figure 1.18). Since the stop photomultiplier receives only the first photon from the sample after each pulse, the accumulation of such photons after every pulse gives a true decay curve only when one (or less) fluorescent photon can reach the stop photomultiplier following every pulse. This is the so called single photon counting condition. This condition can be achieved by adjusting the emission intensity such that the rate of detection of an emitted photon is less than, for example, 1% of the start rate [38].

1.9.3. **Fluorescence excited state lifetime**

The fluorescence excited state lifetime analysis was utilised to investigate the response of a fluorophore to its surrounding environment. This fluorescence

technique provides us useful information relating to the conformational change of a charged polymer in aqueous solution [19].

In this work, the fluorescence excited state lifetimes of fluorophore, single and doubly labelled polymers were measured by using the IBH 5000 spectrofluorometer, which is schematically similar to that 199 system. Typically, 30,000 counts were required to generate a simple exponential fluorescence intensity decay $I(t)$, which is described by using the following equation.

$$I(t) = I_0 \, exp^{-t/\tau_f} \qquad \text{Equation 1.23}$$

Where, I_o represents the initial fluorescence intensity, τ_f is the fluorescence excited state lifetime. To create a τ_f value the gained fluorescence raw data is fitted to a mathematical model utilizing the least squares method. A statistical quantity termed as chi-squared (χ^2) results as a specific number. This number calculates the discrepancy between the mathematical model function and the raw data. It is very favourable to get the minimum value of χ^2 from this process. Ideally, χ^2 value equals one; this means that the fitted function matches the raw data exactly. When χ^2 value is much bigger than one this will inform that the fit is not good this is attributed to that deviations are larger than the statistically expected deviations.

1.10. **Potentiometry of Polyelectrolytes**

Potentiometric titration is mainly used for the experimental measurement of ion concentrations by using a combined electrode [61] (Figure 1.19), this electrode consist of a reference and pH-indicator electrode contained in a single glass tube [62]. Although these electrodes are more costly than separated reference and indicator electrodes, they are more suitable to utilize, particularly for smaller amounts of polyelectrolyte solution [62]. The difference in potential which generate between the reference and pH electrodes can be determined by applying the following equation [62];

$$\mathrm{V} = \mathrm{E}_{constant} + \left(\frac{2.303RT}{F}\right) * pH \qquad \text{Equation 1.24}$$

Where, V is the voltage of the cell, $E_{constant}$ is the reference electrode potential, R is the gas constant, T is the absolute temperature and F represents the Faraday constant.

It can be noted from the above equation that the voltage proportional directly to sample solution temperature, so pH meter should be a combined with a temperature control. pH determinations are primarily used to determine the degree of ionization of polymers, which depends directly on the degree of neutralization [61], the acidity constants (pKa values). In order to identify the pH induced conformational changes of polymer chain, it is necessary to know the acidity constant in order to determine the global charge on a polyelectrolyte at specific pH [61]. These determinations can be achieved via characterizing the electrochemical properties of polyelectrolytes solution [61].

In general, the dissociation constant (*Ka*) of a weak acid (HA dissociating to H^+ and A^-) can be expressed as supposed by the law of mass action as follows [61]:

$$\mathrm{Ka} = \left(\frac{[H^+][A^-]}{[HA]}\right) \qquad \text{Equation 1.25}$$

The *pKa* can be determined by taking the negative logarithm of both sides for the Equation 1.25, this gives:

$$\mathrm{pKa} = pH - log\left(\frac{[A^-]}{[HA]}\right) \qquad \text{Equation 1.26}$$

Where, $[A^-]$ can be linked directly to the degree of neutralization (α) and $[HA]$ to $1 - \alpha$. Eventually, the *pKa* value can be determined by using the Henderson-Hasselbalch equation[61]:

$$\mathrm{pKa} = pH + log\left(\frac{1-\alpha}{\alpha}\right) \qquad \text{Equation 1.27}$$

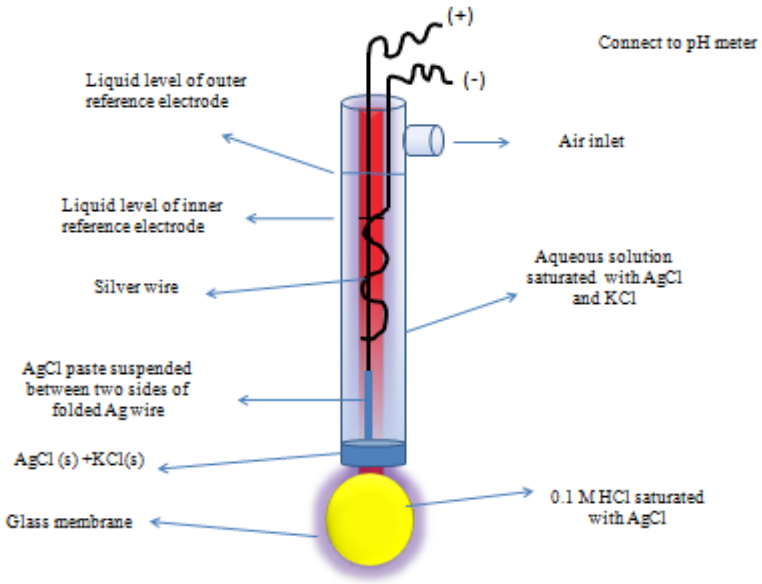

Figure 1.19 A combined electrode.

In this work, a potentiometric titration is carried out by using an automated potentiometric titrator. This is preferred to manual titrations, since they are more accurate and precise. The pH of the polyelectrolyte solution at a constant ionic strength is varied by adding controlled amounts of strong acid (HCl) or strong base (NaOH), and simultaneously detected by a glass electrode. The measured amounts are expressed by the electromotive force of the combined electrode, the volume of strong acid or base added to the analyte container, and the total volume of the sample. From these data, the experimental titration curve (moles added from acid or base against pH) is plotted. The blank titration is carried out, in which only the solvent is titrated with strong acid and then back titrated with base.

A given potentiometric titration curve has a characteristic sigmoid curve of acrylic acid is shown in Figure 1.20, the blank titration curve is also presented. The part of the curve that has the maximum change marks the equivalence point of the titration. From the first derivative, buffer intensity, the *pKa* of sample can be typically determined (Figure 1.21).

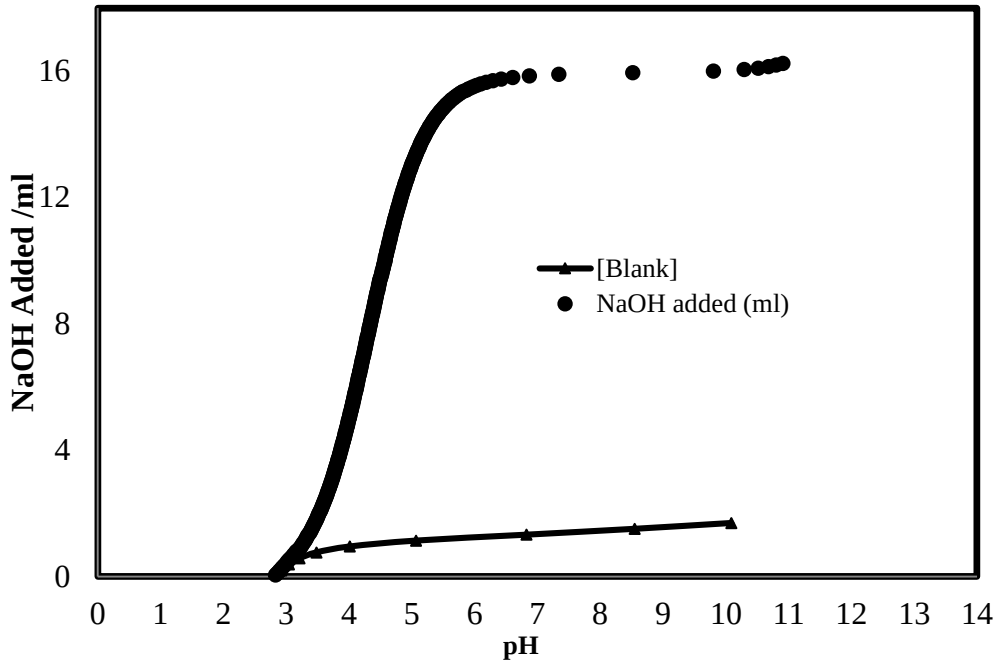

Figure 1.20 A potentiometric titration curve of 0.1 M acrylic acid, blank titration is included.

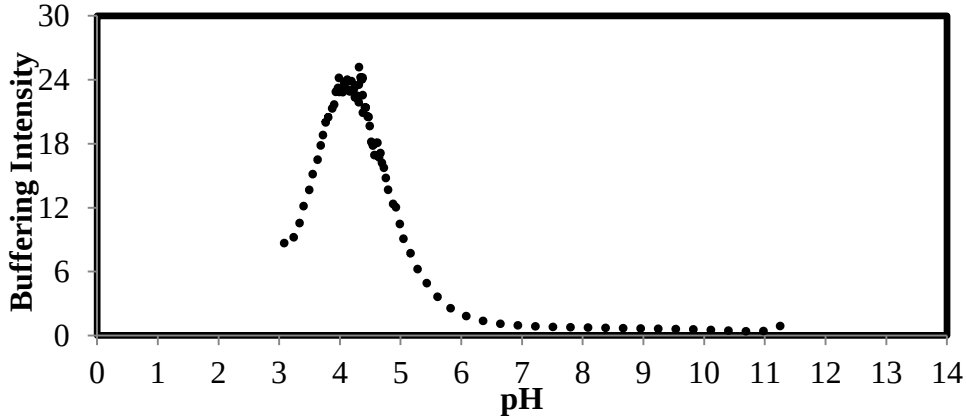

Figure 1.21 A buffer intensity of 0.1 M acrylic acid, pKa=4.03.

1.11. **Hypothesis**

Our hypothesis is that a major step change in elucidating ability at cell and biofilm scale can be delivered by investigating of conformation and dynamics of cell wall macromolecules (LPS) in both bulk solution and at solid surfaces, starting with using simple synthetic polymer (PAA), which should act as model systems for bacterial growth.

1.12. **Objectives**

This project will deliver targeted data sets on the interactions of model polymer with mineral surfaces, such as silica and alumina, to gain insight into interaction forces. The final aim is to extend this study to a bacterial biopolymer. This will be represented by lipopolysaccharide, the main component of the outer membrane of bacteria, as biological models in contact with solid surface. Research investigations will combine fluorescence; potentiometry and inductively coupled plasma mass spectrometry techniques to build a good experience in understanding of the molecular basis for physical and chemical interactions are involved in the attachment of a cell to a mineral surface. A broad set of investigational data on model systems down to the nanometre observation scale is a key deliverable for researchers.

1.12.1. **General Objectives**

- To study conformation changes of model polymers including poly (acrylic acid) (PAA), as model biopolymer and alginic acid, as model bacterial polymer, using fluorescence technique.
- To study conformation changes of biologically produced polymeric substances, such as lipopolysaccharide (LPS), using fluorescence technique.

1.12.2. **Specific Objectives**

Fluorescence study including steady state, excited-state lifetime and time-resolved anisotropy measurements (TRAMS) on:

- Poly(acrylic acid) and alginic acid solutions in the presence of simple electrolytes such as NaCl and $CaCl_2$

- Poly (acrylic acid) and alginic acid solutions in the presence of minerals including alumina and silica.
- Lipopolysaccharide solution in the presence of simple electrolytes such as NaCl and $CaCl_2$
- Lipopolysaccharide solution in the presence of minerals including alumina and silica.
- Determination conformation changes of model and biopolymers by potentiometric titration.
- Compare conformational behaviour between model polymer and biopolymers by fluorescence and potentiometric techniques.
- Measure adsorption isotherms of minerals by inductively coupled plasma mass spectrometry technique.

Chapter 2. EXPERIMENTAL WORK

2.1. **Materials**

All materials were used as received unless otherwise stated.

2.1.1. **Solvents**

(i) Dioxane (Aldrich, spectroscopic grade)
(ii) Methanol (Aldrich, general and spectroscopic grades)
(iii) Ethanol (Aldrich, general and spectroscopic grades)
(iv) Diethyl ether (Aldrich general and spectroscopic grades)
(v) Water (double distilled)
(vi) Tetrahydrofuran (Fisher, general grade)
(vii) Dichloromethane (Fisher, HPLC grade)
(viii) Dimethyl formamide (Aldrich, spectroscopic grade)
(ix) Glycerol (Aldrich, spectroscopic grade)

2.1.2. **General reagents**

(i) Potassium carbonate (Aldrich, 99%)
(ii) Hydrochloric acid (Fluka, ≥ 37%)
(iii) Sodium hydroxide (Sigma-Aldrich, ≥ 97%)
(iv) Tri ethylamine (Aldrich, 99.5%)
(v) Triethyleneglycol monochlorohydrin (Aldrich, 96%)
(vi) Aluminium oxide (50-200 micron) (Acros Organics)
(vii) Sodium chloride (Sigma-Aldrich, ≥ 99.5%)
(viii) Calcium chloride (Sigma, ≥ 96%)
(ix) LUDOX® AS-30 colloidal silica 30 wt% suspension in H_2O (Aldrich)
(x) N,N'-Dicyclohexyl carbodiimide (DCC) (Aldrich, 99%)
(xi) Methacrylic acid (Aldrich, 99%)
(xii) 4-(Dimethyl amino) pyridine (DMAP) (Aldrich, ≥99%)
(xiii) Sodium bicarbonate (Fluka, ≥ 99%)
(xiv) Anhydrous sodium sulphate (Sigma-Aldrich, ≥ 99%)
(xv) N-Hydroxysuccinimide (Sigma-Aldrich, 98%)

2.1.3. **Polymerisation initiators and coupling agents**

2,2′-Azobisisobutyronitrile (AIBN) (BDH, 97%)

2,2'-Azobisisobutyronitrile (AIBN) was recrystallized from methanol three times according to a protocol. Briefly, over a water bath at 40^{o}C, AIBN was dissolved in a small amount of methanol in a flask under stirring. The solution was filtered and left to cool before being placed in the freezer overnight. The recrystallized material was then washed with a small amount of methanol, filtered under a vacuum and dried in a vacuum oven overnight at room temperature. The purity of the AIBN was tested with a Linkam melting point apparatus (Prior England). The purity was judged to be 100% based on the documented AIBN melt point of 100-103 ^{o}C. The purified AIBN was stored in the freezer at -10^{o}C.

N-(3-Dimethylaminopropyl)-N′-ethylcarbodiimide hydrochloride (EDC) (Fluka, ≥99.0%)

Used as received, without any further purification.

N-hydroxysuccinimide (NHS) (Aldrich, 98%)

Used as received, without any further purification.

2.1.4. **Fluorescent labels**

Acenaphthene (Aldrich, 99%)

Used as received, without any further purification.

Acenaphthylene (ACE) (Lancaster, 90%)

Acenaphthylene (ACE) was purified by applying the following procedure: According the supplier acenaphthene is the major impurity exists within the provided ACE. This is removed by multiple recrystallization (1 g of ACE) from methanol followed by vacuum sublimation [63]. The purity of the ACE was tested with a Linkam melting point apparatus (Prior England). The purity was judged to be 100% based on the documented ACE melt point of 86-87^{o}C. The purified monomer was stored at -10 ^{o}C. The product was isolated in ~ 75% yield.

9-Anthracenylmethanol(Aldrich, 97%)

9-Methylanthracene(Aldrich, 98%)

Used as received, without any further purification.

(9-Anthryl)methyl methacrylate (AMMA)

(9-Anthryl)methyl methacrylate (AMMA) was synthesised according to the literature [64] (Figure 2.1):

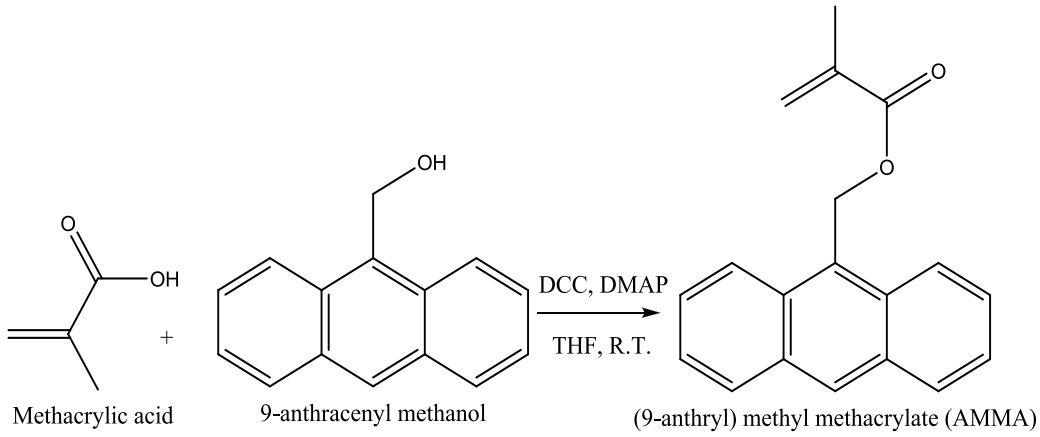

Figure 2.1 Scheme for the synthesis of (9-anthryl) methyl methacrylate (AMMA).

27.7 g (0.13 mol) of 9-anthracenylmethanol was dissolved in 350 mL of tetrahydrofuran (THF). A solution of 11.19 g (0.13 mol) of methacrylic acid in 50 mL of THF was added, and the solution was cooled in an ice-water bath. A solution of 26.82 g (0.13 mol) of dicyclohexyl carbodiimide (DCC) in 50 mL of THF was added upon stirring followed by a solution of 3.2 g of 4-dimethyl amino pyridine (DMAP) in 50 mL of THF. The reaction mixture was kept in the ice-water bath for 5 min and then for 8 hours at room temperature. After this time, thin layer chromatography (TLC) was used to check that all the monomer had been consumed in the reaction. Had all the monomer not been used up the solution would have been left to stir for a longer period, possibly overnight. The resultant solution formed an orange oily liquid and precipitated dicyclohexyl carbamide, which was filtered off and washed with 50 ml of THF on the filter. The solvent was evaporated, and the formed suspension was kept in refrigerator for several hours and then at room temperature for 3 days. Distilled water was added to the mixture, followed by diethyl ether in order to extract the organic layer. The liquid was then poured into a separating funnel and the lower aqueous phase was removed, leaving the orange ether layer (containing the product). The ether layer was filtered with a paper filter then washed with 0.5M HCl solution (3 times) followed by a saturated $NaHCO_3$ solution (4 times). The ether solution was finally washed 4 times with double distilled water and dried over anhydrous sodium sulphate for a period of 16 hours at room temperature. The sodium sulphate was filtered off and the ether solution was evaporated off with a rotary evaporator. The resultant product was recrystallized from spectroscopic grade methanol (3 times).

After the completion of the recrystallization, the monomer was dried in a vacuum oven at 60 ^{o}C for several days. The yellow crystalline solid was tested for purity from its melting point (85-86 ^{o}C) and by obtaining its NMR spectrum in $CDCl_3$. After synthesis, the monomer was stored in the freezer at -10^{o}C. The product was isolated in ~ 44 % yield. ^{1}H NMR (400 MHz, CHLOROFORM-*d*) δ ppm 1.95 (s, 3 H, =C-C**H$_3$**) 5.55 (s, 1 H, -C=C**H**) 6.08 (s, 1 H, -C=C**H**) 6.25 (s, 2 H, **Ar**) 7.52 (t, *J*=6 Hz, 2 H, **Ar**) 7.5 (t, *J*=6 Hz, 2 H, **Ar**) 8.06 (d, *J*=8 Hz, 2 H, **Ar**) 8.41 (d, *J*=9 Hz, 2 H, **Ar**) 8.54 (s, 1 H, **Ar**). m/z = 276 (theoretical: 276.33)

4-amino naphthalene-1-sulfonic acid (AmNS) (Aldrich, 97%)

4-Amino naphthalene-1-sulfonic acid (AmNS) was purified by extraction with warm hexane, the residue was removed, the produced material having melting point 300 -302^{o} C, which had been dried under vacuum over $CaC1_2$. Then it was stored in a dark coloured bottle, in cold place. The product was isolated in ~ 74 %.

2.1.5. **Monomers**

Acrylic acid (AA) (Aldrich, 99%)

Prior to use, the monomer acrylic acid (AA) was passed through a vacuum distillation at room temperature to remove the gas phase inhibitors (monomethyl ether hydroquinone) that are included in the supplied material to prevent polymerisation. The distillation was carried out with the distillate flowing into an iced vessel. The purified AA was stored in the freezer at -10^{o}C.

2.2. **Synthesis of Polymers**

2.2.1. **Synthesis unlabelled and fluorescently labelled poly (acrylic acid) (PAA)**

Acrylic acid was polymerised by a free radical mechanism using AIBN as initiator. Polymers were prepared without any fluorescent label or with ACE label and with both ACE and AMMA labels in trace amounts. Solutions with a monomer to solvent weight ratio of approximately 1:4 were made using 1-4 dioxane as the solvent. The monomer mixes included either 0.5wt% ACE or 0.5 wt% ACE and 1.0 wt% AMMA (100 wt% = 5.2523 g of monomer). The AIBN was used at a concentration of 1000 ppm. The monomers solution were poured in

ampoules, then degassed (to remove dissolved oxygen) using a freeze-pump-thaw on a vacuum line. And finally the ampoules were placed in a water bath at 60 ºC to polymerise where they were left for period of time. The polymers were purified by multiple dissolutions (3 times) and subsequent precipitation using methanol as the solvent and diethyl ether as non-solvent. The produced polymers were then dried in a vacuum oven for at least 24 hours before being weighed.

As a typical polymerisation the table below is listed the amounts of chemicals used for the preparation of PAA, ACE-labelled PAA and ACE-AMMA-labelled PAA, respectively.

Table 2.1 The amounts of chemicals used for the preparation of PAA, ACE-labelled PAA and ACE-AMMA-labelled PAA.

Polymer batch number	Time (h)	Dioxane (ml)	Acrylic acid (mmol)	ACE (mmol)	AMMA (mmol)	AIBN (mmol)
PAA (1)	6	20	72.88	0.00	0.00	0.15
PAA (2)	12					
PAA (3)	24					
ACE-PAA (1)	6	20	72.88	0.17	0.00	0.15
ACE-PAA (2)	12					
ACE-PAA (3)	24					
ACE-AMMA-PAA (1)	6	20	72.88	0.17	0.19	0.15
ACE-AMMA-PAA (2)	12					
ACE-AMMA-PAA (3)	24					

PAA (1) (Yield ~50.0%) ^{1}H NMR (400 MHz, DEUTERIUM OXIDE) δ ppm 1.4 - 1.92 (br. m, 2 H , b:C-C**H$_2$** backbone) 2.0 - 2.45 (br. m, 1 H, a:HOOC -C**H**).

The H^{1} NMR spectrum was quite informative, viewing the typical H^{1} NMR of unlabelled PAA. Additionally, the 1H NMR spectrum showed that no monomer

was found and integration of H^1 NMR peaks gave integral ratios expected for the poly(acrylic acid) (Hb: Ha = 2 : 1). FTIR spectrum (KBr, cm^{-1}): 1715 (C=O; free COOH), 1457 (-CH_2 scissor) and 3150 (-OH stretching). GPC (RI): M_n = 6540 g/mol, M_w = 13014 g/mol, M_v = 11311 g/mol. Viscometry: M_v = 10507 g/mol. (The estimated accuracy of M_n, M_w and M_v is ± 5%).

ACE-PAA (1) (Yield ~35%) ^{1}H NMR (400 MHz, DEUTERIUM OXIDE) δ ppm 1.11 - 1.93 (br. m, 2 H, C-C**H₂** backbone) 2.0-2.50 (br. s., 1 H, HOOC -C**H**) 6.9-7.9 (br. m., 6 H, **Ar**). The H^1 NMR spectrum was quite informative, viewing the typical H^1 NMR peaks of PAA and a broad peak in the aromatic region is supposed to the acenaphthene ring. FTIR spectra of (KBr, cm^{-1}): were indistinguishable from the spectra of PAA due to the low loading of the fluorophore. Fluorescent label content: $(mol\ \%)_{ACE}$ = 2.23 mol%. GPC (RI): M_n = 6579 g/mol, M_w = 13271 g/mol, M_v = 11533g/mol. Viscometry: M_v = 10949 g/mol. (The estimated accuracy of M_n, M_w and M_v is ± 5%).

ACE-AMMA-PAA (1) (Yield ~28%) ^{1}H NMR (400 MHz, DEUTERIUM OXIDE) δ ppm 1.23 - 1.98 (br. m, 2 H, C-C**H₂** backbone) 2.2-2.50 (br. s., 1 H, HOOC -C**H**) 6.9-7.8 (br. m., 15 H, **Ar**). The H^1 NMR spectrum was quite informative, viewing the typical H^1 NMR peaks of PAA and a broad peak in the aromatic region is supposed to the acenaphthene and anthracene rings. FTIR spectra of (KBr, cm^{-1}): were indistinguishable from the spectra of PAA due to the low loading of the fluorophore. Fluorescent label content: $(mol\ \%)_{ACE}$ = 1.88 mol % ; $(mol\ \%)_{AMMA}$ = 1.11 mol %. GPC(RI): M_n = 6614 g/mol, M_w = 13461 g/mol, M_v = 11691 g/mol. Viscometry: M_v = 10417 g/mol. (The estimated accuracy of M_n, M_w and M_v is ± 5%).

PAA (2) (Yield ~61.0%) ^{1}H NMR (400 MHz, DEUTERIUM OXIDE) δ ppm 1.4 - 1.92 (br. m, 2 H , b:C-C**H₂** backbone) 2.0 - 2.45 (br. m, 1 H, a:HOOC -C**H**). The H^1 NMR spectrum was quite informative, viewing the typical H^1 NMR of unlabelled PAA. Additionally, the 1H NMR spectrum showed that no monomer was found and integration of H^1 NMR peaks gave integral ratios expected for the poly(acrylic acid) (Hb: Ha = 2 : 1). FTIR spectrum (KBr, cm^{-1}): 1715 (C=O; free COOH), 1457 (-CH_2 scissor) and 3150 (-OH stretching). GPC (RI): M_n =

12995 g/mol, M_w = 15384 g/mol, M_v = 15022 g/mol. Viscometry: M_v = 13599 g/mol. (The estimated accuracy of M_n, M_w and M_v is ± 5%).

ACE-PAA (2) (Yield ~39%) ^{1}H NMR (400 MHz, DEUTERIUM OXIDE) δ ppm 1.11 - 1.93 (br. m, 2 H, C-C**H$_2$** backbone) 2.0-2.50 (br. s., 1 H, HOOC -C**H**) 6.9-7.9 (br. m., 6 H, **Ar**). The H^1 NMR spectrum was quite informative, viewing the typical H^1 NMR peaks of PAA and a broad peak in the aromatic region is supposed to the acenaphthene ring. FTIR spectra of (KBr, cm^{-1}): were indistinguishable from the spectra of PAA due to the low loading of the fluorophore. Fluorescent label content: (mol %)$_{ACE}$ = 3.33 mol%. GPC (RI): M_n = 8365 g/mol, M_w = 25708 g/mol, M_v = 23018g/mol. Viscometry: M_v = 22098 g/mol. (The estimated accuracy of M_n, M_w and M_v is ± 5%).

ACE-AMMA-PAA (2) (Yield ~39%) ^{1}H NMR (400 MHz, DEUTERIUM OXIDE) δ ppm 1.23 - 1.98 (br. m, 2 H, C-C**H$_2$** backbone) 2.2-2.50 (br. s., 1 H, HOOC -C**H**) 6.9-7.8 (br. m., 15 H, **Ar**). The H^1 NMR spectrum was quite informative, viewing the typical H^1 NMR peaks of PAA and a broad peak in the aromatic region is supposed to the acenaphthene and anthracene rings. FTIR spectra of (KBr, cm^{-1}): were indistinguishable from the spectra of PAA due to the low loading of the fluorophore. Fluorescent label content: (mol %)$_{ACE}$ = 1.99 mol % ; (mol %)$_{AMMA}$ = 1.14 mol %. GPC(RI): M_n = 7718 g/mol, M_w = 14562 g/mol, M_v = 12571 g/mol. Viscometry: M_v = 10917 g/mol. (The estimated accuracy of M_n, M_w and M_v is ± 5%).

PAA (3) (Yield ~80.0%) ^{1}H NMR (400 MHz, DEUTERIUM OXIDE) δ ppm 1.4 - 1.92 (br. m, 2 H , b:C-C**H$_2$** backbone) 2.0 - 2.45 (br. m, 1 H, a:HOOC -C**H**). The H^1 NMR spectrum was quite informative, viewing the typical H^1 NMR of unlabelled PAA. Additionally, the 1H NMR spectrum showed that no monomer was found and integration of H^1 NMR peaks gave integral ratios expected for the poly(acrylic acid) (Hb: Ha = 2 : 1). FTIR spectrum (KBr, cm^{-1}): 1715 (C=O; free COOH), 1457 (-CH_2 scissor), 2939 (-CH_2 stretching) and 3150 (-OH stretching). GPC (RI): M_n = 19580 g/mol, M_w = 47458 g/mol, M_v = 37778 g/mol Viscometry: M_v = 31495 g/mol. (The estimated accuracy of M_n, M_w and M_v is ± 5%).

ACE-PAA (3) (Yield ~65%) ^{1}H NMR (400 MHz, DEUTERIUM OXIDE) δ ppm 1.11 - 1.93 (br. m, 2 H, C-C**H₂** backbone) 2.0-2.50 (br. s., 1 H, HOOC -C**H**) 6.9-7.9 (br. m., 6 H, **Ar**). The H^1 NMR spectrum was quite informative, viewing the typical H^1 NMR peaks of PAA and a broad peak in the aromatic region is supposed to the acenaphthene ring. FTIR spectra of (KBr, cm^{-1}): were indistinguishable from the spectra of PAA due to the low loading of the fluorophore. Fluorescent label content: $(mol\ \%)_{ACE}$ = 1.47 mol%. GPC (RI): M_n = 9995 g/mol, M_w = 31928 g/mol, M_v = 25791 g/mol. GPC (UV): M_n = 19000 g/mol, M_w = 59442 g/mol, M_v = 47986 g/mol. Viscometry: M_v = 43573 g/mol. (The estimated accuracy of M_n, M_w and M_v is ± 5%).

ACE-AMMA-PAA (3) (Yield ~45%) ^{1}H NMR (400 MHz, DEUTERIUM OXIDE) δ ppm 1.23 - 1.98 (br. m, 2 H, C-C**H₂** backbone) 2.2-2.50 (br. s., 1 H, HOOC -C**H**) 6.9-7.8 (br. m., 15 H**, Ar**). The H^1 NMR spectrum was quite informative, viewing the typical H^1 NMR peaks of PAA and a broad peak in the aromatic region is supposed to the acenaphthene and anthracene rings. FTIR spectra of (KBr, cm^{-1}): were indistinguishable from the spectra of PAA due to the low loading of the fluorophore. Fluorescent label content: $(mol\ \%)_{ACE}$ = 1.48 mol % ; $(mol\ \%)_{AMMA}$ = 0.48 mol %. GPC(RI): M_n = 11614 g/mol, M_w = 28840 g/mol, M_v = 20859 g/mol. GPC(UV): M_n = 10060 g/mol, M_w = 25781 g/mol, M_v = 19053 g/mol. Viscometry: M_v = 20382 g/mol. (The estimated accuracy of M_n, M_w and M_v is ± 5%).

Table 2.2 Chemical structures of PAA, ACE-PAA and ACE-AMMA-PAA, respectively, where *n* is importantly larger than *m* and *k*.

Polymer	Chemical structure
PAA	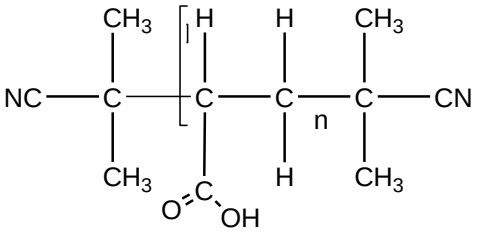
ACE-PAA	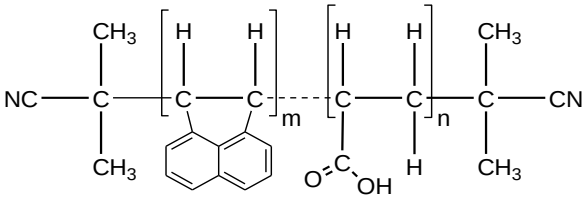
ACE-AMMA-PAA	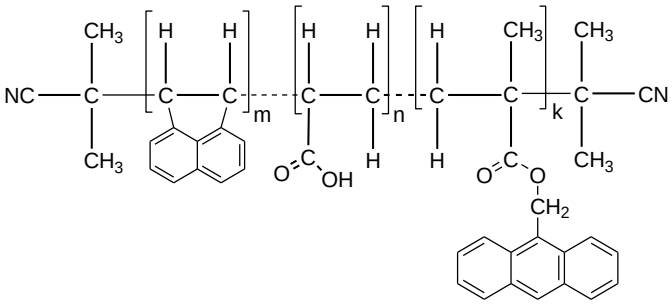

2.2.2. **Synthesis of AmNS-labelled alginate**

Alginate purchased from Sigma-Aldrich was purified by dissolving 5 g in 0.5 M NaOH and stirring for two hours. After that 0.5 M HCl was added slowly until pH 2-3 and stirred for 24 hours. The resulting gel suspension was filtered in a quantitative filter paper and washed with ethanol. The resulting solid was then dried in a vacuum oven at 40 °C for 24 hours. This purification procedure was performed since the commercial reagent presented sodium residue.

Alginate was labelled with 4-amino naphthalene-1-sulfonic acid (AmNS) with a slight modification according to the procedure described elsewhere [65]. Briefly, 3g of alginic acid (18 mmol monosaccharide) was mixed with 80ml water, 30ml of 1,4-dioxane, 50mg(0.15mmol) 4-Amino naphthalene-1-sulfonic

acid and 1g (7.8 mmol) N-(3-dimethylaminopropyl)-N'-ethylcarbodiimide hydrochloride. The mixture was stirred for 3 hours and left overnight .The colour slowly turned orange. Not all alginic acid had dissolved when the reaction was stopped. The mixture was filtered and washed with acetone until the acetone was colourless. The yellow powder was dried before being weighed.

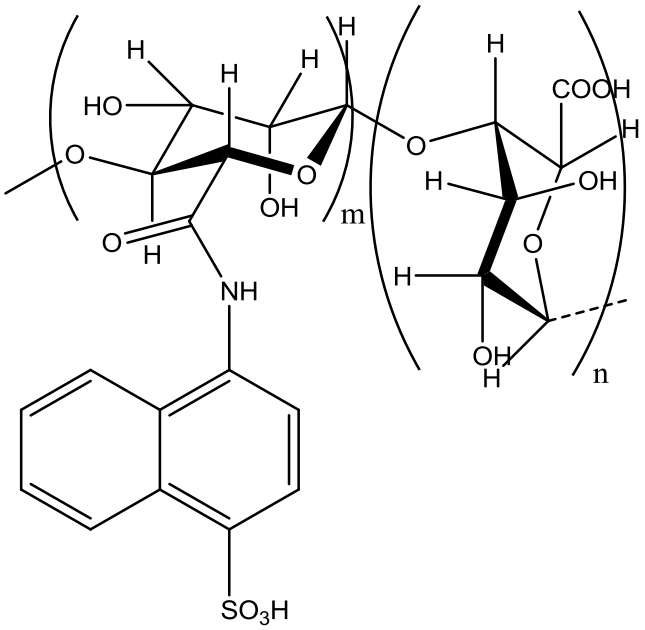

Figure 2.2 Chemical structure of AmNS-labelled alginate, where *n* is importantly larger than *m*.

Alginic acid (Yield ~90 %) ^{1}H NMR (400 MHz, DEUTERIUM OXIDE) δ ppm 2.74 (s, 1 H, C**H-3** of M) 3.62 (br. s., 1 H, C**H-4** of M) 3.77 (br. s., 1 H, C**H-5** of M) 3.89 (br. s., 1 H, C**H-2** of M) 3.98 (br. s., 1 H, C**H-2** of G) 4.04 (br. s., 1 H, C**H-3** of G) 4.31 (br. s., 1 H, C**H-4** of G) 4.50 (br. s., 1 H, C**H-5** of G) 4.85 (br. s., 1 H, C**H-1** of M) 4.90 (br. s., 1 H, C**H-1** of G) [M = mannuronate; G = guluronate]. FTIR spectrum (KBr, cm^{-1}): 3446 (-OH, hydrogen bonded), 12260 (CC); 2929 (CH), 1740 (COOH), 905 (CO). GPC(RI): M_n = 38782 g/mol, M_w = 66480 g/mol, M_v = 62212 g/mol. Viscometry: M_v = 61294 g/mol. (The estimated accuracy of M_n, M_w and M_v is ± 5%).

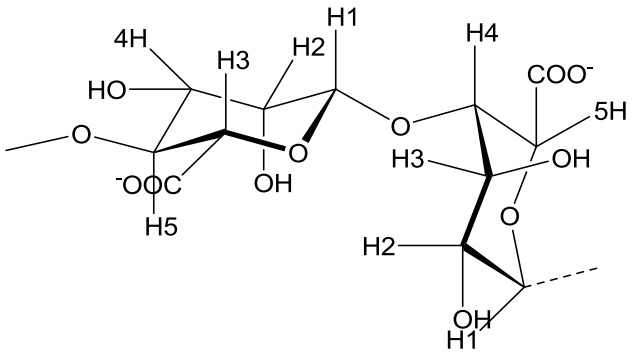

M G

Figure 2.3 Alginate structure, shows *G* and *M* protons.

AmNS-alginate (Yield ~89 %)^{1}H NMR (400 MHz, DEUTERIUM OXIDE) spectra of the product was indistinguishable from the spectra of the unlabelled alginate due to the low content of fluorophore. FTIR spectra of (KBr, cm^{-1}): were indistinguishable from the spectra of alginic acid due to the low loading of the fluorophore. Fluorescent label content: $(mol\ \%)_{AmNS}$ = 0.96 mol%. GPC (RI): M_n = 20965 g/mol, M_w = 31733 g/mol, M_v = 29870 g/mol. Viscometry: M_v = 29507 g/mol. (The estimated accuracy of M_n, M_w and M_v is ± 5%).

2.2.3. **Synthesis of AmNS-labelled lipopolysaccharide**

Lipopolysaccharide (LPS) from *Escherichia coli 0111:B4* provided by Sigma-Aldrich was purified by adding an equal volume of chloroform to the aqueous solution of LPS, then shaking for 10 minutes. After that, the aqueous layer was removed to new tube to which ethanol was added to precipitate LPS. Hence, pure LPS was labelled with 4-amino naphthalene-1-sulfonic acid (AmNS) with applying the modified procedure described elsewhere[44].Lipopolysaccharide (LPS) (4.14g) was dissolved in 80 ml of deionised water, cooled to 0 ^{o}C and allow to react with 18mg of N-(3-dimethylaminopropyl)-N'-ethylcarbodiimide and 11 mg of N-hydroxy succinimide for 30 min. Then 25 mg of 4-amino naphthalene sulfonic acid was added and the resulting mixture was stirred overnight. The product was washed with dichloromethane, and the aqueous layer was evaporated to dryness at reduced pressure to yield the fluorescently labelled LPS.

LPS (Yield ~90 %) The^{1}H NMR (400 MHz, DEUTERIUM OXIDE) spectrum of pure LPS is shown below, it was in good agreement with that in the literature[66]. FTIR spectra of (Solid): 3330 (OH), 2930 (CH), 1650 (CO), 1085 (CN), 1224 (CC). GPC(RI): M_n = 140884g/mol, M_w = 287802 g/mol, M_v = 258552 g/mol . Viscometry: M_v = 266420 g/mol. (The estimated accuracy of M_n, M_w and M_v is ± 5%).

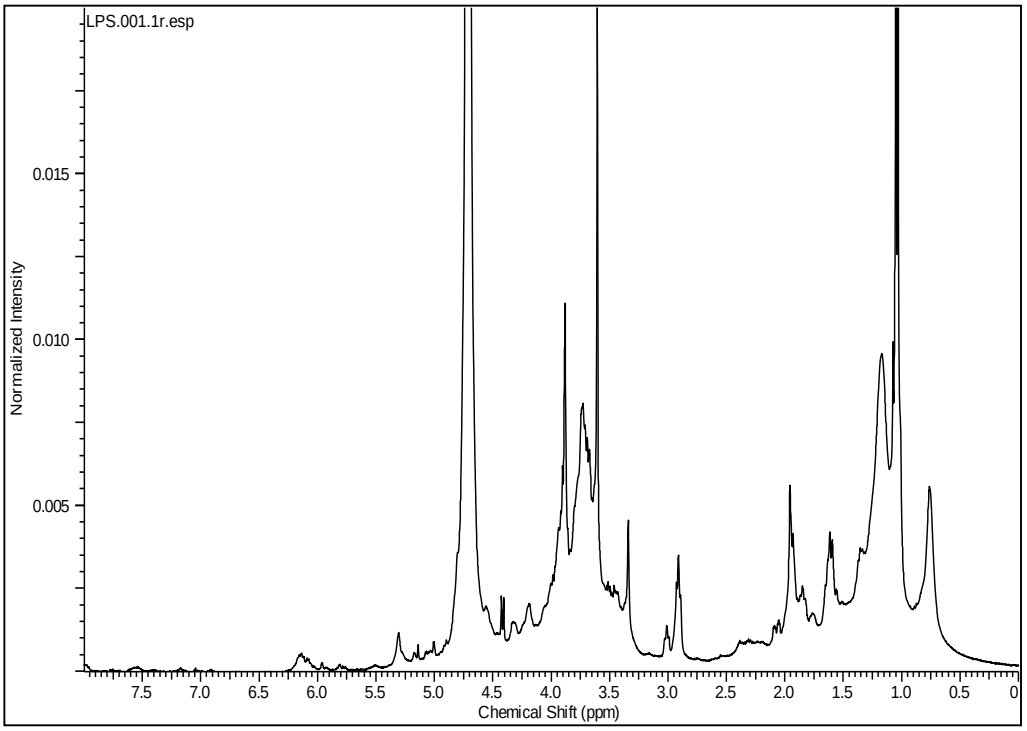

Figure 2.4 H^{1} NMR spectra of pure LPS.

AmNS-LPS (Yield ~90 %) ^{1}H NMR (400 MHz, DEUTERIUM OXIDE) spectra of AmNS-LPS was impossible to differentiate from the spectra of the unlabelled LPS due to the low content of fluorophore. FTIR spectra of (Solid): were indistinguishable from the spectra of LPS due to the low loading of the fluorophore. Fluorescent label content: $(mol\%)_{AmNS}$ = 1.55 mol%. GPC (RI): M_n = 132689 g/mol, M_w = 305486 g/mol, M_v = 270145g/mol. Viscometry: M_v = 256796 g/mol. (The estimated accuracy of M_n, M_w and M_v is ± 5%).

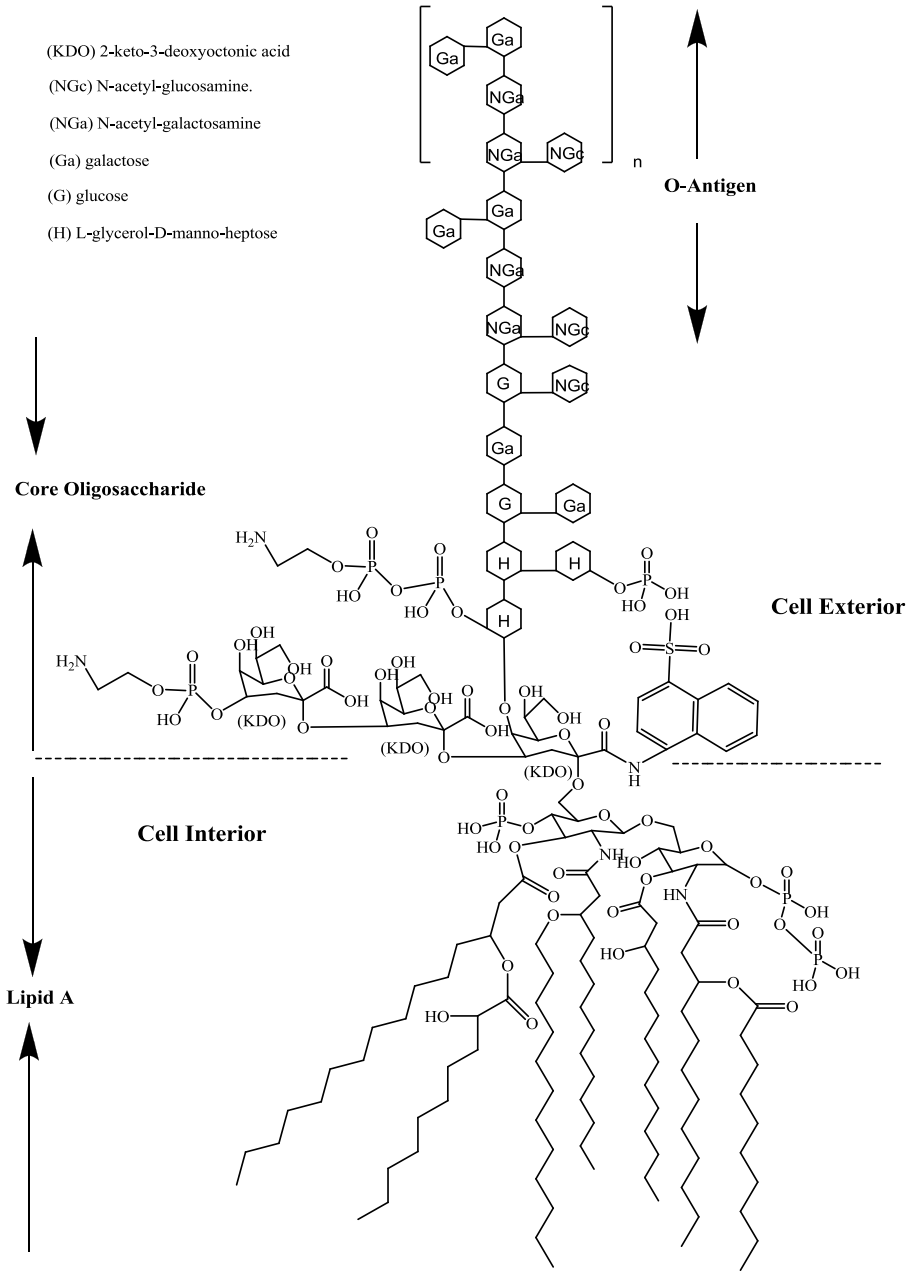

Figure 2.5 Chemical structure of AmNS-labelled LPS, LPS from E. coli O111:B4 structure as proposed by Ohno and Morrison 1989 [67].

2.3. **Purification of Polymers**

2.3.1. **Ultrafiltration**

Typically, ultrafiltration was applied to remove low molecular-weight substances. Ultrafiltration was carried out using a 300ml stirred cell (Millipore, UK) at 400 kPa nitrogen pressure with 70mm cellulose 1000 and 3000 MWCO filters. The procedure was carried out over ca. 1 hour to give a final volume of 20-

50ml. The procedure was three times repeated by addition of more solvent and the solvent was removed from the concentrate by freeze-dried.

2.3.2. **Freeze-drying**

Freeze-drying is a technique was applied to remove residual solvent from a polymer to produce a dry powder that can be safely stored. The dissolved polymer was frozen in liquid nitrogen. The solvent sublimated and was removed by vacuum, leaving a dry powder polymer.

2.4. **Characterisation Techniques**

2.4.1. **Nuclear magnetic spectroscopy (NMR)**

To characterise the monomers, synthetic model polymers and biopolymers proton nuclear magnetic resonance (^{1}H NMR) spectra were recorded on a Bruker AC250 sample changer instrument operating at 400 MHz The monomer and polymer samples were prepared in deuterated solvent (20mg/1ml). The 1D ACDlabs program was used to analyse spectrometer data.

2.4.2. **Fourier transform infrared spectroscopy (FTIR)**

FTIR spectra of polymer samples were recorded in absorbance with 10 scans using Perkin Elmer FTIR Spectrometer. All polymer samples were prepared for the measurements in the form of KBr disks.

2.4.3. **Ultraviolet spectroscopy (UV)**

To estimate the quantity of fluorescent label ($(mol\%)_{fluorophore}$) in the polymers, ultraviolet (UV) spectra were recorded with a Hitachi U-2010 spectrometer. The scan was done from 800 nm to 200nm with a scan speed of 400nm/min. The slits were set at 2nm. Fluorophores were measured at different concentrations in methanol spectroscopic grade, whereas polymer solutions at 10^{-1}wt% in deionised water were prepared and measured at room temperature.
The mol% of the fluorescent label was calculated by the following equation:

$$(mol\%)_{fluorophore} = \frac{C_{fluorophore}}{C_{fluorophore}+C_{Monomer}} x\ 100 \qquad \text{Equation 2.1}$$

Where, $C_{fluorophore}$ and $C_{Monomer}$ are the molar concentration of the fluorescent label and the non fluoro-monomer, respectively.

2.4.4. **Dynamic light scattering (DLS)**

The particle size of materials was determined using a Zeta Plus apparatus by dynamic light scattering. Particle distribution in the size distribution curves was used to determine polydispersity as a measure of homogeneity of the colloids; ionic strength was adjusted to 0.001 M using KCl solution.

2.4.5. **Gel-permeation chromatography (GPC)**

Average molecular weights of prepared macromolecules, were determined by Gel Permeation Chromatography (GPC). Poly (ethylene oxide) (PEO) and poly (ethylene glycol) (PEG) were utilized as standards. The mobile phase was a 0.1M sodium nitrate and 0.01M sodium dihydrogen phosphate aqueous solution. The mobile phase was run through two Viscotek PLGEL-Mixed B columns 30 cm long, with an internal diameter of 7.5 mm. The columns were protected by a guard column and an inline filter, and samples manually injected using a Rheodyne 200 um injection loop. Samples were prepared up to 1 mg ml^{-1} concentration and passed through a nylon syringe filter to remove any remaining undissolved particles. The samples were then injected into the machine individually for analysis. JordiGel sulphonated DVB columns were used for the chromatography, and sample's chromatogram was detected by using a HP 1047A refractive index (RI) and UV detectors.

2.4.6. **Viscometry**

Viscosity average molecular weights of prepared polymers were also calculated by viscometry technique. Values for the efflux time of polymer solutions were measured by Ostwald glass capillary viscometer thermostated at 30 ^{o}C. In addition, measured viscosity values were expressed in terms of reduced (η_{red}) and inherent (η_{inh}) as flows [68]:

$$t_r = \frac{t_p}{t_s} \qquad \text{Equation 2.2}$$

$$\rho_r = \frac{\rho_p}{\rho_s} \qquad \text{Equation 2.3}$$

$$\rho_r \; x \; t_r = \eta_r \qquad \text{Equation 2.4}$$

$$\eta_{sp} = \eta_r - 1 \qquad \text{Equation 2.5}$$

$$\eta_{red} = \frac{\eta_{sp}}{C_p} \qquad \text{Equation 2.6}$$

$$\eta_{inh} = \frac{\ln \eta_r}{C_p} \qquad \text{Equation 2.7}$$

Where, t_r, t_p, and t_s represent the relative efflux time, the efflux time of aqueous polymer solution and the measured efflux time of solvent, respectively. And ρ_r , ρ_p and ρ_s represent the relative density, the density of aqueous polymer solution and the density of solvent, respectively. Whereas, η_r is the relative viscosity of aqueous polymer solution, η_{sp} is the specific viscosity, and C_ρ is the concentration (in mass per volume) of aqueous polymer solution.

Plots of η_{sp} / C_ρ and $\ln \eta_r / C_\rho$ as a function of polymer concentration were constructed. The curves extrapolate to the intrinsic viscosity, [η], at zero concentration. The average viscosity molecular weight, $<M_v>$, was calculated according to the Mark-Houwink equation [68];

$$[\eta] = k \; x < M_v >^a \qquad \text{Equation 2.8}$$

Where, *K* and *a* are constants for a given solvent and temperature.

2.5. **Calculations**

2.5.1. **Yield calculations**

Monomer yields were calculated by a simple calculation such that the mass of end material was expressed as a relative percentage of the mass of starting material. Whereas, the polymer yields were obtained by expressing the mass of end material as a relative percentage of the monomer (or commercial biopolymer) and label(s) used in the reaction mixture. The table below shows the yields of monomers and polymers, respectively.

2.5.2. **Fluorescent label content**

A more accurate concentration (C) can be determined mathematically from the Beer-Lambert's law for the calibration curve as flows [38]:

$$A = \mathcal{E}bC$$ Equation 2.9

Where, A is the absorbance value of fluorophore, $\mathcal{E}$ is the molar absorptivity; b is the bath length of the cell, equal to 1 *cm* and C the concentration of fluorescent label in solution.

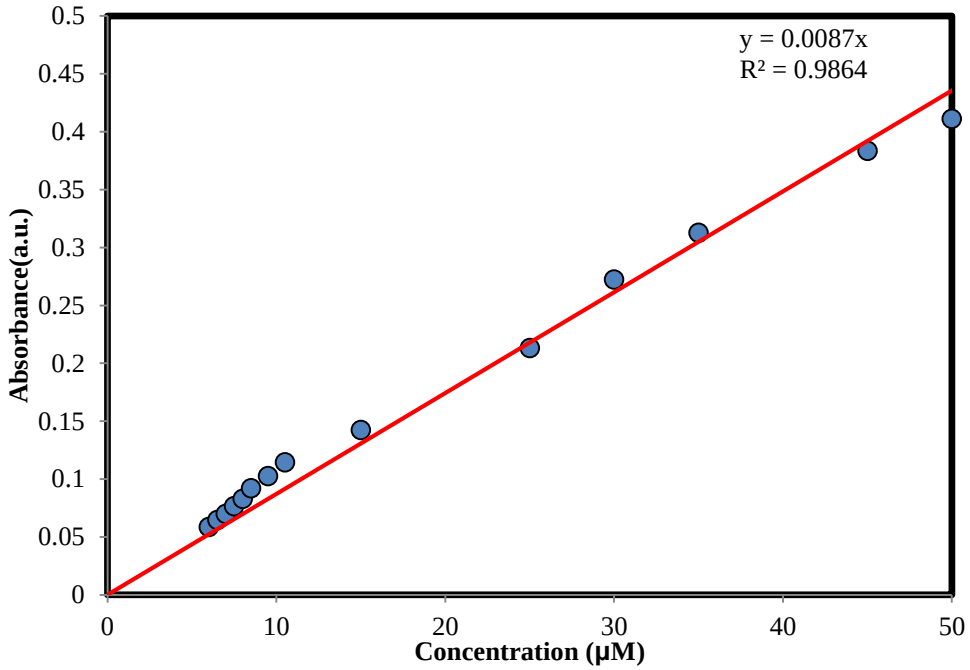

Figure 2.6 Beer-Lambert's law of acenaphthene at different molar concentration in methanol. (λ_{max} = 288 nm).

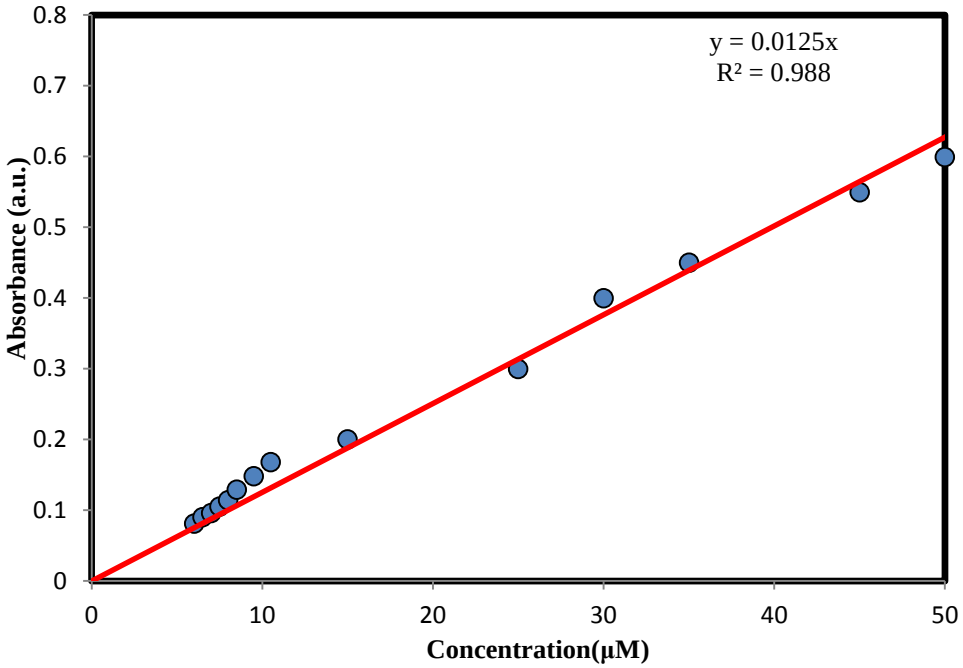

Figure 2.7 Beer-Lambert's law of methylanthracene at different molar concentration in methanol. (λ_{max} = 288 nm).

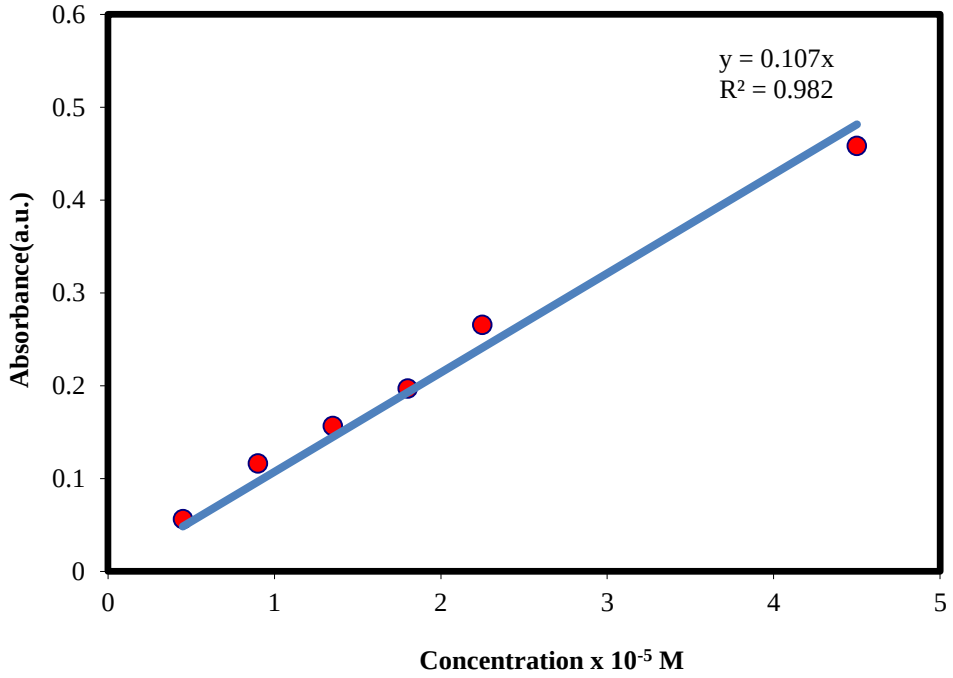

Figure 2.8 Beer-Lambert's law of AmNS at different molar concentration in water. (λ_{max} = 320 nm).

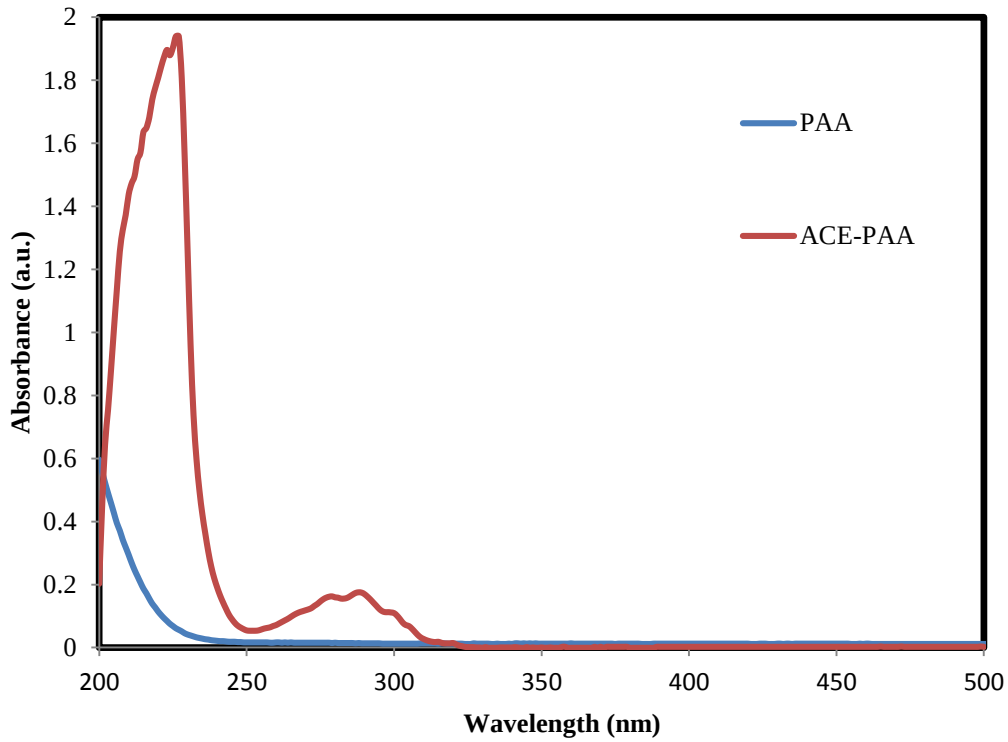

Figure 2.9 UV-Absorption spectra of 0.1 g/L ACE-labelled PAA and PAA.

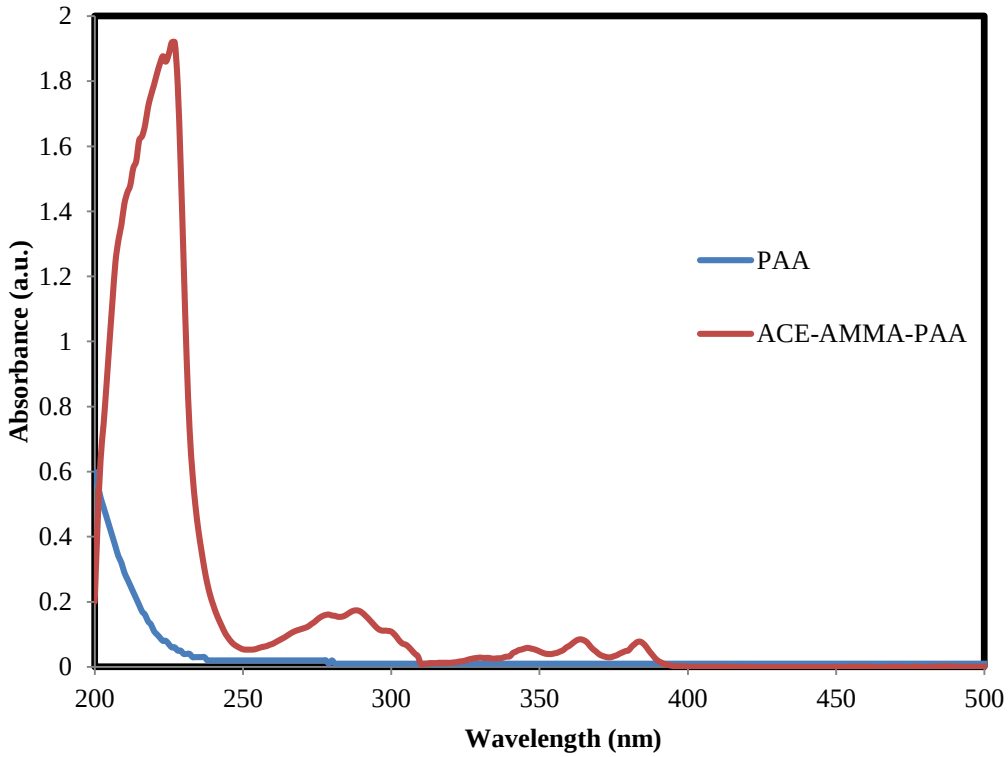

Figure 2.10 UV-Absorption spectra of 0.1 g/L ACE-AMMA-labelled PAA and PAA.

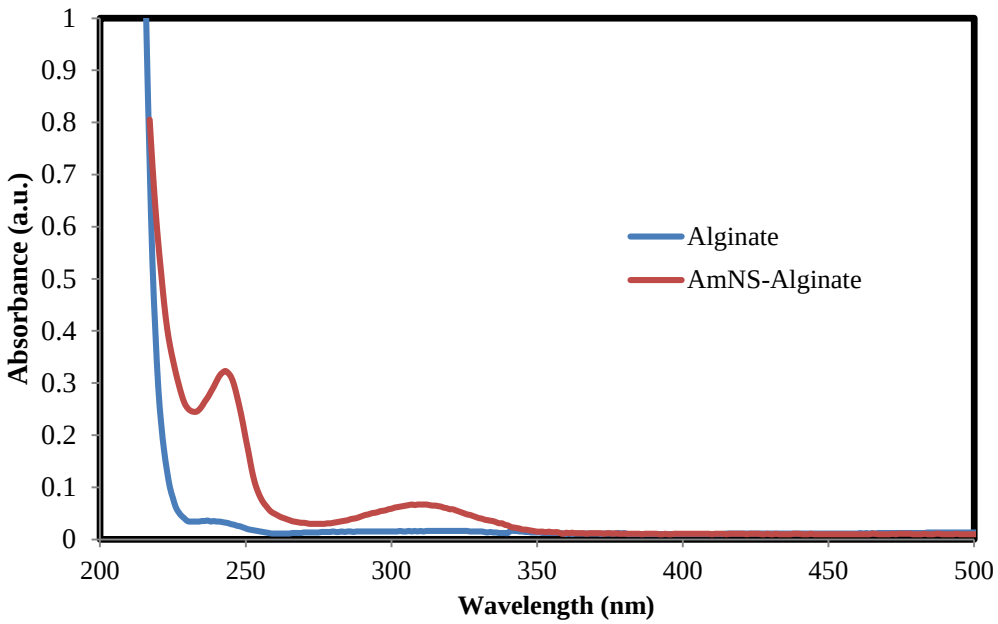

Figure 2.11 UV-Absorption spectra of 0.1 g/L AmNS-labelled alginate and alginate.

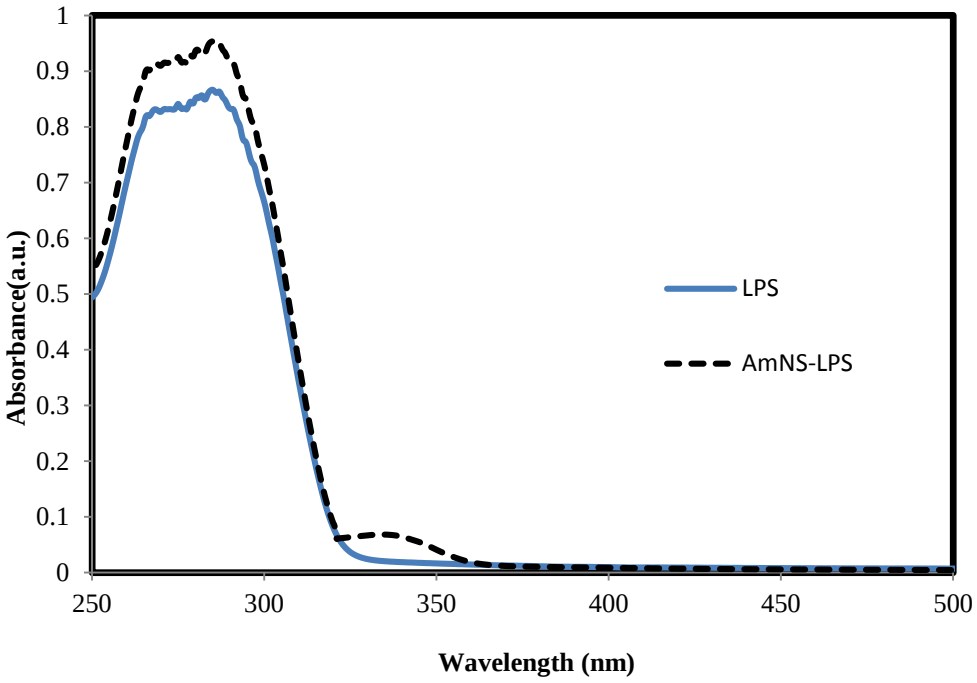

Figure 2.12 UV-Absorption spectra of 0.1 g/L AmNS-labelled LPS and LPS.

2.6. **Characteristics of the Mineral Particles**

Alumina Physical State: Crystalline white powder**.** Particle diameter: 1363.5±72.8 nm (DLS analysis)**.** Surface area: 1.11 m^2/g (Sigma-Aldrich)**.** pH: 8.5 (1 wt% in water) (pH-meter)**.** e.m.f: -94 mv (1 wt% in water) (Potentiometer)**.**

Density: 3.97 g/cm^3 (Sigma-Aldrich)**.** Molecular Formula: Al_2O_3 (Sigma-Aldrich)**.** Molecular Weight: 101.96 g/mol (Sigma-Aldrich).

Silica Physical State: colloidal, 30 wt. % suspension in water. Particle diameter: 34.7±1.4 nm (DLS analysis)**.** Surface area: 225 m^2/g (Sigma-Aldrich)**.** pH: 9.2 (1 wt% in water) (pH-meter)**.** e.m.f: -123 mv (1 wt% in water) (Potentiometer). Density: 1.21 g/cm^3 (Sigma-Aldrich). Molecular Formula: SiO_2 (Sigma-Aldrich). Molecular Weight: 60.08 g/mol (Sigma-Aldrich).

2.7. **Fluorescence Analysis**

Fluorescence steady state measurements were carried out on a Perkin-Elmer LS50 Luminescence Spectrometer or Spectrofluorometer FluoroMax®-4**.** For all ACE and AMMA labelled polymers the excitation wavelength was 290 nm and the emission range was 330-500 nm to detect both ACE and AMMA. An excitation wavelength of 370nm and emission range of 380-550 nm was applied to detect AMMA only. Excitation scans were carried out with emission wavelengths of 340 and 420nm for ACE and AMMA respectively with excitation wavelengths of 245-330 and 245-410 nm. To detect AmNS the samples were excited at 320 nm and the emission range was 360-510nm. Excitation scans from 260-380 nm were applied with 420 nm emission wavelength. Emission and excitation slits were set between 2.5 and 4nm depending on the analysed sample. Ten accumulation scans were made ten times for each reading to ensure smooth spectra. (The accuracy of intensity measurements is ±5% CPS)

Fluorescence excited state lifetime and time resolved measurements were carried out via an IBH 5000 system and Edinburgh Instruments 199 Fluorescence Spectrometers, respectively. Samples were excited at 290nm with the monochromator set to detect fluorescence at 340nm to detect ACE, while AmNS samples were excited at 370 nm with the monochromator set to detect fluorescence at 450 nm. The range was 200ns for ACE samples and 100ns for AmNS samples, and 30,000 counts were obtained for each sample in lifetime measurements, whereas 20,000 counts were obtained for time resolved measurements. A prompt was run after each sample to take into account scattered light from the source during fluorescence analysis.

To detect a measurable conformational change in the synthetic polymers chains, PAA(3), ACE-PAA(3) and ACE-AMMA-PAA(3) were selected in this work, since they all have high molecular weights compared to other prepared polymers.

Fluorescence measurements were all made using 10^{-1} or 10^{-2} wt% polymer solutions with the water purified using Millipore simfilter equipment with the water being filtered at a resistance of 18.2M Ωcm^{-1}. The pH of the polymer solutions was verified using NaOH and HCl with the pH being recorded on a pH meter.

2.8. **Potentiometric Titrations**

Potentiometric titrations were carried out according to protocol previously published [69]. The titrations of polymers were carried out at 25 °C using NaCl as the background electrolyte. The polymer solution was prepared by dissolving a known amount of polymer in degassed ultrahigh quality (UHQ) water. The 0.1 M NaOH and 0.1 M HCl solutions were prepared from NaOH and HCl using UHQ water, and the exact concentration was determined prior to the titration against a primary standard $Na_2B_4O_7.10H_2O$. The samples were dissolved in 25 mL of NaCl electrolyte (0.001, 0.1, or 1.0 M), and the solution was purged with N_2 (> 99.99%) for 1 hour to remove CO_2 before initiating titration, yielding a constant pH value. Following the degassing procedure, a positive pressure of N_2 was maintained by allowing a gentle flow of N_2 into the headspace during the titration. The sample solutions were acidified to pH ≈ 2 using 0.1 M HCl and then titrated to pH ≈ 11 using 0.1 M NaOH. A blank without desired sample was also titrated. To assess reversibility and protonation behaviour, a reverse acidimetric titration was applied following the base titration. Each experiment was done 3 times. All titrations were performed in a glass vessel with a lid as part of a Metrohm 718 STAT-Titrino instrument at 25 °C. The titrator was set to add successive acid or base every 20 seconds. The electrode was standardized on a proton concentration scale, $[H^+]$, and the slope deviation from the theoretical Nernst value was always within 1%.

2.9. **Adsorption Experiments**

2.9.1. **Adsorption of polymers on alumina**

Polymer solutions of the desired concentrations were prepared in aqueous solution and the solution pH adjusted as required. 10 ml of a polymer solution was then placed in 20 ml centrifuge tube and the necessary amount of alumina powder was added slowly while being stirred. The suspensions were then stirred or shaken overnight. After equilibration, samples were centrifuged at 5000 rpm for 40 minutes, and then the upper-level solution was taken and centrifuged at 5000 rpm for another 40 minutes. Aliquots of the supernatant were then carefully removed.

2.9.2. **Adsorption of polymers on silica**

The correct proportions of each polymer and silica solution was measured and then mixed with the pH of the sample adjusted to the required value. The mixture was shaken overnight to ensure that adsorption had reached equilibrium. The solution were then centrifuged at 50000 rpm (Beckman Coulter Optima LE-80K Ultracentrifuge) for 2 hours to sediment the solid phase from the aqueous phase. The supernatant was then carefully withdrawn from the top of the centrifuge tube.

Fluorescence steady state analysis

Fluorescence steady state analysis was run of polymer mineral solution before and after separation. The percentage of the adsorbed amount was calculated from the difference in maximum fluorescence intensity.

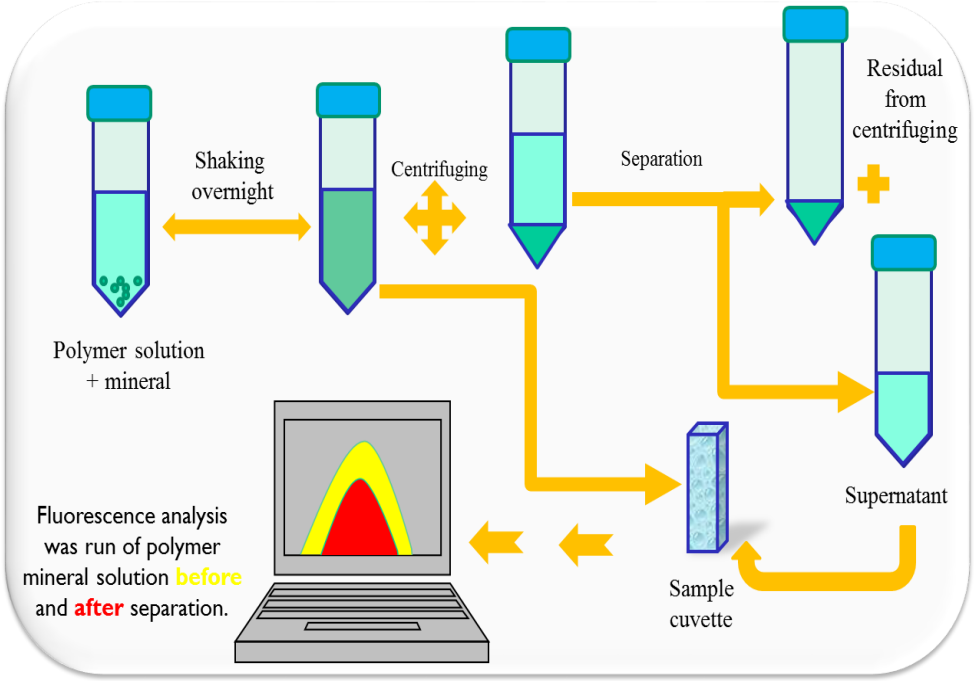

Figure 2.13 Adsorption experiment scheme.

Inductively Coupled Plasma Mass Spectrometry analysis (ICP-MS)

The inductively coupled plasma mass spectrometer (ICP-MS, Perkin Elmer Elar 400 DRC II) was used to determine the attached minerals according to the following steps:

1- The ICP-MS machine was turned on and left to warm up for about 1 hour then purged by a blank solution.
2- The machine was calibrated with standards alumina and silica at different concentration ranges.
3- The equilibrated mineral polymer solution was transferred into ultrafiltration cylinder (pore size1kDa), free mineral was passed through the filter and collected in a flask.
4- The eluent was diluted and acidified (1% v/v HNO_3) and the ICP-MS analysis was carried out.
5- The adsorbed mineral amount = the initial concentration – the free mineral.

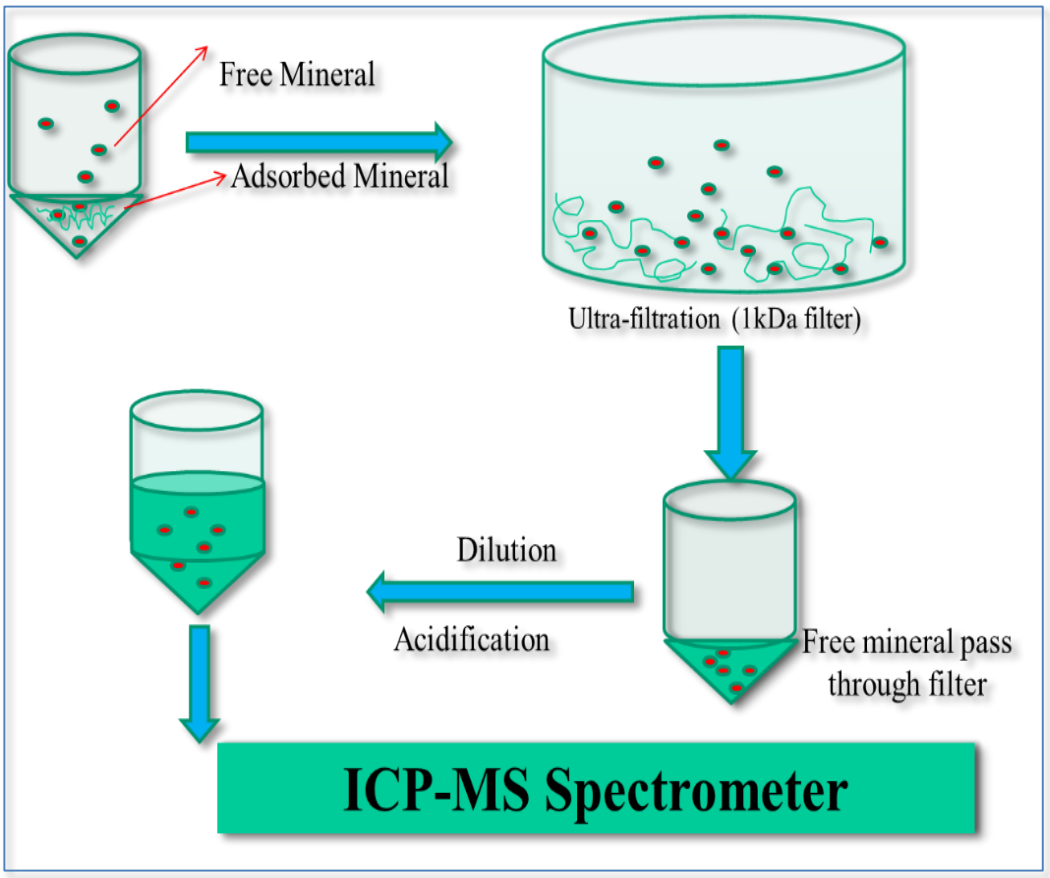

Figure 2.14 Mineral analysis scheme.

2.10. **Error bars**

The variability of data in this thesis are graphically represented by statistical significance bars, known as error bars, and are used on graphs to indicate the error, or uncertainty in a measurement [70]. In this work, error bars represent the standard deviation of the mean from three replicate experiments.

Chapter 3. CONFORMATIONAL BEHAVIOUR OF POLY (ACRYLIC ACID) IN BOTH BULK SOLUTION AND AT SOLID/LIQUID INTERFACES

3.1. **Fluorescence Spectroscopic Study of Water-Soluble Polymers**

Fluorescence techniques, such as fluorescence quenching, energy transfer, excimer formation and fluorescence anisotropy, have been shown to be powerful, versatile and sensitive tools for the study of the physical behaviour of water-soluble polymers [34, 41, 71]. Fluorescence time-resolved anisotropy measurements (TRAMS) of fluorescently labelled polymers are the most useful in the investigation of the conformational behaviour of macromolecules, as they can directly examine the segmental dynamic of polymers in both a bulk solution and at solid-liquid interface [34, 71, 72]. However, few TRAMS studies have been conducted on water-soluble polymers [71].

In this chapter, fluorescence and potentiometric techniques were applied to study the effect of pH and ionic strength on the conformational behaviour of the diluted aqueous solution, as well as the behaviour of singly and doubly labelled poly (acrylic acid) and the corresponding model compounds. The interaction of model polymers with silica and alumina was also investigated. The adsorption isotherms of minerals on poly (acrylic acid) were determined by the inductively coupled plasma mass-spectroscopy (ICP-MS) technique.

3.2. **Conformational Behaviour of Poly (acrylic acid) at Solid/Liquid Interfaces**

Before studying the effect of surrounding conditions, such as pH on the behaviour of poly (acrylic acid) conformations in both bulk solution and at the solid/liquid interface, the free fluorophore response to external stimuli was firstly investigated to prove that any change in the fluorescent behaviour was due to the polymer chain response.

3.3. **Fluorescent Behaviour of Acenaphthene as a Function of pH**

In this work, acenaphthene (ACEN) (Figure 3.1) was selected as a typical model molecule for acenaphthylene (ACE) (Figure 1.12) (Chapter 1), because of the absence of the double bond in ACEN structure, making it mimics electronic structure to the covalently attached ACE in PAA (Table 2.2 Chapter 2).

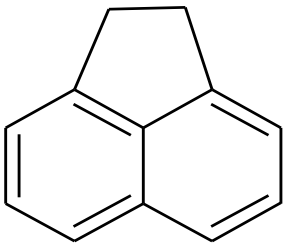

Figure 3.1 Chemical structure of acenaphthene (ACEN).

3.3.1. **Fluorescence steady state spectra of acenaphthene as a function of pH**

Figure 3.2 displays the fluorescence emission spectra of 10^{-5} M acenaphthene dissolved in deionized water at pH values 3, 7 and 11, respectively. All samples were excited at 290 nm at fixed bandwidth. It can be observed that all the fluorescence emission spectra displayed the well-known structured band of the ACEN fluorophore [73], giving a maximum emission at about 333 nm. The spectra also showed that the location and intensity of maximum emission does not depend on the pH value of the solution. This result confirms that any change in fluorescence intensity in the following experiments will not be due to the fluorophore itself.

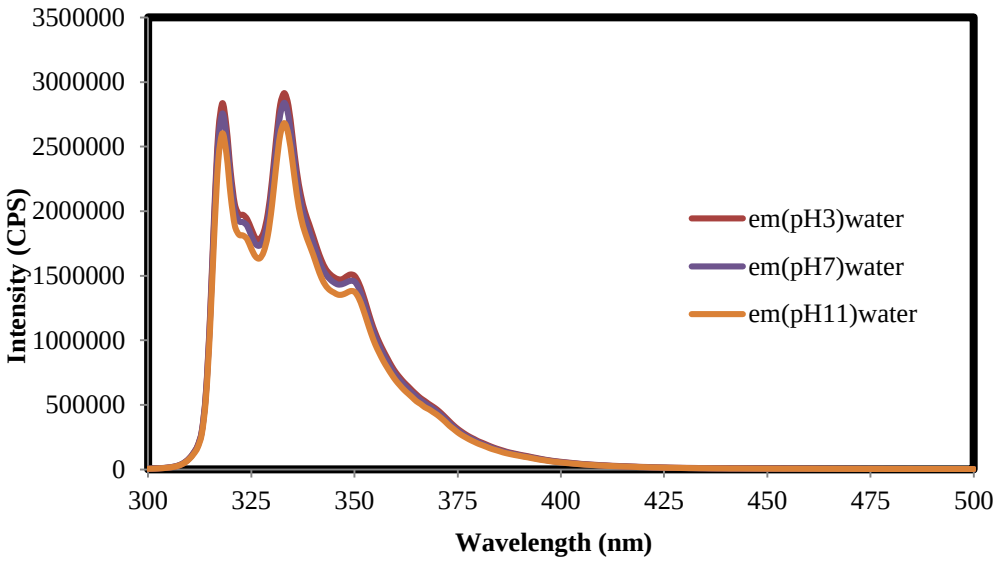

Figure 3.2 Fluorescence emission scan in a range equal to 300-500 nm at fixed excitation (λ_{ex}= 290 nm) for Acenaphthene (10^{-5} M in water) at different pH values.

3.3.2. Fluorescence exited state lifetimes of acenaphthene as a function of pH

To confirm the results, obtained by the fluorescence steady state, the fluorescence excited state life times were measured after each steady state scanning. Fluorescence lifetimes are typically independent of the fluorophore concentration so that it is more accurate technique than the fluorescence steady state [38]. Additionally, the fluorescence lifetime was measured to investigate the surrounding effect on a fluorophore; this surrounding can be varied by changing, pH, ionic strength or hydrophobicity of the solution.

Fluorescence intensity decays for 10^{-5} M ACEN in aqueous solution at different pH values are shown in Figure 3.3. The samples were excited at 290 nm and fluorescence emission was measured at 340 nm. It should be noted that the decays at pH 3, 7 and 11 are superimposed over each other. This means that the fluorescence intensity decay of ACEN is pH independent.

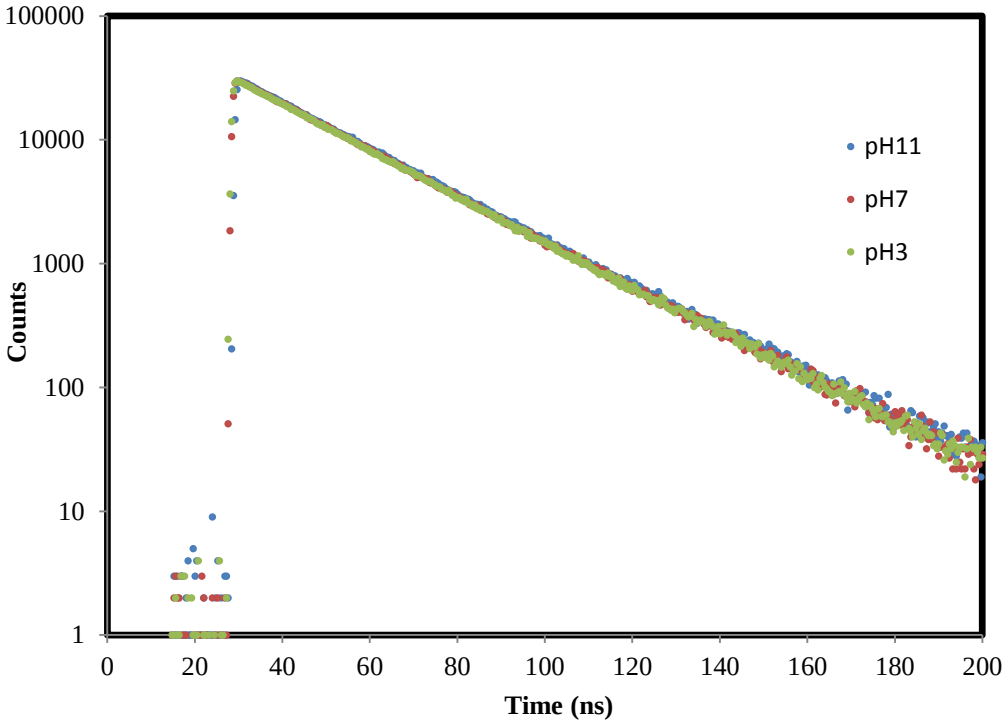

Figure 3.3 Fluorescence excited state lifetime decays of 10^{-5} M acenaphthene in water at different pH values.

To determine the excited state lifetime values (τ_f) (Table 3.1), the decays were fitted by using a single exponential model decay function as follows:

$$I(t) = A + B\ exp^{-t/\tau_f} \qquad \text{Equation 3.1}$$

Where, $I(t)$ is fluorescence intensity as a function in time, A and B are constants, and t is time in nanoseconds. The data was statistically tested for its goodness of fit by the chi-squared (χ^2) value. Approaching the value of one indicates a reliable analysis.

From Table 3.1, it can be observed that there is no important difference in the value of lifetime when the pH was changed. This means that the ACEN photophysical behaviour is not affected by changing the acidity of the environment. Accordingly, it can be suggested that any variation in lifetime values of ACE-labelled polymer versus the pH of the solution is not because of the fluorophore itself, this will be discussed further in section 3.6.

Table 3.1 Fluorescence excited state lifetime values of 10^{-5} M acenaphthene in water at different pH values.

pH	τ_f (ns)	χ^2
3	23.06 ± 0.06	1.0
7	23.08 ± 0.07	1.1
11	23.24 ± 0.11	1.2

3.3.3. **Fluorescence Time-resolved anisotropy measurements (TRAMS) of acenaphthene as a function of pH**

As previously mentioned (Section 1.9.2. in Chapter 1), the TRAMS technique is utilised to directly measure the dynamic of fluorescently labelled polymers by measuring the correlation time values, using Equation 1.21 or Equation 1.22. However, the anisotropy decays of 10^{-5} M ACEN shown in Figure 3.4 display an extremely short correlation time to reach up to 0.10 ns at pH 3, 7 and 11. Moreover, all decays are superimposable on each other; this supposes that the anisotropy of free fluorophore is not affected by the pH change.

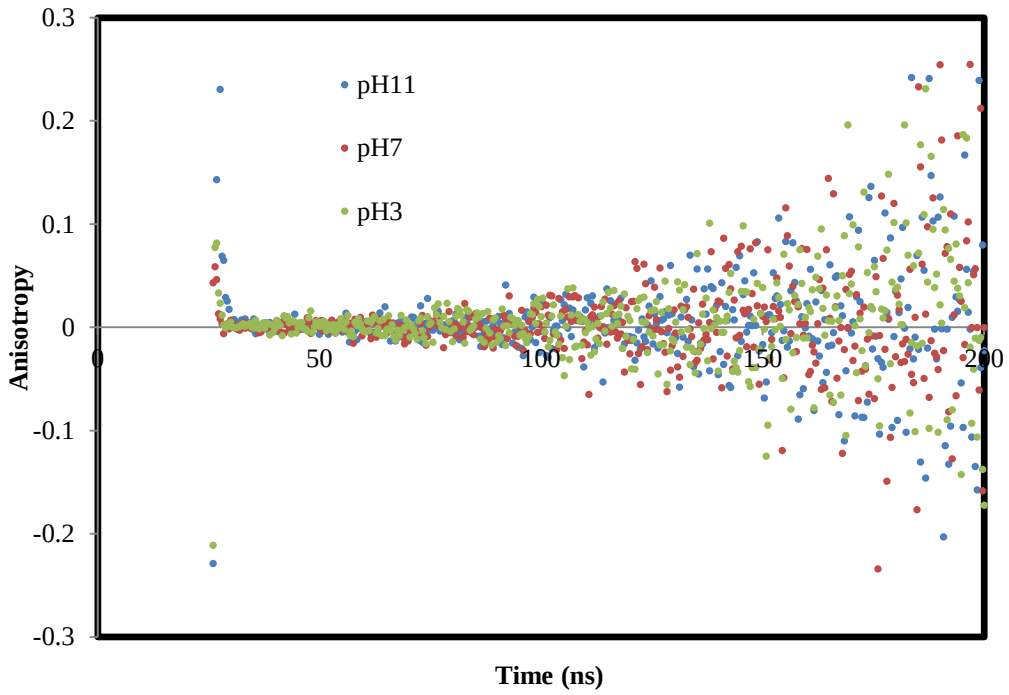

Figure 3.4 Anisotropy decays of 10^{-5} M acenaphthene in water at different pH values.

3.4. **Fluorescent Behaviour of Acenaphthene in the Presence of Silica as a Function of pH**

To prove that the free fluorophore does not interfere with the solid and that any attachment between the polymer and mineral is due to the polymer, the fluorescence analysis of ACEN, dispersed in colloidal silica solution, was carried out.

3.4.1. **Fluorescence steady state spectra of acenaphthene in the presence silica as a function of pH**

Fluorescence steady-state spectra were recorded of 10^{-5} M ACEN in 1 wt% silica solution at pH values 3, 7 and 11 before and after separation of the solid components by centrifugation, are shown in Figure 3.5 to Figure 3.7, respectively. The occurrence of adsorption was derived from the difference in maximum fluorescence intensity before and after centrifugation.

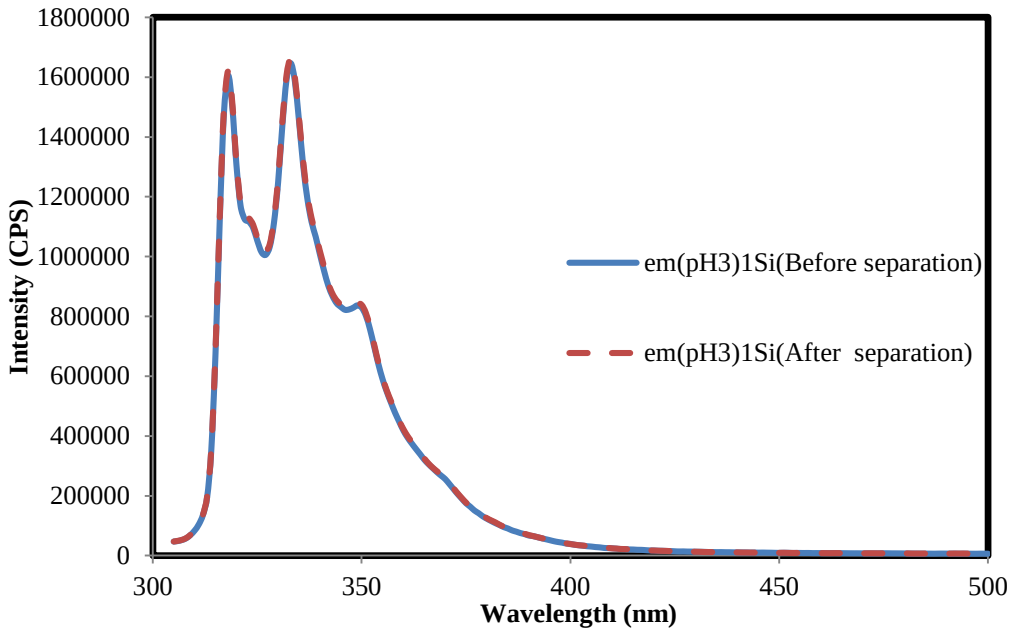

Figure 3.5 Fluorescence emission scan in a range equal to 300-500 nm at fixed excitation (λ_{ex}= 290 nm) for acenaphthene (10^{-5} M in 1wt% silica), before and after separation at pH 3.

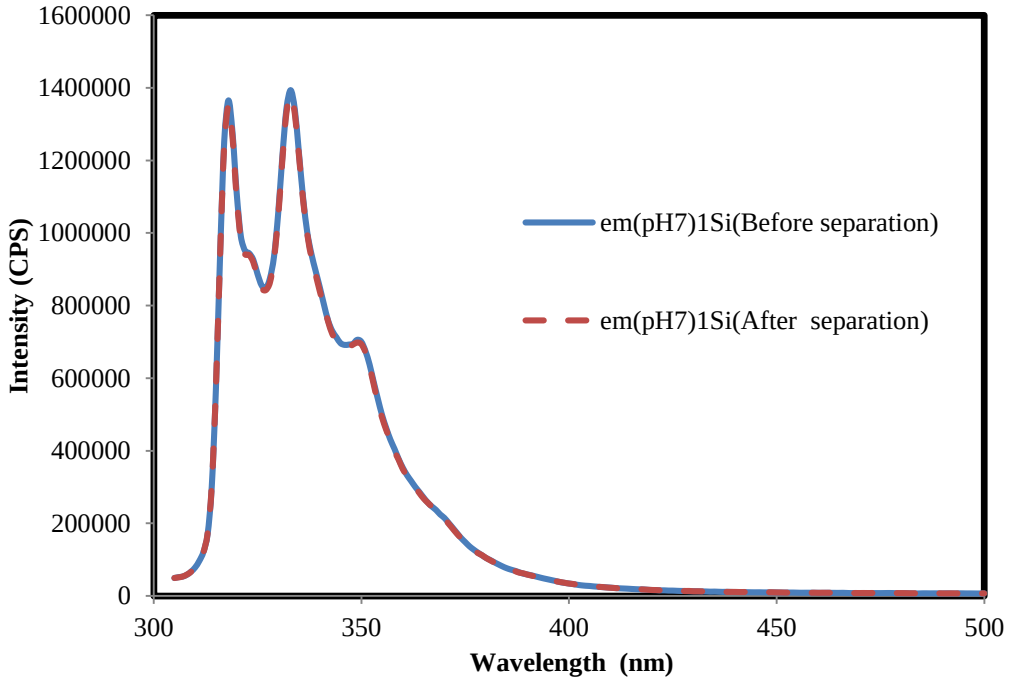

Figure 3.6 Fluorescence emission scan in a range equal to 300-500 nm at fixed excitation (λ_{ex}= 290 nm) for acenaphthene (10^{-5} M in 1wt% silica), before and after separation at pH 7.

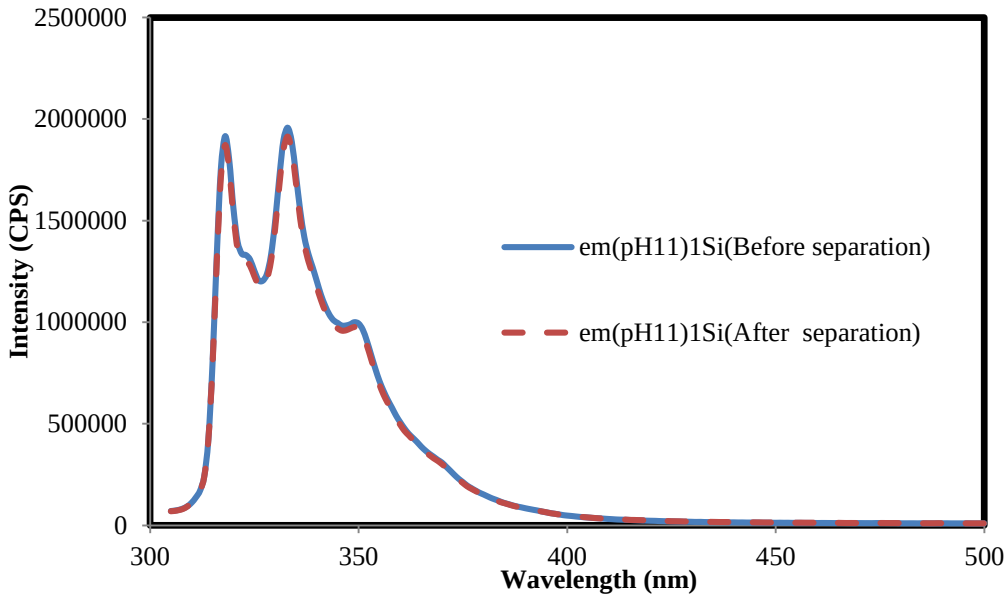

Figure 3.7 Fluorescence emission scan in a range equal to 300-500 nm at fixed excitation (λ_{ex}= 290 nm) for acenaphthene (10^{-5} M in 1wt% silica), before and after separation at pH 11.

At all pH values, it was found that the fluorescence intensity before separation (blue spectra) was indistinguishable from that after separation (red spectra). This similarity in the intensity of fluorescence proves that the free fluorophore remains dispersed in the bulk solution and is not adsorbed into the surface of silica. This would indicate that in the case of finding a difference in fluorescence intensities in the polymer adsorption experiment, attachment occurs as a result of the interaction between the polymer and the mineral.

3.4.2. **Fluorescence time-resolved anisotropy measurements (TRAMS) of acenaphthene in the presence of silica as a function of pH**

The anisotropy decays of ACEN in silica, represented in Figure 3.8, confirm that the free fluorophore is not absorbed into the mineral surface. This can be noted from the duration of fluorescence anisotropy decays, which are similar to that of ACEN in water at pH values 3, 7 and 11, see Figure 3.4. Moreover, an increase in the correlation time should occur in case of ACEN attaching to silica, but this was not observed from the anisotropy analysis of ACEN in silica.

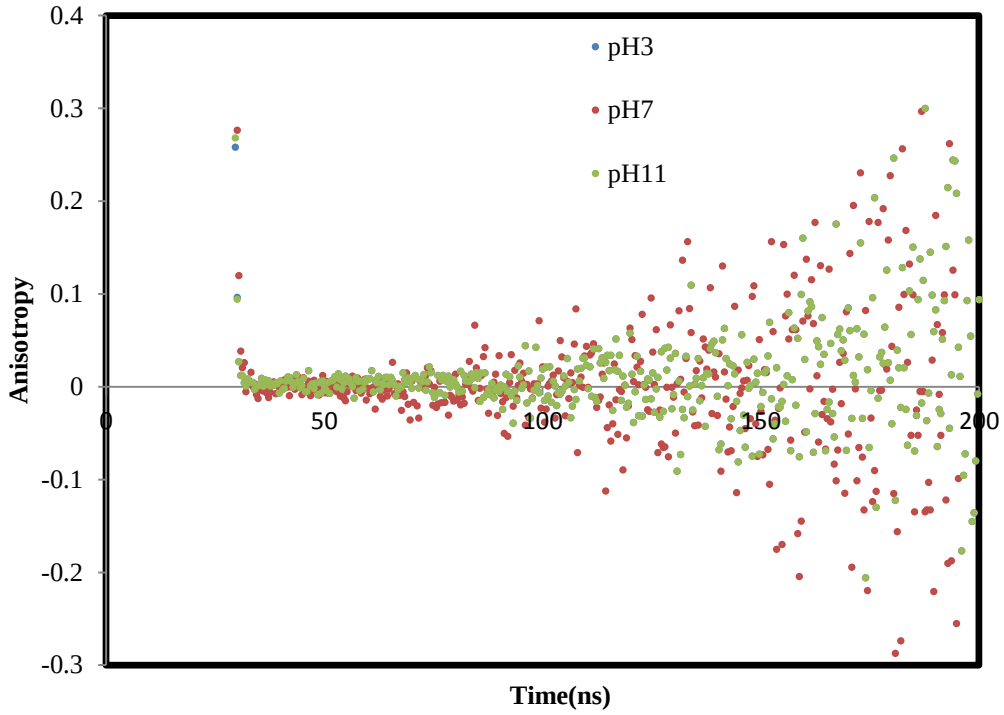

Figure 3.8 Anisotropy decays of 10^{-5} M acenaphthene in 1wt% Silica at different pH values.

3.5. **Fluorescent Behaviour of Acenaphthene in the Presence of Alumina as a Function of pH**

As in the previous section, the fluorescence analysis of ACEN dispersed in alumina solution was carried out to prove that no direct adsorption could happen between the free fluorophore and mineral.

3.5.1. **Fluorescence steady state spectra of acenaphthene in the presence of alumina as a function of pH**

Figure 3.9 to Figure 3.11 display the fluorescence steady-state spectra of 10^{-5} M ACEN in 1 wt% alumina solution at pH values 3, 7 and 11 before and after separation, respectively.

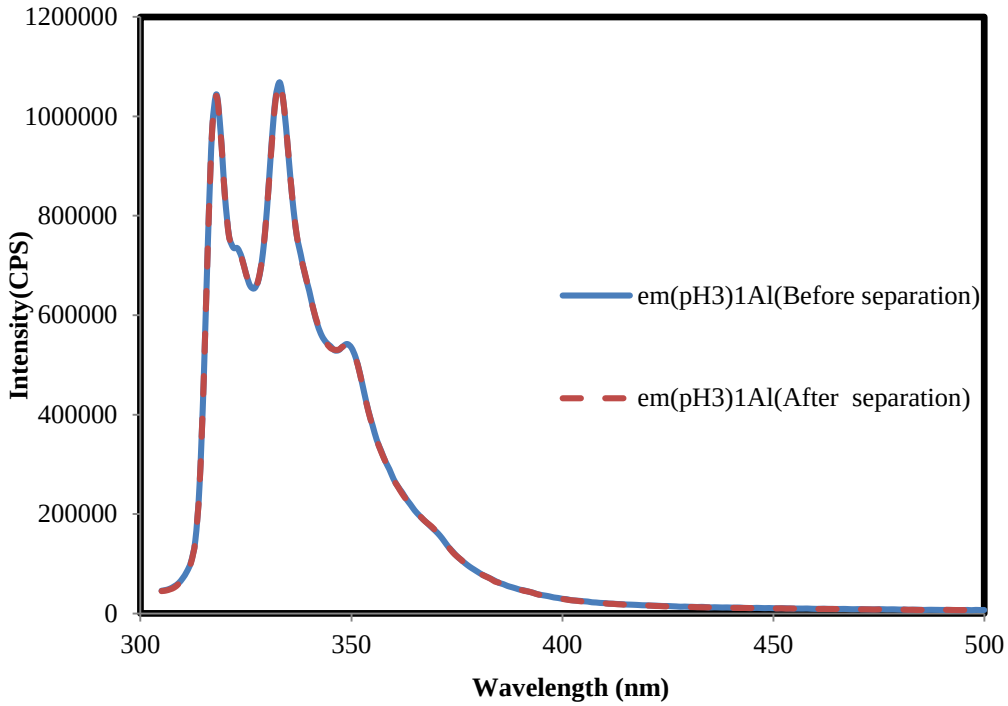

Figure 3.9 Fluorescence emission scan in a range equal to 300-500 nm at fixed excitation (λ_{ex}= 290 nm) for acenaphthene (10^{-5} M in 1 wt % Alumina), before and after separation at pH3.

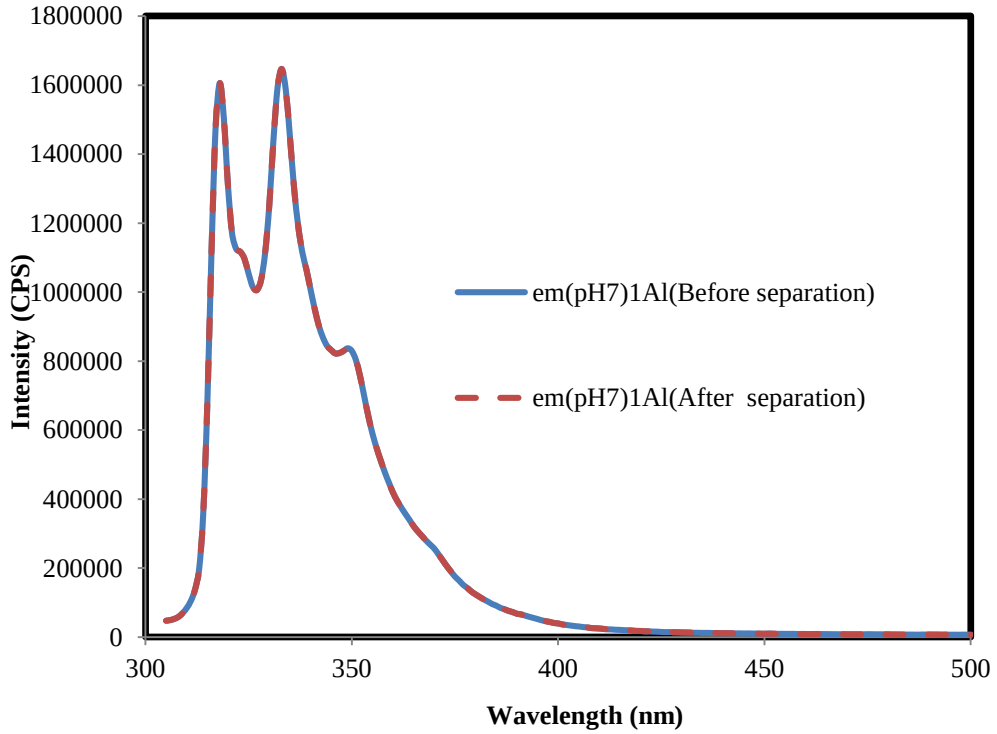

Figure 3.10 Fluorescence emission scan in a range equal to 300-500 nm at fixed excitation (λ_{ex}= 290 nm) for acenaphthene (10^{-5} M in 1 wt % Alumina), before and after separation at pH7.

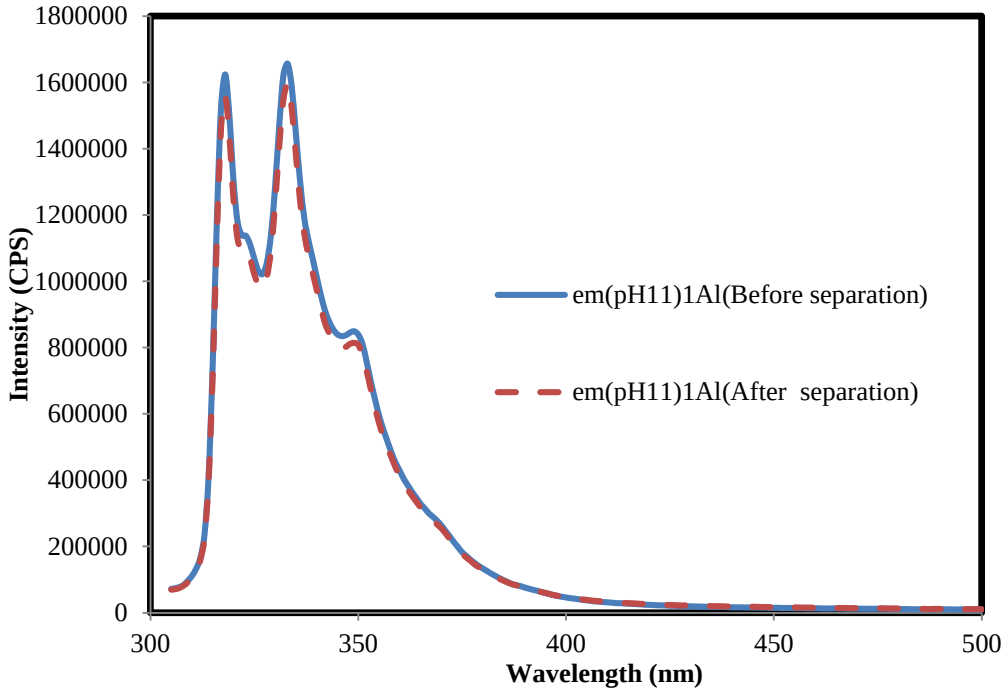

Figure 3.11 Fluorescence emission scan in a range equal to 300-500 nm at fixed excitation (λ_{ex}= 290) nm for acenaphthene (10^{-5} M in 1 wt % Alumina), before and after separation at pH11.

It can be noted that the fluorescence intensity before separation is identical to that after separation. This could be attributed to the fact that the free fluorophore remains dispersed in the bulk solution and is not adsorbed on the surface of alumina. In addition, it would be said that in polymer work, any gap in the fluorescence intensity before and after separation would point to the conclusion that attachment occurs because of the interaction between the polymer and alumina.

3.5.2. **Fluorescence Time-resolved anisotropy measurements (TRAMS) of acenaphthene in the presence of silica as a function of pH**

The anisotropy decays of acenaphthene at alumina surface, showed in Figure 3.12, prove that the free ACEN does not adsorb onto the mineral surface. This can be observed from the duration of fluorescence anisotropy decays, which are analogous to that of ACEN in water at pH 3, 7 and 11, see Figure 3.4. Furthermore, an increase in the correlation time should occur in case of ACEN attaching to alumina, but this was not derived from the anisotropy analysis of ACEN in alumina.

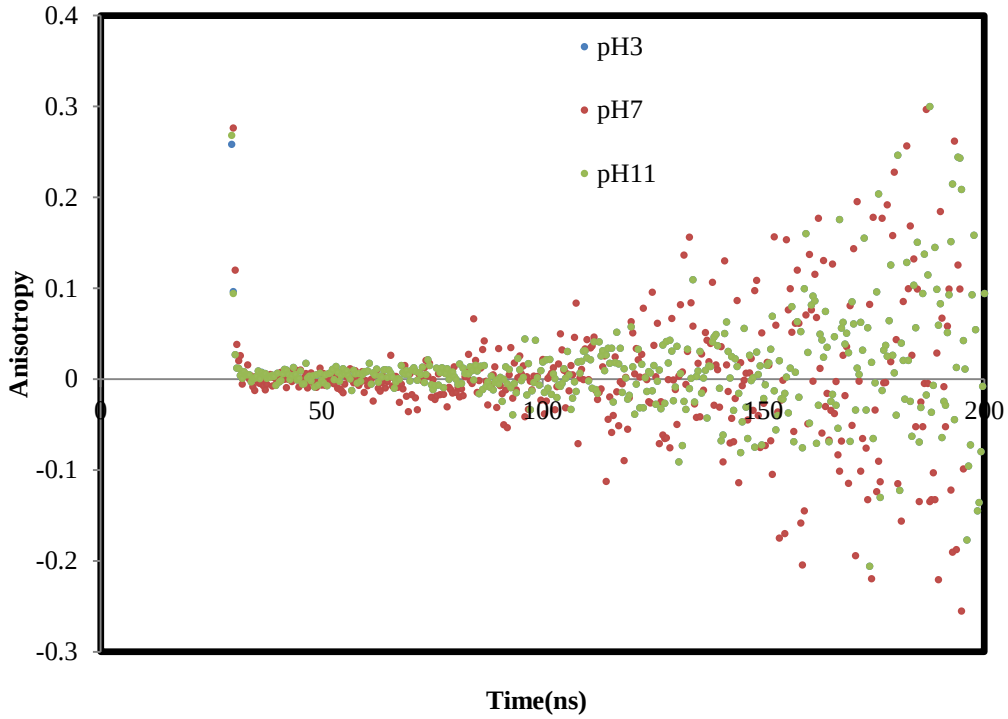

Figure 3.12 Anisotropy decays of 10^{-5} M acenaphthene in alumina at different pH values.

3.6. Conformational Behaviour of ACE- labelled PAA as a Function of pH

3.6.1. Fluorescence steady state spectra of ACE- labelled PAA as a function of pH

Figure 3.13 shows the fluorescence emission spectra of 10^{-2} wt% ACE-labelled-PAA over a pH range of 1-12. It can be distinguished that the unlabelled poly (acrylic acid) is non-fluorescent and the ACE label is responsible for that fluorescence emission. These emission spectra are well known for the acenaphthene fluorophore and characterised by a structured band, centred at ~340 nm when it was excited at 290 nm. The maximum emission peak position is independent of the pH of the polyelectrolyte solution. Moreover, no marked difference in the spectra is recorded when the pH of the solution is varied. This means that no important dependence in the fluorescence intensity of ACE label with the structural conformation of the polymer chain to which it is covalently linked.

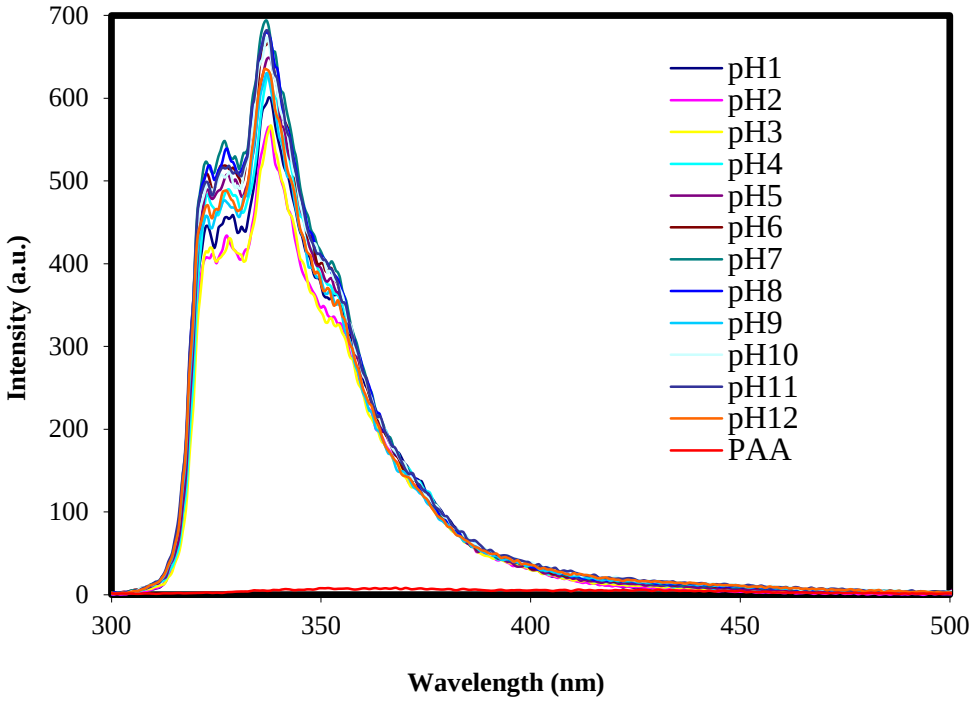

Figure 3.13 Fluorescence emission scan in a range equal to 300-500 nm at fixed excitation λ_{ex}= 290 nm for ACE- labelled PAA in water (10^{-2} wt%) at different pH values.

3.6.2. **Fluorescence exited state lifetimes of ACE- labelled PAA as a function of pH**

Figure 3.14 shows fluorescence intensity decays for 10^{-2} wt% ACE-labelled-PAA over a pH range of 1-12. From the data it can be observed that at high pH (> pH 4), the ACE-labelled polymer shows shorter duration decays compared to that at low pH. This could be attributed to the fact that polyelectrolyte chains begin to deprotonate and adopt a partly expanded form due to the repulsive electrostatic force among the ionized carboxylic moieties (COO^-) [22] (see Figure 1.6 in Chapter 1). Then the ACE labels are exposed to aqueous environment, and their lifetime decays become quenched. On the contrary, in acidic conditions such decays become longer than those in basic conditions. Since the polymer chains are partially collapsed because of the protonation of carboxylate groups of PAA [22]. This is consistent with solubilisation of ACE in the protective domains of the coiled conformation.

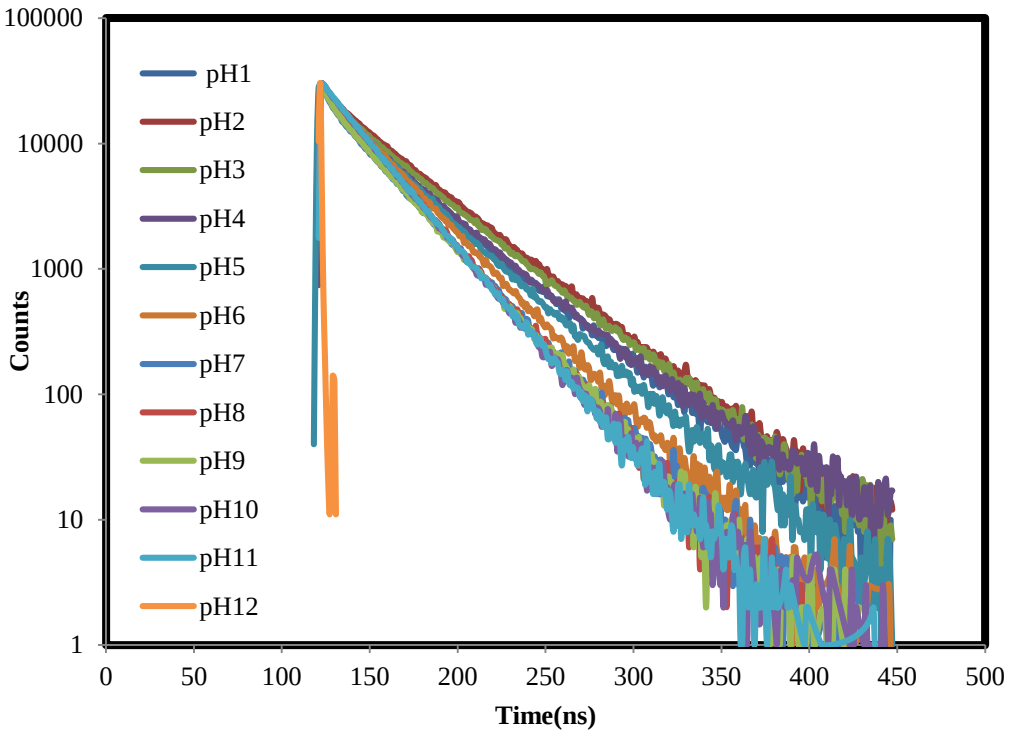

Figure 3.14 Fluorescence intensity decays as a function of pH for ACE-labelled PAA in water (10^{-2} wt %).

Fluorescence excited state analysis was carried out by fitting the raw data to mathematical functions. The statistical value (χ^2), which represents the residuals of decay, can determine the fit goodness. This means that if χ^2 is close to unity, then we have chosen a good fit. However, single exponential fit was unsatisfactory, since it generated large χ^2 values. To improve these values, a double fit was applied to all raw fluorescence intensity decays data. Single and double exponential fits can be expressed as following;

$$I(t) = A + B\ exp^{-t/\tau_f} \quad \text{(Single exponential fit)} \qquad \text{Equation 3.2}$$

$$I(t) = A + B_1\ exp^{-t/\tau_{f1}} + B_2\ exp^{-t/\tau_{f2}} \quad \text{(Double exponential fit)} \qquad \text{Equation 3.3}$$

Where A and B are constants, t is time and τ_f is fluorescence excited state lifetime. Two τ_{f1} and τ_{f2} values are generated by double exponential fit. The τ_{f1} is usually in the nanoseconds range, while τ_{f2} is in 10^{-10} seconds range. This point to the conclusion that the decay has two components, a longer decay component

followed by a relatively short decay component. Figure 3.15 shows a sample of fluorescence intensity decay with its fit and residuals data of ACE-PAA.

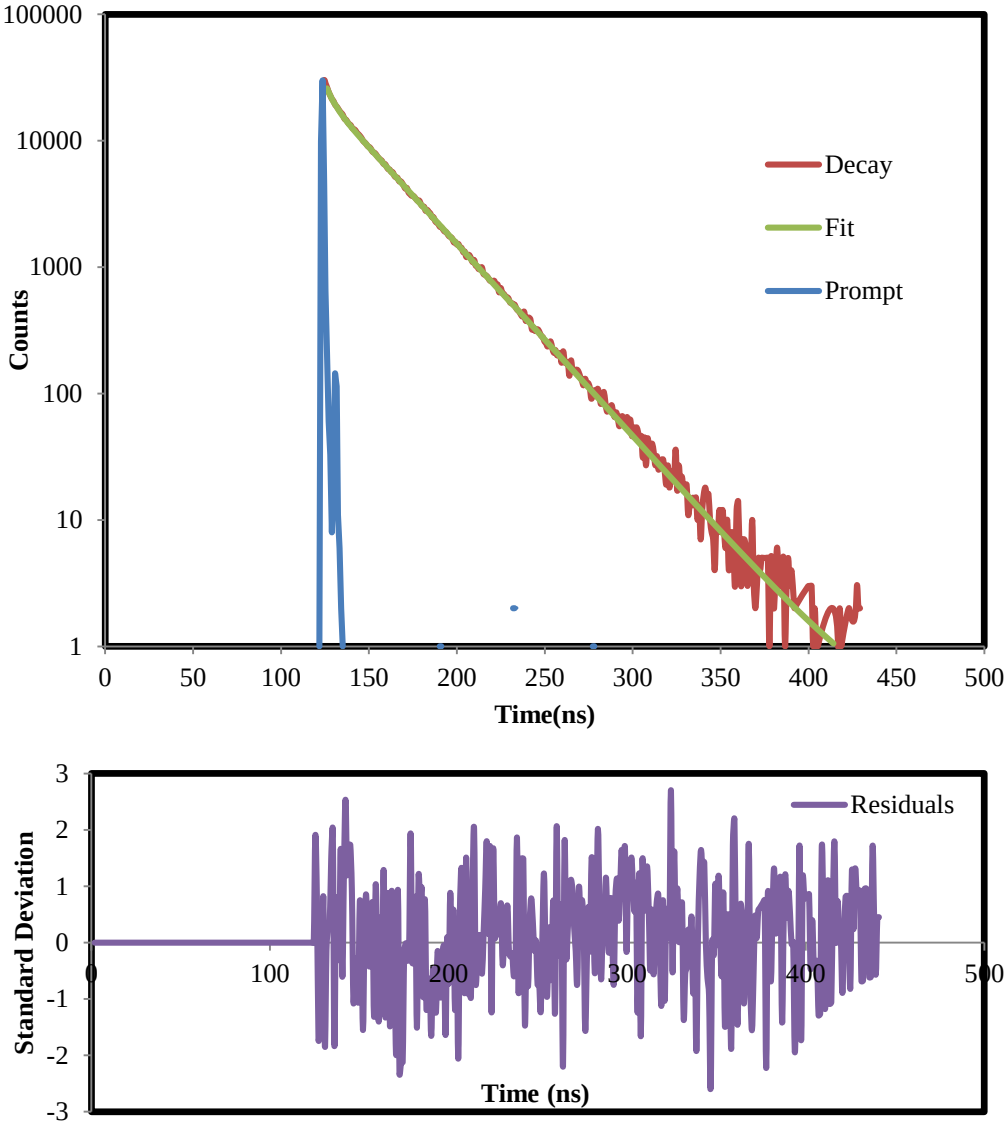

Figure 3.15 Fluorescence intensity decay of 10^{-2} wt% ACE- labelled PAA in aqueous solution at pH 7, prompt and the associated double-exponential fit with the distribution of residuals. (λ_{ex} = 295nm and λ_{em}=350nm).

The average excited state fluorescence lifetime $<\tau_f>$ was determined by means of the following equation;

$$< \tau_f >= \frac{[B_1(\tau_{f1})^2 + B_2(\tau_{f2})^2]}{[(B_1\tau_{f1}) + (B_2\tau_{f2})]} \qquad \text{Equation 3.4}$$

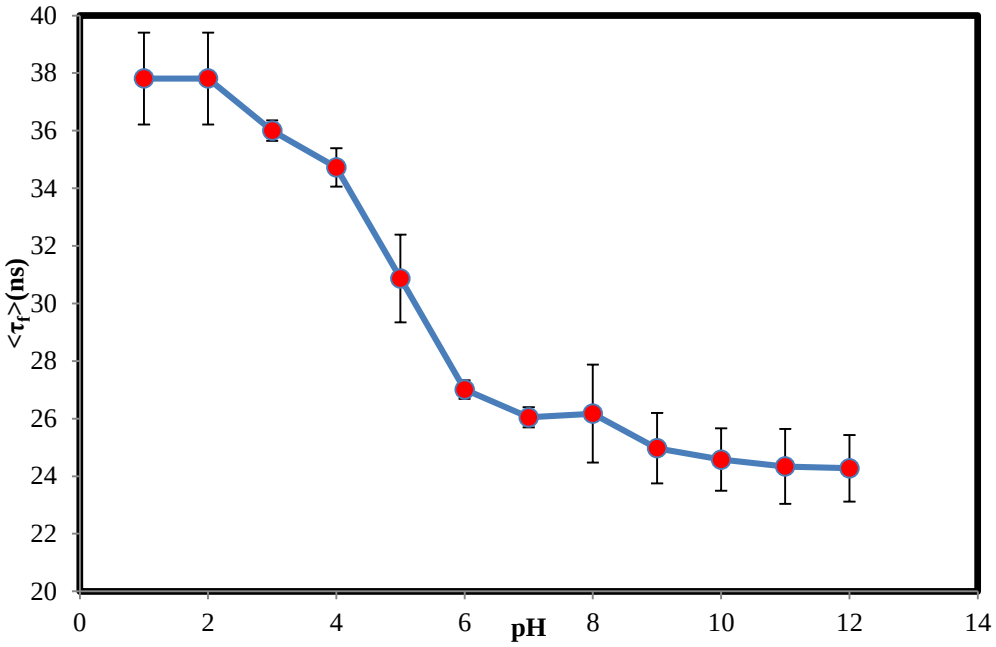

Figure 3.16 Fluorescence excited-state average lifetime, <τf>, as a function of pH for ACE- labelled PAA in water (10^{-2} wt%).

Figure 3.16 shows average ACE lifetime at emission of 350 nm from ACE-PAA as a function in pH. Average lifetime values suggest that the model polymer collapses at low pH and the ACE labels are exposed to hydrophobic environment and become more solubilised, hence their lifetime decays are enhanced (ca 37 ns). While a marked decrease in these values (ca 24 ns) is noted at higher pH. This is evidence that the polymer chains are expanded due to the electrostatic repulsion, which occurs between the carboxylate anion groups [22]. Consequently, the hydrophobic label is exposed to hydrophilic environment and becomes undissolved.

3.6.3. Fluorescence Time-resolved anisotropy measurements (TRAMS) of ACE- labelled PAA as a function of pH

In order to monitor the change in the mobility of poly (acrylic acid) chain, fluorescence time-resolved anisotropy measurements were carried out, and the correlation time of the ACE was estimated as the measure of the motion of the macromolecule chain.

For the time-resolved anisotropy work parallel and perpendicular fluorescence decays are generated after excitation with vertically polarized light analysed at 350 nm from ACE- labelled PAA in aqueous solution, as presented in Figure 3.17 and Figure 3.18. This leads to the anisotropy decay of the ACE-PAA

polymer. Selective samples are shown in Figure 3.19. Since the expanded PAA chains rotated without restrictions overall, shortly after excitation, the two polarized fluorescence decays were superimposed on each other (see Figure 3.17) and anisotropy decay quickly decays to zero (see the red decay in Figure 3.19). Once the pH decreased to 1, the motion of ACE label was hindered by the aggregation of PAA chain, and a tramline gap was generated between the two polarized decays for a slower time, as depicted in Figure 3.18. As a result, the anisotropy decay doses not reach the zero for a longer period, as shown in Figure 3.19 (the blue decay).

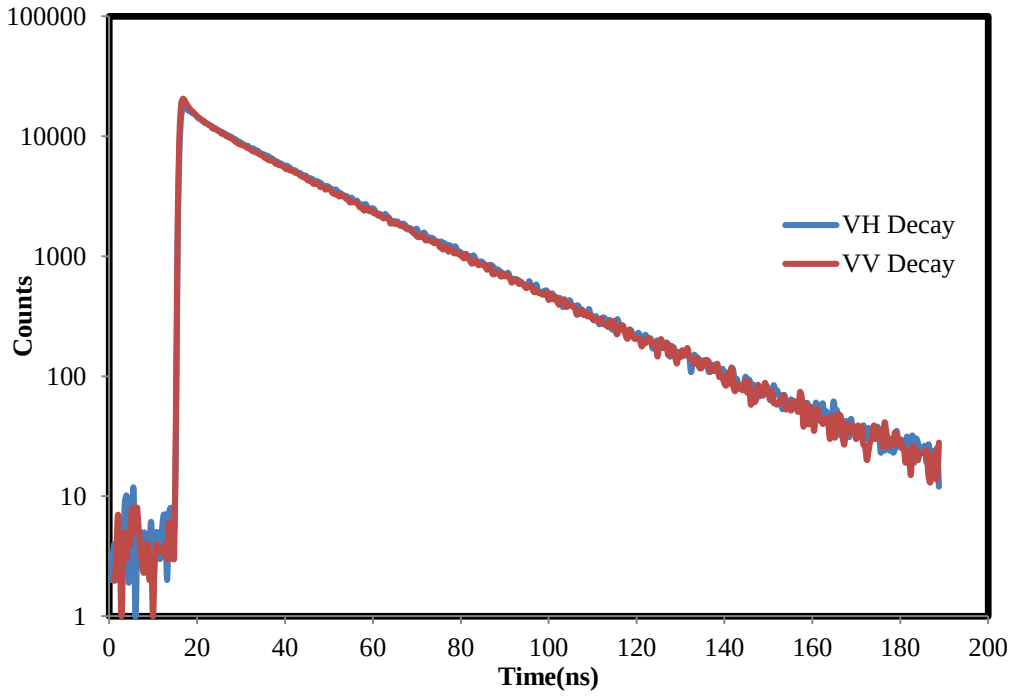

Figure 3.17 Parallel (red curve) and perpendicular (blue curve) fluorescence intensity decay curves following excitation with vertically polarized light (λ_{ex}= 295 nm) analysed at 350 nm from 10^{-2} wt% ACE- labelled PAA in aqueous solution at pH =12.

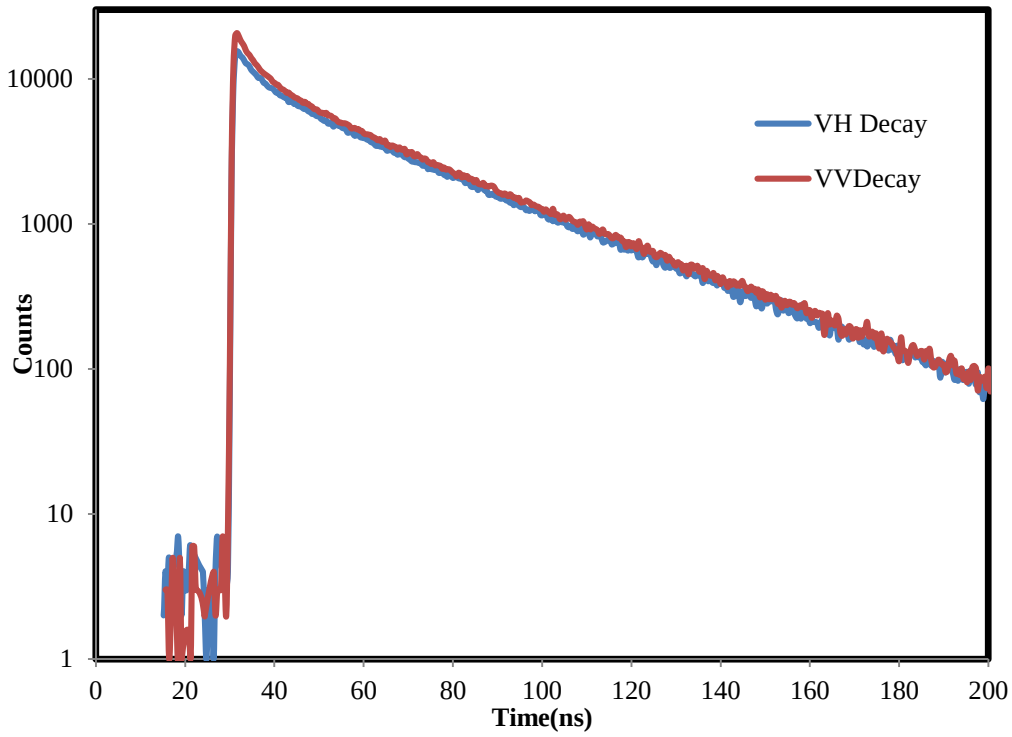

Figure 3.18 Parallel (red curve) and perpendicular (blue curve) fluorescence intensity decay curves following excitation with vertically polarized light (λ_{ex}= 295 nm) analysed at 350 nm from 10^{-2} wt% ACE- labelled PAA in aqueous solution at pH = 1.

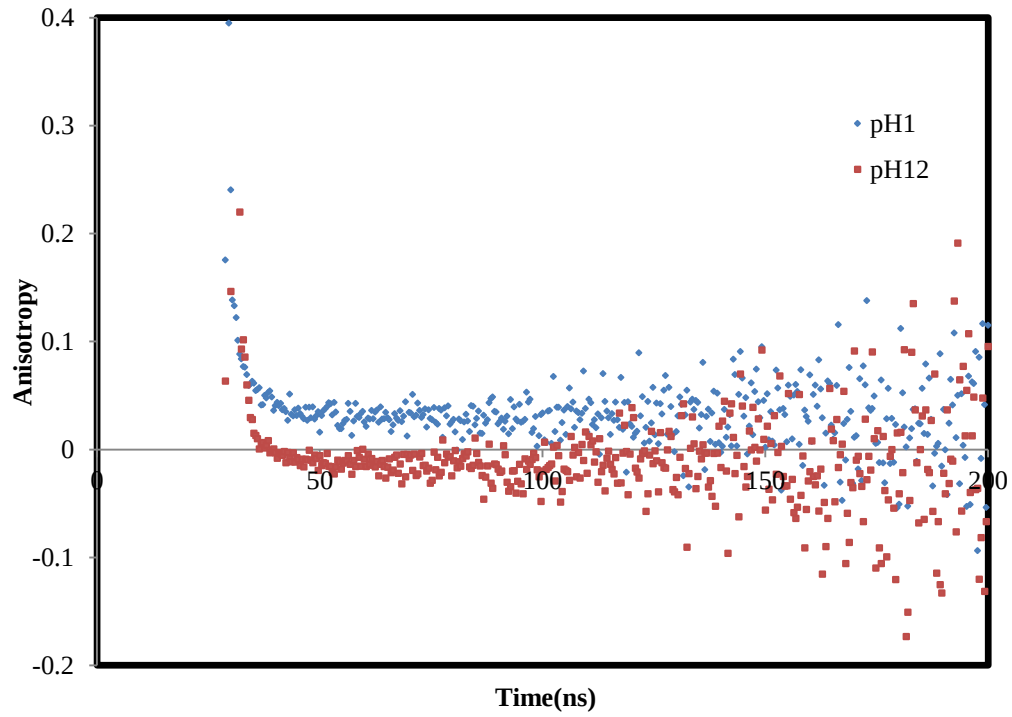

Figure 3.19 Fluorescence time-resolved anisotropy decays of 10^{-2} wt % ACE-labelled PAA in aqueous solution at pH 1(blue curve) and pH12 (red curve). (λ_{ex} =295nm and λ_{em}=350nm).

A direct analysis using a single exponential function was applied to fit the anisotropy decays curves (see Figure 3.20), which can reflect the polymer backbone motion. These TRAMS results reveal an obvious differentiation between the collapsed and expanded shapes of polymer.

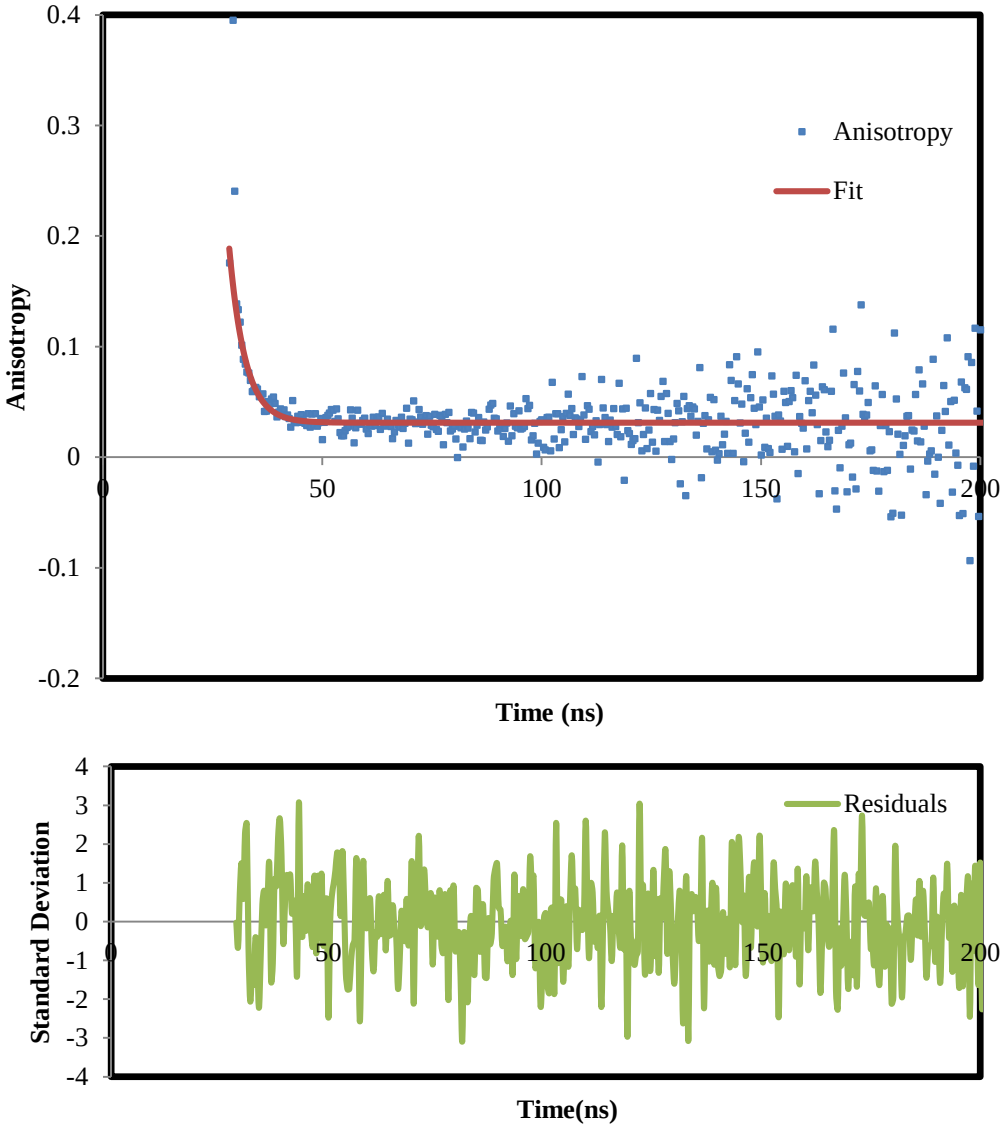

Figure 3.20 Decay of anisotropy, r(t), of 10^{-2} wt% ACE-labelled PAA in aqueous solution at pH 7, and the associated single-exponential fit with the distribution of residuals. (λ_{ex} =295nm and λ_{em}=350nm).

Figure 3.21 shows the rotational correlation time of ACE-PAA as a function of pH. A maximum increase in correlation time value is observed at pH 2 (ca 8 ns). This value decreased to a minimum (ca 1.8 ns) at pH 7. It can be assumed that an increase in correlation time values occurs because of ACE label rotation about an axis defined by the single bond, linking the label to the polymer

backbone. Additionally, it can be expected that at lower pH the polymer chain will move more slowly. This could be attributed to the collapse of the chain, in which hydrogen bonding between carboxylic groups and any remaining carboxylate ions enhances the rigidity of the polymer chain [74, 75], which leads to an increase in the rotational correlation time. On the other hand, in basic media a partially expanded shape is dominate, which makes the label rotate very fast, hence a short correlation time is expected. There is consistent agreement in the literature that the PAA chain undergoes a switch from a collapsed coil to an expanded chain as the pH increases [19, 25]. This behaviour is characterised by potentiometric titration for the linear PAA [26] and can also be observed using optical density (OD) measurements as a function of pH [27].

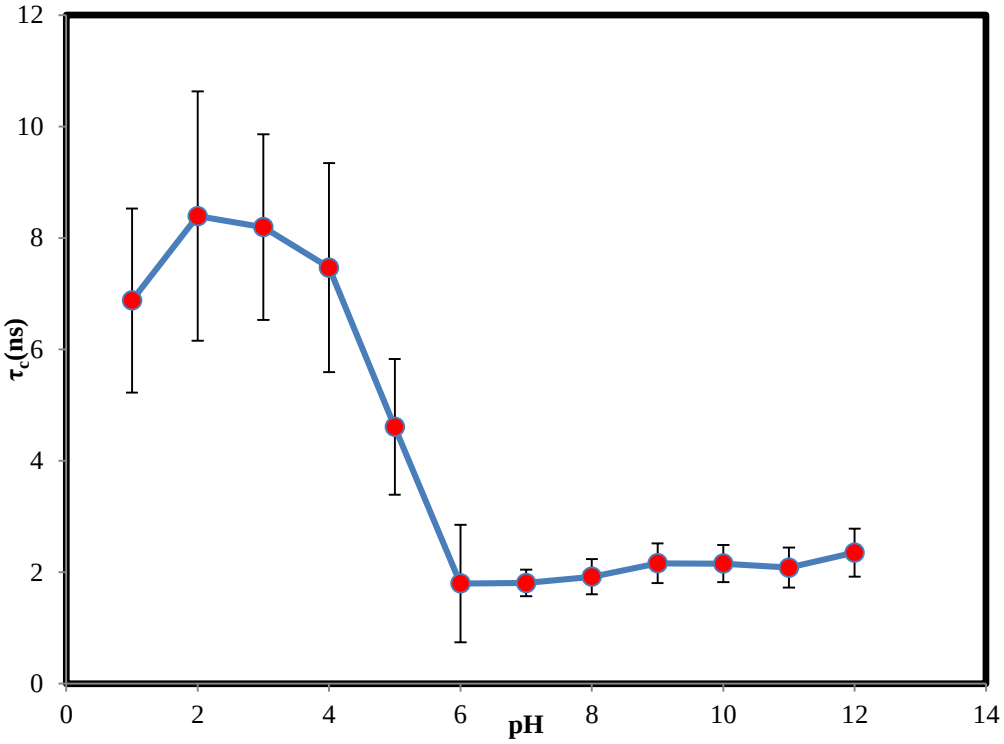

Figure 3.21 Correlation times(τ_c) for molecular segmental motion of 10^{-2} wt% ACE- labelled PAA in aqueous solution at different pH values. (λ_{ex} =295nm and λ_{em}=350nm).

3.7. **Conformational Behaviour of ACE-labelled PAA and Its Interaction with NaCl**

The addition of cations, mainly Na^+ and $Ca^{2+,}$ present in the natural water system, is supposed to aggregate the polyelectrolyte chain at natural pH. The effect

of salt addition (NaCl) on water solutions of the polymer was studied. The fluorescence steady-state and time resolved anisotropy data was collected for the ACE-labelled-PAA at different pH values as a function of sodium chloride concentration.

3.7.1. **Fluorescence steady state spectra of ACE-labelled PAA as a function of NaCl concentration**

The steady-state fluorescence emission plots versus the NaCl concentration at pH 3 and 9, with NaCl concentration ranging from 1 M to 5 M (the solubility limit of NaCl in water), are shown in Figure 3.22 and Figure 3.23, respectively. The fluorescence emission spectra of aqueous ACE-labelled-PAA remain unchanged over the all NaCl concentration range at pH3 (Figure 3.22). On the other hand, the addition of salt induces a slight increase in the fluorescence intensity at pH 9 (Figure 3.23). The observation suggests that the intensification in the fluorescence spectra for high NaCl concentrations results from the collapse of the PAA chain. Possibly, the anionic carboxylate groups of PAA with its expanded chain are neutralized by Na^+ cations [75]. The collapse of the polymer chain creates pockets of the macromolecule that entrap the ACE label, resulting in a localised hydrophobic environment. This may result then in an increasing of the fluorescent intensity of the ACE fluorophore. Possible conformation models for the PAA structure under influence the sodium chloride salt is depicted in Figure 3.28.

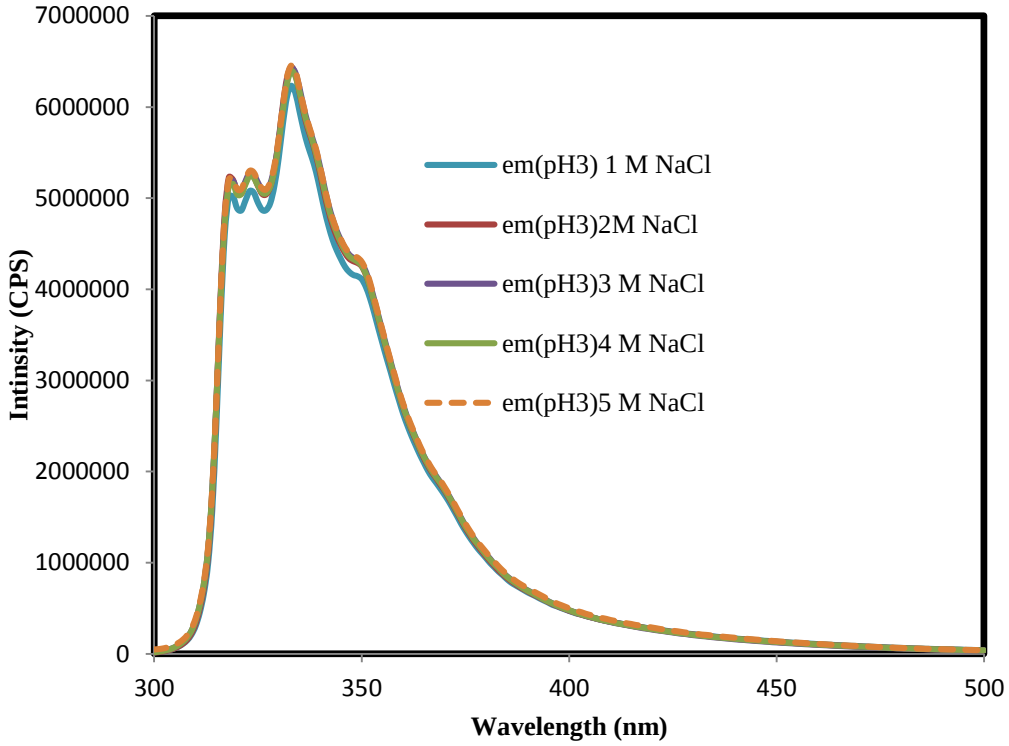

Figure 3.22 Steady state fluorescence emission spectra of aqueous ACE-labelled PAA (10^{-2} wt %) as a function of NaCl concentration at pH3. (λ_{ex}= 290 nm and λ_{em}= 340nm).

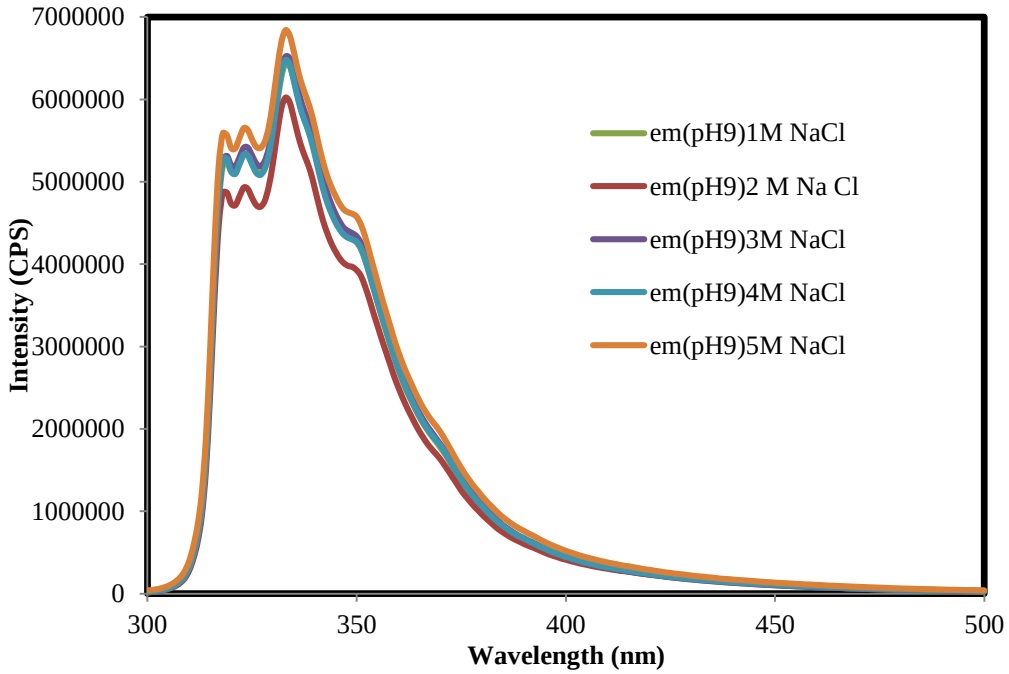

Figure 3.23 Steady state fluorescence emission spectra of aqueous ACE-labelled PAA (10^{-2} wt %) as a function of NaCl concentration at pH9. (λ_{ex}= 290 nm and λ_{em}= 340nm).

3.7.2. **Fluorescence time-resolved anisotropy measurements (TRAMS) of ACE-labelled PAA as a function of NaCl concentration**

The interaction of sodium ions with the carboxylate anions groups of poly (acrylic acid) was also investigated by measuring the correlation times as a function in NaCl concentration at pH 3 and 9, respectively, see Figure 3.24. A marked increase of correlation times (ca. 134 ns) with increasing concentration of NaCl was recorded at pH 9, whereas a slight increase was noted at pH 3. However, over the entire concentration range the rate of increment in these values at pH 9 is more than in those at pH 3. The noticeable increase can be attributed to the interaction, which occurs between Na^+ ions and COO^- of PAA [75]. This interaction screens the carboxylate groups charge and leads to the collapse of the polyelectrolyte chain, which in turn inhibits the motion of the ACE-PAA chain. This in agreement with the static and dynamic light scattering study [76], which was applied to characterise a variety of poly (acrylic acid) samples in dilute aqueous solutions with added NaCl. It was found that an increase of the NaCl concentration caused in a decrease of hydrodynamic radius of PAA chain.

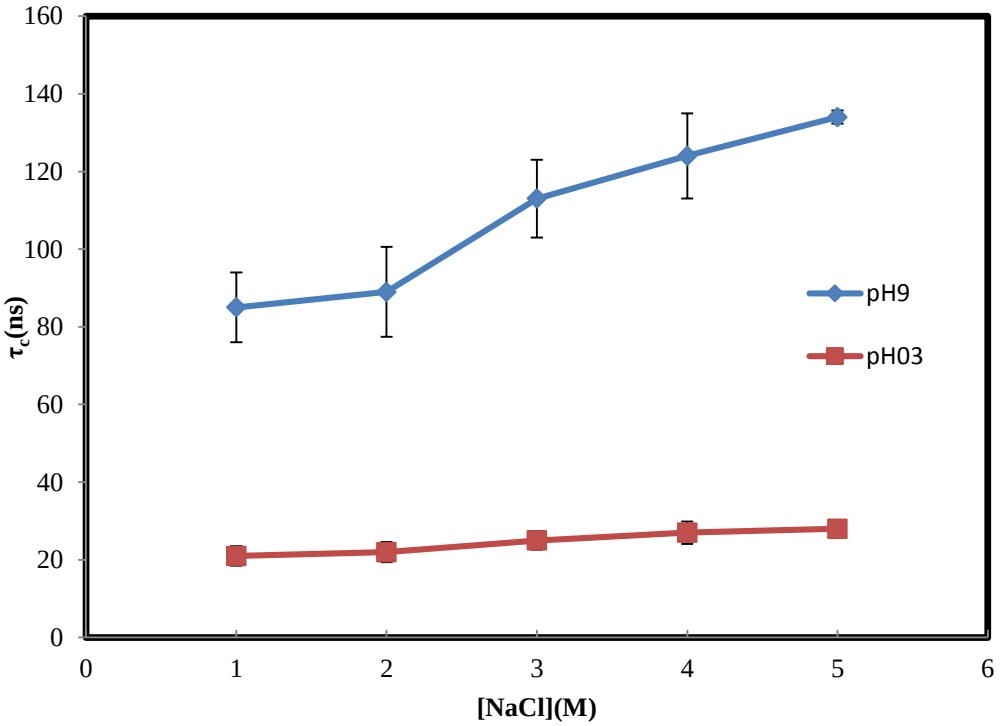

Figure 3.24 Correlation times of ACE-labelled PAA as a function of NaCl at pH 3(red curve) and pH9 (blue curve).

3.8. **Conformational Behaviour of ACE- labelled PAA and Its Interaction with $CaCl_2$**

The influence of divalent salt ($CaCl_2$) on the conformational behaviour of poly (acrylic acid) was also investigated. The fluorescence steady-state and time resolved anisotropy records were collected for the ACE-labelled-PAA at different pH values as a function of calcium chloride concentration.

3.8.1. **Fluorescence steady state spectra of ACE-labelled PAA as a function of $CaCl_2$ concentration**

The steady-state fluorescence emission plots against the calcium chloride concentration at pH 3 and 9, with $CaCl_2$ concentration ranging from 10^{-5} M to 0.15 M, are presented in Figure 3.25 and Figure 3.26, respectively. The fluorescence intensity spectra of aqueous ACE-labelled-PAA remain unaffected over the whole $CaCl_2$ concentration range at pH 3 (Figure 3.25). In contrast, the addition of $CaCl_2$ induces an increase in the fluorescence intensity at pH 9 (Figure 3.26). This result suggests that the increase in the fluorescence spectra for high $CaCl_2$ concentrations results from the aggregation of the PAA chain. Probably, the COO^- groups of PAA with its expanded chain are interacting with an equivalent amount of Ca^{2+} ions [77, 78]. The collapse of the PAA chain creates pockets of the macromolecule that entrap the ACE label localised hydrophobic environments. This may result then in an increasing of the fluorescent intensity of the ACE fluorophore. Possible conformation models for the PAA structure under influence the calcium chloride salt are depicted in Figure 3.28.

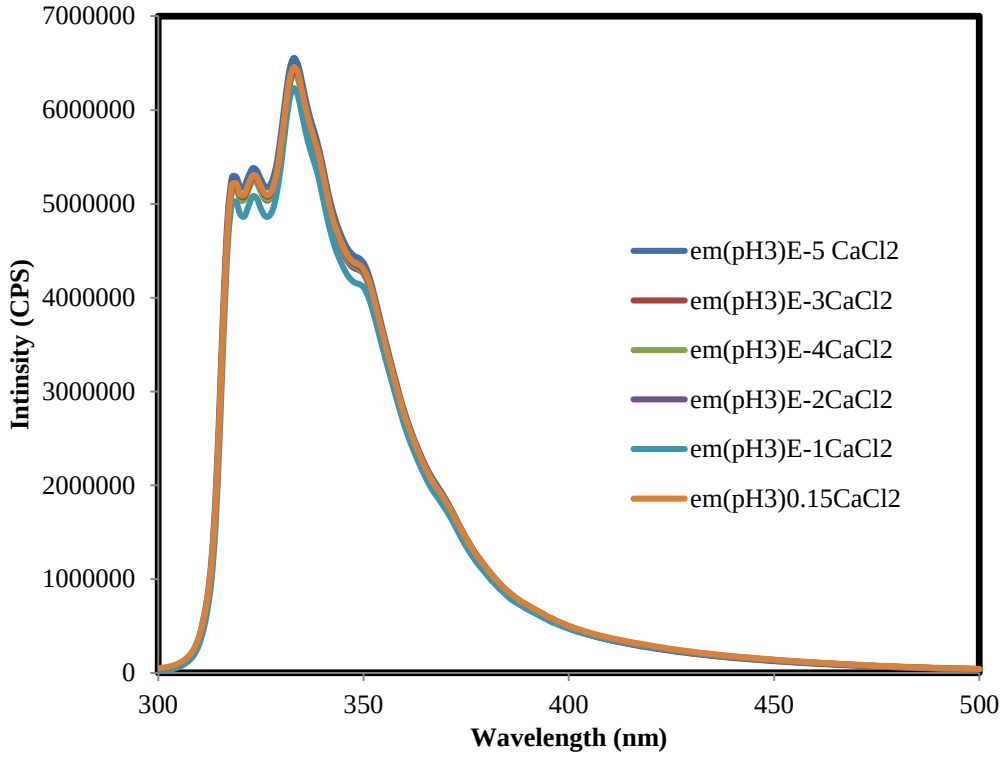

Figure 3.25 Steady state fluorescence emission spectra of aqueous ACE-labelled PAA (10 $^{-2}$ wt %) as a function of $CaCl_2$ concentration at pH3. (λ_{ex}= 290 nm and λ_{em}= 340nm).

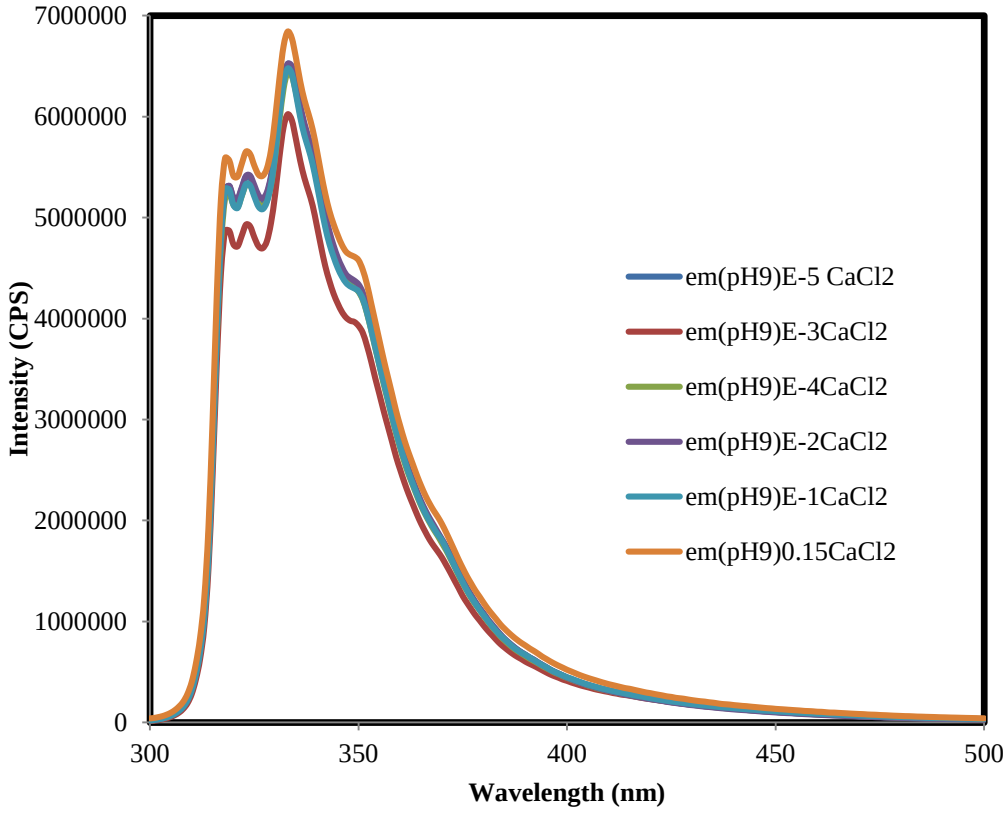

Figure 3.26 Steady state fluorescence emission spectra of aqueous ACE-labelled PAA (10 $^{-2}$ wt %) as a function of $CaCl_2$ concentration at pH9. (λ_{ex}= 290 nm and λ_{em}= 340nm).

3.8.2. **Fluorescence time-resolved anisotropy measurements (TRAMS) of ACE-labelled PAA as a function of $CaCl_2$ concentration**

The cross-linking of poly (acrylic acid), which is induced by the interaction of Ca^{2+} ions with the carboxylate anions groups, was also examined by measuring the correlation times as a function in calcium chloride concentration at pH 3 and 9, see Figure 3.27. A dramatic increase in correlation times (from 85 to 218 ns) with increasing concentration of $CaCl_2$ was recorded at pH 9, while a small increase was demonstrated at pH 3. However, over the entire concentration range the rate of increment in these values at pH 9 is more than in those at pH 3. The obvious increase can be attributed to the interaction, which occurs between Ca^{2+} ions and two COO^- of PAA [78]. This interaction screens the carboxylate groups charge and leads to the collapse of the polyelectrolyte chain, which in turn inhibits the motion of the ACE-PAA chain. This in agreement with the static and dynamic light scattering study [77], which was applied to investigate the collapse of PAA chain calcium chloride solutions. It was reported that the bidentate complex formation (see Figure 3.28) could lead to intramolecular bridging, which further decreases the coil dimensions of PAA chain.

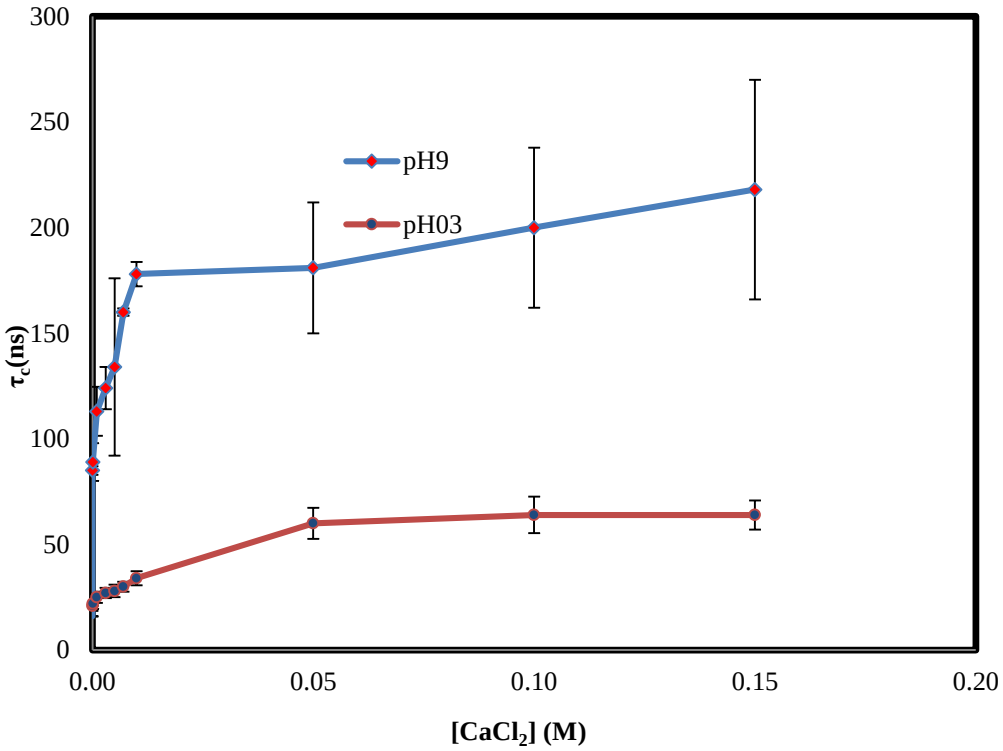

Figure 3.27 Correlation time of ACE-labelled PAA as a function of $CaCl_2$ at pH 3 (red curve) and pH 9 (blue curve).

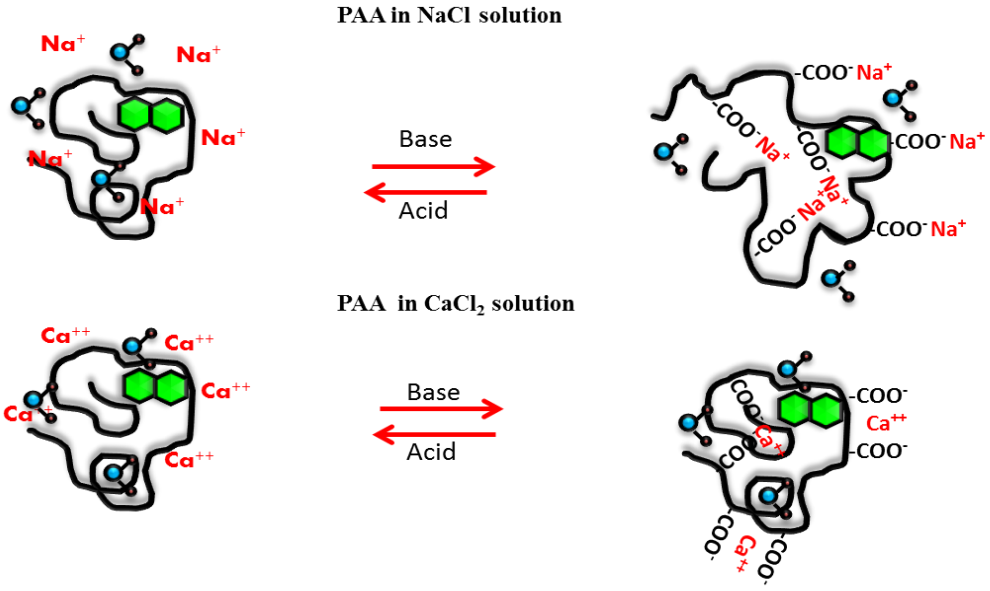

Figure 3.28 Proposed conformations of PAA chain in the presence of salts.

3.9. **Adsorption of ACE-PAA on Silica as a Function of pH**

Fluorescence steady-state and anisotropy measurements were carried out on the ACE-PAA in the presence of silica, with confidence that the free fluorophore remains dispersed in the bulk solution and is not adsorbed into the silica after separation. Any difference in the fluorescence intensities before and after separation would point to attachment occurring because of the interaction between the polymer and silica.

3.9.1. **Fluorescence steady state spectra of ACE-PAA on silica as a function of pH**

Figure 3.29 to Figure 3.32 show the fluorescence emission spectra of 0.01 wt % of ACE-PAA at pH 3 and 11 in 0.0001 and 10 wt% silica, respectively. The spectra were recorded before and after centrifuging, as described in the adsorption experiment (see section 2.9. in Chapter 2). At extremely low concentrations of silica (herein we just present 0.0001 wt%, 0.001, 0.01 were also measured), the supernatant displays similar fluorescence intensity compared to of the value before centrifuging at pH 3 and 11 (Figure 3.29 and Figure 3.30). This could be attributed to the fact that the polymer exists in the bulk solution and does not adsorb onto silica. Alternatively, when the silica concentration was increased up to 1 wt%, the fluorescence intensity of the supernatant was markedly quenched at pH 3 compared to a slight reduction at pH11, see Figure 3.31 and Figure 3.32. It can be concluded that a considerable amount of polyelectrolyte attached to silica at pH 3 and a lower quantity is adsorbed at pH 11.

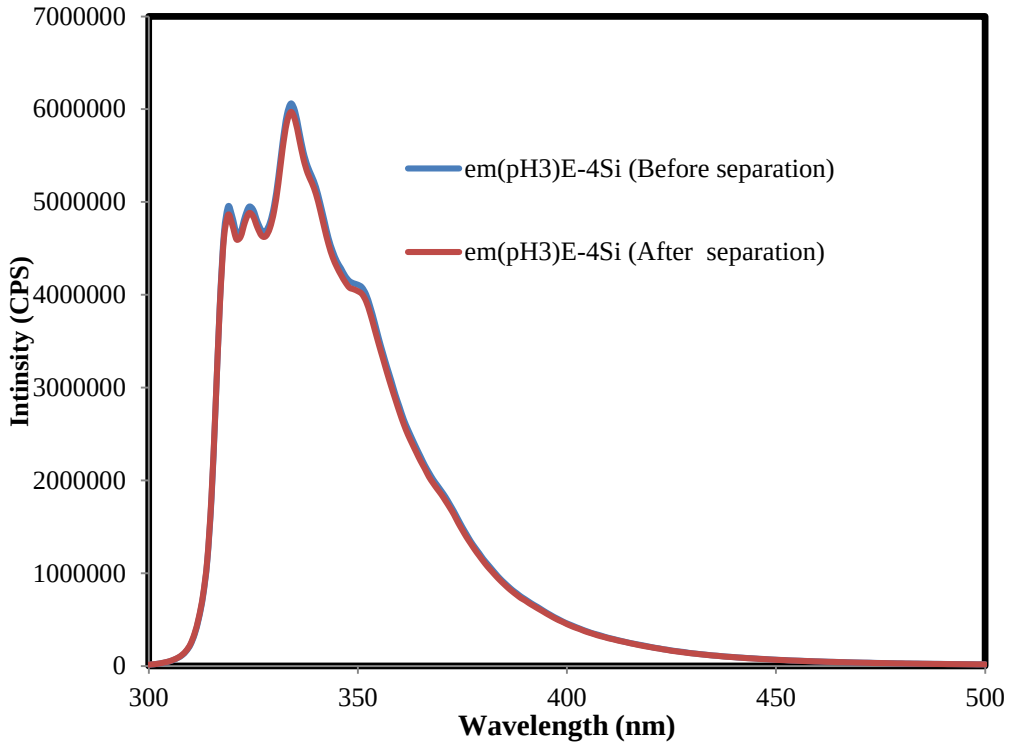

Figure 3.29 Steady state fluorescence emission spectra of aqueous ACE-labelled PAA (10^{-2} wt%) and silica (10^{-4}wt%) solutions before and after the separation at pH3. (λ_{ex}= 290 nm and λ_{em}= 340nm).

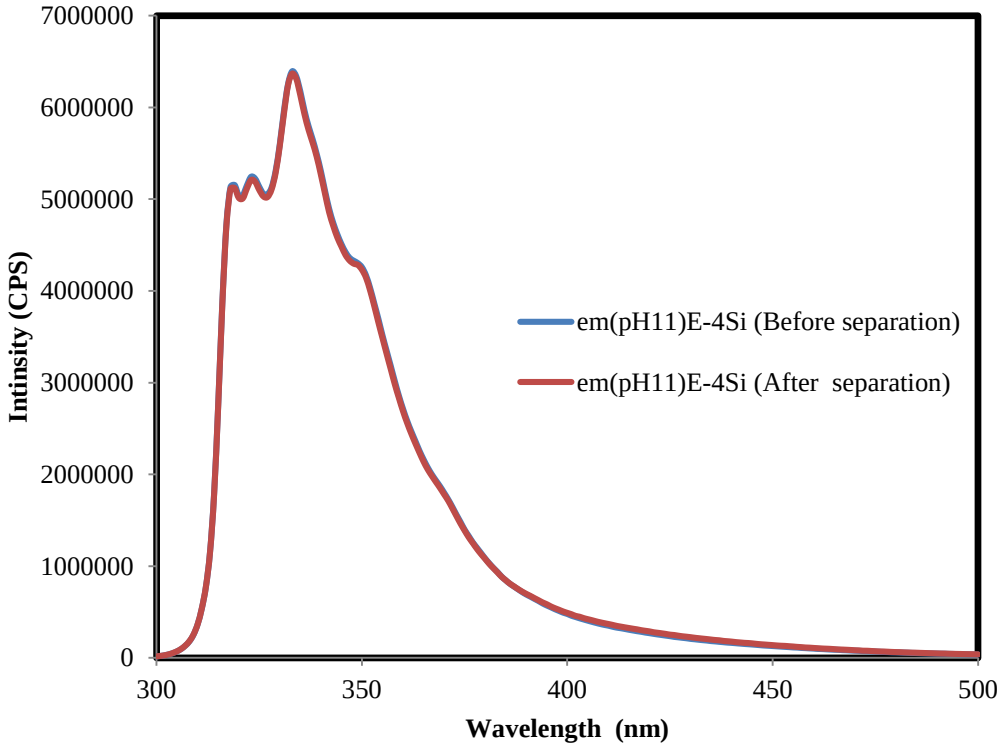

Figure 3.30 Steady state fluorescence emission spectra of aqueous ACE-labelled PAA (10^{-2} wt %) and silica (10^{-4}wt%) solutions before and after the separation at pH11. (λ_{ex}= 290 nm and λ_{em}= 340nm).

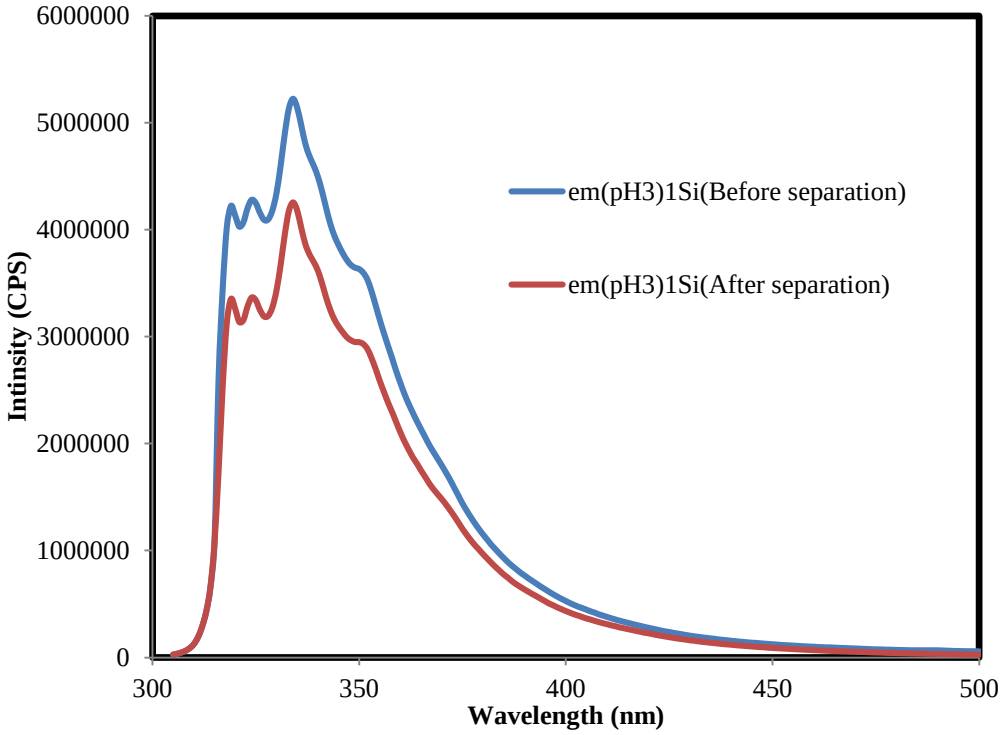

Figure 3.31 Steady state fluorescence emission spectra of aqueous ACE-labelled PAA (10^{-2} wt %) and silica (1wt%) solutions before and after the separation at pH3. (λ_{ex}= 290 nm and λ_{em}= 340nm).

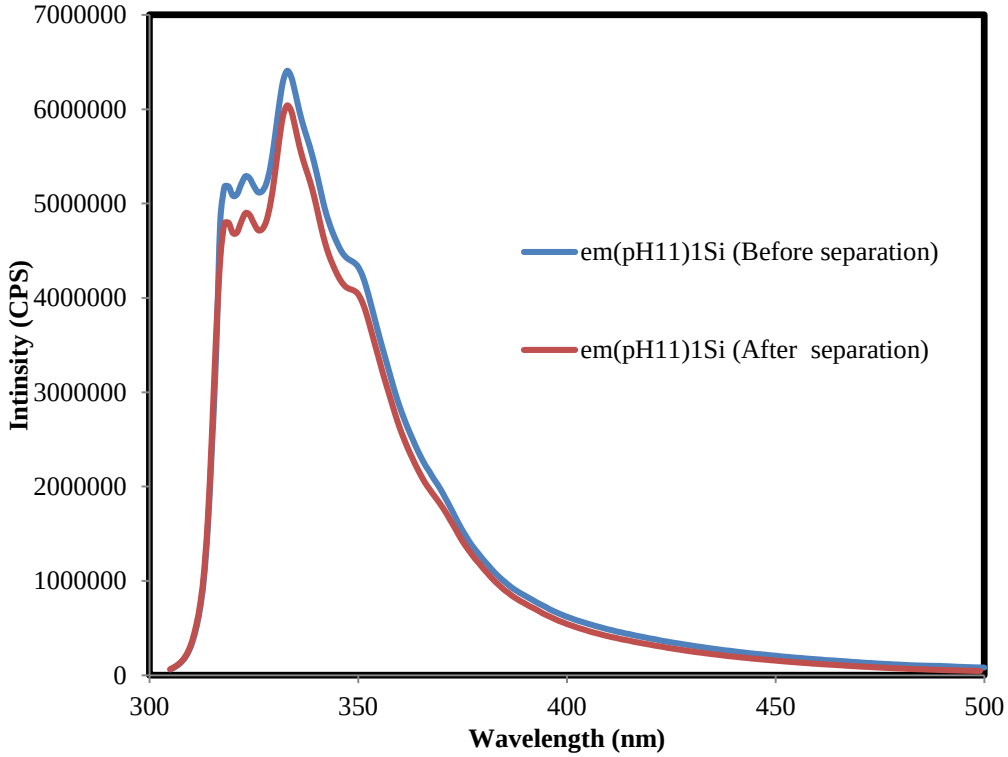

Figure 3.32 Steady state fluorescence emission spectra of aqueous ACE-labelled PAA (10^{-2} wt %) and silica (1wt%) solutions before and after the separation at pH11. (λ_{ex}= 290 nm and λ_{em}= 340nm).

Figure 3.33 shows the percentage amount of adsorbed polymer as a function in pH and silica concentration. The percentage value of adsorbed polymer was calculated, using the following equation:

$$< \% >= 100 - \frac{(I_{max})\text{Before separation}}{(I_{max})\text{After separation}} x100 \qquad \text{Equation 3.5}$$

Where, I_{max} is the maximum fluorescent emission of the attached ACE label.

As an overall trend, the amount of adsorbed polymer increases by decreasing the pH from 11 to 2. This pH dependence can be explained in terms of zero points of charge (pHzpc) for PAA and silica, the pHzpc concept will be discussed further in section 3.16. Several researchers have reported that the PAA as well as silica are uncharged at pH 3 [16, 79-81]. It means that except for pH 2 the relative charges of SiO_2 and PAA are negative over the studied pH range. In this situation, the electrostatic repulsion between polymer chain and the silica suspension occurs. pH increase causes the decrease of PAA adsorption because of electrostatic repulsion between the COO^- groups in PAA and the negatively charged silica particle is becoming strong. The adsorption of PAA on the silica suspension could be attributed to that non-electrostatic forces occur between PAA and the silica surface. Otherwise, the interaction of similarly charged materials should not occur [80]. Similar results were obtained for adsorption of poly (acrylic acid) on SiO_2 [80]. For all examined molecular weights of PAA, it was found that the maximum amount for adsorption of PAA at pH 3 (~ 0.25 mg/m^2 PAA adsorbed). The adsorbed amounts decrease to ~ 0.08 mg/m^2 with the increasing pH of the solution to pH 10.

Besides the pH of solution, increasing the amount of silica leads to an increase in the amount of adsorbed PAA. Specifically, from 10^{-4} to 10^{-2} wt % of added SiO_2, there is a small increase in the adsorbed polymer at pH 2 and 3, but no important adsorption is recorded at pH levels 5, 7, 9 and 11. When the concentration of added SiO_2 was increased further to 1 wt %, the adsorbed amount of PAA reached the maximum (~20% of PAA) at pH 2 and 3. Less polymer was attached silica suspensions (~5 % of PAA) when the pH of solution increased to pH 11.

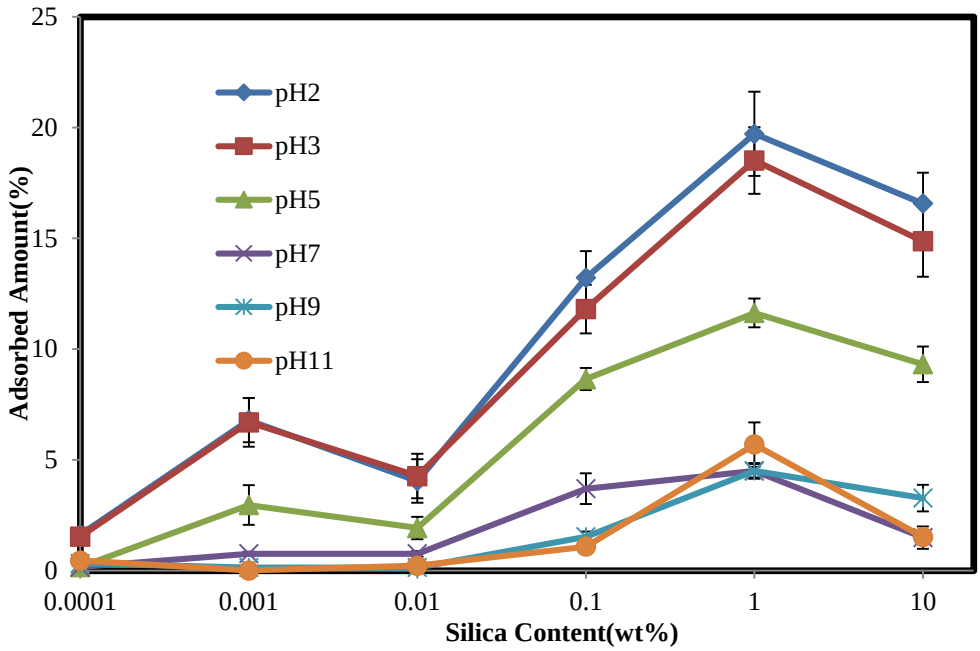

Figure 3.33 Adsorption of ACE-labelled poly (acrylic acid) on the silica as a function of silica concentration at various pH values. Concentration of polymer in the solution is 10^{-2} wt %.

3.9.2. Fluorescence time-resolved anisotropy measurements (TRAMS) of ACE-PAA on silica as a function of pH

The adsorption of polyelectrolyte onto solid is accompanied by changes in the mobility of the adsorbate [34]. Techniques like TRAMS, which monitor polymer dynamics, should be useful for investigating macromolecule-surface interfaces. In this section, we describe a preliminary experiment aimed at assessing the applicability of TRAMS to monitor the adsorption of fluorescently labelled polyelectrolyte onto solid particles. We present here the results of a mathematical analysis of the raw anisotropy decays from the polymer-silica system, and discuss the dynamic behaviour of PAA on a silica surface.

Figure 3.34 shows the fluorescence time-resolved decays of ACE-labelled poly (acrylic acid) in dilute aqueous solution. Parallel and perpendicular fluorescence intensities are plotted logarithmically against time on the nanosecond time range. Since the polyelectrolyte chains rotated without restrictions overall, shortly after excitation the two polarized fluorescence decays were superimposed on each other. Contrarily, once the polymer was adsorbed onto the silica, rotational motion was impeded, and the two polarized decays did not superimpose on each other for a longer time, as displayed in Figure 3.35.

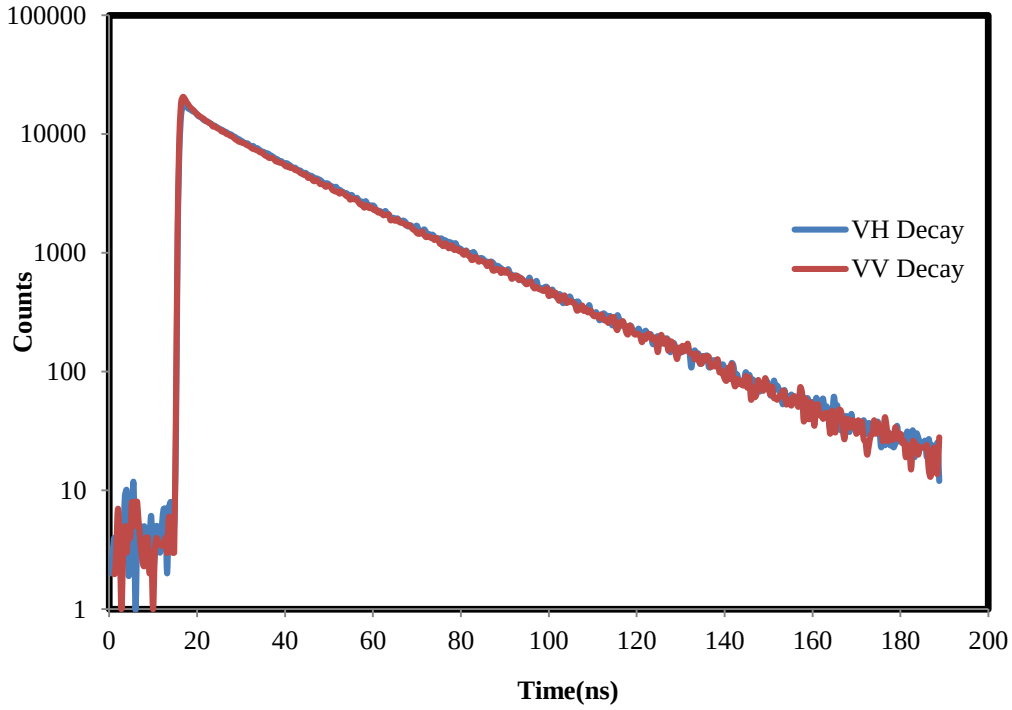

Figure 3.34 Parallel (red curve) and perpendicular (blue curve) fluorescence intensity decay curves following excitation with vertically polarized light (λ_{ex}= 295 nm) analysed at 350 nm from 10^{-2} wt% ACE- labelled PAA in aqueous solution in the absence of silica.

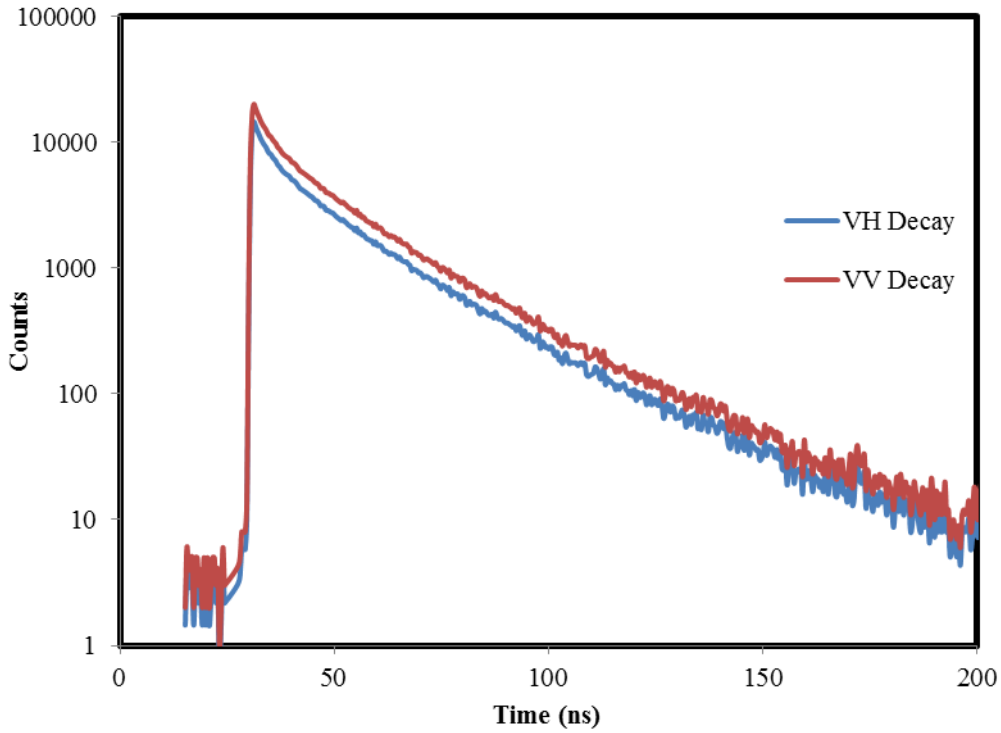

Figure 3.35 Parallel (red curve) and perpendicular (blue curve) fluorescence intensity decay curves following excitation with vertically polarized light (λ_{ex}= 295 nm) analysed at 350 nm from 10^{-2} wt% ACE- labelled PAA in aqueous solution at silica concentration of 1 wt%.

Figure 3.36 compares the fluorescence anisotropy decays of ACE-labelled-PAA in water in the absence and presence of silica and shows that the anisotropy decays rapidly to zero in the absence of silica. Conversely, in the presence of silica, the anisotropy decays slowly to zero. This photophysical behaviour can be explained as follows. Since the label was randomly attached to the polymer backbone, it seems possible that it can exist only within the loops of adsorbed chains. Since chains require physical contact with the solid surface, but our control experiments proved that ACE alone did not adsorb onto silica, this indicates that the polymer chain attaches to a mineral. This, in turn leads to the restriction of the segmental motion of fluorescently labelled polymer. Long anisotropy decay is observed accordingly.

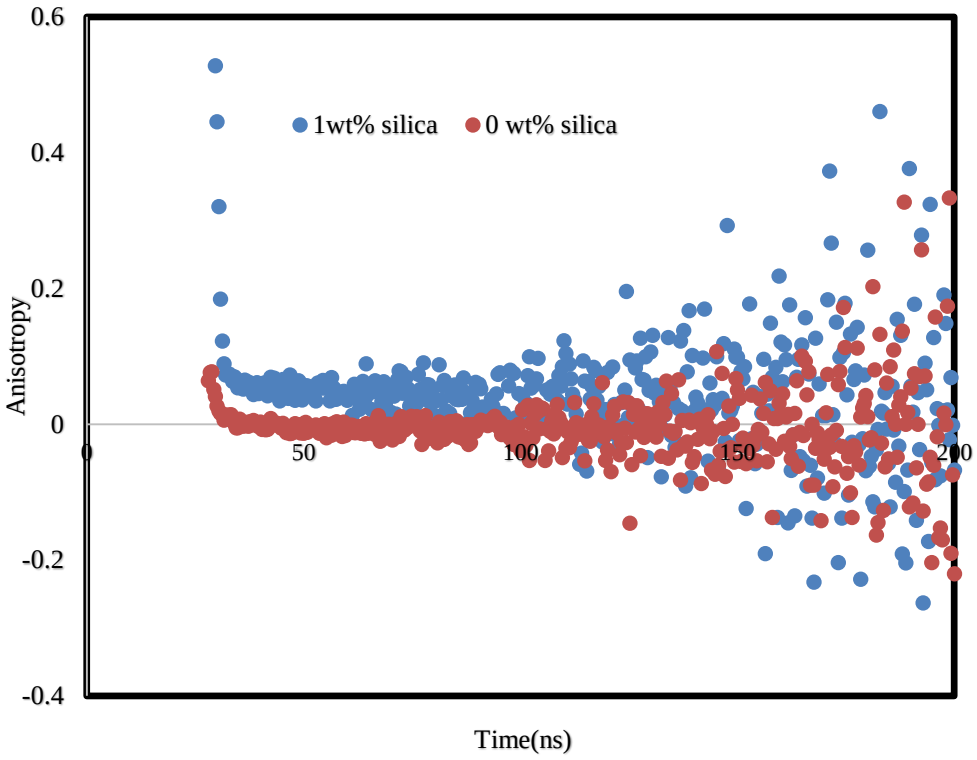

Figure 3.36 Fluorescence time resolved anisotropy data of aqueous ACE-labelled PAA solution(10^{-2} wt%) in the absence of silica(red dots) and at the silica concentration of 1wt%(λ_{ex}= 295 nm and λ_{em}= 350 nm).

Similarly, the anisotropy decay of the polymer in the presence of silica was found to be pH dependent. Figure 3.37 presents the anisotropy decays of PAA in the presence of 10 wt % silica at pH 2 and 11, respectively. It was found that the anisotropy decays rapidly to zero at pH11, whereas at pH 2 the anisotropy decays slowly to zero. Probably, the aggregated adsorbed PAA chain at acidic pH moves slower than the expanded one.

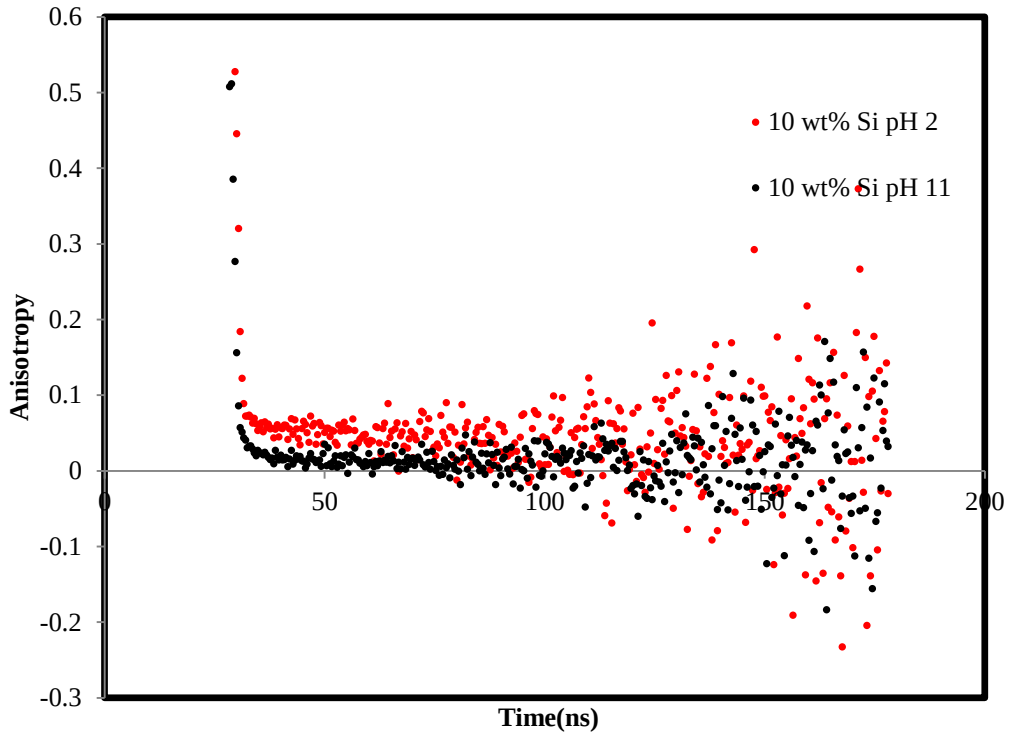

Figure 3.37 Fluorescence time resolved anisotropy data of aqueous ACE-labelled PAA solution (10^{-2} wt %) in 10 wt% silica at pH 11(black dots) and at pH 2 (red dots) (λ_{ex}= 295 nm and λ_{em}= 350nm).

The correlation times derived from mathematical analysis of anisotropy decays of ACE-labelled-PAA (10^{-2} wt %) were plotted against the silica content at different pH values, see Figure 3.38. When the concentration of added silica is low, for example at 10^{-4}, 10^{-3} and 10^{-2} wt % no important adsorption occurs and the ACE label exists in a homogeneous environment. In such cases, a single exponential function (Equation 1.21) is applied to determine the correlation time values in nanoseconds. When the concentration of colloid is increased to 10 wt %, absorption begins and some of polymer remains in the bulk solution. In this complex situation, a double exponential fit (Equation 1.22) is suited to such anisotropy decays.

In general, the correlation time increases by decreasing the pH from 11 to 2, while increasing the amount of silica causes an increase in the correlation time values. Specifically at a low concentration of silica, from 10^{-4} to 10^{-2} wt%, there was a slight increase in the correlation time values at pH 2 and 3, but no change was recorded at pH values 5,7,9 and 11. On the other hand, a marked rise was detected when the silica concentration increased to 1wt% at pH values 2,3 and 5, at 10 wt% of silica the correlation time remained roughly constant, This can be

explained with saturation between the polyelectrolyte chain and the silica. However, a small increase was recorded at pH values 7, 9 and 11 from silica concentration range from 10^{-1} to 10 wt %.

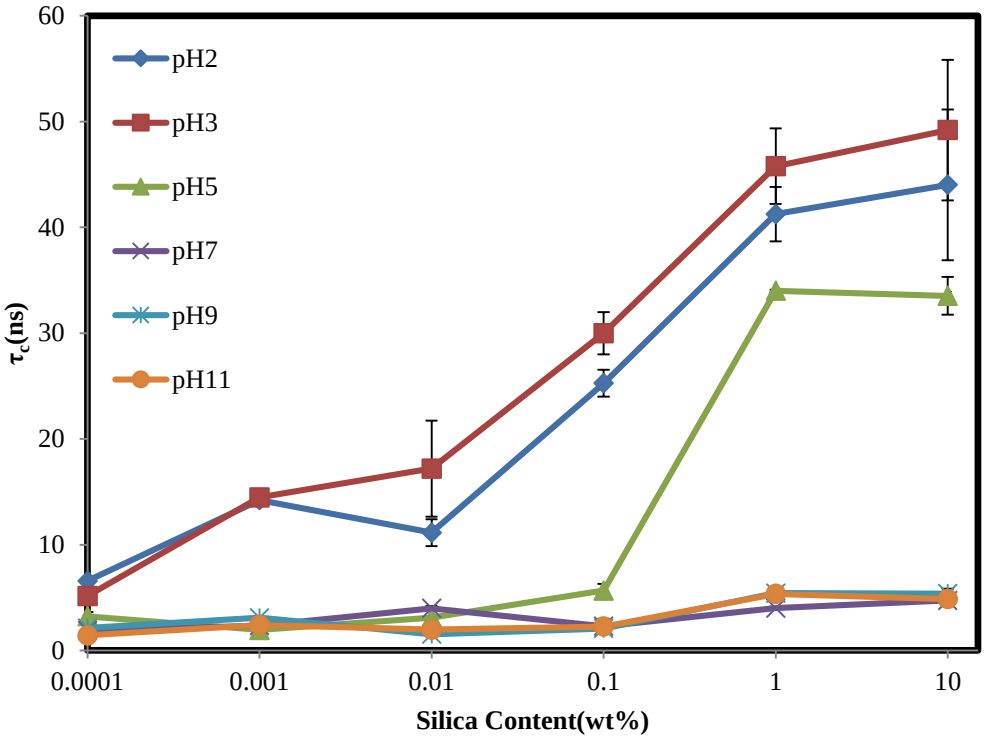

Figure 3.38 Correlation times of ACE-labelled PAA as a function of silica concentration at various pH values.

3.10. **Adsorption of ACE-PAA on Alumina as a Function of pH**

The adsorption of fluorescently labelled polymer was also carried out on larger particle size mineral, such as alumina (particle diameter ~1000 nm). Fluorescence steady-state and anisotropy techniques were applied to examine the attachment of ACE-PAA onto alumina, after making sure that the free fluorophore can not to attach at the alumina surface (see section 3.5.). Any difference in the fluorescence intensities before and after separation would point to the conclusion that adsorption occurs because of the interaction between the polymer and alumina.

3.10.1. **Fluorescence steady state spectra of ACE-PAA on alumina as a function of pH**

The fluorescence emission spectra of 0.01 wt% of ACE-PAA at pH 3 and 11 in 0.0001, 0.1 and 1 wt% alumina are displayed in Figure 3.39 to Figure 3.44, respectively. As discussed before in the practical part of the absorption experiment (Chapter 2) the fluorescence intensities were recorded before and after separation. Overall results showed that the polymer chain adsorbs strongly on alumina compared to silica, at low pH values.

At extremely low concentrations of alumina, for example at 0.0001 wt%, the fluorescence intensity after centrifuging is comparable to that before separation at pH 3 and 11, see Figure 3.39 and Figure 3.40. This confirms that the polyelectrolyte remains present in the bulk solution and does not adsorb onto the silica after separation. On the other hand, when the alumina content is increased to 0.1 wt% the fluorescence intensity of the supernatant is reduced at pH 3 compared to a minor decline at pH11, see Figure 3.41 and Figure 3.42. Then again, when 1 wt% of alumina is added, the fluorescence intensity of supernatant disappears at pH3, as shown in Figure 3.43, but a tiny reduction is shown at pH 11 (Figure 3.44), suggesting that, at high mineral concentration a large quantity of polymer attaches to alumina at pH 3 while a smaller quantity is adsorbed at pH 11.

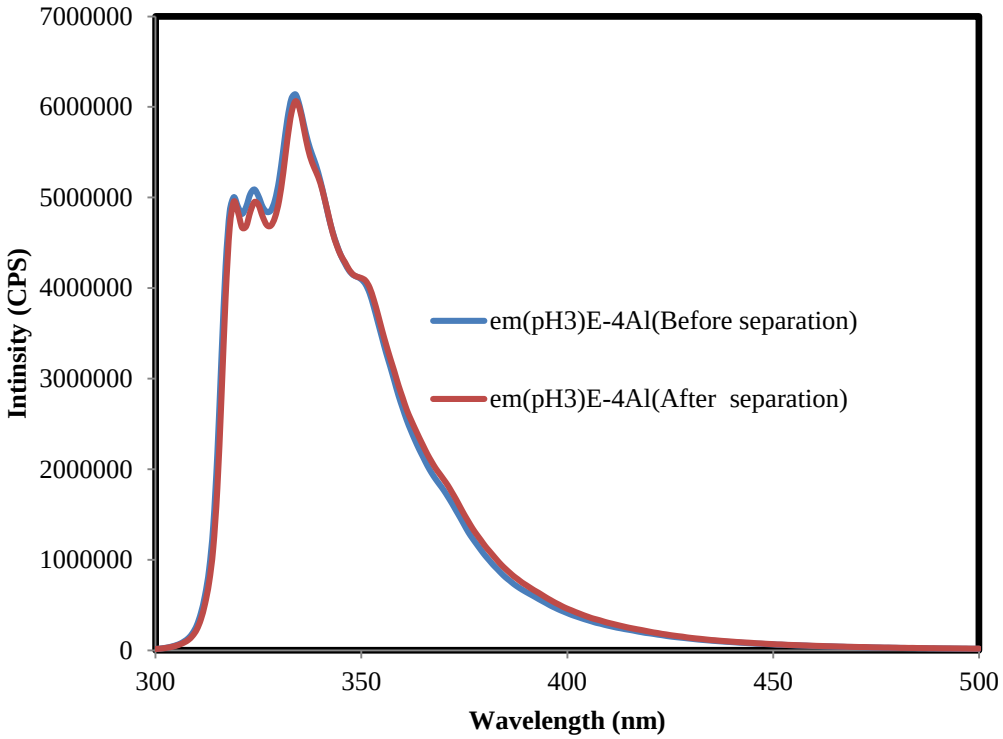

Figure 3.39 Steady state fluorescence emission spectra of aqueous ACE-labelled PAA (10^{-2} wt %) and alumina (10^{-4}wt %) solutions before and after the separation at pH3. (λ_{ex}= 290 nm and λ_{em}= 340nm).

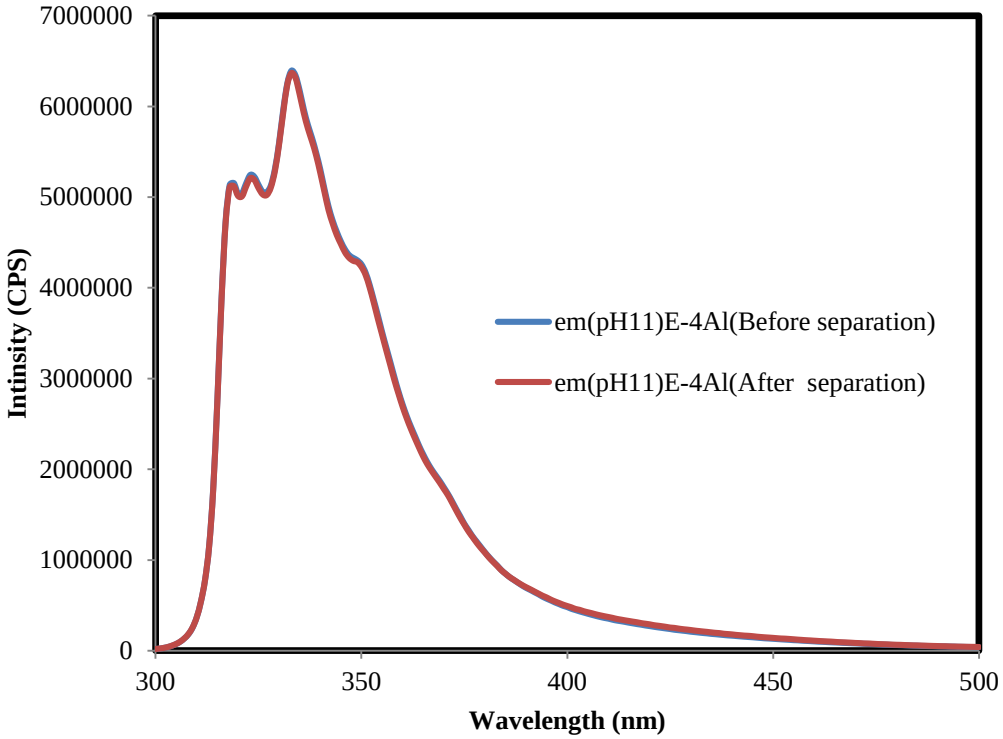

Figure 3.40 Steady state fluorescence emission spectra of aqueous ACE-labelled PAA (10^{-2} wt %) and alumina (10^{-4}wt%) solutions before and after the separation at pH11. (λ_{ex}= 290 nm and λ_{em}= 340nm.

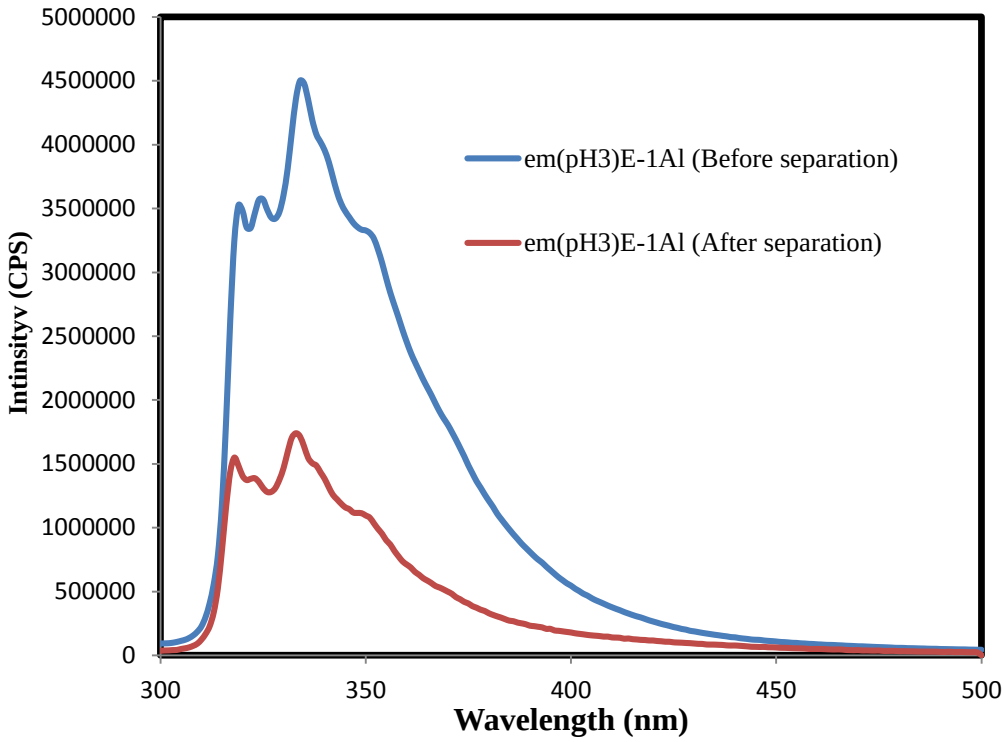

Figure 3.41 Steady state fluorescence emission spectra of aqueous ACE-labelled PAA (10^{-2} wt %) and alumina (0.1wt%) solutions before and after the separation at pH3. (λ_{ex}= 290 nm and λ_{em}= 340nm).

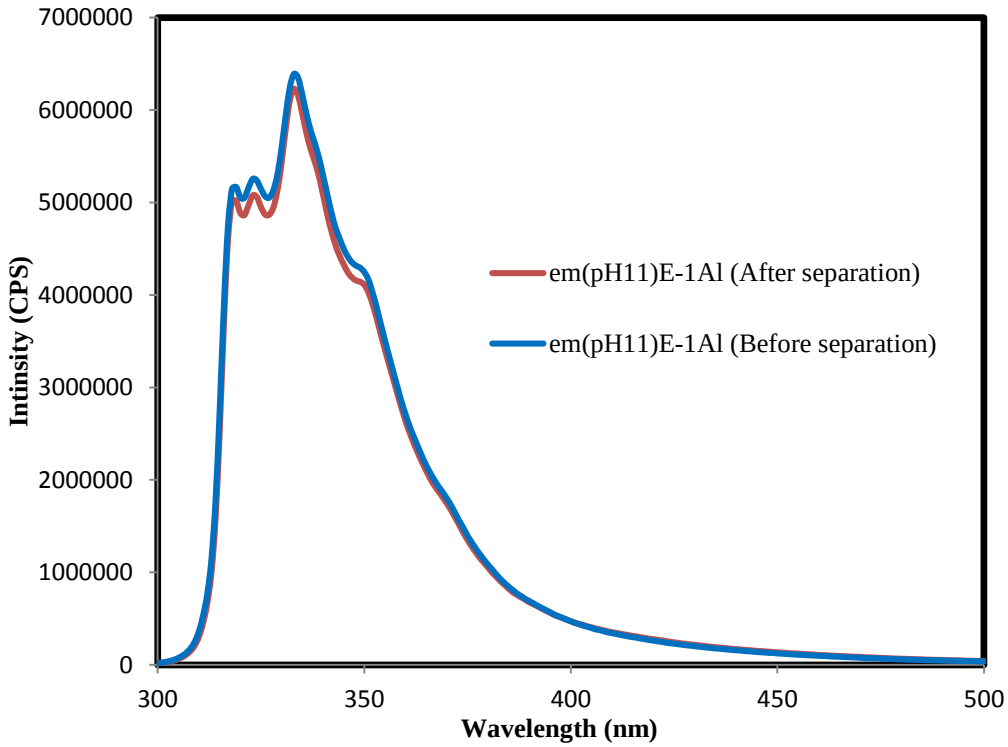

Figure 3.42 Steady state fluorescence emission spectra of aqueous ACE-labelled PAA (10^{-2} wt %) and alumina (0.1wt %) solutions before and after the separation at pH11. (λ_{ex}= 290 nm and λ_{em}= 340nm).

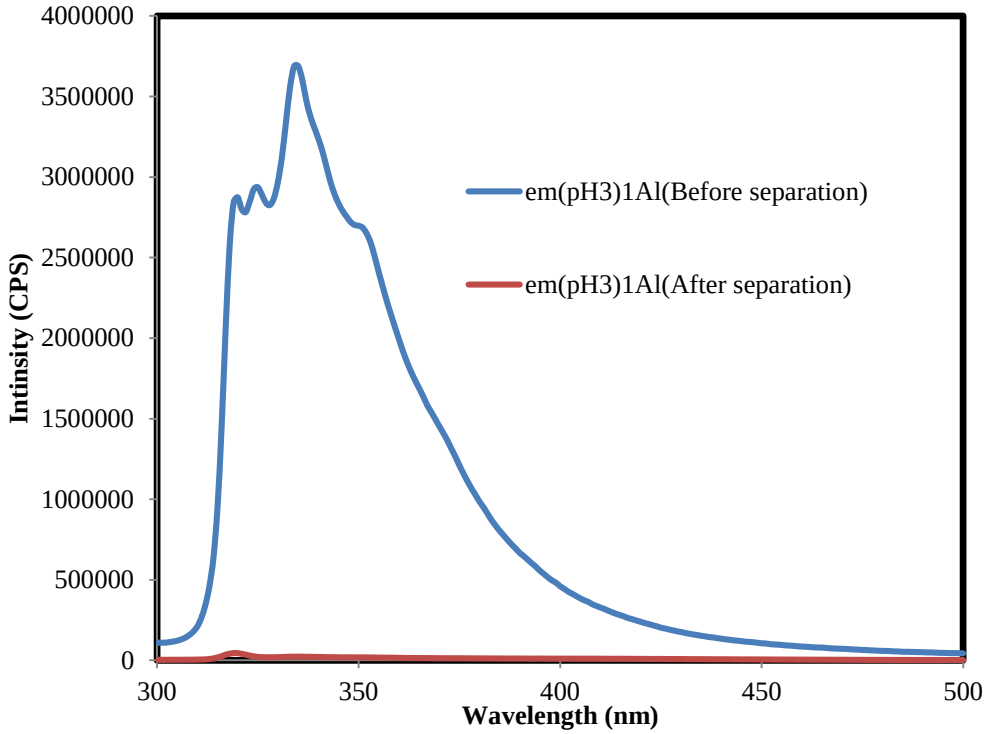

Figure 3.43 Steady state fluorescence emission spectra of aqueous ACE-labelled PAA (10^{-2} wt %) and alumina (1wt%) solutions before and after the separation at pH3. (λ_{ex}= 290 nm and λ_{em}= 340nm).

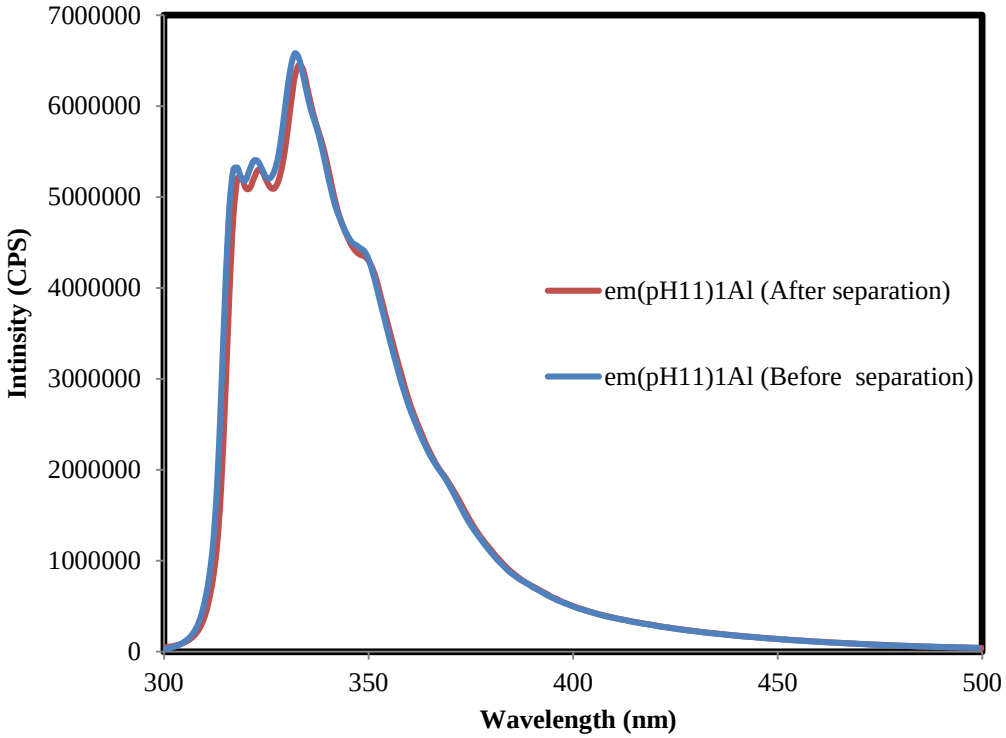

Figure 3.44 Steady state fluorescence emission spectra of aqueous ACE-labelled PAA (10^{-2} wt %) and alumina (1wt%) solutions before and after the separation at pH11. (λ_{ex}= 290 nm and λ_{em}= 340nm).

Figure 3.45 presents the percentage amount of adsorbed poly (acrylic acid) as a function in pH and alumina concentration. The amount of labelled PAA adsorbed on the alumina particles is determined by using Equation 3.5. The results are displaying an increase in the percentage of adsorbed PAA with a decrease on pH. This could be attributed to the zero point of charge (pHzpc) for the polymer and mineral. The pHzpc term will be discussed further in section 3.16. Researchers [16, 79] have reported that the pHzpc for PAA and alumina are ~3 and ~ 9, respectively. It means that apart from pH 9 and 11 the surface of alumina is positively charged, while the PAA bears a negative charge in the pH range from 5 to 11. So, the increase of PAA adsorption by decreasing the pH is because of electrostatic attraction between the negatively charged COO^- groups in PAA and the positively charged alumina particles is becoming strong (from pH 7-3). At pH 9 and 11, the adsorption of PAA on the alumina could be because of that non-electrostatic forces occur between the polymer and the mineral. Otherwise, the interaction of similarly charged materials should not take place [80]. At pH 2 besides that non-electrostatic force, the hydrogen bonding could be responsible for adsorption. The effect of pH on the adsorption of PAA on alumina was investigated elsewhere [82]. Similar results were found, since a strong adsorption for PAA on alumina was recorded at pH 3 (~0.9 mg/m^2), whereas only 0.2 mg/m^2 of PAA was adsorbed onto alumina surface at pH12. However, the role of the zero point of charge in the adsorption behaviour of polymer will be discussed further in the section 3.16. On contrary, the polymer adsorption increases by increasing the quantity of added mineral (from 10^{-4} to 10 wt %). In particular, a minor increase in the adsorbed PAA at pH values of 5, 7, 9 and 11. While, a dramatic increase is observed at pH 2 and 3, as the percentage of adsorbed PAA reaches the maximum value (~100%). In such a condition only ~20 % of PAA is adsorbed onto the silica. This could be attributed to that in acidic media, the unionized carboxylic acid groups (COOH) adsorb via hydrogen bonding between the PAA carbonyl group and hydroxyls on alumina surface. Hence, at lower pH values the adsorption mechanism is predominantly hydrogen bonding in nature, and PAA does not adsorb significantly onto silica due to electrostatic repulsion [16].

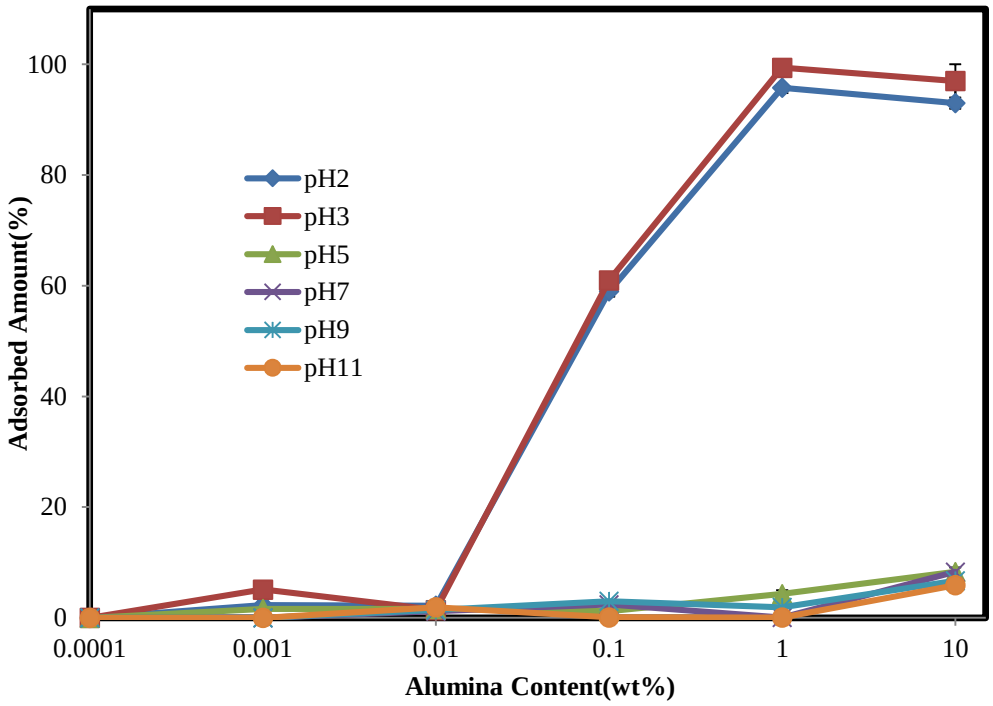

Figure 3.45 Adsorption of ACE-labelled poly (acrylic acid) on the alumina as a function of alumina concentration at various pH values. Concentration of polymer in the solution is 10^{-2} wt %.

3.10.2. Fluorescence time-resolved anisotropy measurements (TRAMS) of ACE-PAA on alumina as a function of pH

The parallel and perpendicular fluorescence intensities of ACE-labelled-PAA (10^{-2} wt %) adsorbed onto Al_2O_3 are plotted logarithmically against time on the nanosecond time range, as shown in Figure 3.46. Unlike in the absence of mineral (Figure 3.34), after excitation the two polarized fluorescence decays are clearly separated from each other for a longer time. This suggests that sites on the polymer chain are attached onto the mineral surface, which leads to restricted fluorophore and consequently, macromolecular mobility.

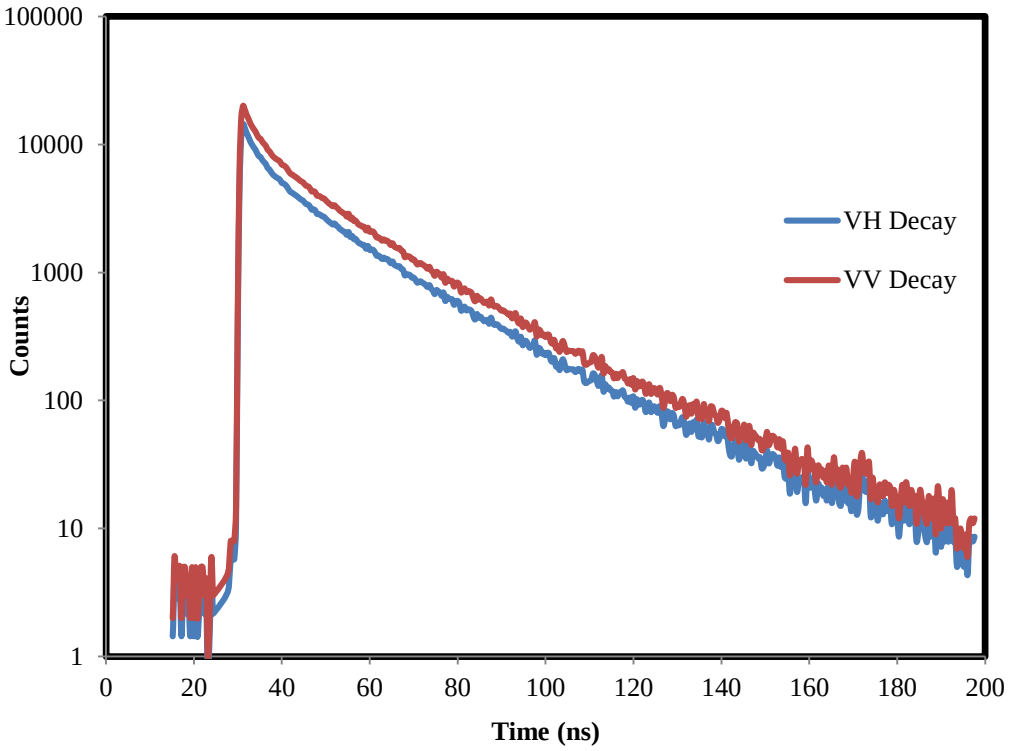

Figure 3.46 Parallel (red curve) and perpendicular (blue curve) fluorescence intensity decay curves following excitation with vertically polarized light (λ_{ex}= 295 nm) analysed at 350 nm from 10^{-2} wt% ACE- labelled PAA in aqueous solution at alumina concentration of 1 wt%.

Figure 3.47 matches the fluorescence anisotropy decays of ACE-labelled-PAA in water in the absence and presence of alumina. It was found that the anisotropy quickly drops to zero in the absence of alumina. Respectively, the presence of alumina slowly lowers the anisotropy decays to zero. These results assume that the macromolecule chain adsorbs onto the alumina particles, which would slow down the segmental motion of fluorescently labelled polymer, hence long anisotropy decay is observed in presence of 1 wt % of alumina.

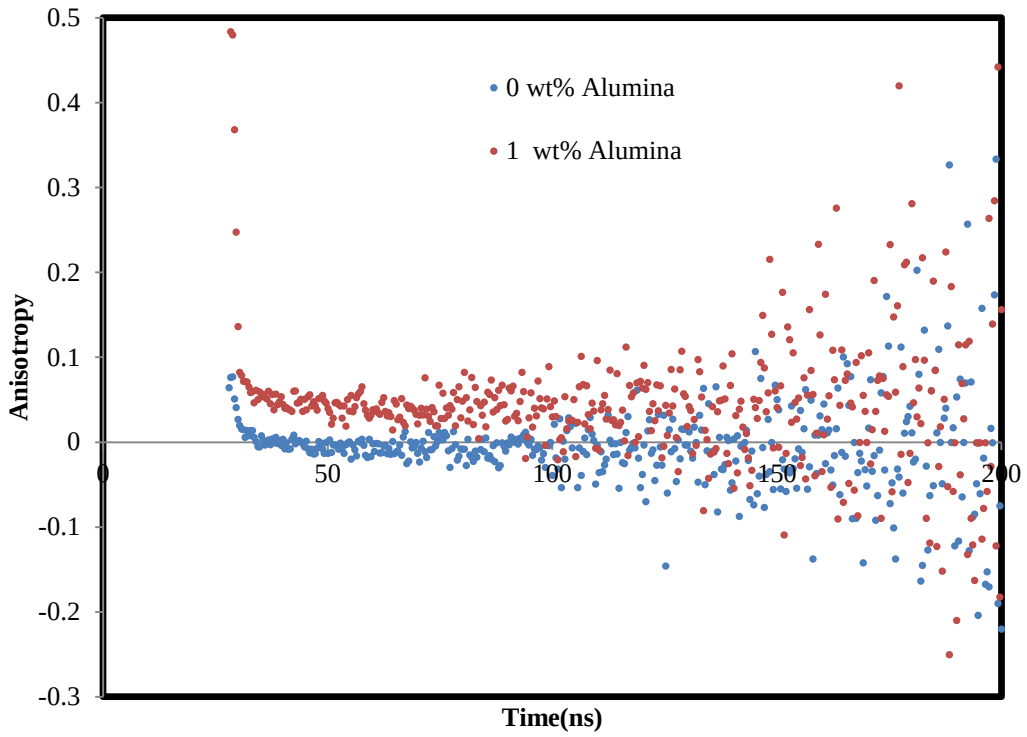

Figure 3.47 Fluorescence time resolved anisotropy data of aqueous ACE-labelled PAA solution (10^{-2} wt %) in the absence of alumina (red dots) and at the alumina concentration of 1wt % (λ_{ex}= 295 nm and λ_{em}= 350 nm).

In addition, the anisotropy decay of poly (acrylic acid) in the presence of alumina was found to be pH sensitive. Figure 3.48 demonstrates the anisotropy decays of PAA in the presence of 10 wt % alumina at pH 2 and 11, respectively. It was detected that the anisotropy decays rapidly to zero at pH11, whereas at pH 2 the anisotropy decays slowly to zero. This proposes that a greater amount of the collapsed PAA adsorbs onto the surface of alumina (~100%) in acidic media, in contrast to the expanded form (~0.04%) at the same mineral concentration and pH. As a result, the strong adsorption leads to restricted fluorophore mobility and consequently macromolecular mobility.

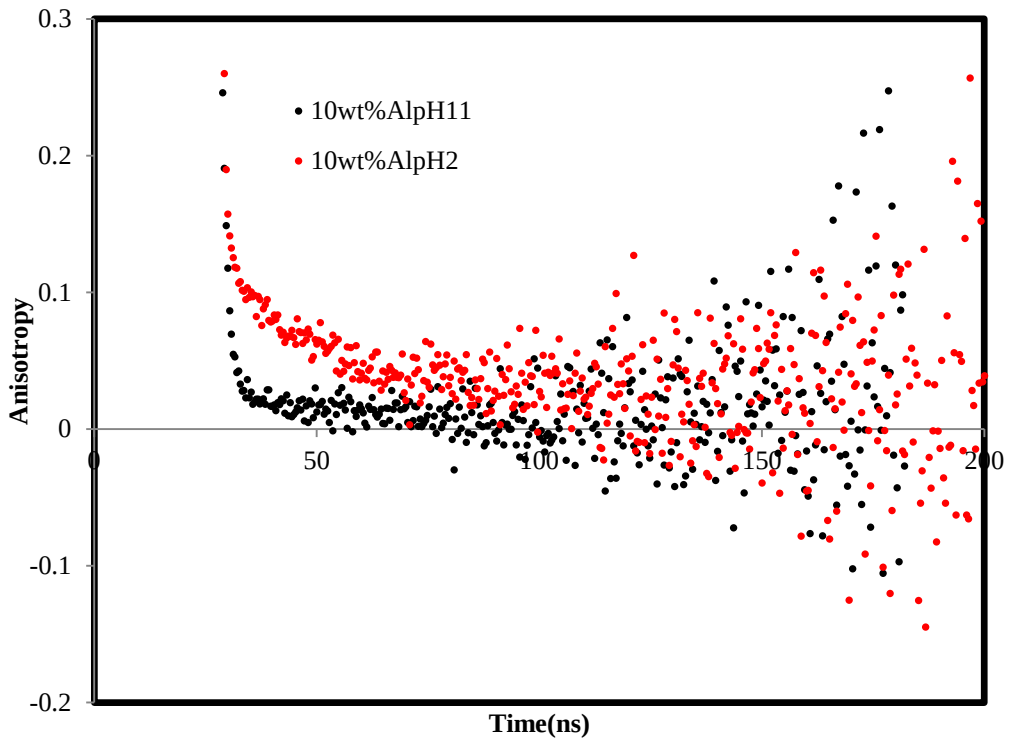

Figure 3.48 Fluorescence time resolved anisotropy data of aqueous ACE-labelled PAA solution (10^{-2} wt%) in 10 wt% alumina at pH 11(black dots) and at pH 2 (red dots)(λ_{ex}= 295 nm and λ_{em}= 350nm).

Figure 3.49 shows the correlation times (τ_c) of ACE-labelled-PAA (10^{-2} wt %) as a function of alumina concentration at different pH values. When the concentration of added alumina is low, for example at 10^{-4}, 10^{-3} and 10^{-2} wt %, weak adsorption occurs and the ACE label exists in homogeneous environment. In such cases, a single exponential fit is applied to calculate the correlation time values in nanoseconds. When the concentration of alumina is increased to 10 wt %, strong adsorption occurs. In this situation, a single exponential fit is also believed to be suited to fit such anisotropy decays. While a double exponential fit is selected to fit the anisotropy decays, at a concentration of alumina content equal to 0.1wt %, the polymer partially adsorbs onto alumina, which means that the ACE label is dispersed in two phases, solid and bulk solution. However, the correlation times increase by reducing the pH from 11 to 2. Increasing the amount of alumina also causes an increase in the correlation time values.

When alumina concentration varied from 10^{-4} to 10^{-2} wt%, a small increase in the correlation time values is recorded over the entire pH range. Once the alumina concentration is increased to 1 wt %, a marked increase is recorded at pH values 2, 3 and 5.

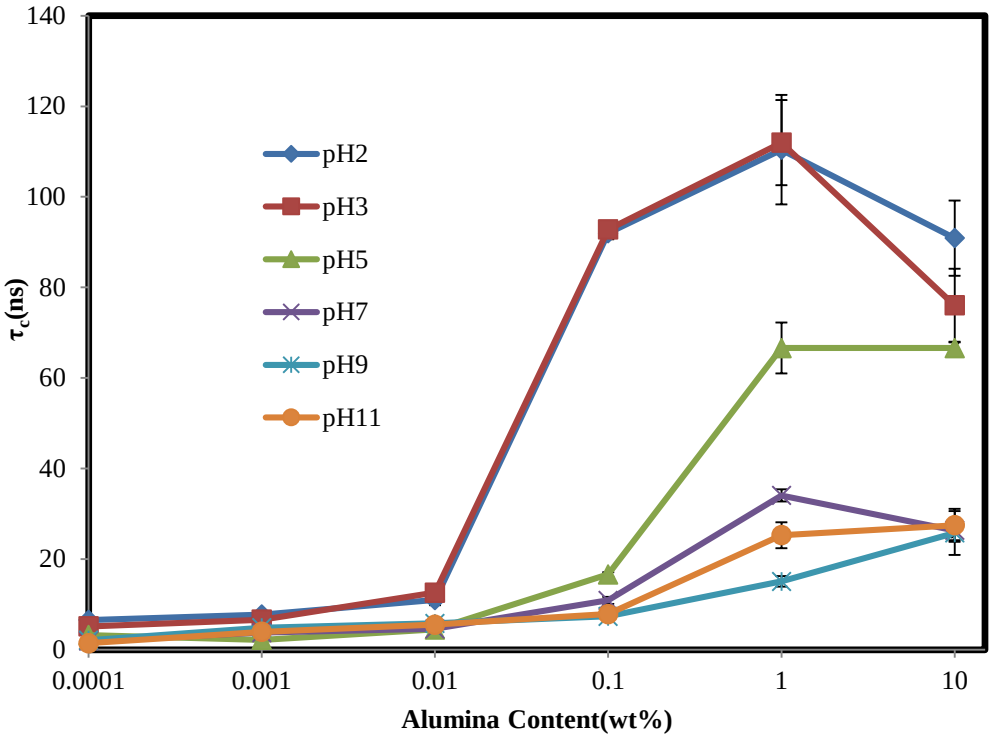

Figure 3.49 Correlation times of ACE-labelled PAA as a function of alumina concentration at various pH values.

3.11. **Conformational Behaviour of ACE-AMMA-PAA as a Function of pH**

The conformational behaviour of ACE (donor) labelled polymer has been discussed in the previous section, for aqueous samples of ACE-labelled-PAA, in which the donor is directly excited at about 290 nm. Herein, the behaviour of donor (ACE)-acceptor (AMMA) labelled PAA is discussed. This type of study provides us with more information about distance distribution of a polymer chain, since we use ACE and AMMA labels covalently bound to poly (acrylic acid) backbone. As previously mentioned, the donor and acceptor labelled are randomly distributed within the chain. An energy transfer experiment was performed for the donor-acceptor pair upon steady-state fluorescence intensity and excited state lifetime measurements under different conditions, such as pH and ionic strength. The principle behind fluorescence resonance energy transfer is displayed in Figure 1.11 (Chapter 1).

3.11.1. **Fluorescence steady state spectra of ACE-AMMA-PAA as a function of pH**

Figure 3.50 displays an emission scan of ACE-AMMA-labelled-PAA in aqueous solution as a function of pH. A 10^{-2} wt% of polymer concentration is dilute enough to investigate single macromolecule conformational behaviour[54]. The excitation wavelength is fixed at 290 nm, a characteristic of the donor. The emission range includes the emission wavelengths of ACE (~340 nm) and AMMA (~420 nm), respectively.

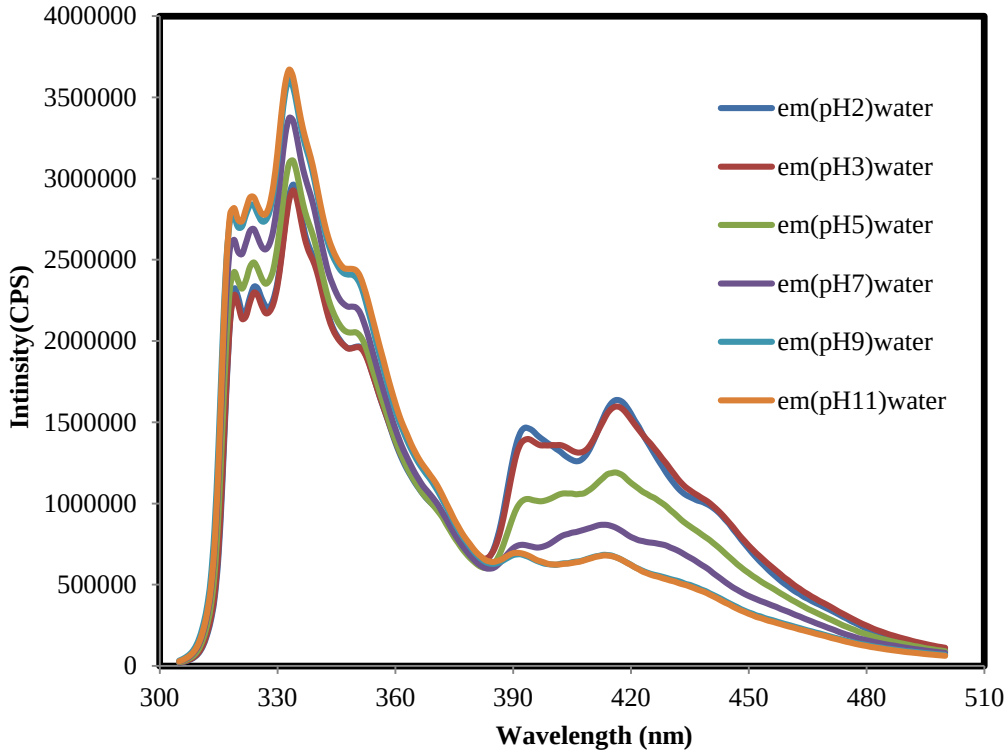

Figure 3.50 Emission scan in a range equal to 300-500 nm at fixed excitation λ_{ex}= 290 nm for ACE-AMMA-PAA (10^{-2} wt % in water) at different pH values.

From above figure, it can be observed that ACE label (donor) emits at ~340 nm when it is directly excited at 290 nm, whereas AMMA (acceptor) emits at ~420 nm, this emission could be because of both some direct absorption at 290 nm, which is enough for its emission, and some energy transfer of excitation from the donor molecule. In acidic media, pH below 7, the ACE emission peak decreases because of excitation of the AMMA fluorophore, whose emission increases because of *ET* from donor.

This transition in the energy indicates that the distance between the donor and the acceptor becomes shorter, which suggests that the polymer chain exists in a collapsed shape due to the protonation process, see Figure 1.6 (Chapter 1). In contrast, under basic conditions the AMMA emission peak quenches and any observable peaks could be attributed to a direct excitation of an acceptor molecule rather than *ET,* which cannot occur when the polyelectrolyte chain exists in an expanded form due to the repulsion of carboxylic groups (see Figure 1.6).

Experimentally, the energy transfer efficiency (*ET*) has been calculated as a function of pH from the maximum fluorescence intensity peaks of ACE-AMMA-PAA emission spectra, as shown in the following equation:

$$\mathrm{ET} = \frac{Enhansed\ acceptor\ emission}{Quenched\ donor\ emission} = \frac{I_A(\lambda_{max}=420\ nm)}{I_D(\lambda_{max}=340\ nm)} \qquad \text{Equation 3.6}$$

Where *ET* is energy transfer efficiency, I_A represents the maximum fluorescence intensity peak of the acceptor, I_D is the maximum fluorescence intensity peak of the donor.

Figure 3.51 shows the energy transfer efficiency as a function of pH. It can be observed that the ratio of acceptor peak to donor peak increases as the pH decreases, a collapsed form is shaped, while its decrease when the pH increases results in an expanded form.

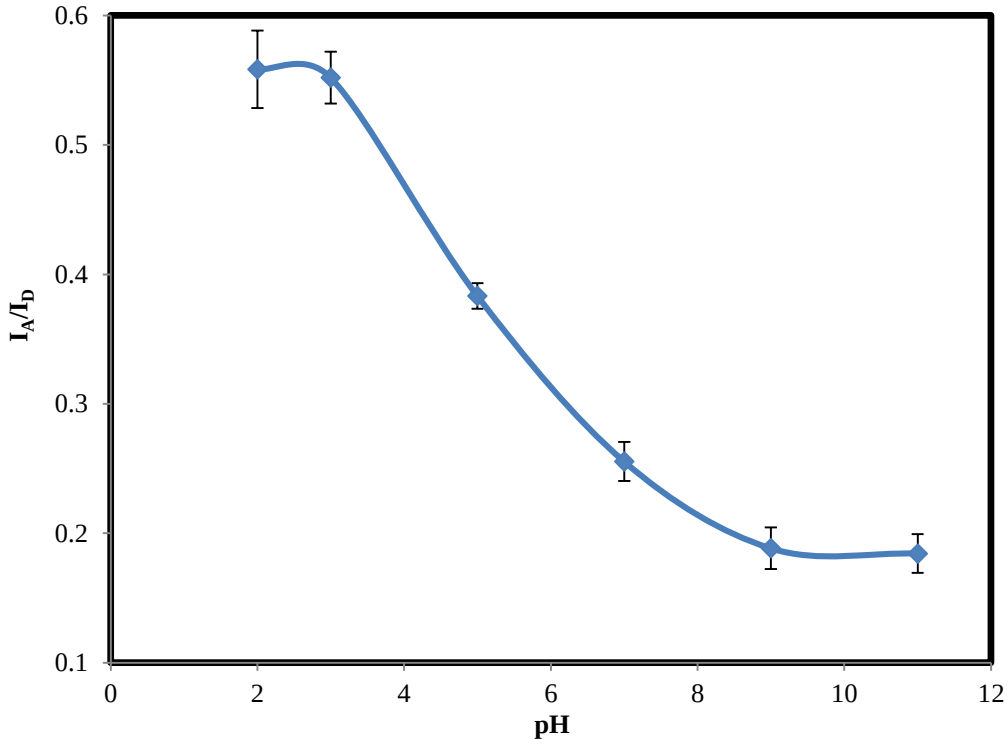

Figure 3.51 Ratio of emission at λ_{em} = 420nm (AMMA) to emission at λ_{em} = 340nm (ACE) exciting at 290nm with varying pH for 10^{-2} wt% from ACE-AMMA-PAA in water.

In particular, at pH 2 and 3 the ratio is at maximum ~0.55 indicating ~55% efficiency of energy transfer in the partially coiled form of poly (acrylic acid) chain, since at theses pH values the vast majority of carboxylate groups are protonated [22]. When the transition in conformation occurs, pH value between 4 and 6 a marked decrease in I_A/I_D ratio is recorded, this means that some of carboxylic groups become deprotonated and accordingly bear a negative charge, which in turn leads to a partially expanded form [22]. Contrary to this, the ratio declines to ~0.20 in pH >7, which suggests that the polyelectrolyte chain exists in a more expanded form at strong basic media. In other words, more carboxylic groups become deprotonated, hence additional negative charges are produced.

3.11.2. **Fluorescence exited state lifetimes of ACE-AMMA-PAA as a function of pH**

For the purpose of an additional explanation for the phenomenon of energy transfer, which provides us with more information about the distance distribution of a polymer chain, ACE fluorescence decays were collected over the whole pH range for ACE-AMMA-PAA as previously measured for a singly labelled

polymer (see section 3.6.2.). A triple exponential function of the form of Equation 3.7 was applied to adequately interpret the fluorescence decay data when energy transfer occurs, meaning under acidic conditions, while at basic media the use of a double exponential (Equation 3.3) was enough to fit the decay data. The average lifetimes were calculated using Equation 3.8.

$$I(t) = A + B_1\ exp^{-t/\tau_{f1}} + B_2\ exp^{-t/\tau_{f2}} + B_3\ exp^{-t/\tau_{f3}} \qquad \text{Equation 3.7}$$

$$< \tau_f >= \frac{[B_1(\tau_{f1})^2 + B_2(\tau_{f2})^2 + B_3(\tau_{f3})^2]}{[(B_1\tau_{f1}) + (B_2\tau_{f2}) + (B_3\tau_{f3})]} \qquad \text{Equation 3.8}$$

By relating average lifetimes for ACE-PAA and ACE-AMMA-PAA, listed in Table 3.2, we note that at pH < 6 the $<\tau_f>$ values are lower for the donor in the presence of AMMA than for ACE without acceptor. Specifically, at pH 1 the ACE fluorophore in ACE-PAA remains excited ~4.5 ns larger than the donor in ACE-AMMA-PAA. This indicates that the maximum efficiency of energy transfer occurs when the polymer chain is collapsed at low pH values.

Table 3.2 Average lifetimes <τf> comparison for ACE-PAA and ACE-AMMA-PAA samples in aqueous solution at different pH values.

pH	<τf> (ns)/ACE-PAA	<τf> (ns) ACE-AMMA-PAA
1	37.81 ± 0.53	33.22 ± 0.25
2	37.81 ± 0.53	33.41 ± 0.23
3	36.00 ± 0.12	34.33 ± 0.31
4	34.73 ± 0.22	34.19 ± 0.37
5	30.87 ± 0.50	30.82 ± 0.50
6	27.01 ± 0.10	28.61 ± 0.12
7	26.05 ± 0.11	26.45 ± 0.06
8	26.17 ± 0.57	26.37 ± 0.08
9	24.97 ± 0.40	25.03 ± 0.05
10	24.58 ± 0.36	25.18 ± 0.07
11	24.34 ± 0.43	25.03 ± 0.13
12	24.28 ± 0.38	25.22 ± 0.13

There are no important differences in average lifetime values of ACE in ACE-PAA and ACE-AMMA-PAA polymers, when the pH varied from 6 to 12 (above the conformational transition pH). In this range of pH, higher expansion of the polyelectrolyte chain occurs because of the electrostatic repulsions of negatively charged COO^- groups [22]. As a result, the distance between the donor and the acceptor is longer and thus no important energy transfer is observed.

Average lifetimes for ACE-PAA and ACE-AMMA-PAA, listed in the above are plotted versus pH in Figure 3.52. Both curves display the similar pattern obtained from the I_A/I_D ratio against pH, see Figure 3.51. Therefore, the shape of the plot may also be attributed to the conformational transition occurring for the PAA chain when pH is changed. Such a transition goes from a partially expanded chain at high pH, short $<\tau_f>$ is recorded, to a partially collapsed form at low pH, longer $<\tau_f>$ is observed. In addition, we can see from Figure 3.52 that the conformational transition pH (~5) which separates both forms is approximately matched for ACE-PAA and ACE-AMMA-PAA polymers. This similarity for double and single labelled polymers suggests that the attachment of covalently bound AMMA does not affect the conformational behaviour of the poly (acrylic acid) chain.

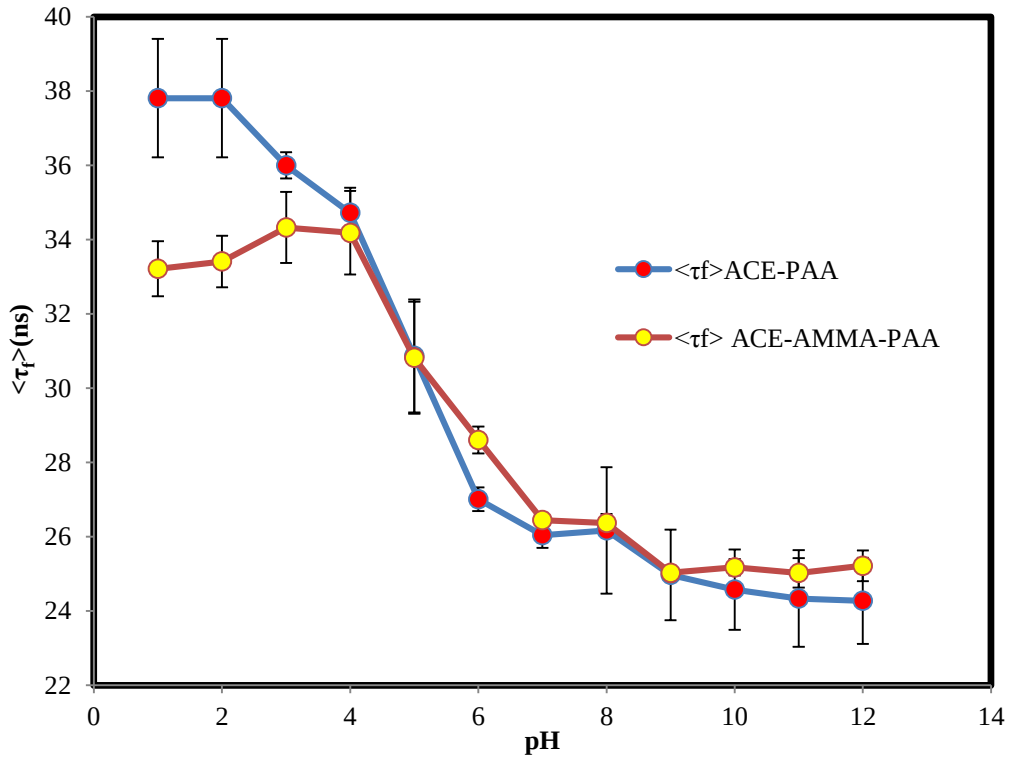

Figure 3.52 Average donor lifetime <τf> for ACE-PAA and ACE-AMMA-PAA as a function of pH (λ_{ex} = 295 nm and λ_{em} = 340 nm).

When donor-acceptor pairs are randomly attached to the polyelectrolyte chain, the distribution of distances between such pairs is related to the chain dimensions. Since fluorescence steady-state data cannot be used to measure the distance distribution of fluorescently doubly labeled polymer. We used average lifetimes for ACE-PAA and ACE-AMMA-PAA to determine such distribution, as described in next equation:

$$r^6 = \left(\frac{R_o^6}{ET}\right) - R_o^6 \qquad \text{Equation 3.9}$$

Where r is the actual separation distance in a particular system, R_o, the distance for ACE-AMMA pair involved in our studies, is 2.3 nm [19], and ET is the energy transfer efficiency, which can be determined, using the following equation:

$$ET = 1 - \frac{<\tau_{ET}>}{<\tau_D>} \qquad \text{Equation 3.10}$$

Where $<\tau_{ET}>$ represents the average lifetime of the ACE-AMMA-PAA and $<\tau_D>$ represents the average lifetime of the ACE-PAA.

Table 3.3 presents the actual separation distance in the poly (acrylic acid) chain as a function of pH. As expected, a decrease in the separation distance between the donor and acceptor is noted when the pH is decreased, this short distance indicates that the polymer chain is in a collapsed form. In contrast, an expanded form causes an increase in the separation distance when the pH is increased.

We particularly found that at pH 1, the distance between ACE and AMMA was 3.50 nm, which is within the Förster distance for donor-to-acceptor energy transfer [38]. At the higher pH of 5 (transition point) the ACE and AMMA rise up to 7.29, but at more than pH 5 the distance cannot be determined. This is because in this case the separation distance is believed to be more than 10 nm, which is completely out of ET range. All the separation distance numbers are within the range of the values obtained by dynamic light scattering technique [83].

Table 3.3 The distance between donor and acceptor as a function of pH.

pH	r/nm
1	3.50 ± 0.11
2	3.53 ± 0.13
3	4.15 ± 0.05
4	4.99 ± 0.8
5	7.29 ± 0.12

3.12. **Conformational Behaviour of ACE-AMMA-PAA and Its Interaction with NaCl Concentration**

As we observed in sections (sections 3.11.1. and 3.11.2.), under basic conditions the separation distance between ACE and AMMA is long and no ET was detected. This was attributed to the polyelectrolyte chain existing in an expanded form due to the mutual repulsion of negatively charged carboxylate groups (COO^-). Therefore, the effect of salt addition (NaCl) on the separation distance in an expanded polymer chain was studied. The fluorescence steady state

and lifetime data are collected for the ACE-AMMA-labelled-PAA at fixed pH value as a function of sodium chloride concentration.

3.12.1. **Fluorescence steady state spectra of ACE-AMMA-PAA as a function of NaCl concentration**

Figure 3.53 shows the energy transfer efficiency as a function of the sodium chloride concentration at pH 9. It can be seen that the acceptor to donor ratio increases as the NaCl concentration increases, this suggests that the polyelectrolyte chain collapses when Na^+ ions are added.

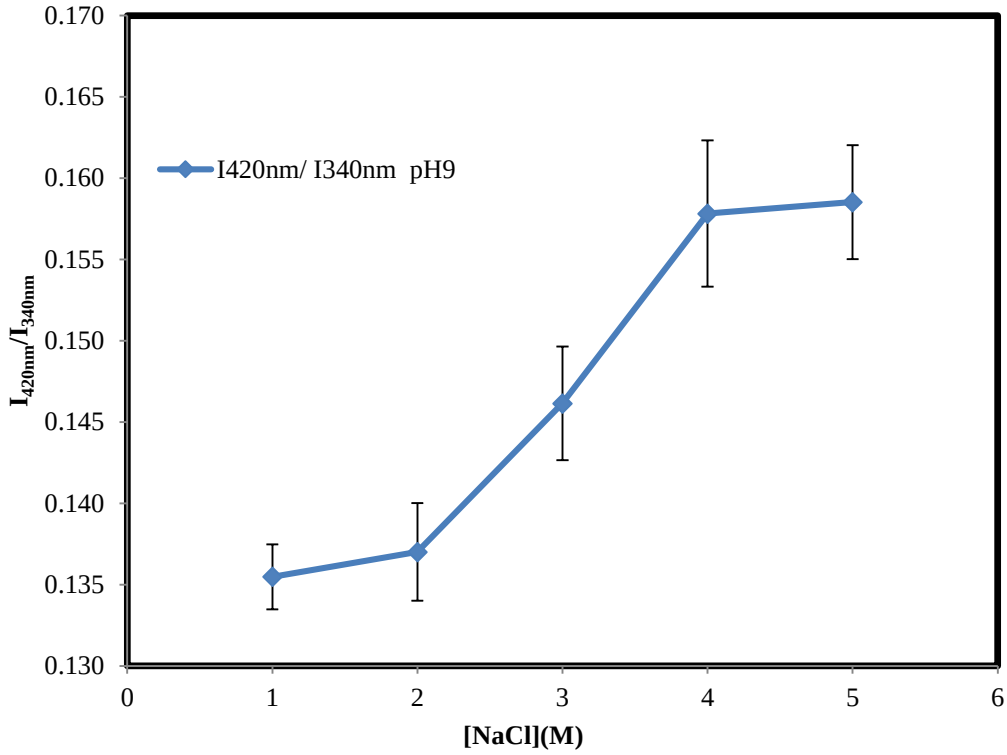

Figure 3.53 Fluorescence emission intensity ratio, I_A/I_D of 10^{-2} wt % ACE-AMMA-labelled PAA as a function of NaCl concentration at pH 9. (λ_{ex} = 290nm).

In particular, at 4 and 5 M NaCl added the ratio is at maximum ~0.16 indicating ~16% efficiency of energy transfer in the partially coiled form of PAA chain, since at these extremely concentrated values of Na^+ ions, several of negatively charged carboxylate groups are screened by sodium cations (see Figure 3.28). When the transition in conformation occurs, at 3 M of NaCl, a noticeable increase in I_A/I_D ratio is observed, this suggests that a few of the carboxylate groups become neutralised and hence lead to the conversion of the

expanded chain to a partly aggregated form. In contrast, the ratio drops to ~0.13 at low NaCl concentration (1 and 2 M), which suggests that the polyelectrolyte chain still exists in an expanded form compared to PAA in water.

3.12.2. **Fluorescence excited state lifetimes of ACE-AMMA-PAA as a function of NaCl concentration**

Average donor lifetimes for ACE-AMMA-PAA are plotted against [NaCl] in Figure 3.54. As it can be observed, the curve exhibits the opposite pattern obtained from the I_A/I_D ratio against NaCl concentration, see Figure 3.53. However, the shape of the plot could be attributed to the fact that a conformational transition occurs for the polymer chain, when the concentration of added salt is increased. Such a transition goes from a partially expanded chain at low NaCl concentration, long $<\tau_f>$ is observed, to a partially collapsed form at high concentration of NaCl, $<\tau_f>$ is slightly quenched to ~ 20 ns due to energy transfer to acceptor.

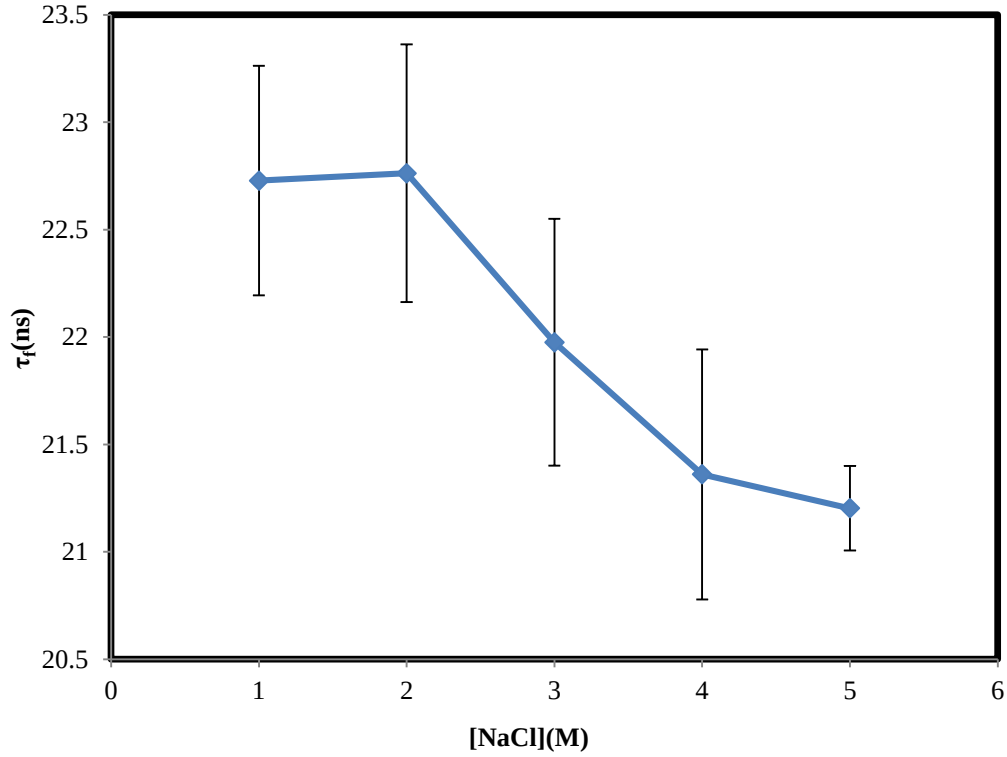

Figure 3.54 Fluorescence excited state average lifetimes of 10^{-2}wt%ACE-AMMA-labelled-PAA as a function of NaCl at pH 9 (λ_{ex}= 295nm and λ_{em}= 340nm).

3.13. **Conformational Behaviour of ACE-AMMA-PAA and Its Interaction with $CaCl_2$**

Similarly, the effect of divalent cations, such as calcium on the separation distance in an expanded polyelectrolyte chain is also investigated. The fluorescence steady state and lifetime data were collected for the ACE-AMMA-labelled-PAA at a fixed pH value as a function of the calcium chloride concentration.

3.13.1. **Fluorescence steady state spectra of ACE-AMMA-PAA as a function of $CaCl_2$ concentration**

Figure 3.55 shows the energy transfer efficiency in ACE-AMMA-PAA as a function of the calcium chloride concentration at pH 9. It can be observed that the I_A/I_D ratio increases as the $CaCl_2$ concentration increases, suggesting that the acceptor gets close to the donor when Ca^{2+} ions are added.

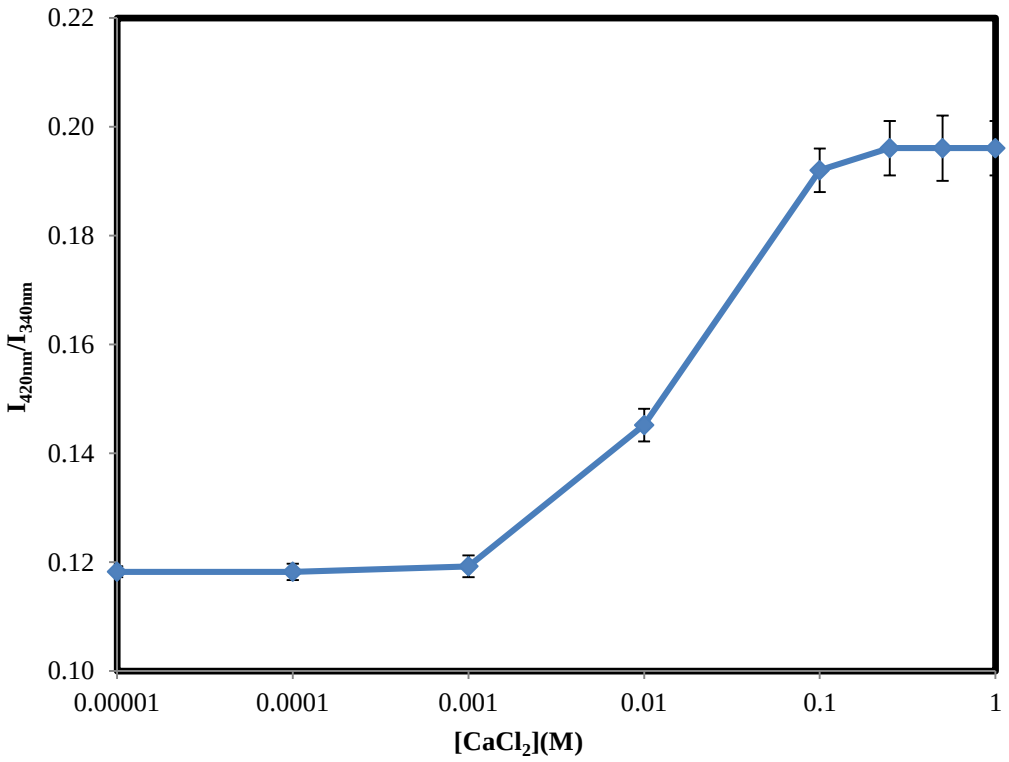

Figure 3.55 Fluorescence emission intensity ratio, I_A/I_D of 10^{-2} wt% ACE-AMMA-labelled PAA as a function of $CaCl_2$ concentration at pH 3 and pH 9.(λ_{ex} = 290nm).

When the concentration of salt is increased from 0.1 to 1M, the acceptor to donor ratio reaches the extreme ~0.20, indicating ~20% efficiency of energy transfer in the partially coiled form of polyelectrolyte chain. Since at theses concentrated values from calcium chloride, negatively charged carboxylate groups are linked by Ca^{2+} ions, this crosslinking leads to chain aggregation (see Figure 3.28). When the transition in conformation occurs, at 0.01 M of $CaCl_2$, a marked increase in I_A/I_D ratio is observed, suggesting that the existence of a sufficient amount of Ca^{2+} ions to crosslink the carboxylate groups and ,accordingly, lead to the conversion of the expanded chain to a partially aggregated form. In contrast, the ratio falls to ~0.11 at low $CaCl_2$ concentration (0.00001 to 0.001 M), suggesting that the polyelectrolyte chain still exists in an expanded form compared to PAA conformation in water.

3.13.2. **Fluorescence excited state lifetimes of ACE-AMMA-PAA as a function of $CaCl_2$ concentration**

Average donor lifetimes for ACE-AMMA-PAA are plotted against [$CaCl_2$] in Figure 3.56. It can be seen that the curve shows the reverse pattern gained from the I_A/I_D ratio against $CaCl_2$ concentration, as presented in Figure 3.55. Nevertheless, the shape of the plot can tell us about a conformational transition occurring in the polyelectrolyte chain when the concentration of added calcium chloride is increased from 0.00001 to 1 M. This transition goes from a partially expanded chain at low $CaCl_2$ concentration (from 0.00001-0.001 M), long $<\tau_f>$ is recorded ~25 ns, to a partially collapsed form at high concentration of $CaCl_2$, $<\tau_f>$ is slightly quenched to ~ 21 ns due to an energy transfer to the acceptor.

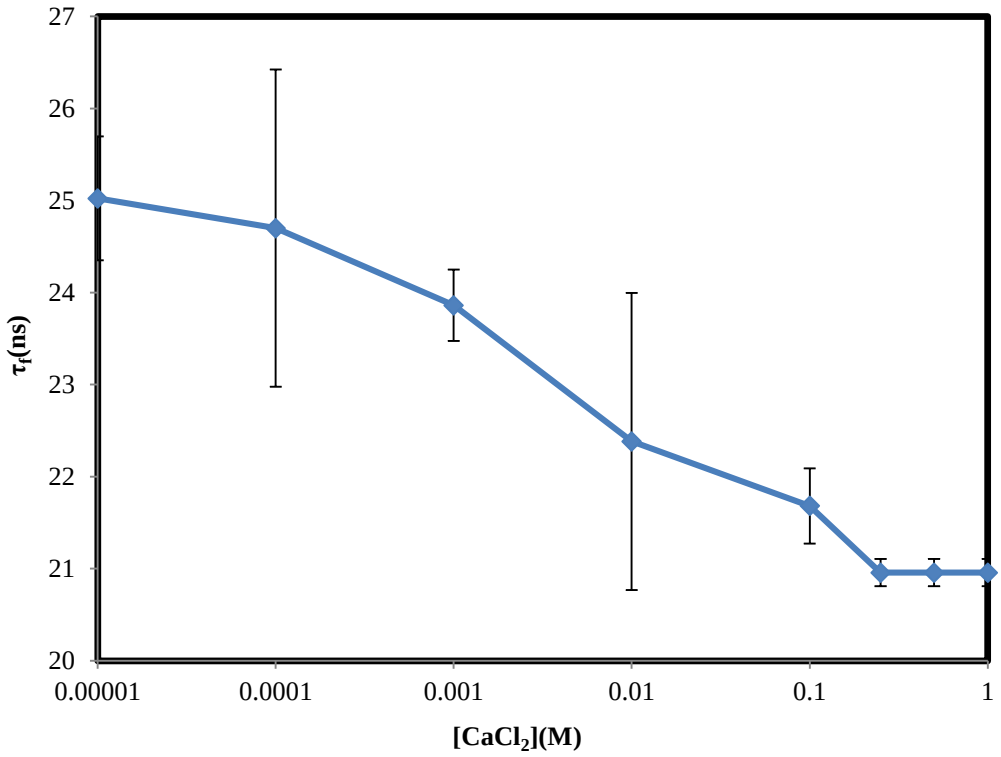

Figure 3.56 Fluorescence excited state average lifetimes of 10^{-2}wt%ACE-AMMA-labelled-PAA as a function of $CaCl_2$ at pH 9 (λ_{ex}= 295nm and λ_{em}= 340nm).

3.14. **Adsorption of ACE-AMMA-PAA on Silica as a Function of pH**

In this section, the adsorption behaviour of a fluorescently doubly labelled poly (acrylic acid) on silica was investigated as a function of mineral concentration and pH. Fluorescence analysis includes steady state and excited state lifetimes, applied to investigate the conformations of poly (acrylic acid), adsorbed at the water-mineral interface.

The application of fluorescence resonance energy transfer (FRET) to investigate the conformational change of a polymer at the solid-liquid interface is the aim of this experiment.

3.14.1. **Fluorescence steady state spectra of ACE-AMMA-PAA on silica as a function of pH**

Figure 3.57 to Figure 3.60 show the fluorescence emission spectra of 0.01 wt% of ACE-AMMA-PAA at pH 2 and 11 in water and 1 wt% silica. The spectra were recorded before and after centrifuging, as described in the adsorption experiment (Chapter 2). At absence of silica, the supernatant displays similar

emission intensity compared to that prior to centrifuging at pH 2 and pH 11 (Figure 3.57 and Figure 3.58). This suggests that the polymer does not settle down by itself during the centrifuging. On the other hand, when the mineral concentration was increased to 1 wt % the emission intensity of the supernatant was quenched at pH 2 compared to pH 11 (see Figure 3.59 and Figure 3.60). It can be concluded that a considerable amount of polymer attached to silica at pH 2 and negligible amount is adsorbed at pH 11.

As can be observed in Figure 3.59, the acceptor emission peaks (at about 420nm) appear when the pH was decreased for the adsorbed polymer on silica in a similar way as was presented for the polyelectrolyte in a solution, see Figure 3.57. This similar photo-physical behaviour supposes that in both the cases of the free and, the absorbed solution, the polymer exhibits a collapsed conformation at acidic pH, where the AMMA peak is generated**.** On the other hand, a deprotonation of the carboxylic acid groups makes the chain backbone bear a negative charge, which leads to an electrostatic repulsion and as a result, the vast majority of the polymer expands in the bulk solution and a tiny amount of it on the surface of the silica. This expansion can be noted by quenching the AMMA peaks at pH11.

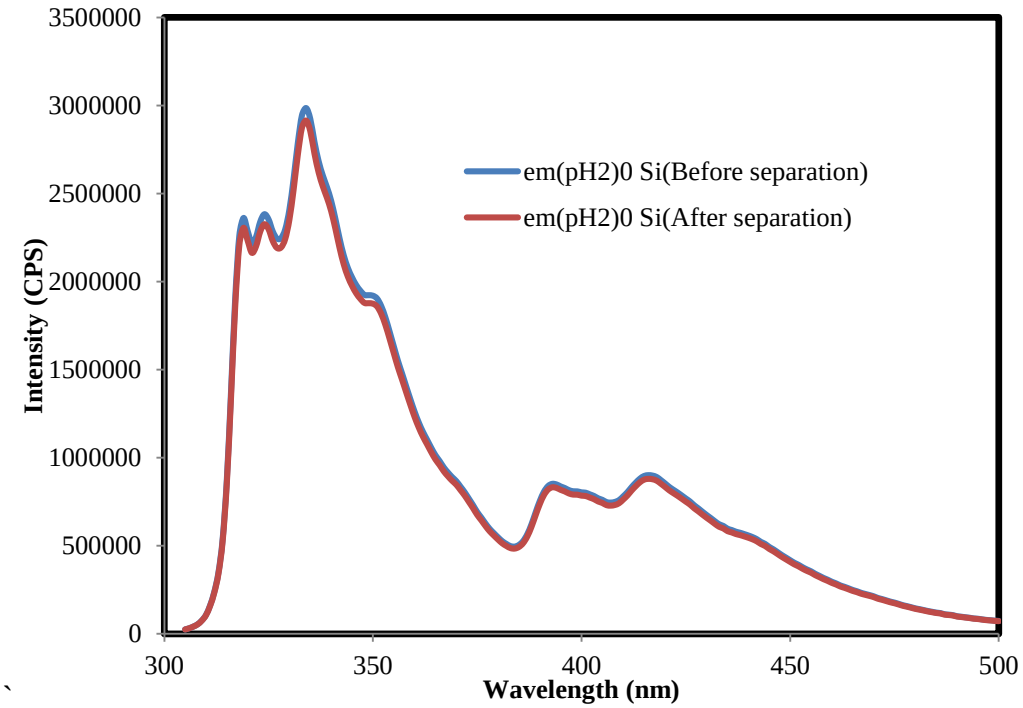

Figure 3.57 Emission spectra for ACE-AMMA-PAA (10^{-2} wt% in water) before and after separation at pH 2.

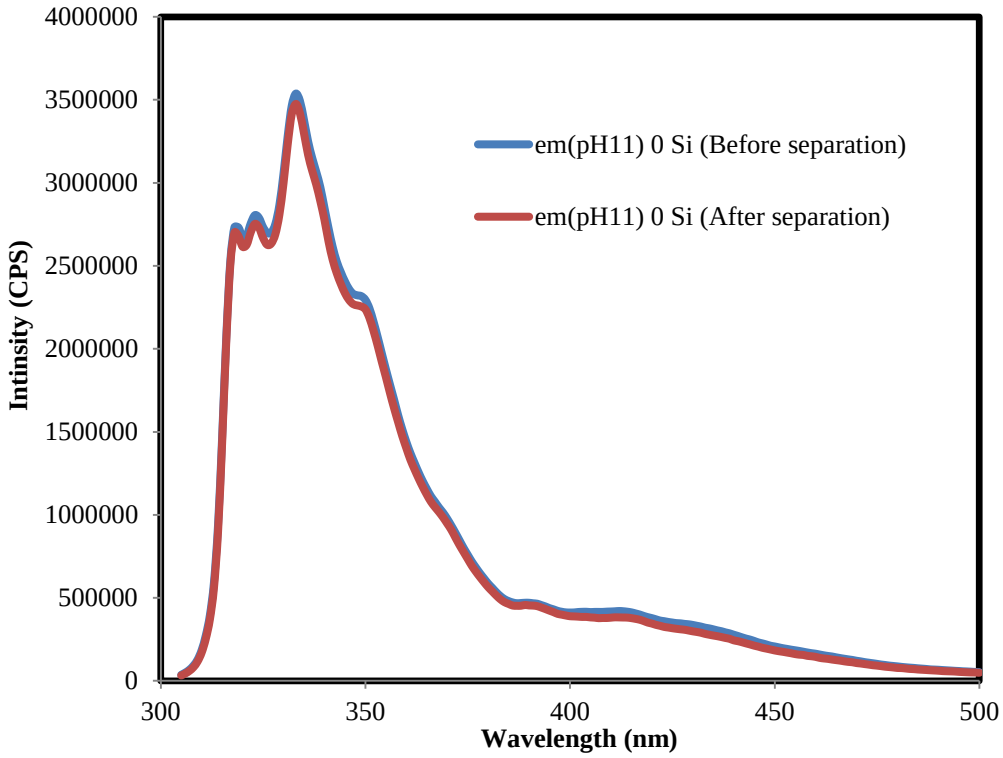

Figure 3.58 Emission spectra for ACE-AMMA-PAA (10^{-2} wt % in water) before and after separation at pH 11.

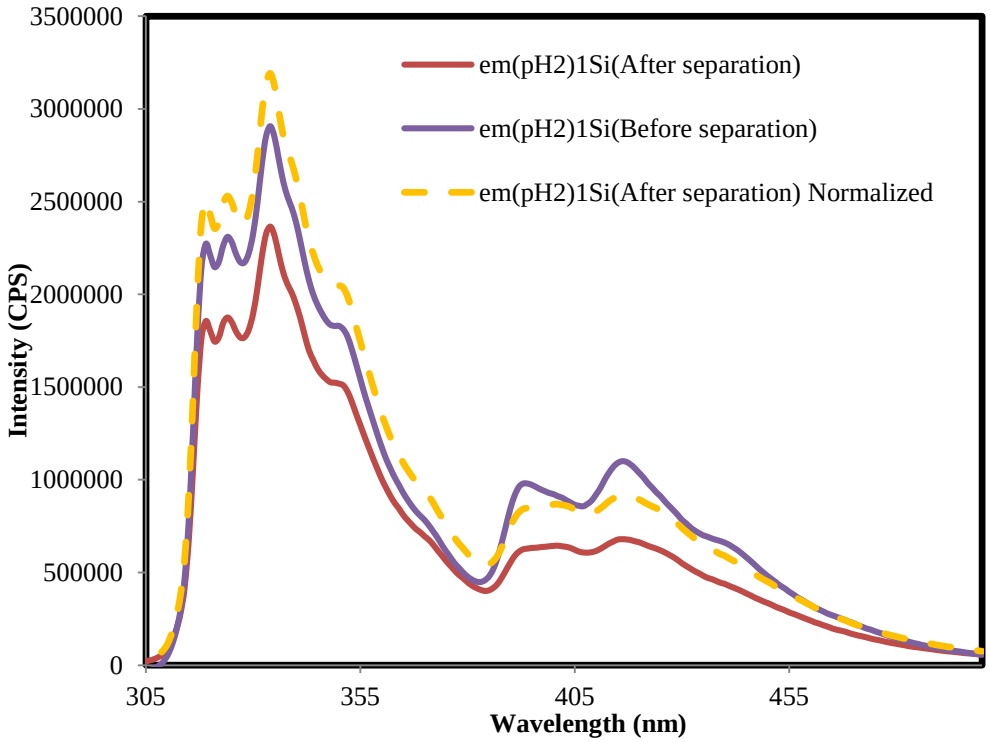

Figure 3.59 Emission spectra for ACE-AMMA-PAA (10^{-2} wt% in 1wt% Si) before and after separation at pH 2.

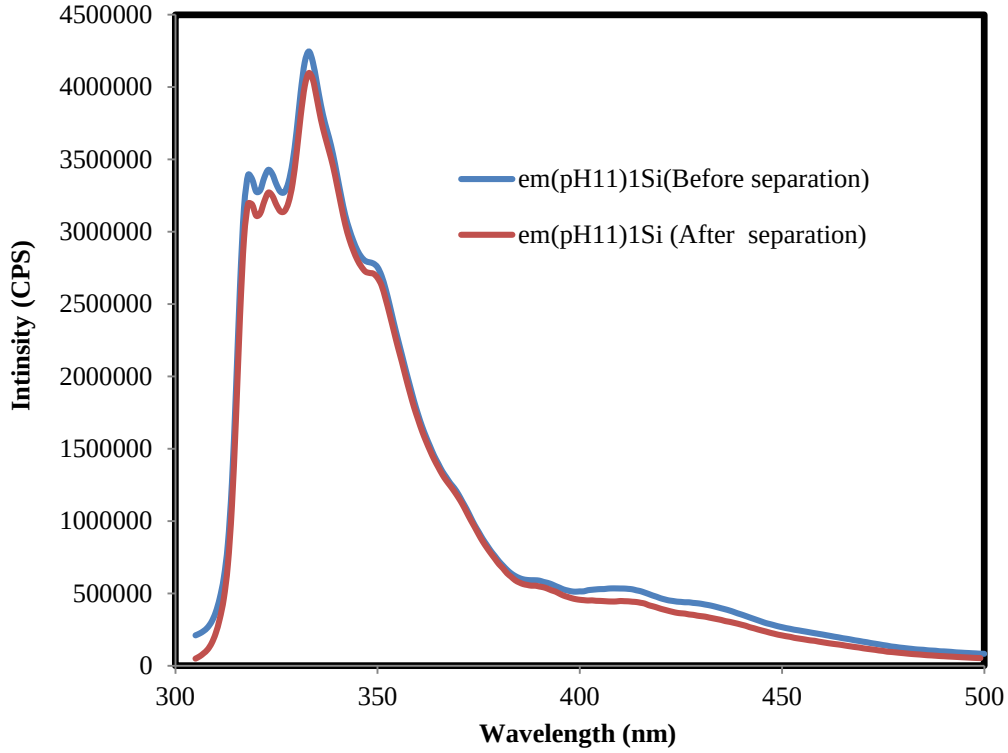

Figure 3.60 Emission spectra for ACE-AMMA-PAA (10^{-2} wt % in 1wt% Si) before and after separation at pH11.

In the previous *ET* experiments we showed that the I_A/I_D ratio increases when the separation distance between donor and acceptor decrease. Since a large value of I_A/I_D indicates polymer chain contraction, while a small value suggests polymer chain expansion. Thus, comparisons of the dependence of acceptor-donor ratio in free solution (after separation), and at adsorbed state (before separation) provides information about donor-acceptor separation distance, and hence the conformation of PAA chain in both bulk solution and at liquid-solid interface.

We carried out energy transfer experiments to understand the conformational behaviour of polymer when it is attached to mineral surface. Figure 3.61 to Figure 3.63 show ratio of emission I_A/I_D with varying pH for 10^{-2} wt % from ACE-AMMA-PAA in different concentration from silica before and after centrifuging, respectively. Generally, it can be seen that the fluorescence intensity ratio varies as a function of pH for adsorbed polymer on silica (before separation) in a similar fashion as was displayed for polymer in solution (after separation). This proposes the adsorption model schemed in Figure 3.64. At low pH values, the adsorbed polymer coils such that higher I_A/I_D ratio is recorded. On

the contrary, as deprotonation of the carboxylic acid moieties occurs, the polymer chain expands on the silica surface.

When the concentration of silica is increased from 10^{-3} to 1 wt %, a dramatic difference is observed in the fluorescence intensity ratios of ACE-AMMA-PAA before and after separation. At 10^{-3} wt% of silica, the I_A/I_D ratio before and after centrifuging is almost identical, this means that at low concentration of mineral the conformational change of adsorbed polymer behaves exactly like that change in free solution, but at high silica content the energy transfer efficiency before separation is greater than that after separation specially at low pH values. This suggests that the polymer chain is more collapsed at adsorbed state, since the separation distance between the donor and acceptor is closer.

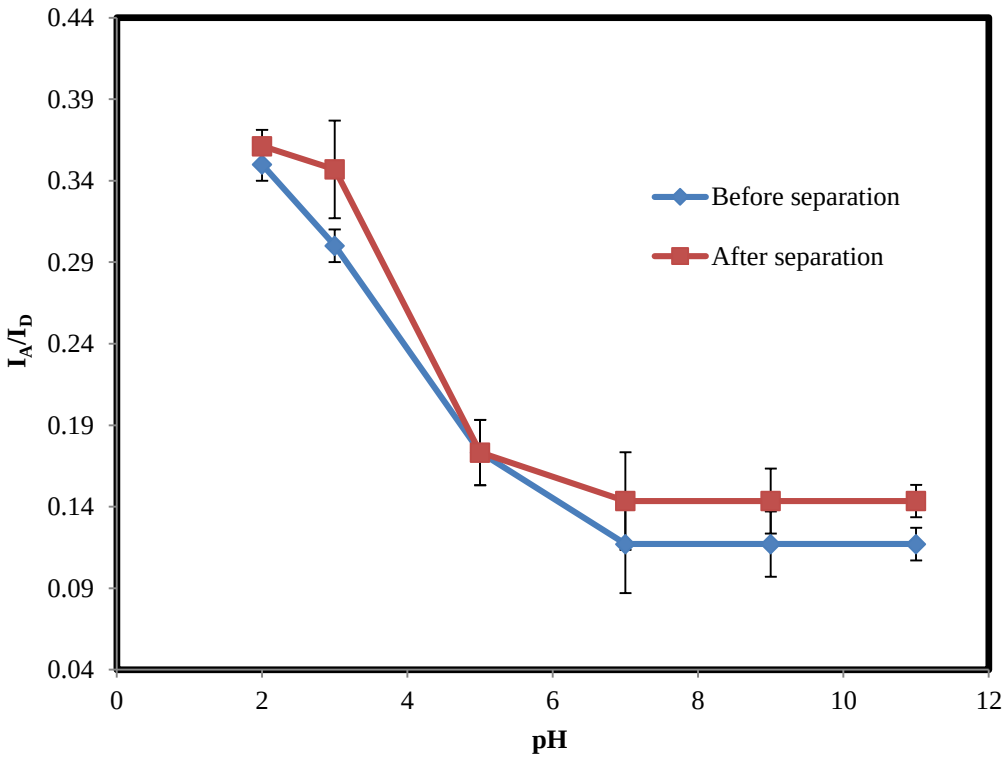

Figure 3.61 Ratio of emission I_A/I_D as a function of pH for 10^{-2} wt% from ACE-AMMA-PAA in 10^{-3}wt% silica, before and after separation.

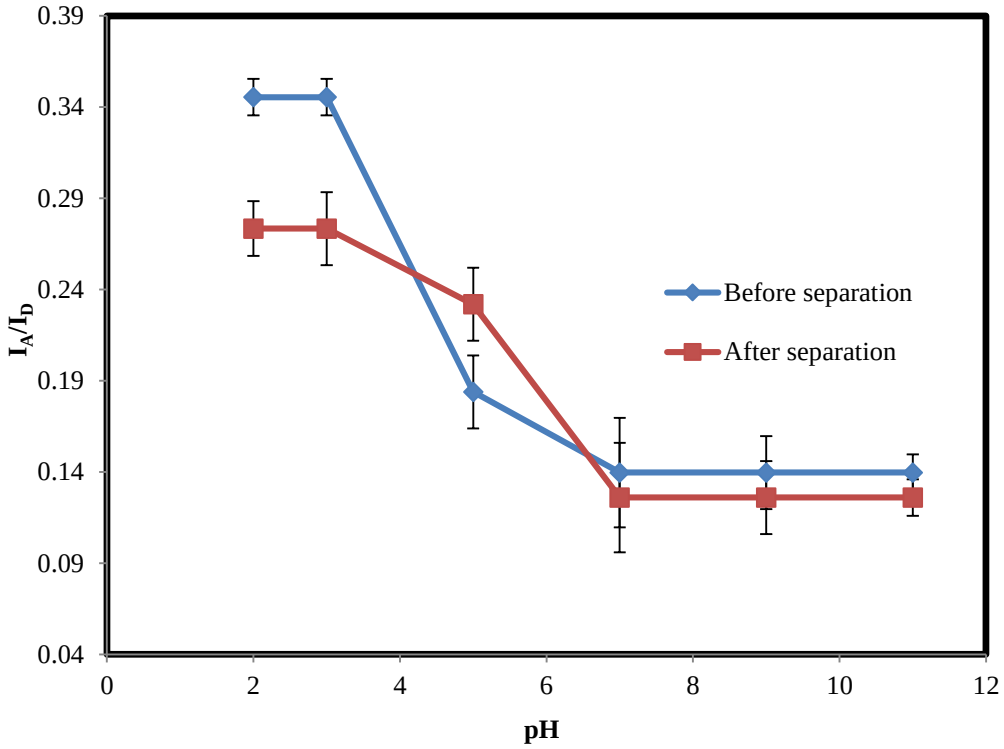

Figure 3.62 Ratio of emission I_A/I_D as a function of pH for 10^{-2} wt % from ACE-AMMA-PAA in 10^{-1}wt% silica, before and after separation.

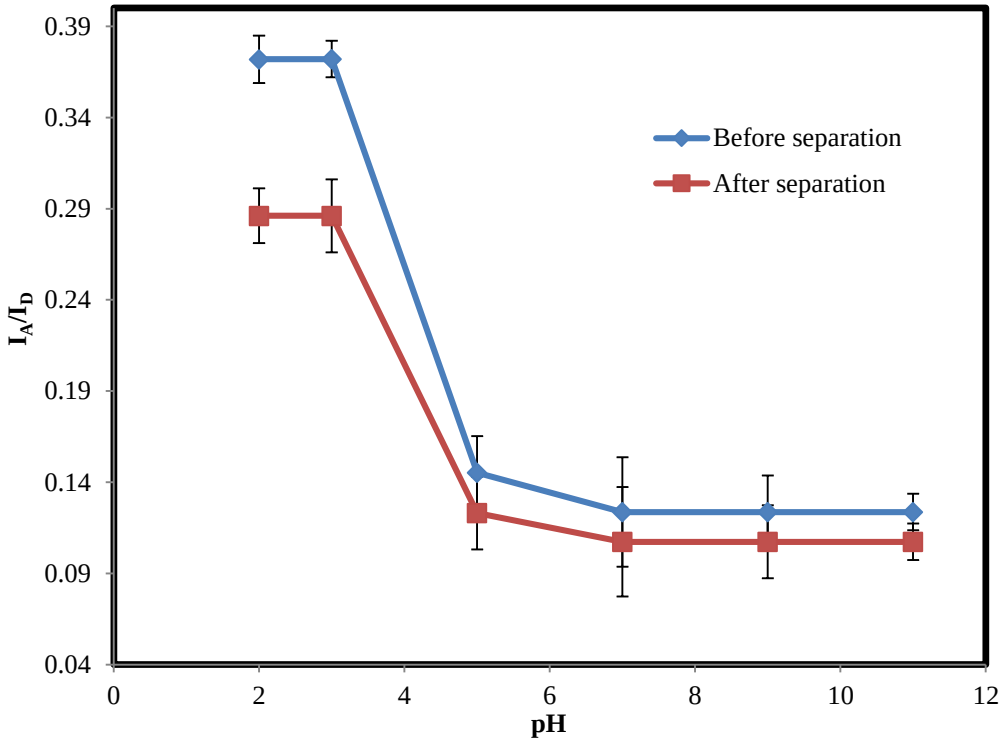

Figure 3.63 Ratio of emission I_A/I_D as a function of pH for 10^{-2} wt % from ACE-AMMA-PAA in 1 wt% silica, before and after separation.

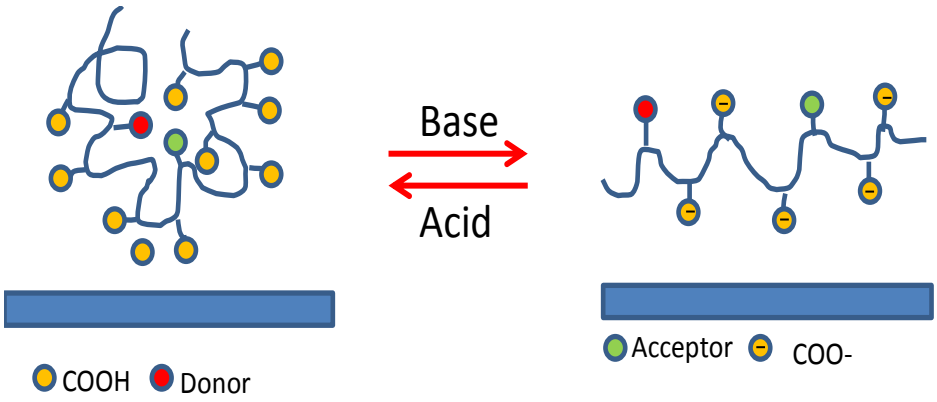

Figure 3.64 Schematic representation of the adsorption of polyelectrolyte on the mineral surface in coiled and extended form.

3.14.2. Fluorescence excited state lifetimes of ACE-AMMA-PAA on silica as a function of pH

Average donor lifetimes <τ> for ACE-PAA and ACE-AMMA-PAA as a function of pH at different silica concentration are plotted in Figure 3.65 to Figure 3.67. All average lifetime values decrease over the pH range involved. Moreover, the rate of decline in these values in ACE-AMMA-PAA is less than in those in ACE-PAA polymer, except at high pH. However, the shape of the plots is due to a conformational transition happening in the polyelectrolyte chain when the pH varies. Such a transition goes from a relatively expanded coil at high pH, which in turn leads to short lifetime values, to a collapsed form at low pH. Longer lifetime values are recorded at these points.

As can be noted from all figures, at pH values 2 and 3, the $<\tau_f>$ values are shorter for donor in ACE-AMMA-PAA, when the silica concentration is increased. This decrease in lifetimes could be attributed to the maximum efficiency of energy transfer occurring from the donor to the acceptor. This maximum transfer is a result of a more compact collapsed polymer being formed by adding more silica.

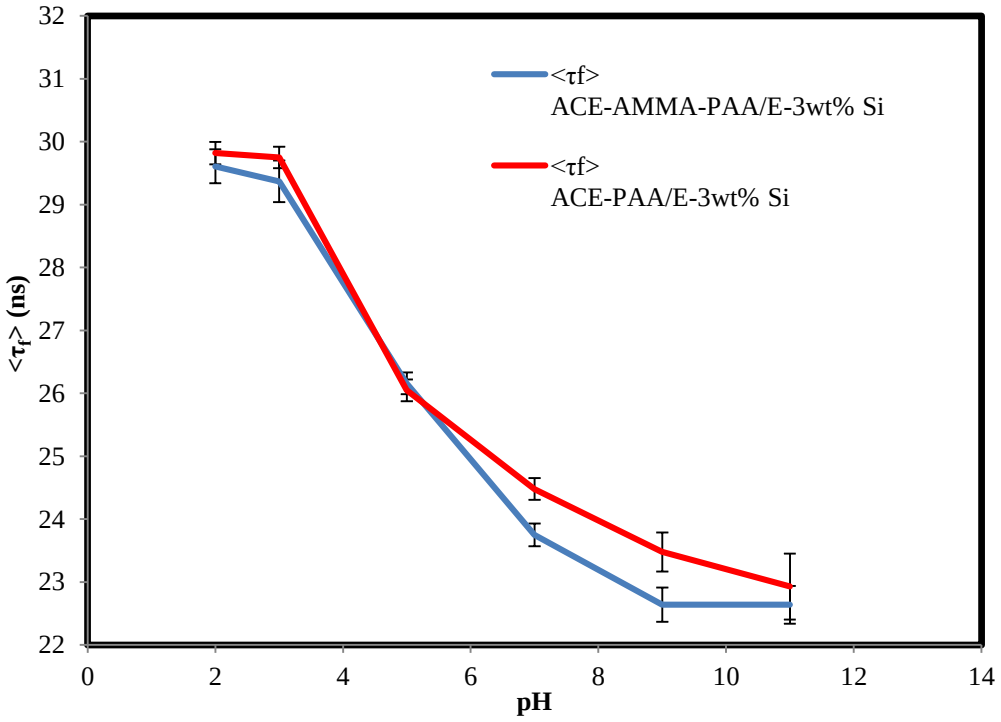

Figure 3.65 Average donor lifetime <τ_f> for ACE-PAA and ACE-AMMA-PAA (10^{-2}wt %) as a function of pH at 10^{-3}wt% silica concentration (λ_{ex} = 295 nm and λ_{em} = 340 nm).

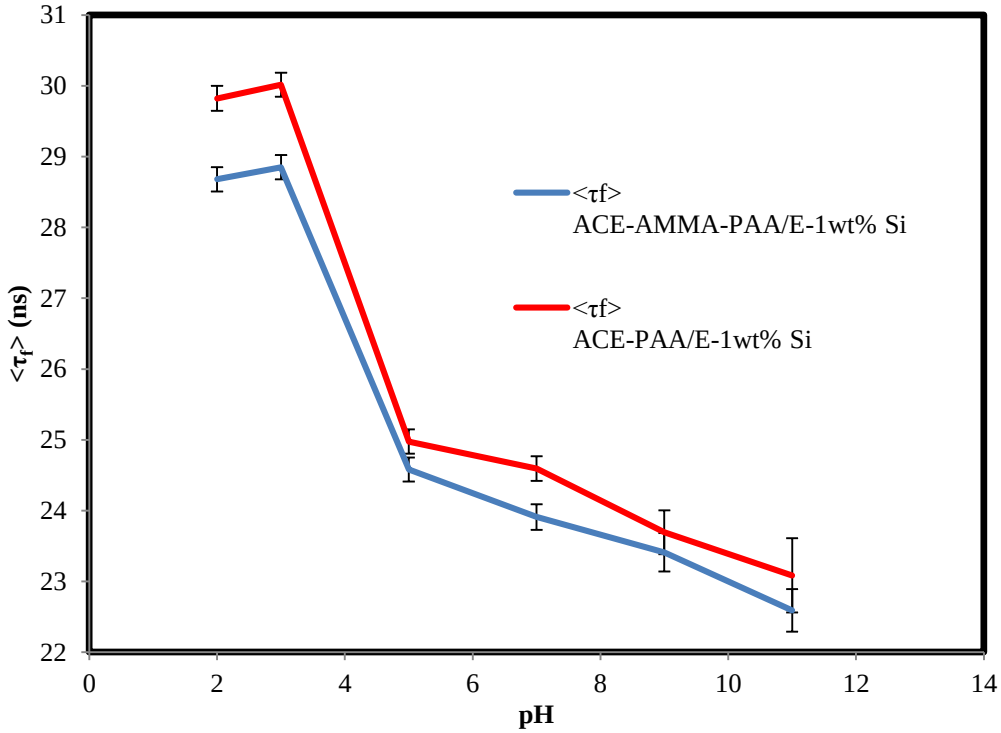

Figure 3.66 Average donor lifetime <τ_f> for ACE-PAA and ACE-AMMA-PAA (10^{-2}wt %) as a function of pH at 10^{-1}wt% silica concentration (λ_{ex} = 295 nm and λ_{em} = 340 nm).

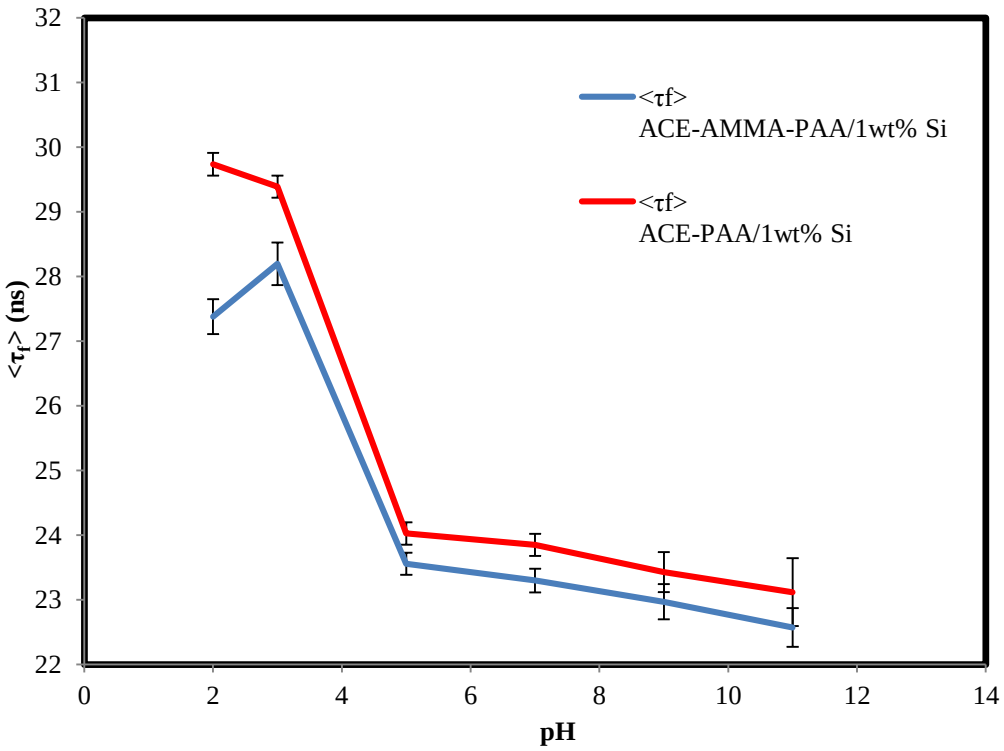

Figure 3.67 Average donor lifetime <τ_f> for ACE-PAA and ACE-AMMA-PAA (10^{-2}wt %) as a function of pH at 1 wt% silica concentration (λ_{ex} = 295 nm and λ_{em} = 340 nm).

3.15. Adsorption of ACE-AMMA-PAA on Alumina as a Function of pH

Similarly, to section 3.14. , the effect of other minerals, such as alumina (Al_2O_3), on the adsorption behaviour of poly (acrylic acid) is investigated as a function of mineral concentration and pH by the FRET principle. Since fluorescence technique, includes steady state and excited state lifetime, is applied to investigate the conformations of PAA adsorbed at the water-mineral interface.

3.15.1. Fluorescence steady state spectra of ACE-AMMA-PAA on alumina as a function of pH

The fluorescence emission spectra of 0.01 wt % of ACE-AMMA-PAA at pH 2 and 11 in 10^{-4} and 1 wt% alumina are presented in Figure 3.68 to Figure 3.71, respectively. The spectra were generated before and after mineral separation via centrifugation technique as previously mentioned in adsorption experiment (Chapter 2). However, at extremely low concentrations of alumina (10^{-4} wt %), the supernatant exhibits an emission intensity identical to that before separation at pH 2 and pH 11 (Figure 3.68 and Figure 3.69). This match suggests that such a low

concentration of solids is not enough to attach to the polymer chain. In other words, the macromolecule still moves freely in the bulk solution. Alternatively, when the alumina concentration was increased to 1 wt%, the emission intensity of the supernatant was sharply quenched at pH 2 compared to pH 11 (Figure 3.70 and Figure 3.71). It can be decided that the vast majority of the polymer chain is attached to the alumina surface at pH 2 and only a small amount is adsorbed at pH 11.

Interestingly, Figure 3.70 also shows that the acceptor emission peak is more intense at pH 2 for the polymer, adsorbed on alumina (before separation), compared with the AMMA peaks for the polyelectrolyte in solution (after separation), see normalized spectra in Figure 3.70. This dissimilar photo-physical behaviour suggests that at the adsorbed state, the PAA chain becomes more coiled at acidic pH than the conformation of the polymer chain in solution**.**

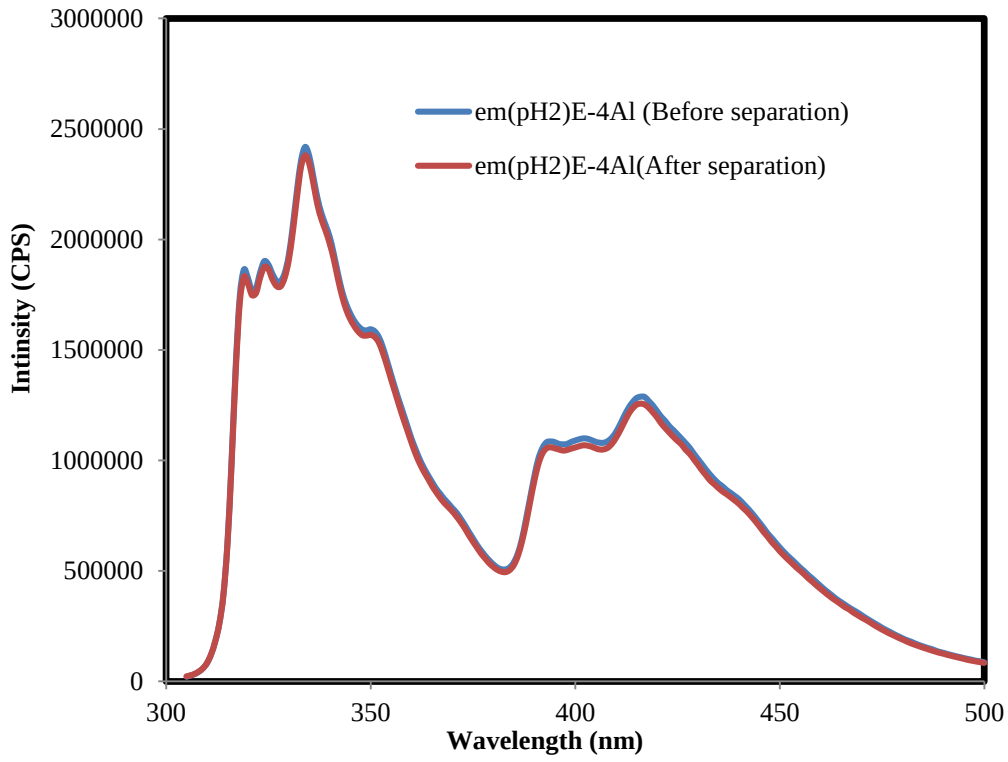

Figure 3.68 Emission spectra for ACE-AMMA-PAA (10^{-2} wt% in 10^{-4}wt% Al) before and after separation at pH 2.

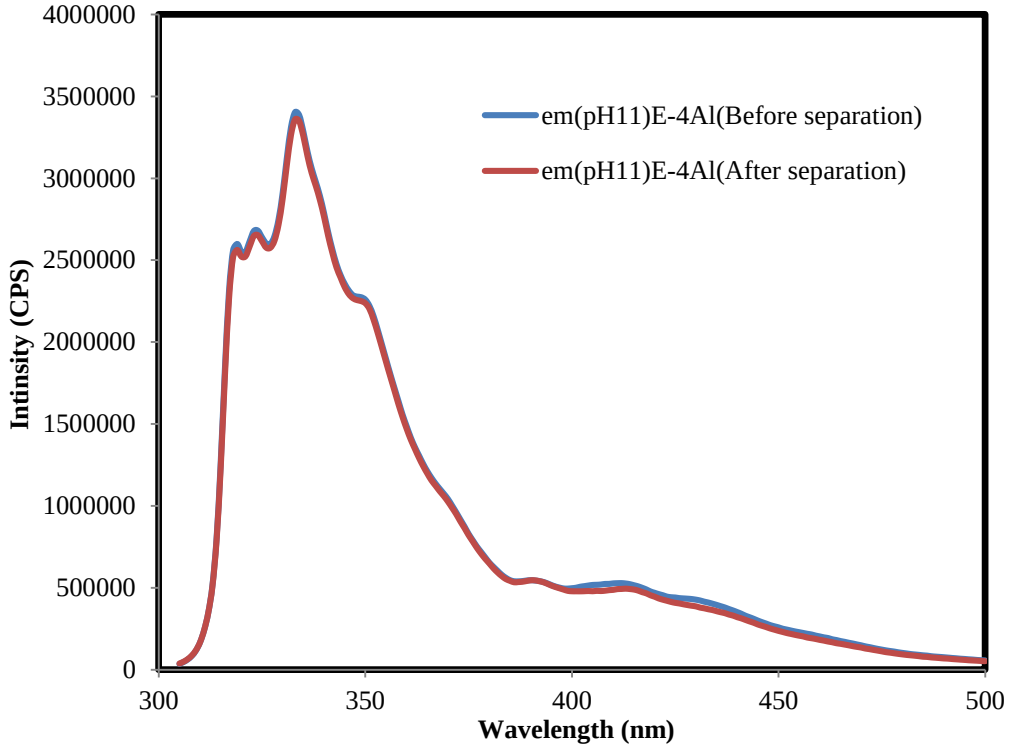

Figure 3.69 Emission spectra for ACE-AMMA-PAA (10^{-2} wt % in 10^{-4}wt% Al) before and after separation at pH 11.

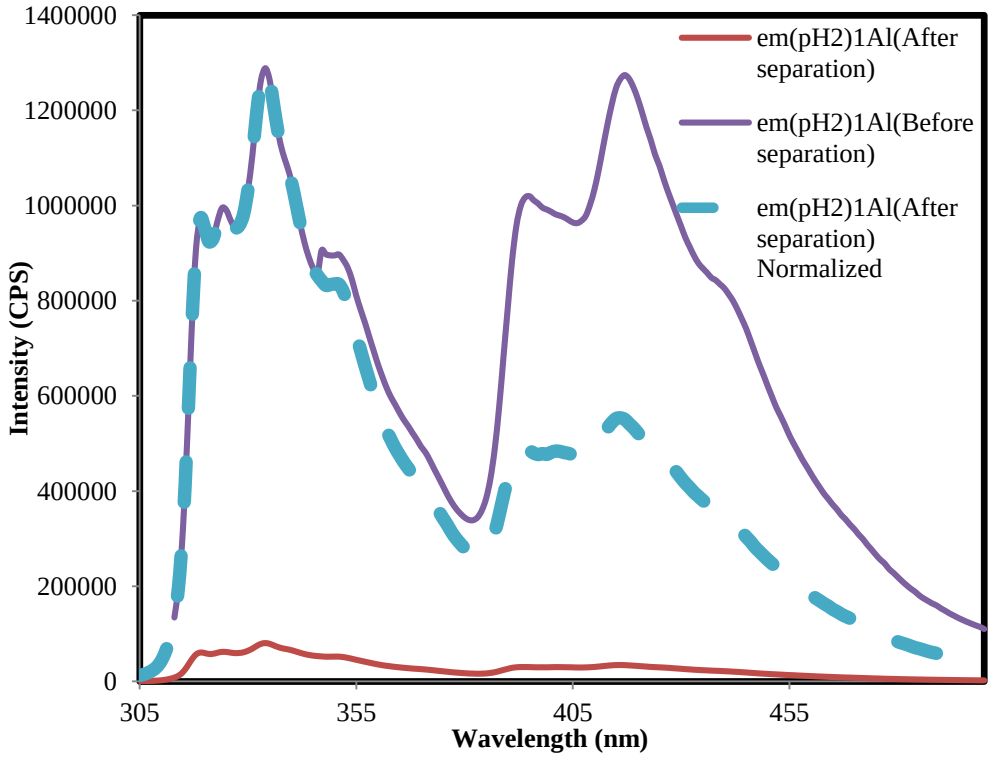

Figure 3.70 Emission spectra for ACE-AMMA-PAA (10^{-2} wt% in 1wt% Al) before and after separation at pH 2.

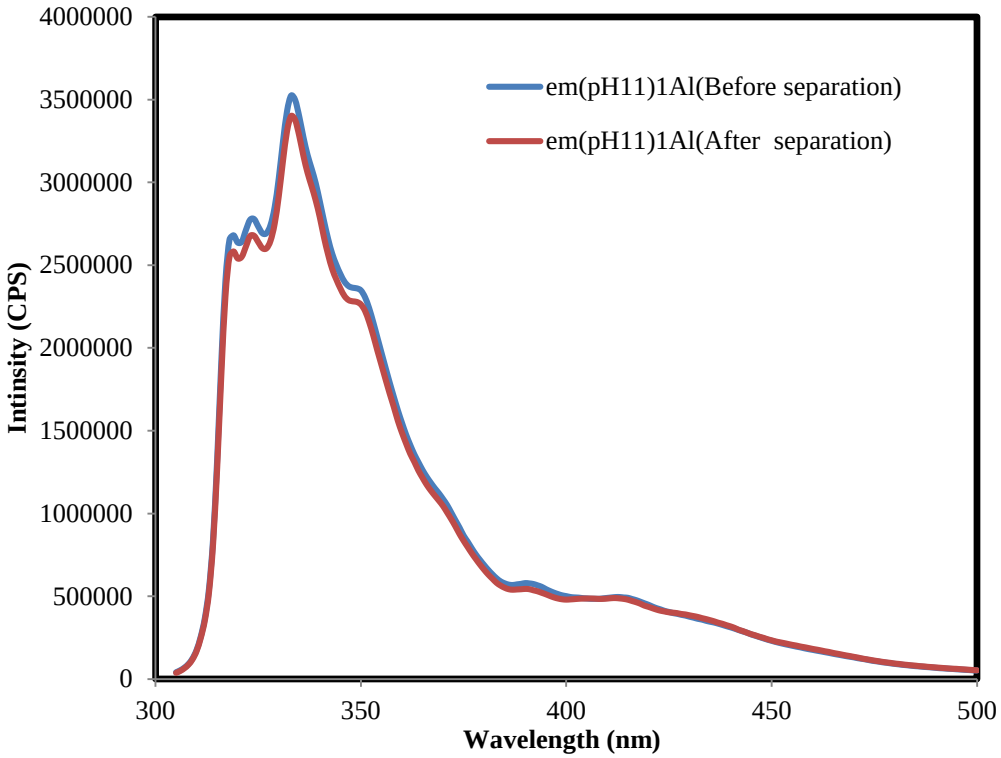

Figure 3.71 Emission spectra for ACE-AMMA-PAA (10^{-2} wt % in 1wt% Al) before and after separation at pH 11.

As previously mentioned in section 3.14.1, the comparison of conformational change of PAA chain in both bulk solution and at liquid-solid interface can be investigated by calculating the acceptor-donor ratio of a doubly labelled polymer in free solution (after separation) and in an adsorbed state (before separation). Thus, the energy transfer experiments are carried out for a better understanding of the conformational behaviour of the polyelectrolyte, when it is attached to the alumina surface.

Figure 3.72 and Figure 3.73 demonstrate the ratio of fluorescence intensity I_A/I_D as a function of pH for 10^{-2} wt % from ACE-AMMA-PAA in 10^{-4} and 1 wt % concentration of alumina before and after separation, respectively. Generally, it can be noted that the I_A/I_D ratio differs, when changing the pH for an adsorbed polymer (before separation) in an analogous mode as was exhibited for PAA in a solution (after separation). This suggests the adsorption model schemed in Figure 3.64. As presented in the scheme, at low pH values, the adsorbed polyelectrolyte becomes coiled, which can be seen when the value of the I_A/I_D ratio increases. In contrast, as deprotonation of the carboxylic acid moieties arises, the PAA chain expands on the alumina surface, thus the I_A/I_D ratio is decreased.

At 10^{-4} wt% of alumina (Figure 3.72), the I_A/I_D ratio before and after separation is almost identical over the whole pH range. When the solid content is increased from 10^{-4} to 1 wt%, a marked difference is recorded in the fluorescence intensity ratios of ACE-AMMA-PAA before and after separation at low pH values (Figure 3.73). This confirms that at a low concentration of alumina, the conformational change of the adsorbed polymer behaves similarly to the change in free solution, but at a higher concentration of alumina, the fluorescence intensity ratio before separation is bigger than that after separation at low pH values. This shows that the polyelectrolyte chain is more coiled in the adsorbed state, since the separation distance between the donor and acceptor becomes shorter.

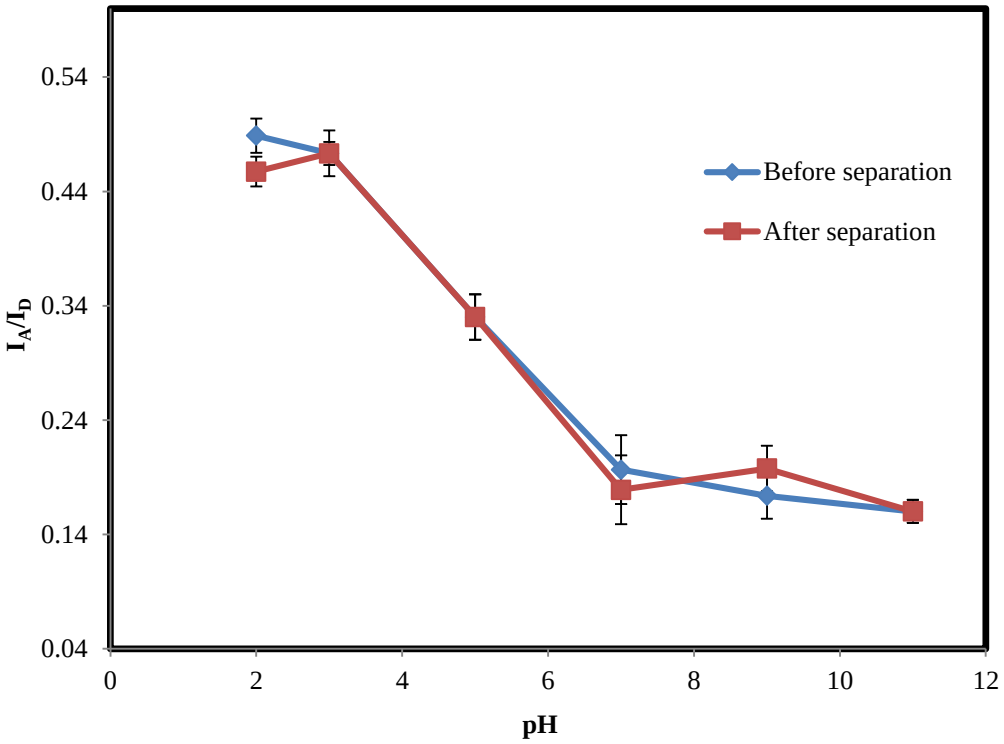

Figure 3.72 Ratio of emission I_A/I_D as a function of pH for 10^{-2} wt % from ACE-AMMA-PAA in 10^{-4}wt% alumina, before and after separation.

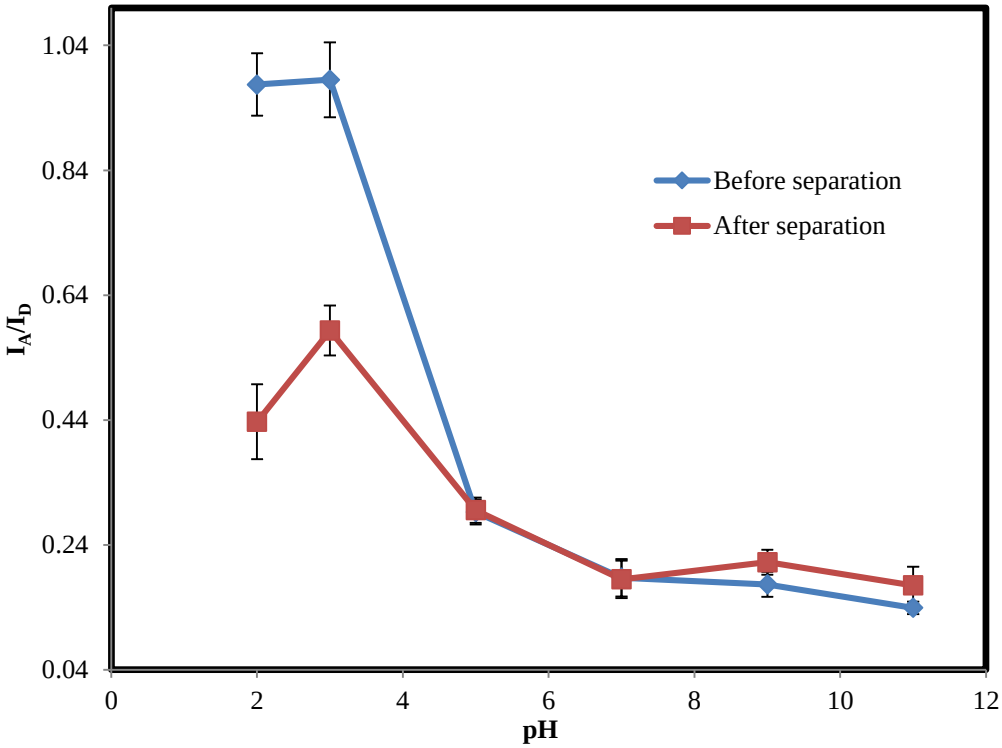

Figure 3.73 Ratio of emission I_A/I_D as a function of pH for 10^{-2} wt % from ACE-AMMA-PAA in 1 wt% alumina, before and after separation.

3.15.2. Fluorescence excited state lifetimes of ACE-AMMA-PAA on alumina as a function of pH

Fluorescence excited state lifetime analysis is the second technique, applied in this section to elucidate the conformational behaviour of fluorescently labelled polymer on Al_2O_3 surface. However, Figure 3.74 and Figure 3.75 present average donor lifetimes $<\tau_f>$ for ACE-PAA and ACE-AMMA-PAA as a function of pH at 10^{-4} and 1 wt % alumina content, respectively. Generally, all average lifetime values decrease over the whole pH scale. Additionally, the rate of decrease in $<\tau_f>$ values in ACE-AMMA-PAA is less than in those in ACE-PAA polymer at low pH values. However, the shape of the plots can also be attributed to the conformational transition occurring in the PAA chain when pH is changed. Such a transition goes from a relatively open coil at high pH, which in turn leads to quenching the lifetime values, to a coiled shape at low pH, when longer lifetime values are displayed.

Exclusively, it can be noted from Figure 3.74, that at pH values equal to 2 and 3, the $<\tau_f>$ values are shorter for donor in ACE-AMMA-PAA than those for ACE-PAA. This small difference in $<\tau_f>$ values could be because a small energy

transfer occurs from the donor to the acceptor. This *ET* is a result of a collapsed polymer, formed by adding alumina to acidic media. When the alumina content is increased to 1 wt % (Figure 3.75), a marked decrease (~25 ns) in the $<\tau_f>$ values is recorded for the donor in a doubly labelled polymer. Similarly, such a big difference in average lifetime values could be attributed to the maximum energy transfer occurring from the ACE to AMMA, which is a result of a more coiled macromolecule chain, shaped by adding more alumina to the acidic media.

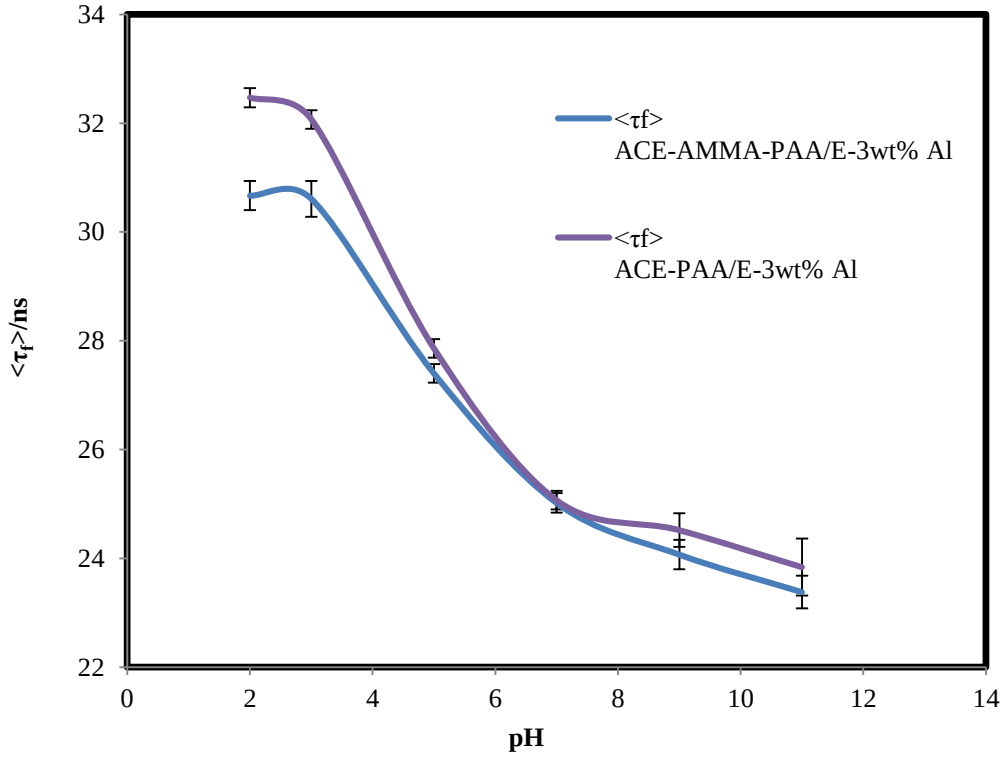

Figure 3.74 Average donor lifetime <τ> for ACE-PAA and ACE-AMMA-PAA (10^{-2} wt %) as a function of pH at 10^{-4}wt% alumina concentration. (λ_{ex} = 295 nm and λ_{em} = 340 nm).

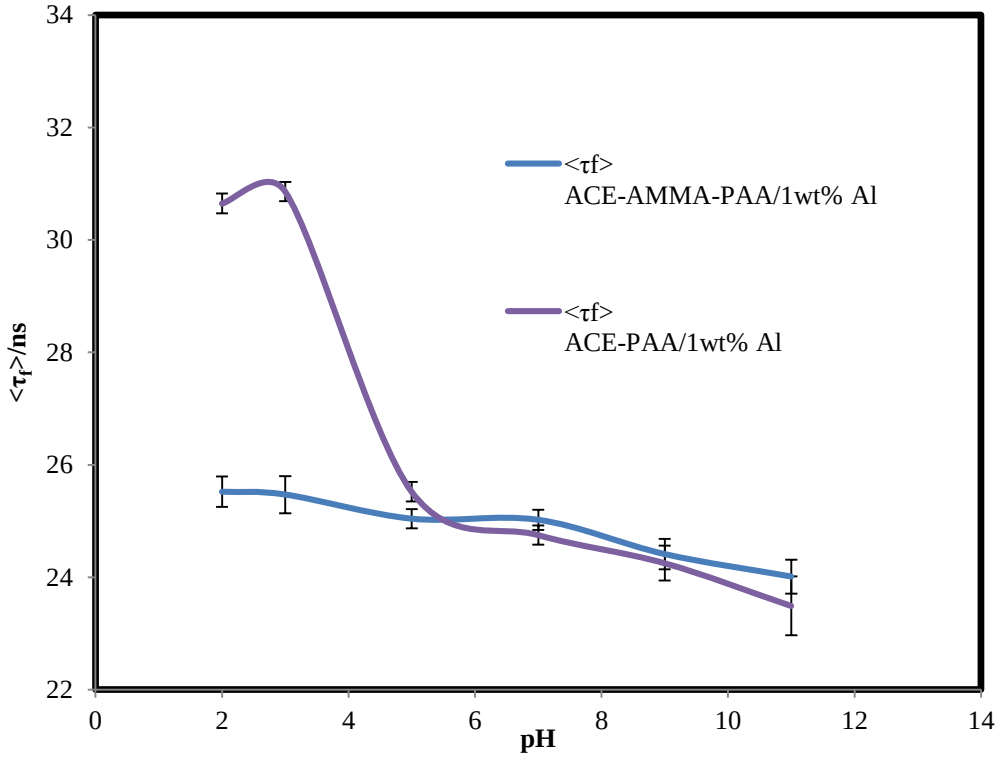

Figure 3.75 Average donor lifetime $<\tau_f>$ for ACE-PAA and ACE-AMMA-PAA (10^{-2} wt %) as a function of pH at 1 wt% alumina concentration. (λ_{ex} = 295 nm and λ_{em} = 340 nm).

3.16. **Potentiometric Titration of Poly (acrylic acid)**

Unlike a simple electrolyte, a polyelectrolyte undergoes conformational change both in a solution and in the adsorbed state [82]. Due to the multifunctional groups that exist within polymer backbone, the adsorption of macromolecules onto minerals is different from that of small molecules. In other words, the chemistry of polymers is a key factor governing their conformational behaviour [82]. In this section, the potentiometric technique is applied to study the acid-base behaviour of polymers as well as the effect of pH and ionic strength on the conformational behaviour of the semi-diluted aqueous solution of unlabelled poly (acrylic acid).

As shown in Figure 1.5 (Chapter 1), poly (acrylic acid) chain bears a carboxylic acid (COOH) repeating unit. In this work about 272 available carboxylic acid groups exist in macromolecule backbone (M_n =19580 g/mol). A fraction of COOH groups dissociates to COO^- when the pH of the solution is changed (Equation 1.1). The polyelectrolyte charge varies from relatively neutral

to highly negative when the fraction dissociated (α) increases from 0 to 1, the relation between α and pH is shown in Equation 1.2. Because of this change in the charge, the conformational behaviour of the charged polymer in solution depends on the external conditions like pH and ionic strength.

However, the fraction of dissociated COOH groups for poly (acrylic acid) as a function of pH and at different NaCl concentration is depicted in Figure 3.76. As it can be observed, the degree of ionization (α) and, consequently, the negative charge of the PAA increase by increasing the pH and NaCl concentration. Exclusively, at pH values > 10 the macromolecule chain bears more negative charges and the COOH groups are completely dissociated with α approaching 1**.** Under these strong basic condition, the fluorescence experiment showed that the poly (acrylic acid) chain in a solution is in the form of relatively expanded random coil (coil size >7 nm). This conformation is due to the electrostatic repulsion between the negatively charged COO^- groups. When the pH is decreased, the anion carboxylate moieties are converted to COOH groups until the polyelectrolyte becomes efficiently neutral near pH 2 and α approaches zero. In this acidic condition, the poly (acrylic acid) chains become relatively insoluble, and form a partially coiled chain (coil size ~3.5 nm). As proven, using the fluorescence technique.

It is believed that the COO-H bonds at low concentrations in water dissociate to COO^- and H_3O^+ (hydronium ion) [84]. Due to the fact that the potentiometric titration is used only to determine dissociated hydronium ions, a reasonable explanation for the effect of the NaCl concentration on the degree of ionization (α) is as follows: the dissociated COO^- anions are stabilized by the surrounding Na^+ cations. This means that the COO^- Na^+ bonding stability is increased by adding more salt and hence the possibility of hydronium ions binding with existing COO^- groups to produce COOH decreases. This explains why increasing the salt concentration leads to an increase in ionization of carboxyl groups.

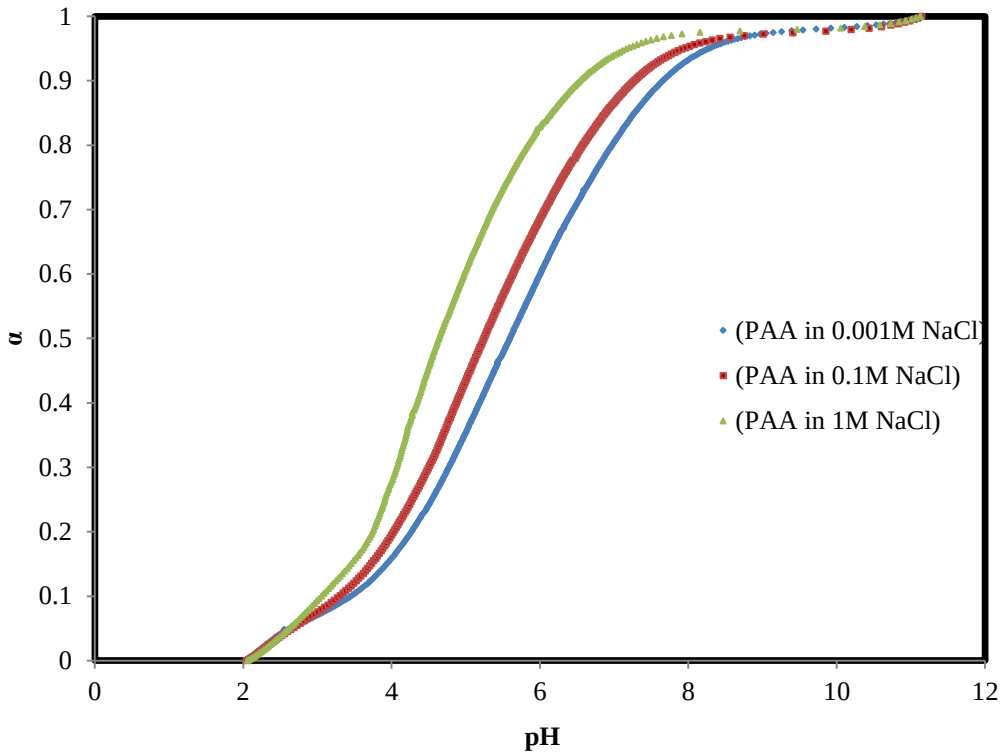

Figure 3.76 Fraction of acid groups ionized versus pH at different NaCl concentration for poly (acrylic acid) (1 wt %).

The *pKa* values of unlabelled and labelled PAA, obtained from the first derivative of titration curves are presented in Table 3.4. The numbers shown suggest the presence of carboxyl groups of poly (acrylic acid) and not acrylic acid monomer, where the *pKa* value of acrylic acid is 4, while that of poly (acrylic acid) reaches up to 5, which is in accordance with what was expected from the fluorescence experiment. In addition, no significant difference has been recorded in the *pKa* values of labelled and unlabelled polymers, see Table 3.4. This means that the same physicochemical behaviour is assumed for both the labelled and unlabelled polymers in aqueous solution, and the fluorescent labels do not disturb the polymer system.

Table 3.4 pKa Constants and pHzpc of labelled and unlabelled polymers as determined by titration curves.

System	NaCl (M)	pKa	pHzpc
PAA	0.1	4.82	2.92
ACE-PAA	0.1	4.92	2.96
ACE-AMMA-PAA	0.1	5.04	2.97

Table 3.4 also displays the zero point of charge (pHzpc), which is known as the pH value at which the whole polymer charge is equal to zero[85]. In other words, when the pH value is lower than the pHzpc number, the surface of the polymer exhibits a global positive charge due to the protonation of the carboxylic groups. In contrast, when the pH value is higher than pHzpc value, the polyelectrolyte backbone acquires a negative charge because of the deprotonation of the carboxyl groups. The results in the above table show that the pHzpc value of labelled and unlabelled PAA is approximately equal to three. This means that any conformational change in the synthetic polymer chains may occur due to the change in external conditions, such as pH. Neither ACE, nor AMMA labels can affect the physicochemical behaviour of the PAA chain. However, the role of the zero point of charge for polymers and minerals in the adsorption behaviour of polyelectrolytes will be discussed further in the following section.

Figure 3.77 shows the charge density on the surface of Al_2O_3 and SiO_2 particles as a function of pH. There are a large number of neutral, negative and positive sites at each pH. The charge density value (on the y-axis) gives the net charge density of material. At the pHzpc, the numbers of positive and negative sites are equal, and the net charge equals zero. For the alumina particles, the pHzpc is ~9 and for the silica it is ~3. This means that, for example, at pH 3 the net charge is positive on Al_2O_3 particles and neutral on SiO_2 particles, but at high pH levels like pH11 both solids bear negative net charges.

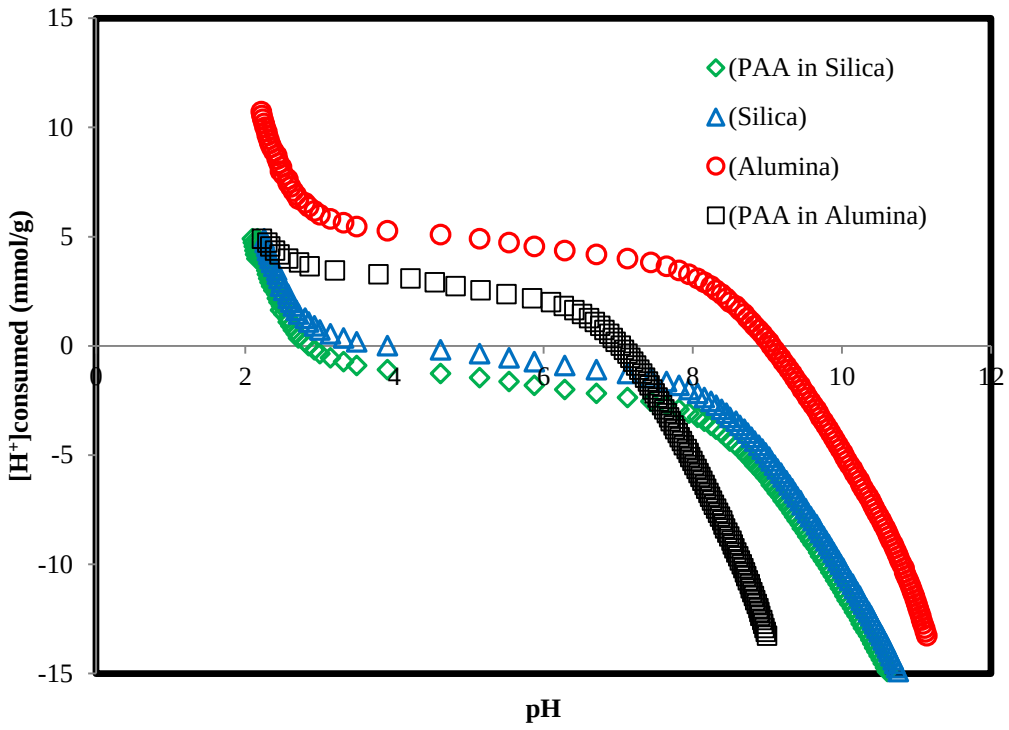

Figure 3.77 Relative charge versus pH for silica, alumina, poly (acrylic acid) in silica, and poly (acrylic acid) in alumina.

The variation in the relative charge density of silica and alumina particles in the absence and presence of adsorbed poly (acrylic acid) is depicted in the above Figure. As it can be observed clearly, the adsorption of the anionic polyelectrolyte decreases the positive charge importantly and lowers the pHzpc of the alumina, but no substantial effect on the relative charge behaviour of silica suspension is recorded. These results suggest that electrostatic interactions are predominantly responsible for the adsorption of poly (acrylic acid) on Al_2O_3 molecules, whereas weak forces, such as Van der Waals are assumed to control the interaction between PAA and SiO_2 suspension. Since in acidic condition, the fluorescence experiment showed that the percentage of adsorbed polyelectrolyte reaches the value (~100%) on alumina, while only ~20% on silica. This is because at low pH levels, the net charge on alumina is positive and PAA is negatively charged (except at pH 2), whereas the silica particles are neutral.

3.17. **Inductively Coupled Plasma Mass Spectrometry Measurements (ICP-MS) of silica and alumina Adsorption on PAA**

Inductively coupled plasma mass spectrometer (ICP-MS) was used to determine the adsorbed minerals on unlabelled PAA according to the method outlined in the experimental chapter.

Because poly (acrylic acid) is a poly (acid) polymer[29], the pH of the solution plays an important role in its adsorption behaviour on the mineral surface. Figure 3.78 shows the effect of pH on the adsorption of Al_2O_3 and SiO_2 on unlabelled PAA. As it can be seen, for the two minerals examined, the adsorbed amounts increase when the pH of the solution is decreased. However, the rate of increment in these amounts for silica is less than in those for alumina over the entire pH range.

It is mentioned in Table 3.4 that the pHzpc value of unlabelled PAA approximately equals 2.92. It means that the global charge of PAA is negative in the whole studied pH range, except at pH 2, where it is positive. In contrast, for the alumina particles the pHzpc is ~9 and ~3 for the silica. This means that the surface of Al_2O_3 is positively charged in the entire studied pH scale, excluding at pH 9, where it is neutral and at pH11, where it is negative. Figure 3.78 shows the difference between the adsorption behaviour of alumina above and below the pHzpc. At pH < 9, the adsorption behaviour is of the high-affinity type, which means that the alumina strongly attaches to the polyelectrolyte. In contrast, at pH > 9, the electrostatic repulsion between the polyelectrolyte chain and the alumina surface causes the decrease of mineral adsorption. This adsorption behaviour coincides with the recent polyelectrolyte adsorption theory established by Van der Schee and Lyklema [32], which can be summarized as follows: adsorption of a negatively or partly negatively charged macromolecule on a positively charged mineral is influenced by electrostatic forces.

In spite of the above facts, the poly (acrylic) acid can adsorb onto the alumina, as well as the silica surfaces over the entire studied pH range, even when the pH, at which both polymer and solid bear the same kind of charge. This could be attributed to the fact that non-electrostatic forces, such as Van der Waals, control the adsorption between mineral and polyelectrolyte [86]. Otherwise, the

adsorption of an anionic polyelectrolyte chain on the negatively charged mineral surface should not occur.

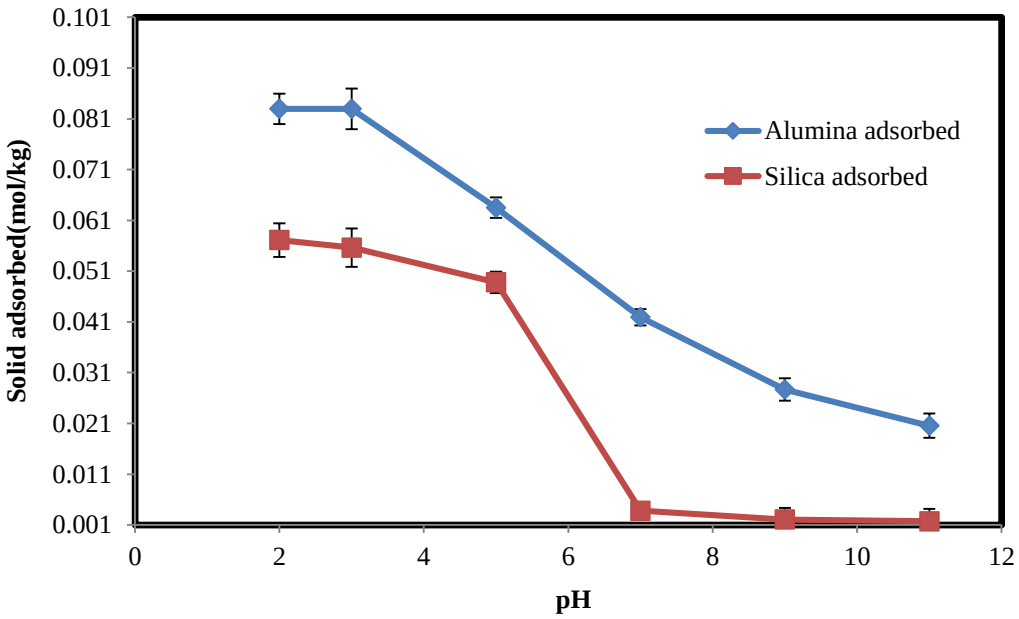

Figure 3.78 Effect of pH on the adsorption of alumina and silica on poly (acrylic acid) (solid added 0.1M).

Besides pH, solid concentration influences the adsorption process of minerals on a polyelectrolyte. Figure 3.79 displays the adsorption isotherms for alumina and silica on PAA at pH 7. These adsorption measurements were carried out at the same concentration of polymer (10^{-2} wt %). The analysis of these isotherms leads to the conclusion that mineral adsorption on the polyelectrolyte increases with the solid concentration increase at low and high pH values. The obtained isotherms are fitted to the Henry adsorption model according to Equation 3.11, in this model the affinity of the mineral for the polyelectrolyte remains constant over the completely investigated concentration range. It can be used at much diluted solutions from the macromolecule, where the strongest adsorption sites of solid are far away from being fully saturated [14].

$$[Solid]_{\text{adsorbed}} = K_{\text{h}}[Solid]_{\text{added}} \qquad \text{Equation 3.11}$$

Where, *[Solid]* $_{adsorbed}$ is the concentration of adsorbed mineral in mol/kg, *[Solid]* added is the concentration of added mineral in *M*, and K_h is Henry or affinity constant, since large K_h means that the mineral is strongly adsorbed on polymer,

and vice versa. These linear dependencies enable calculation of the affinity constants of mineral adsorption from the slope of the above equation. The obtained K_h and goodness of fit (R^2) values are given in Table 3.5. Considering the values of R^2 the Henry model is good to describe such isotherms. It can be noted that, over the complete pH range the affinity of minerals to adsorb on the PAA increases by decreasing the pH of solution. This could also attribute to the attraction of oppositely charged materials. However, under the identical condition Al_2O_3 particles have a greater affinity for the PAA than SiO_2 suspensions. This is due to the effects of the zero point of charge for minerals. The most efficient adsorption occurred at lower pH values, under these conditions, where the alumina particles bear a positive charge, so that they are strongly attracted to negatively charged PAA, and yield larger Henry's constant values. Silica suspensions have a weak affinity for PAA due to the electrostatic repulsion of negative silica molecules with anionic polyelectrolytes.

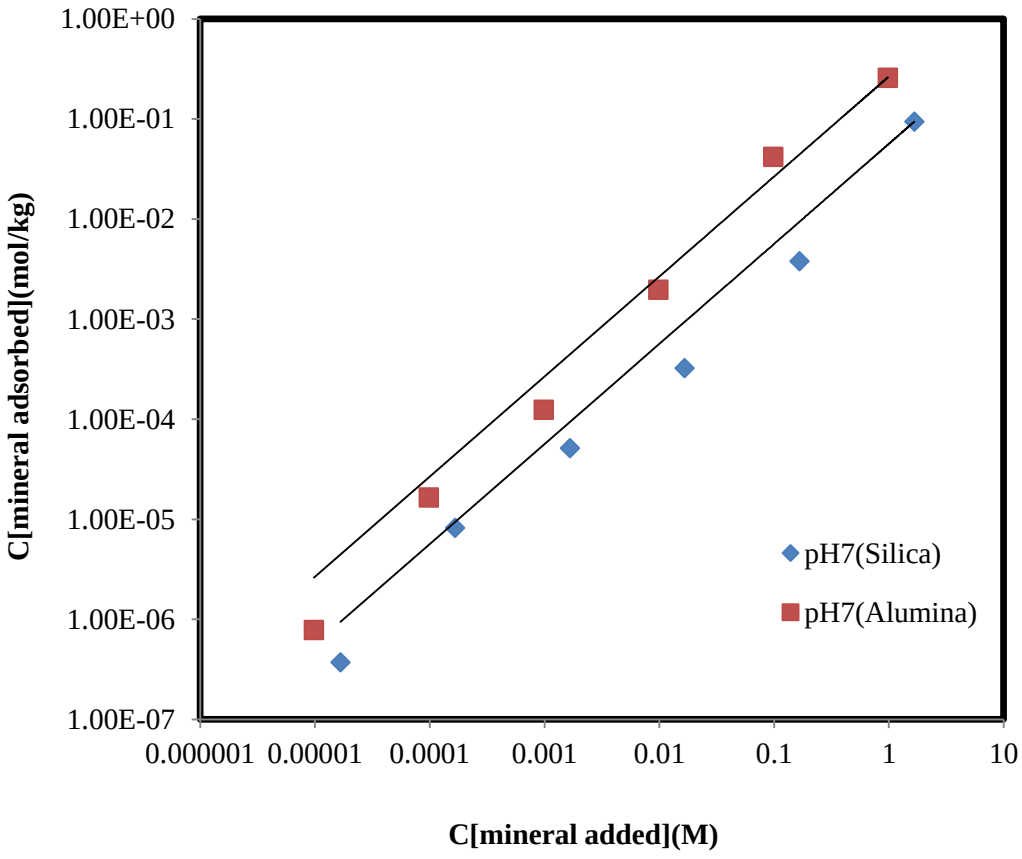

Figure 3.79 Henry adsorption isotherm of alumina and silica adsorbed onto poly (acrylic acid), at pH 7.

Table 3.5 Henry (affinity) constants of alumina and silica adsorbed onto poly (acrylic acid) and the goodness of fit values, at different pH values.

pH	K_h (L/kg) (Alumina)	R^2 (Alumina)	K_h (L/kg) (Silica)	R^2 (Silica)
2	0.9097	0.9999	0.336	0.9995
3	0.6145	0.9998	0.2006	0.9876
5	0.2875	0.9796	0.1813	0.9951
7	0.2663	0.9953	0.0566	0.8891
9	0.2296	0.9993	0.0468	0.9956
11	0.2289	0.9999	0.0432	0.9737

3.18. **Conclusions**

- Fluorescence techniques, including steady state, lifetime and time resolved anisotropy, are extremely powerful in elucidating the conformational behaviour of dilute poly (acrylic acid) (PAA) solutions, and when attached to solid surfaces, such as alumina and silica, respectively.
- Fluorescence steady state and lifetime investigations of the polymer in solution and in the adsorbed state showed that the conformation of the macromolecular chain changes from an open form to a collapsed coil under the influence of several factors such as pH, ionic strength and additives, such as silica and alumina. They also proved that the macromolecule chain is expanded at high pH values, while becoming partially collapsed in acid media.
- Fluorescence steady-state experiment showed that a large amount of the fluorescently labelled polymer adsorbs onto alumina in acidic media, but less adsorbs onto colloidal silica at a similar pH.
- The correlation time (τ_c) of labelled polymer increases as the amount of mineral increases and the pH decreases, this suggests that the polyelectrolyte chains interact strongly with the surface, form a more collapsed form at low pH to an expanded structure on the surface of a solid.
- The results obtained from potentiometric analysis suggested that electrostatic interactions were predominantly responsible for the adsorption of poly (acrylic acid) on Al_2O_3 particles, whereas weak forces, such as Van der Waals are assumed to control the interference between a PAA chain and an SiO_2 surface. This is due to the fact that at low pH (i.e. 3) the net charge of alumina is positive and PAA is negatively charged, whereas the silica particles are neutral.
- ICP-MS demonstrated that PAA had a high adsorption affinity for Al_2O_3, in contrast to the weak interaction on the SiO_2 surface. Strong adsorption was observed at low pH for both minerals. The dependence of adsorption with mineral concentration was also examined under different pH conditions: the adsorption amount was observed to increase by increasing the alumina concentration. Adsorption isotherms obtained at low and high solid concentrations were found to be Hennery in type.

- Collectively, these results demonstrate that a combination of fluorescence, ICP-MS and potentiometric techniques can sensitively elucidate the conformational behaviour of the simple model polymer, PAA. The use of these techniques can now be applied with confidence to investigate the adsorption behaviour of more complex biopolymers onto mineral surfaces, which should act as model systems for bacterial growth. This will be discussed in the following chapter.

Chapter 4. CONFORMATIONAL BEHAVIOUR OF ALGINATE IN BOTH BULK SOLUTION AND AT SOLID/LIQUID INTERFACES

4.1. **Chemistry of Alginates**

Alginic acid is an important mediator of cell adhesion [87], and it is known as a typical model extracellular polymeric substance (EPS) that can be employed to study biofilm systems [88]. The understanding of alginic acid behaviour in aqueous solution begins with an understanding of the basic chemistry. Alginic acid, also known as alginate is a biocompatible linear polyelectrolyte isolated from brown seaweeds or soil bacteria. This polysaccharide is composed of (1→ 4) linked β-D-mannuronic acid (M) and its C-5 epimer, α-L-guluronic acid (G) [89-94], as shown in Figure 4.1. The natural random biopolymer formation produces different quantities of G-block, M-block and MG-block. The pKa values of M and G are 3.38 and 3.65, respectively[95]. This means that the alginate chains can form hydrophilic-hydrophobic aggregates in aqueous solution by changing the pH of the medium [95].

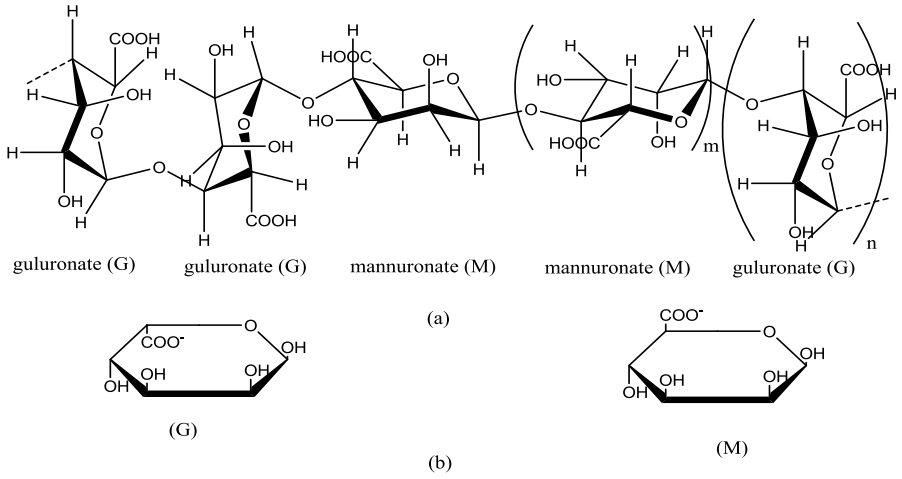

Figure 4.1 Compositional structure of alginic acid (a). Structures of the α-L-guluronate (G) and β-D-mannuronate (M) residues of which it is composed of (b).

4.2. **Physicochemical Behaviour of Alginate in Aqueous Solution and as a Sorbate**

Alginate has a unique physicochemical behaviour, which is affected by its composition and the environment surrounding it [90, 91, 96-98]. Many studies [90, 91, 96-98] have reported that the conformational behaviour of alginate is influenced by factors such as concentration, pH of the medium, ionic strength and presence of some cations such as Ca^{2+}, Mg^{2+}, Na^{+} and K^{+}. In fact, the molecular interactions of an aggregated alginate solution are not fully understood. However, it has been known that alginate can form gels at pH less than the pKa values of alginate monomers [92, 93, 96].

The alginic acid monomers contain carboxyl and hydroxyl groups that may interact with mineral surfaces. The carboxyl group can potentially interact with a surface via electrostatic forces, while the hydroxyl group may interact via hydrogen bonding [99]. The stability of biomacromolecules, such as alginic acid, when in presence of solid surfaces is influenced by the conformation adopted by these macromolecules [100]. However, the conformational behaviour of adsorbed alginate is not well understood.

In this chapter, we aim to use the techniques previously described including fluorescence and inductively coupled plasma mass-spectroscopy to study a more complicated bacterial biopolymer. The photophysical behaviour of the diluted aqueous solution of fluorescently labelled alginate and the corresponding model compounds were investigated using fluorescence spectroscopy. Fluorescence and potentiometric techniques are applied to study the effect of pH and ionic strength on the conformational behaviour of an alginate chain. The interaction of this biopolymer with silica and alumina is also studied. The adsorption isotherms of alginate on minerals were derived by determining aqueous aluminium and silica concentrations using inductively coupled plasma mass-spectroscopy (ICP-MS).

4.3. **Fluorescent Behaviour of AmNS as a Function of pH**

As a preliminary study, the free fluorophore response to external stimuli was investigated to evaluate whether it can disturb the photophysical behaviour of alginate. In this chapter, 4-amino naphthalene-1-salfonic acid (AmNS) (Figure 1.12 in Chapter 1) was selected as a model compound. All fluorescent label samples were prepared and analysed reliably to those reported in section 2.7.

UV absorption spectroscopy was utilised to determine the maximum absorption wavelength of the sample λ_{ex} and was found equal to ~320 nm (see Figure 2.11 in Chapter 2), this wavelength was selected to get the optimum emission wavelength λ_{em} (420 nm) from fluorescence steady state spectra.

4.3.1. **Fluorescence steady state spectra of AmNS as a function of pH**

Figure 4.2 displays the fluorescence emission spectra of 10^{-5} M AmNS dissolved in deionized water at pH values of 3, 7 and 11. All samples were excited at 320 nm. It can be observed that all the fluorescence emission spectra displayed the well-known shapeless band of the AmNS fluorophore [101], giving a maximum λ_{em} at ~420 nm. At pH 3 in this experiment the effect of protonation at the amino group in the AmNS moiety [102] (pKa ~ 4.2) was apparent, which quenched the fluorescence intensity, while at pH values 7 and 11 identical emission spectra were obtained.

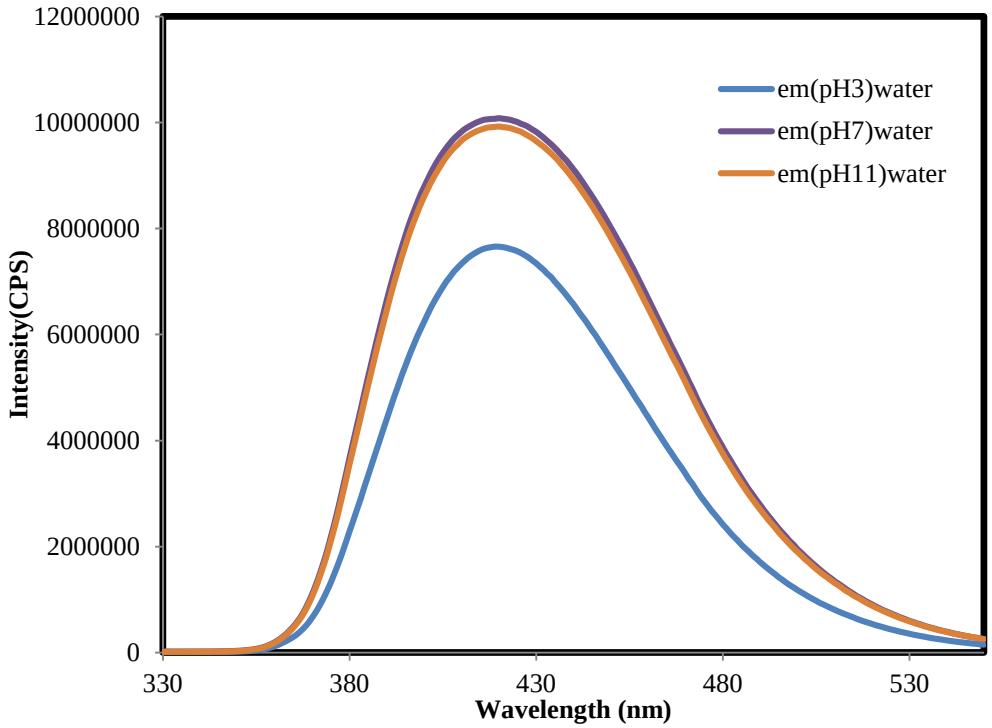

Figure 4.2 Fluorescence emission spectra for 10^{-5} M AmNS in aqueous solution at varied pH values (λ_{ex}= 320 nm).

4.3.2. **Fluorescence exited state lifetimes of AmNS as a function of pH**

The fluorescence intensity decays for 10^{-5} M AmNS in aqueous solution at different pH values are shown in Figure 4.3. For each pH the generated fluorescence decay was successfully resolved with a single exponential model decay function, which was statistically tested for its goodness of fit by application of weighted residual analysis and the chi-squared parameter. All fitted decays gave χ^2 = ~1. At pH3 a relatively short-duration decay was obtained (τ_f = ~6 ns) compared with the values obtained at pH 7 and 11 where the decay time value was doubled (τ_f = ~11 ns). The quenching in the excited state lifetime occurred in the acidic media due to the binding of the amino group for AmNS with H^+ ion [102].

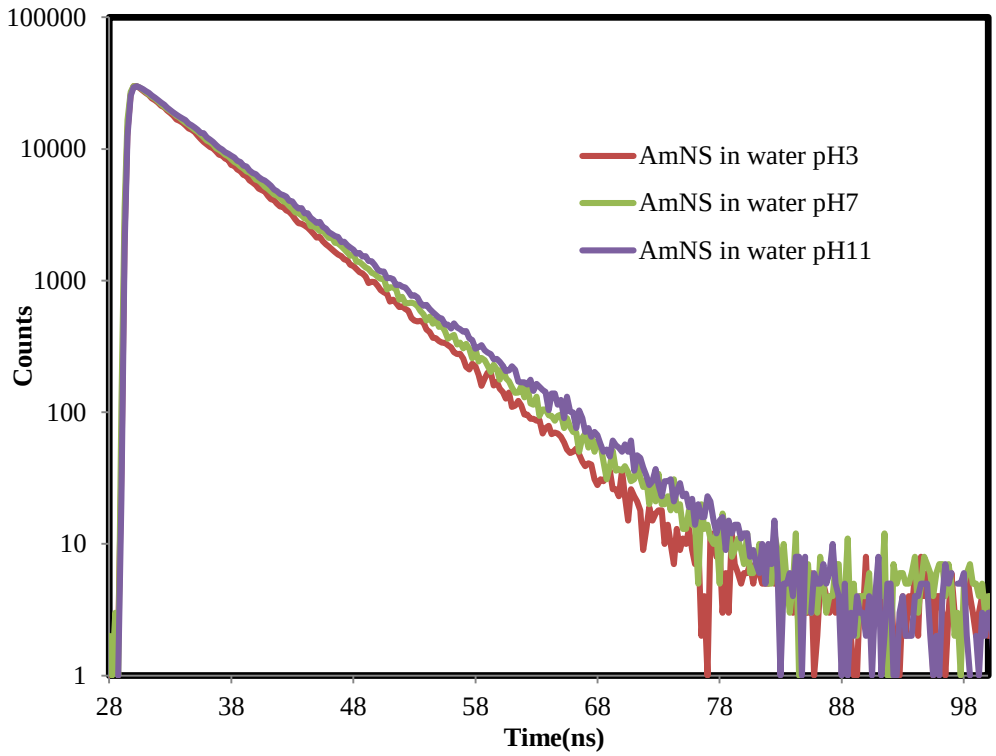

Figure 4.3 Fluorescence excited state lifetime decays of 10^{-5} M AmNS in water at varied pH values.

4.3.3. **Fluorescence time-resolved anisotropy measurements (TRAMS) of AmNS as a function of pH**

The results from previous sections showed that both the fluorescence intensities and lifetimes are quenched in acidic conditions. In this section, the pH effect on the dynamic behaviour of free fluorophore will be discussed.

Figure 4.4 shows the anisotropy decays of 10^{-5} M AmNS in aqueous solution at pH 3, 7 and 11. The TRAMS of AmNS at room temperature exhibits a fast depolarization of the fluorescence. This is accompanied by an extremely short rotational time of AmNS in solution at different pH values (~0.1 ns) as would be expected from a freely rotating small molecule in extremely dilute solution. The TRAMS spectra also show that unlike the fluorescence steady state and lifetime results, the dynamic behaviour of free fluorophore is not affected by the acid quenching, since all decays are superimposable on each other. This pH-independence makes TRAMS technique the most powerful fluorescence

technique capable of resolving the photophysical behaviour of AmNS-labelled macromolecules as a function of pH.

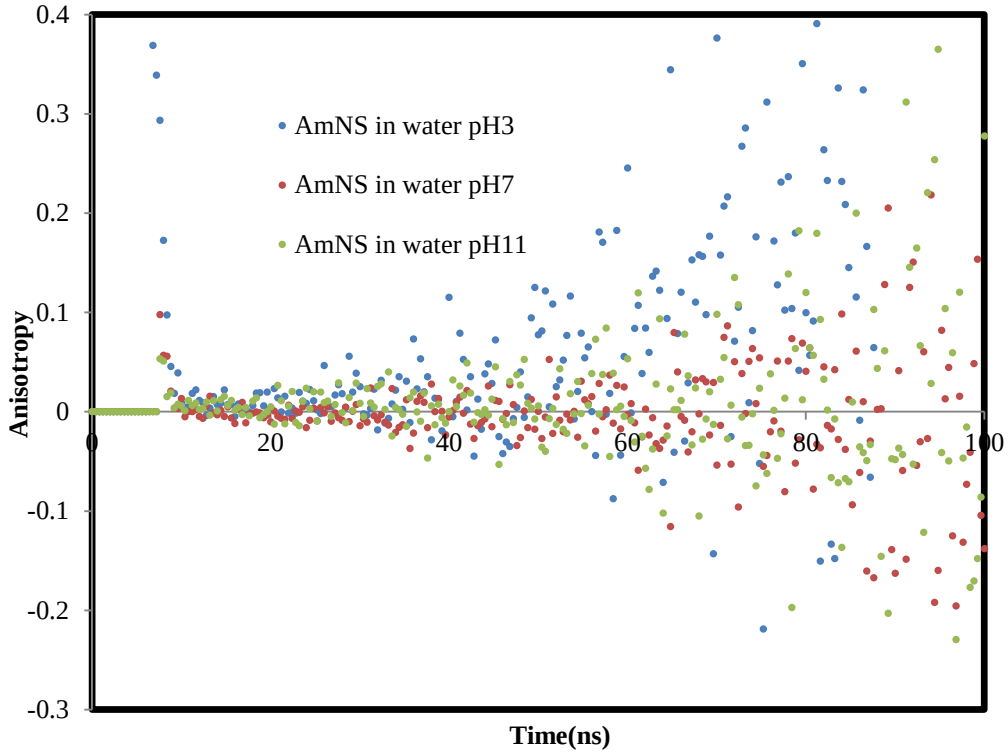

Figure 4.4 Anisotropy decays of 10^{-5} M AmNS in water at different pH values.

4.4. Fluorescent Behaviour of AmNS in the presence of Silica as a Function of pH

In this section, we present the results of an experiment undertaken to support the argument that any adsorption between the AmNS-alginate and the solid surface is absolutely because of interactions between these two components and independent of any interference from the AmNS label. The free fluorophore was dispersed in a solution containing colloidal silica in order to determine whether any adsorption onto the surface occurs.

4.4.1. Fluorescence steady state spectra of AmNS at silica surface as a function of pH

Figure 4.5 and Figure 4.6 show the fluorescence steady-state spectra of 10^{-5} M AmNS in 1 wt % silica solution at pH 3 and pH11 before and after separation

of the solid components by centrifugation. At both pH values, it was found that the fluorescence intensity before separation was indistinguishable from that after separation. This is evidence that the free AmNS remains dispersed in the bulk solution and does not interact with silica.

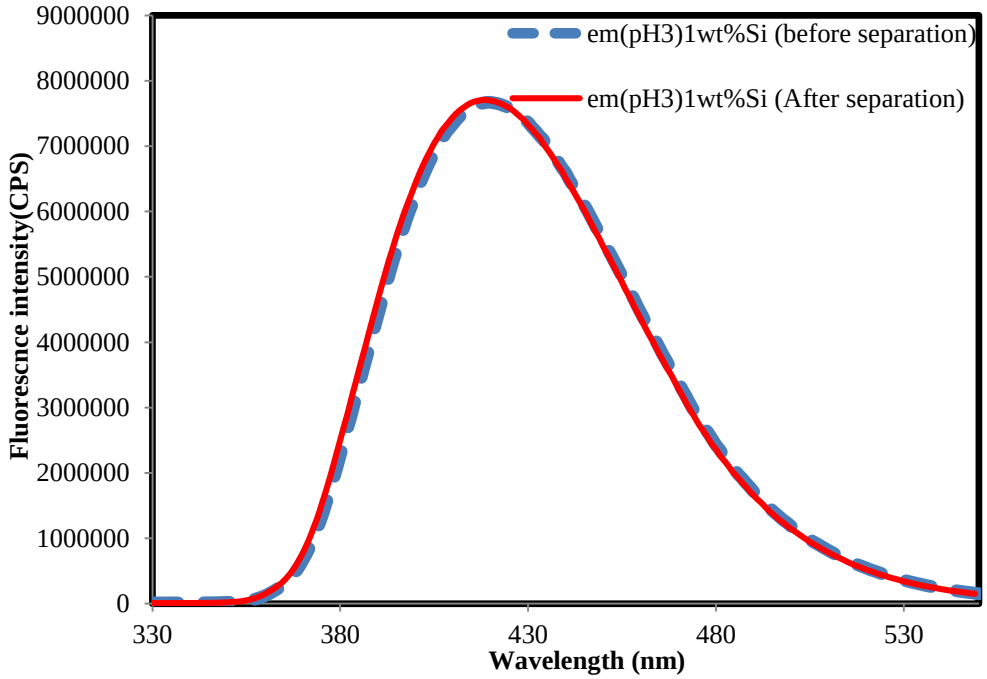

Figure 4.5 Emission scan in a range equal to 330-550 nm at fixed excitation λ_{ex}= 320 nm for AmNS (10^{-5} M in 1wt % Silica), before and after separation at pH 3.

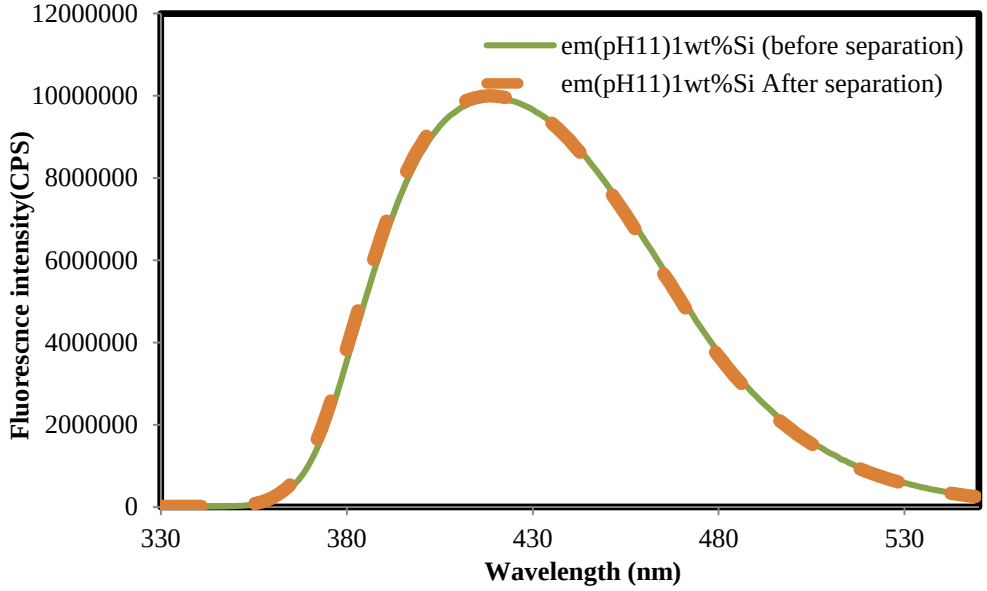

Figure 4.6 Emission scan in a range equal to 330-550 nm at fixed excitation λ_{ex}= 320 nm for AmNS (10^{-5} M in 1wt% Silica), before and after separation at pH 11.

4.4.2. **Fluorescence time-resolved anisotropy measurements (TRAMS) of AmNS at silica surface as a function of pH**

The anisotropy decays of AmNS in silica (Figure 4.7) confirm that the free fluorophore is not absorbed to the silica surface. This can be concluded from the value obtained for the duration of fluorescence anisotropy decays, which are similar to that of AmNS in water at pH values 3, 7 and 11 (see Figure 4.4). If the AmNS fluorophore was attached to the silica surface, an increase in the correlation time should have occurred. However, this increase was not observed during the anisotropy analysis.

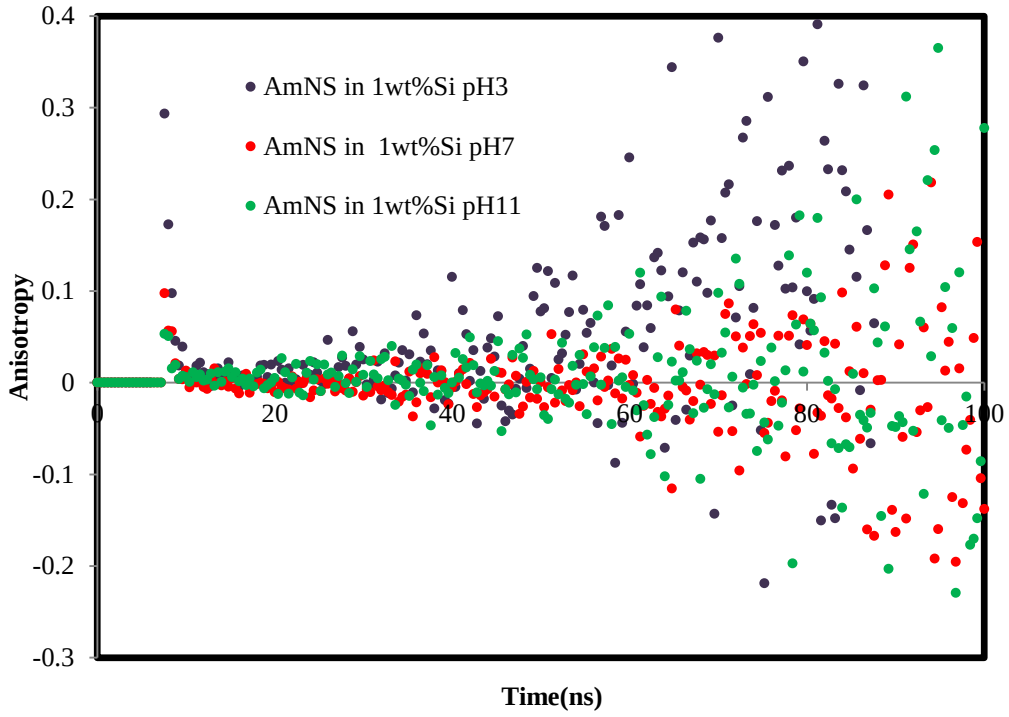

Figure 4.7 Anisotropy decays of 10^{-5} M AmNS in 1 wt % Silica at different pH values.

4.5. **Fluorescent Behaviour of AmNS at Alumina Surface as a Function of pH**

In order to further confirm the argument that any attachment between the AmNS-alginate and the alumina surface is independent of any interference from the AmNS label. The free AmNS was dispersed into the alumina solution in order to determine whether any adsorption at the surface happens.

4.5.1. **Fluorescence steady state spectra of AmNS at alumina surface as a function of pH**

Figure 4.8 and Figure 4.9 display the fluorescence steady-state spectra of 10^{-5} M AmNS in 1 wt% alumina solution at pH 3 and pH 11 before and after separation. The results show that the fluorescence intensity values obtained before separation by centrifugation is identical to that obtained after separation. This could be attributed to the fact that the free AmNS remains dispersed in the bulk solution and is not attached on the surface of alumina.

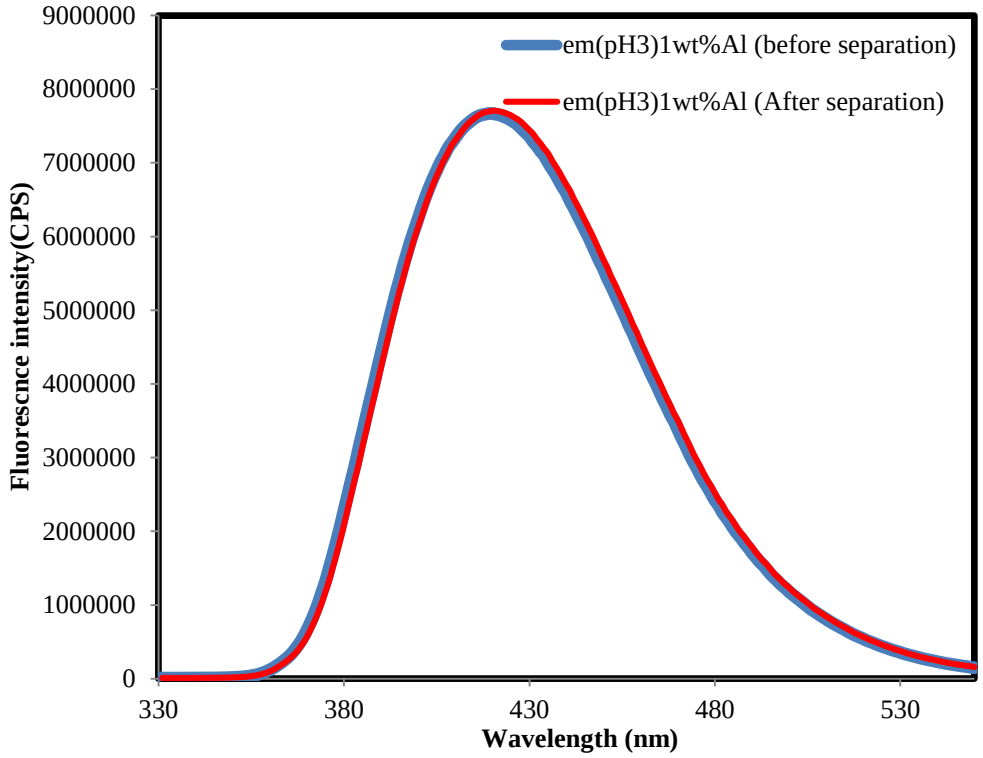

Figure 4.8 Emission scan in a range equal to 330-550 nm at fixed excitation λ_{ex}= 320 nm for AmNS (10^{-5} M in 1wt % Alumina), before and after separation at pH 3.

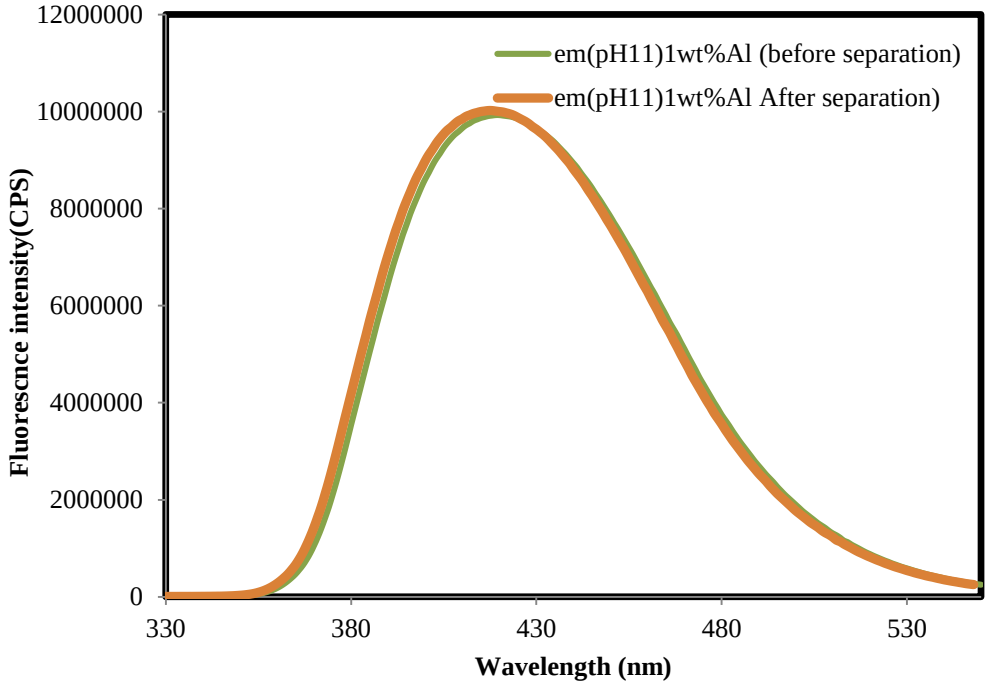

Figure 4.9 Emission scan in a range equal to 330-550 nm at fixed excitation λ_{ex}= 320 nm for AmNS (10^{-5} M in 1 wt% Alumina), before and after separation at pH 11.

4.5.2. **Fluorescence time-resolved anisotropy measurements (TRAMS) of AmNS at alumina surface as a function of pH**

The anisotropy decays of AmNS in the presence of an alumina surface are shown in Figure 4.10, The shape of the decays at in presence of alumina indicate that the free AmNS does not adsorb onto the mineral surface. This can be observed from the duration of fluorescence anisotropy decays, which are analogous to that of AmNS in water at pH 3, 7 and 11, see Figure 4.4. Furthermore, no change in the correlation times of AmNS was recorded from the anisotropy analysis. All these results confirm that AmNS remains free in solution and does not interact with the alumina surface.

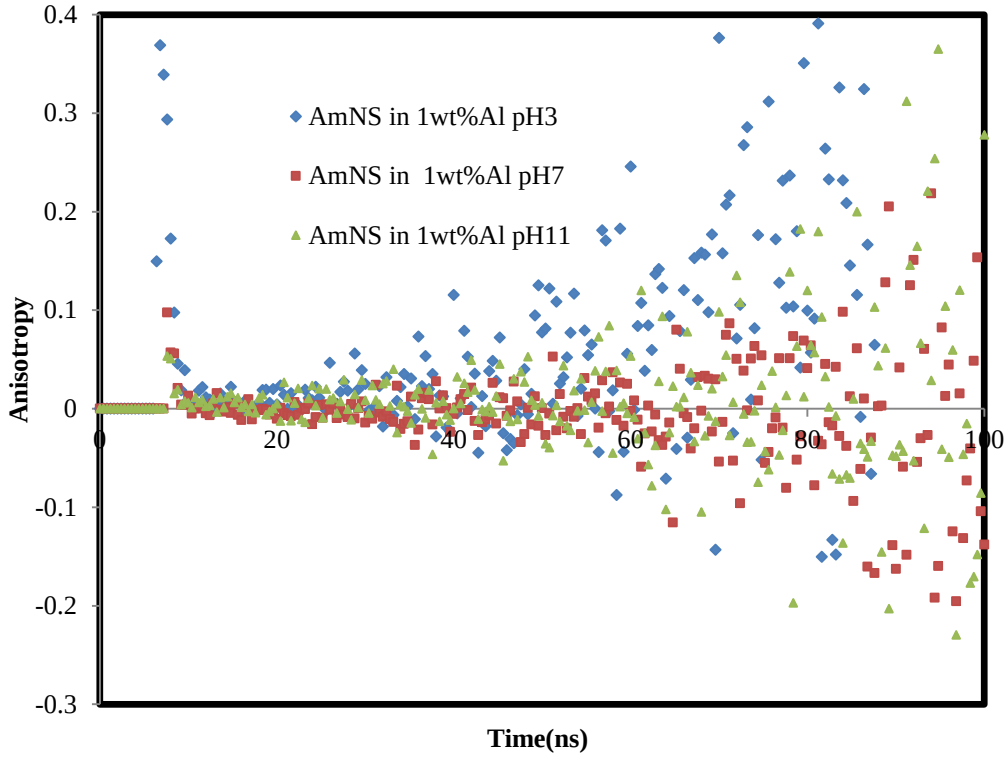

Figure 4.10 Anisotropy decays of 10^{-5} M AmNS in 1 wt % alumina at different pH values.

4.6. Conformational Behaviour of AmNS -Alginate as a Function of pH

4.6.1. Fluorescence steady state spectra of AmNS -alginate as a function of pH

Figure 4.11 presents the fluorescence emission spectra of 10^{-1} wt % unlabelled alginate and AmNS-labelled-alginate over a pH range of 1-12. The data clearly shows the difference in fluorescent intensity for the unlabelled vs. labelled polymer. The unlabelled material did not produce a fluorescent response, while the labelled polymer produced a distinguishable fluorescent spectrum. From this result, it can be concluded that AmNS solely is responsible for the fluorescence intensity observed. The emission spectra produced by the AmNS-labelled alginate are in agreement with earlier work for the bound AmNS label which is characterised by a shapeless spectrum [102], centred at 420 nm when an excitation wavelength of 320 nm is used. The maximum intensity of the emission peak position is dependent of the pH of the biopolymer solution. The dramatic decrease of the fluorescence intensity at acidic pH for AmNS results from the protonation

of the amino group [102], which also leads to a decline in the excitation spectra of AmNS (data not presented). However, from pH 5 to 10 (above the pKa of AmNS) the fluorescence intensity is not affected by an acid quenching, so any dependence of the fluorescence intensity during the change of pH may be due to the conformational transition of the alginate chain. Additionally, the enhancement in the fluorescence intensity from pH 5 to 10 could be attributed to the existence of the hydrophilic fluorophore in an aqueous environment, since the alginate chain becomes partly expanded in basic media due to the electrostatic repulsion of COO^- groups [103]. In addition, the gradual decrease of the fluorescence intensity at extremely high pH (11 and 12) is due to dynamic quenching by OH^- ions [102].

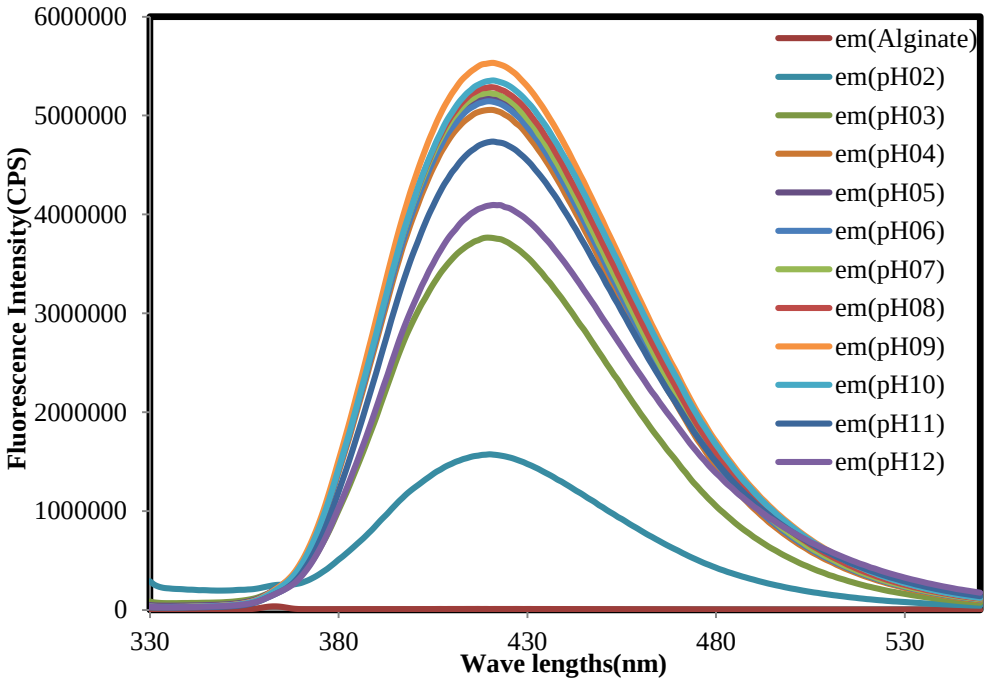

Figure 4.11 Fluorescence emission spectra for 10^{-1}w% AmNS-Alginate in water as a function of pH at λ_{ex}= 320 nm.

4.6.2. **Fluorescence exited state lifetimes of AmNS -alginate as a function of pH**

Figure 4.12 shows the fluorescence intensity decays for 10^{-1} wt% AmNS-labelled-alginate over a pH range of 1-12. From the data it can be observed that at basic pH the fluorescence lifetime of the AmNS-labelled biopolymer has longer duration decay compared to that at low pH (pH > pKa of AmNS). This could be attributed to the fact that natural polyelectrolyte chains are expanded due to the

deprotonation process (Figure 4.13), and the AmNS labels are exposed to aqueous environment and become more solubilised, hence their lifetime decays are enhanced. This behaviour was not evident from the data obtained at pH 11 and pH 12. On the contrary, in acidic conditions such decays become shorter than those in basic conditions, since the biopolymer chains are partially collapsed due to the protonation of carboxylate groups. This allowed the presence of undissolved AmNS in the hydrophobic domains of the coiled conformation, as a result the fluorescence excited state lifetime is quenching. In support of the above discussion, the sensitivity of AmNS to the hydrophobicity of its surrounding environment was tested and an increase in the fluorescence lifetime of AmNS in water was recorded (τ_f = 11.4 ns) compared to a less hydrophilic solvent, such as butanol (τ_f = 7.0 ns). This increase could be attributed to that increase in the solubility of AmNS in aqueous media relative to butanol.

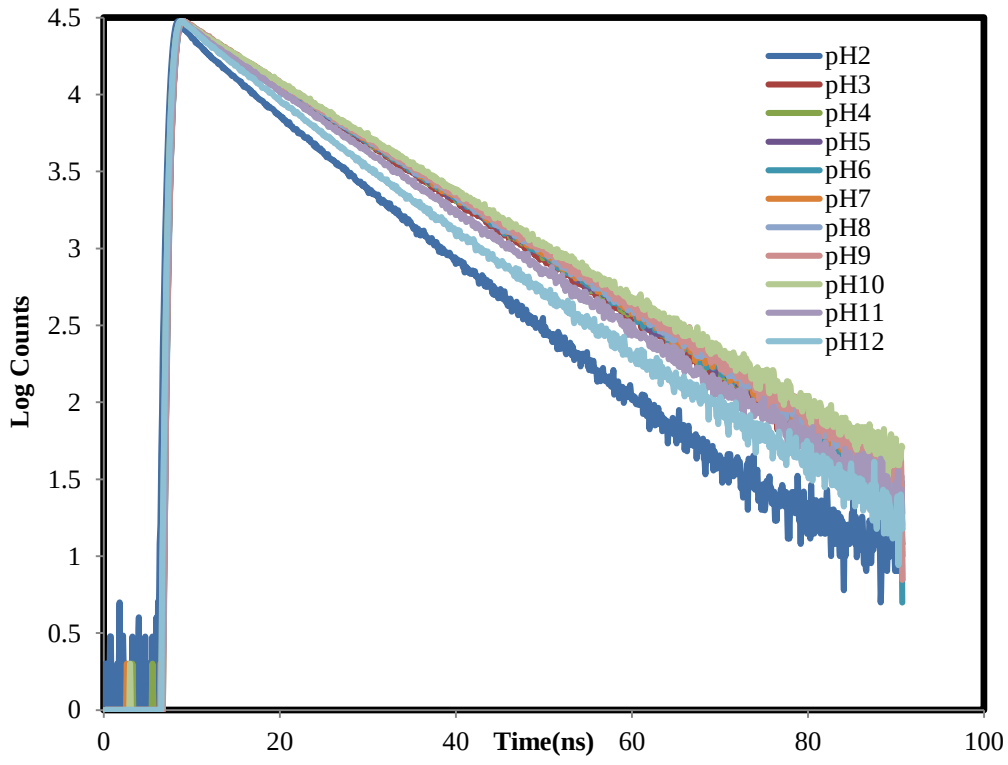

Figure 4.12 Fluorescence intensity decays for 10^{-1}w%AmNS-Alginate in water as a function of pH at λ_{ex}= 370 nm and λ_{em}= 450 nm.

Based on fluorescence intensity and lifetime results, it is possible then to propose structures for the alginate molecules as a function of pH. The following Figure shows a schematic representation of the conformation of alginate chain with adding acid or base:

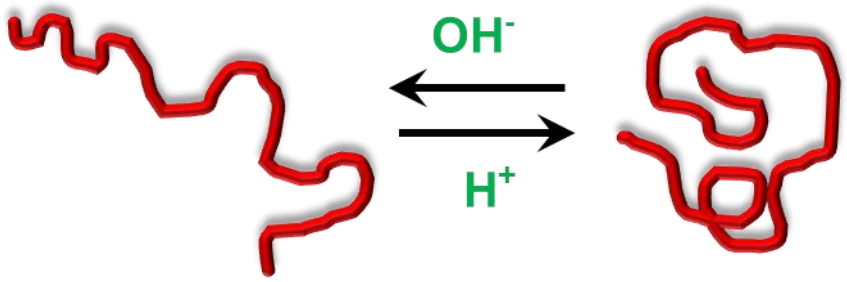

Figure 4.13 Schematic illustration for the conformation of alginate chain with adding acid or base.

4.6.3. **Fluorescence time-resolved anisotropy measurements (TRAMS) of AmNS -alginate as a function of pH**

The chain mobility of alginate in aqueous solutions has been examined using the TRAMS technique. Carboxyl groups of alginate were covalently labelled with AmNS molecules (0.96 mol%) as the fluorescent probe, and the rotational time of the probe was estimated as the measure of the mobility of the biopolymer chain.

For the time-resolved anisotropy work, parallel and perpendicular fluorescence intensity decay curves were generated after excitation with vertically polarized light analysed at 450 nm from 10^{-1} wt% of AmNS- labelled alginate in aqueous solution. This contributed to resolve the anisotropy decay of the AmNS-labelled biopolymer. Selective decays are shown in Figure 4.14. As it can be observed, a long duration anisotropy decay is given at pH 2 compared to pH 12, which indicates that the mobility of the macromolecule is restricted when the alginate chain is coiled in acidic media. Apart from pH 3, the raw curves for each of the samples were similar to Figure 4.14 (anisotropy pH 12). However, gradual changes in the correlation times as a function of pH are noted and this can be attributed to a conformational change in the alginate structure.

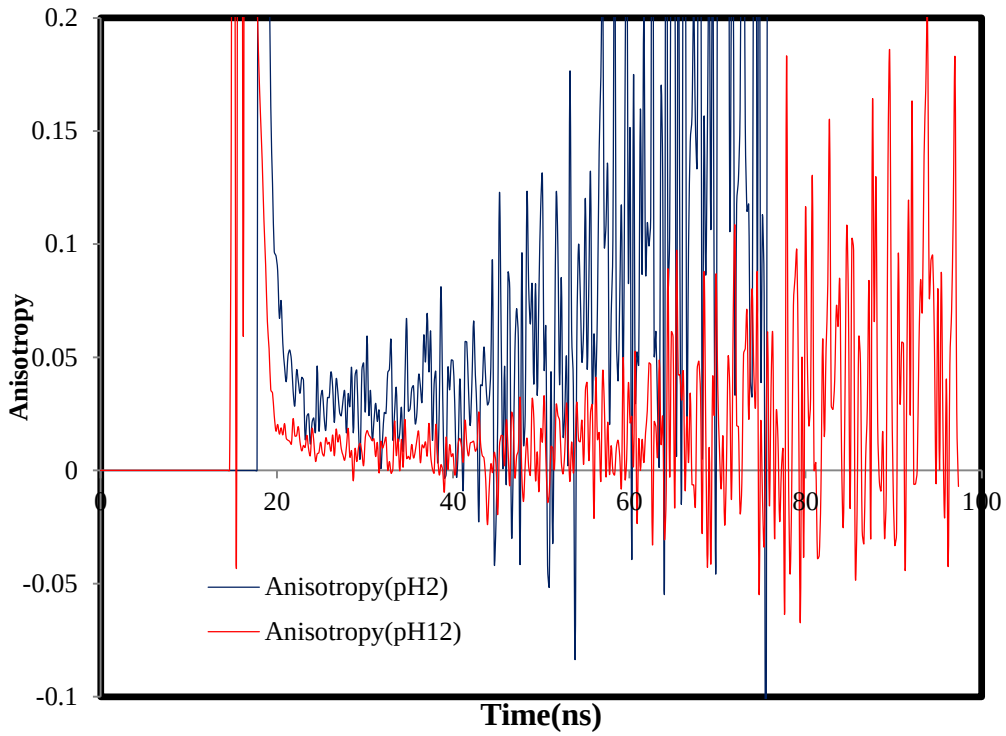

Figure 4.14 Decay of anisotropy, r(t), of 10^{-1} wt% AmNS- labelled alginate in aqueous solution at pH 2(blue line) and pH 12(red line). (λ_{ex}=370nm and λ_{em}=450nm).

Figure 4.15 displays the rotational correlation time of AmNS-alginate as a function of pH, indicating the pH dependence of τ_c for alginate in aqueous solutions. As can be seen, between pH 2 and 6 the τ_c decreases from ~6.5 ns to ~2 ns, this suggests that within this range there is a change in the alginate chain conformation from a coiled to an expanded form as the pH is increased. Additionally, the figure shows that the chain mobility of alginate decreases (i.e. high τ_c value) with decreasing pH. This could be attributed to the fact that carboxyl groups dissociate to become negatively charged under high pH conditions causing an expansion of the biopolymer chain[103]. At low pH conditions the carboxylic group exist as neutral moiety resulting in a collapsed polymer form (Figure 4.13). The pH dependence observed in Figure 4.15 implies that the mobility of the collapsed alginate chain is slower than that of the partly expanded chain. It can be noted that the pH dependence of the conformation of alginic acid is clearly similar to the behaviour of synthetic poly (acrylic acid) discussed in Chapter 3. The pH

dependence of the conformation of the alginate chain is also in agreement with recent research, which reports the aggregation of alginic acid occurring at pH less than 4.1[95].

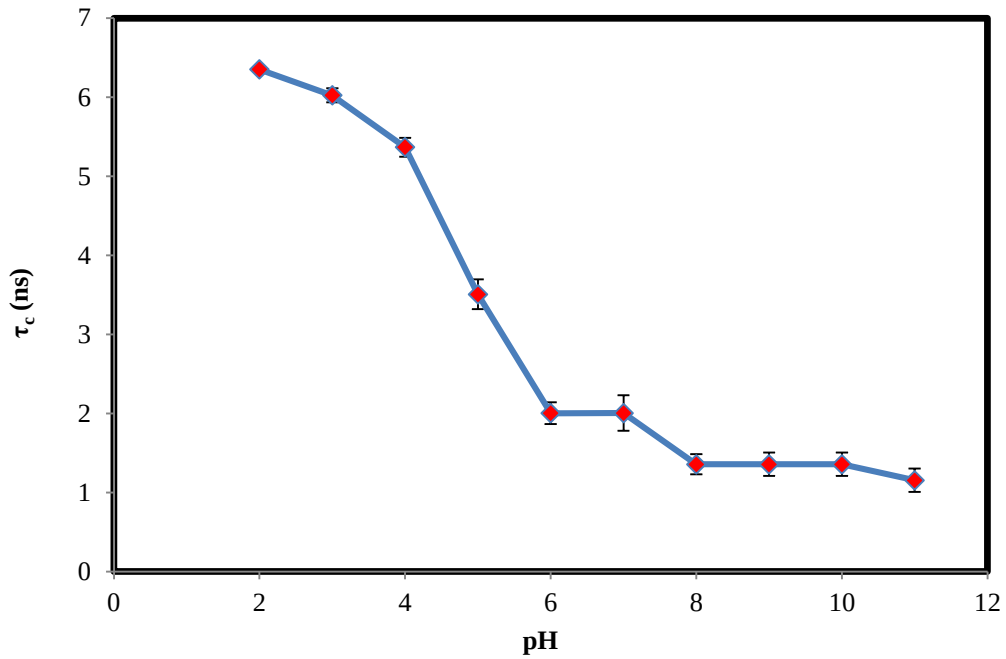

Figure 4.15 Correlation times(τ_c) for molecular segmental motion of 10^{-1} wt% AmNS- labelled alginate in aqueous solution at different pH values. (λ_{ex}=370nm and λ_{em}=450nm).

This conformational assumption is also supported by the fact that at pH levels of 5 and above, a single exponential function is adequate to describe the anisotropy decay. While at values below 5 a double exponential function is needed to obtain a χ^2 value close to unity suggesting that the fluorescence label is present in a more complicated system (a collapsed form: the AmNS is distributed in hydrophobic and hydrophilic media). This in agreement with the alginate conformations that was determined by DLS at different pH values [103]. It was found that an increase in the aggregation diameter between pH 4.5 and 8.0, and the size of aggregations expands almost from ~325 nm to ~625 nm.

4.7. **Conformational Behaviour of AmNS-Alginate and Its Interaction with Sodium Ions**

The interaction of alginate with monovalent cations such as Na^+ was investigated in order to evaluate their effect on the anionic polyelectrolyte conformations. The fluorescence steady state and TRAMS data were collected for the AmNS-labelled-alginate as a function of sodium chloride concentration. Fluorescence studies enabled the observation of changes in the alginate conformation, aggregation and expansion. The results of the TRAMS provides a better understanding of conformational changes in the presence of multivalent cations.

4.7.1. **Fluorescence steady state spectra of AmNS-alginate as a function of NaCl concentration**

The steady-state fluorescence emission plots collected at pH 9 in water and in presence of NaCl concentrations ranging from 1 M to 5 M, are shown in Figure 4.16. The fluorescence intensity of aqueous AmNS-labelled-alginate is gradually quenched by increasing the NaCl concentration. Since the control experiment does not show any possibility that, the fluorescence of the free AmNS is quenched by the presence of NaCl (Figure 4.17), the observation suggests that the decrease in the fluorescence intensity for high salt concentrations results from the collapse of the biopolymer chain. This could be attributed to the decrease of the electrostatic repulsion between the ionized carboxylic groups and alcoholic moieties because of the sodium ions since screening of the negatively charged alginate chain by Na cations cause a transition of the open form to the partly coiled shape [104, 105].

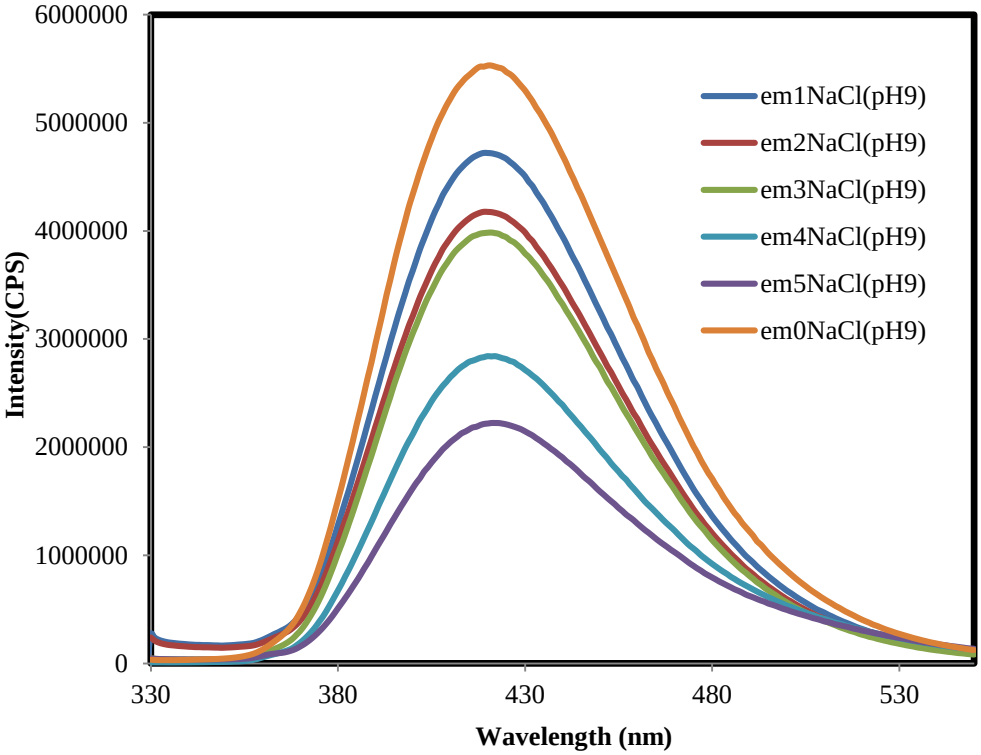

Figure 4.16 Fluorescence emission spectra for 10^{-1}w%AmNs-alginate in water as a function of NaCl concentration ranging from 1 M to 5 M at pH=9, λ_{ex}= 320nm.

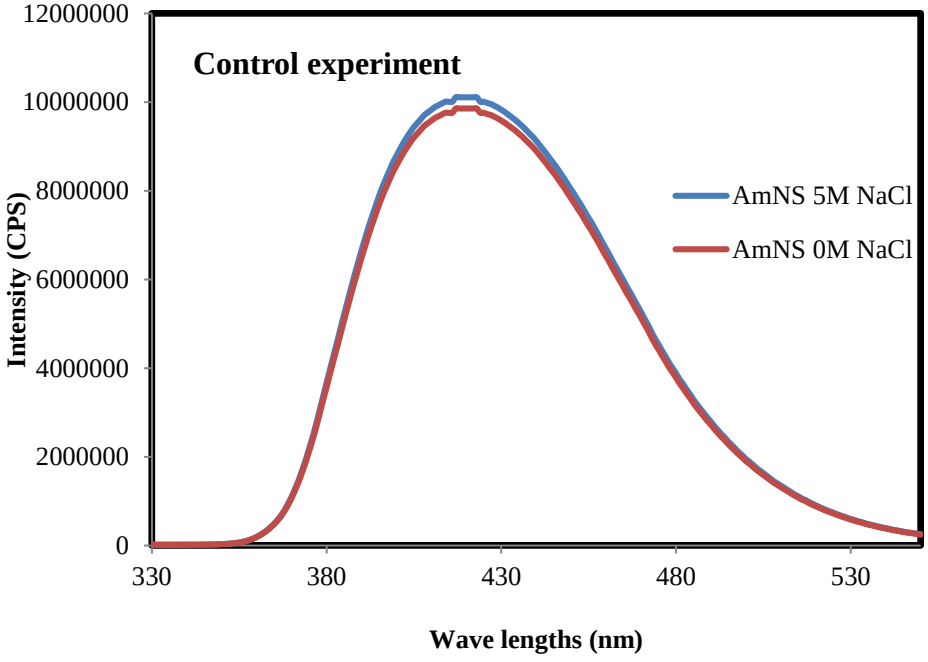

Figure 4.17 Fluorescence emission spectra for 10^{-5} M AmNS in water and in 5 M NaCl at pH=9, λex= 320nm.

4.7.2. **Fluorescence time-resolved anisotropy measurements (TRAMS) of AmNS-alginate as a function of NaCl concentration**

Figure 4.18 presents the plots of τ_c with respect to the concentration of NaCl added to the AmNS-alginate solutions at pH 3 and 9. A marked increase of correlation times (ca.~7 to ~ 29 ns) with increasing concentration of NaCl was recorded at pH 9, whereas a much smaller increase was noted at pH3. However, over the entire concentration range the increment in correlation time values at pH 9 is higher than in those at pH 3. The Figure also illustrates that τ_c is independent of the NaCl concentration up to 2 M at both pH values. The possible effect of Na^+ cations at pH 9 is a shielding effect on the electrostatic repulsions between the anionic COO^- groups and C-O^- moieties in polyelectrolytes [104, 105]. This may lead to the screening of the electrostatic repulsion in the entire alginate chain. As a result, the collapsed biopolymer chains move slower than the expanded coils. This has been previously observed in relation to changes in viscosity of a polysaccharide solution. It has been reported that the intrinsic viscosity for polysaccharides solution decreases with an increasing concentration of salt in basic medium, which indicates that the electrolyte polysaccharide chains assume coiled conformations at high salt concentration [106].

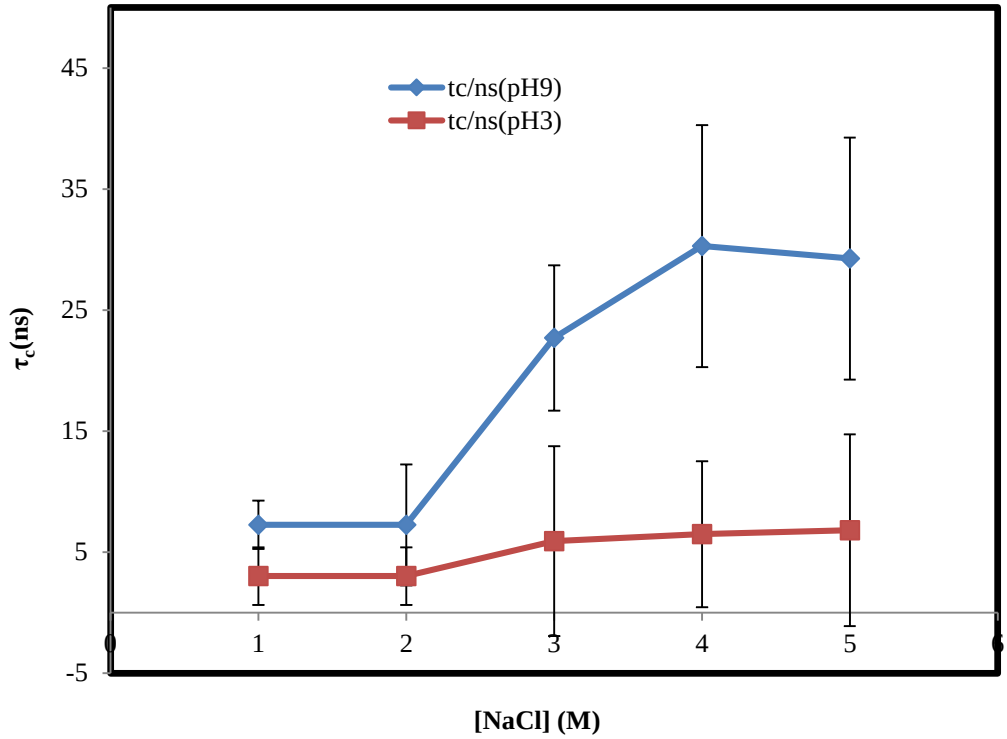

Figure 4.18 Correlation times(τ_c) for molecular segmental motion of 10^{-1} wt% AmNS- labelled alginate in aqueous solution in different NaCl concentration(M) at pH9(blue curve) and pH 3(red curve). (λ_{ex}=370nm and λ_{em}=450nm).

4.8. Conformational Behaviour of AmNS-Alginate and Its Interaction with Calcium Ions

The influence of cations in solution may be different between monovalent and divalent. It is expected that divalent ions will have a higher attractive interaction with deprotonated carboxylate groups due to higher charge. This may lead to a change in conformation that would be related to the charge of the cation. A better understanding of the conformational changes exhibited by the alginate interaction with Ca^{2+} ions in dilute aqueous solution can be investigated by the fluorescence technique. The fluorescence steady-state and time resolved anisotropy records were collected for the AmNS-labelled alginate as a function of calcium chloride concentration.

4.8.1. **Fluorescence steady state spectra of AmNS-alginate as a function of $CaCl_2$ concentration**

Figure 4.19 shows the steady-state fluorescence emission plots versus the $CaCl_2$ concentration at pH 9, with calcium chloride concentration ranging from 0.1 M to 1.5 M. Below 0.1 M no important effect of Ca^{2+} ions were observed (data are not presented), and above 1.5 M is the solubility limit of $CaCl_2$ in water. The spectra indicate the gradual decrease of the fluorescence intensity of aqueous AmNS-labelled-alginate by increasing the $CaCl_2$ concentration. Since the control experiment does not show any possibility that, the fluorescence of the free AmNS is quenched by the presence of $CaCl_2$ (Figure 4.20). The observation suggests that the decrease in the fluorescence intensity for high salt concentrations results from the collapse of the biopolymer chain. This could be attributed to the neutralising of COO^- and $C\text{-}O^-$ groups by linking with Ca^{2+} ions. Which leads to the aggregation of the anionic biopolymer chain [104, 105, 107], and hence the hydrophilic AmNS becomes sparingly soluble in a hydrophobic environment. This leads to quenching of the fluorescence intensity.

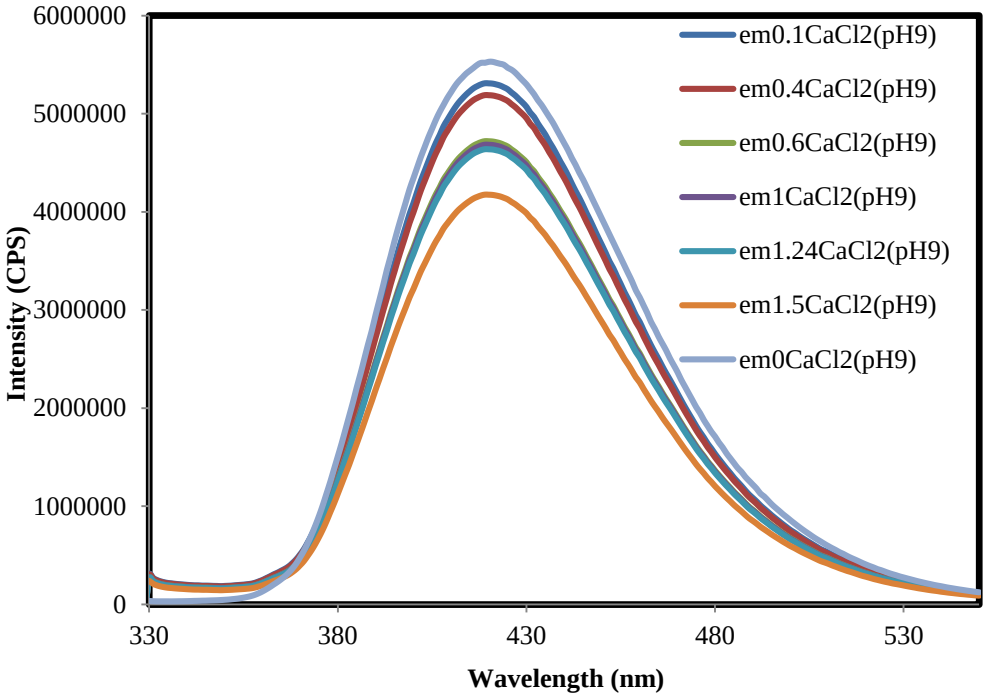

Figure 4.19 Fluorescence emission spectra for 10^{-1}w% AmNS-Alginate in water as a function of $CaCl_2$ concentration ranging from 0.1 M to 1.5 M at pH=9, λ_{ex}= 320 nm.

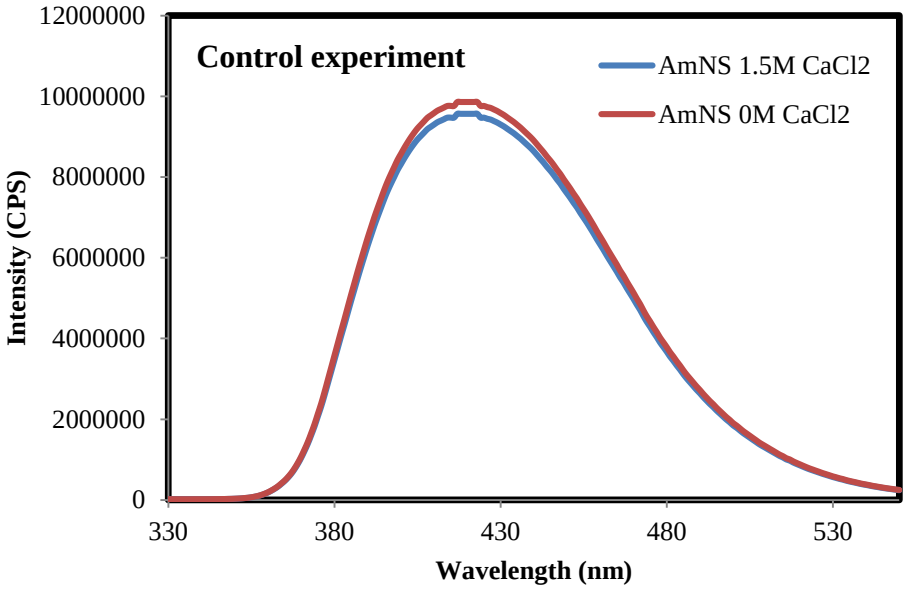

Figure 4.20 Fluorescence emission spectra for 10^{-5} M AmNS in water and in 1.5 M $CaCl_2$ at pH=9, λex= 320nm.

4.8.2. **Fluorescence time-resolved anisotropy measurements (TRAMS) of AmNS-alginate as a function of $CaCl_2$ concentration**

The cross-linking of alginic acid chain, which is induced by the interaction of Ca^{2+} ions with the carboxylate and $C\text{-}O^-$ anions groups, was also examined by measuring the correlation times as a function of calcium chloride concentration at pH 3 and 9, respectively, see Figure 4.21. A marked increase in correlation times (from 34 to 71 ns) with increasing concentration of $CaCl_2$ was recorded at pH 9, while a small increase was demonstrated at pH3 (from 4 to 18 ns). However, over the entire concentration range the rate of increment in τ_c values at pH 9 is more than in those at pH 3. The increase can be attributed to the interaction between Ca^{2+} ions and COO^- and $C\text{-}O^-$ groups of alginic acid [104, 105, 107]. Since the COOH and C-OH groups are deprotonated at pH9 compared to neutral groups present at pH 3, the interaction with Ca^{2+} ions is favoured. However, this interaction screens the carboxylate and alkoxy groups charge and leads to the collapse of the natural polyelectrolyte chain, which in turn inhibits the motion of the AmNS-alginate chain. The chelation of calcium cations by COO^- groups of alginate has been examined by atomic force microscopy (AFM) [108]. It was found that the addition of Ca^{2+} ions transformed the alginate solution into a thin gel, which indicates that the anionic polysaccharide chains assume coiled conformations in the presence of $CaCl_2$ salt. In other study [107], FTIR analysis showed that both COOH and C-OH functional groups in alginate are involved in the metal binding.

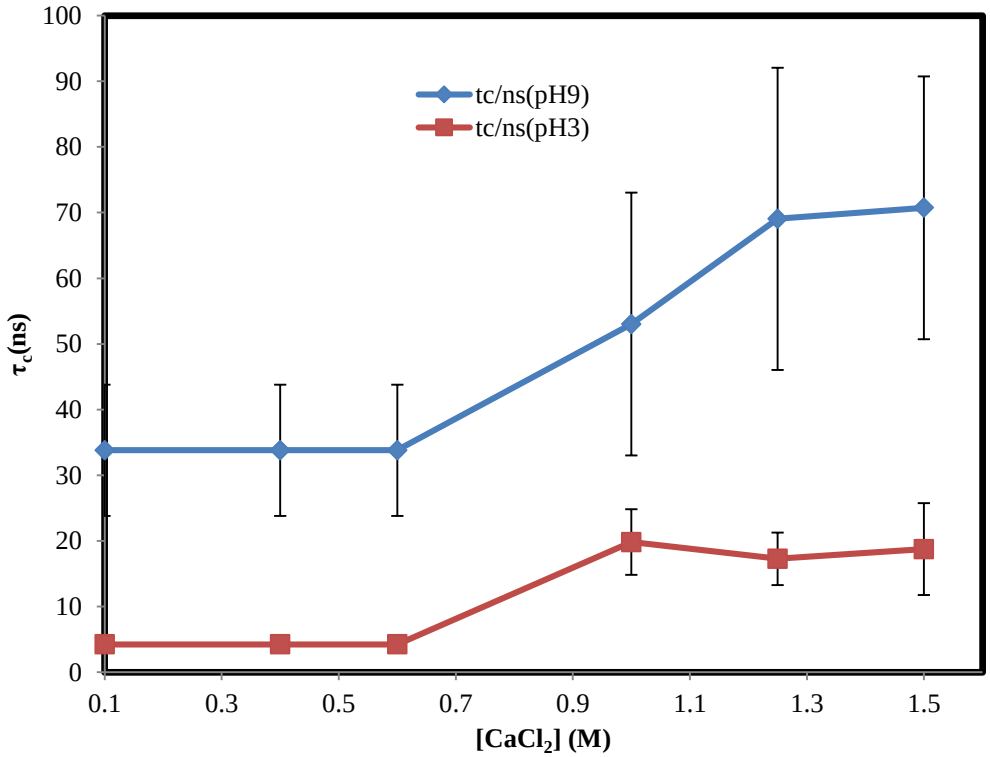

Figure 4.21 Correlation times(τ_c) for molecular segmental motion of 10^{-1} wt% AmNS- labelled alginate in aqueous solution in different $CaCl_2$ concentration at pH9(blue curve) and pH 3(red curve). (λ_{ex}= 370nm and λ_{em}=450nm).

4.9. **Adsorption of AmNS-Alginate on Silica Surface as a Function of pH**

Fluorescence steady state and anisotropy measurements were carried out on the AmNS-alginate at different silica concentration as a function of pH, with confidence that the free AmNS remains dispersed into the bulk solution and does not interact with silica after separation. Fluorescence steady-state spectroscopy was used to quantify the adsorbed amount of biopolymer on silica particles, while TRAMS was applied to investigate the dynamic behaviour of adsorbed alginate.

4.9.1. **Fluorescence steady state analysis of AmNS-alginate at silica surface as a function of pH**

Figure 4.22 shows the amount of adsorbed biopolymer (as percentage) as a function of pH and silica concentration. The percentage value of adsorbed alginate was calculated, using Equation 3.5. As an overall trend, the amount of adsorbed biopolymer increases by decreasing the pH from 11 to 2. The analysis of

surface charge of alginate and silica with the change of pH is essential to clarify the obtained dependencies. The zero point of charge of alginate is 2.83 [85], whereas it is ~3 of silica [16, 79, 80]. It means that apart from pH 2 the surfaces of SiO_2 and alginate are negatively charged in the completely studied pH range changing from 2 to 11. Under such conditions, the electrostatic repulsion between alginate chains and the silica particles takes place. pH increase causes the decrease of biopolymer adsorption due to electrostatic repulsion between the COO^- groups in alginate and the negatively charged silanol groups on the silica particle is becoming strong. The adsorption of alginate on the silica surface could be attributed to that non-electrostatic forces appear between alginate and the silica surface. Otherwise, the interaction of similarly charged materials should not occur [80]. X-ray photoelectron spectroscopy (XPS) and atomic force microscopy (AFM) have been used in the literature to characterize the adsorption of alginic acid to TiO_2 surface (pHzpc~5) as a function of solution pH [99]. It was found that alginic acid adsorbs in greater quantity at acidic pH than at basic pH. However, the role of the zero point of charge in the adsorption behaviour of biopolymer will be discussed further in the section 4.11.

In contrast, increasing the amount of SiO_2 leads to an increase in the amount of adsorbed polysaccharide. At low silica concentration, from 10^{-4} to 10^{-2} wt %, there is a slight increase in the adsorbed amount of alginic acid at pH 2 and 3, whereas no important adsorption was noted at pH levels 5, 7, 9 and 11. A gradual increase was recorded when the silica concentration was increased to 10 wt% at pH 2 and 3. Under these conditions, 11 % was the maximum percentage of the biopolymer attachment to silica particles. Although this amount is considered small, the fluorescence technique is sensitive enough to detect such low percentage from an adsorbed macromolecule. However, it should be noted that under the same conditions, twice the amount for poly (acrylic acid) is adsorbed (Figure 3.33) (Chapter 3). This could be attributed to that the COOH group of simple synthetic polymer (PAA) can easily contact with the silica particle, whereas the COOH groups of alginate suffer from a steric hindrance caused by the bulkier sugar units would have an impact on the COOH ability to attract to the silica surface.

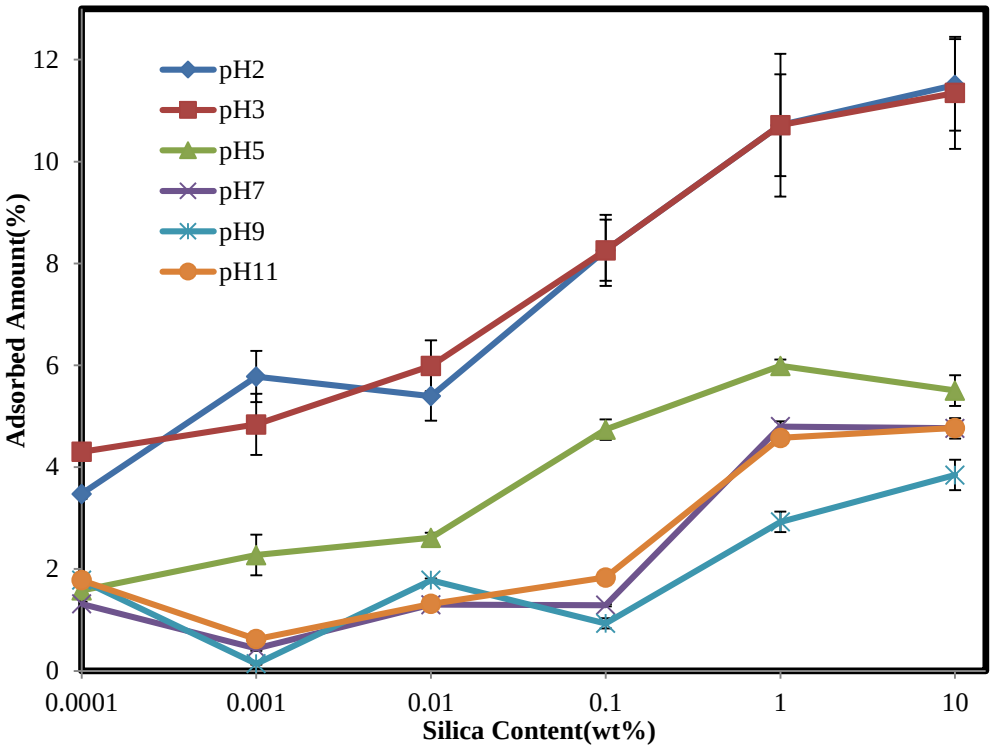

Figure 4.22 Adsorption of AmNS-labelled alginate on the silica as a function of silica concentration at various pH values. Concentration of biopolymer in the solution is 10^{-1} wt %.

4.9.2. Fluorescence time-resolved anisotropy measurements (TRAMS) of AmNS-alginate at silica surface as a function of pH

From the previous chapter, it can be concluded that the adsorption of synthetic polyelectrolyte, such as PAA to a solid surface is accompanied by changes in its segmental mobility. Techniques like TRAMS, which monitor polymer dynamic, should be useful for investigating biomacromolecule-surface interactions and interfaces. In this section, we describe a preliminary experiment aimed at assessing the applicability of TRAMS to monitor the adsorption of fluorescently labelled biopolymer onto solid particle. We present here the results of a mathematical analysis of the raw anisotropy decays from the biopolymer-silica system, and discuss the dynamic behaviour of alginate on a silica surface.

Figure 4.23 shows the fluorescence time-resolved decays of AmNS-labelled alginate (10^{-1} wt %). Parallel and perpendicular fluorescence intensities

are plotted logarithmically against time on the nanosecond time range. Shortly after excitation, the two polarized fluorescence decays were separated from each other for long time, when the biopolymer was adsorbed onto the silica.

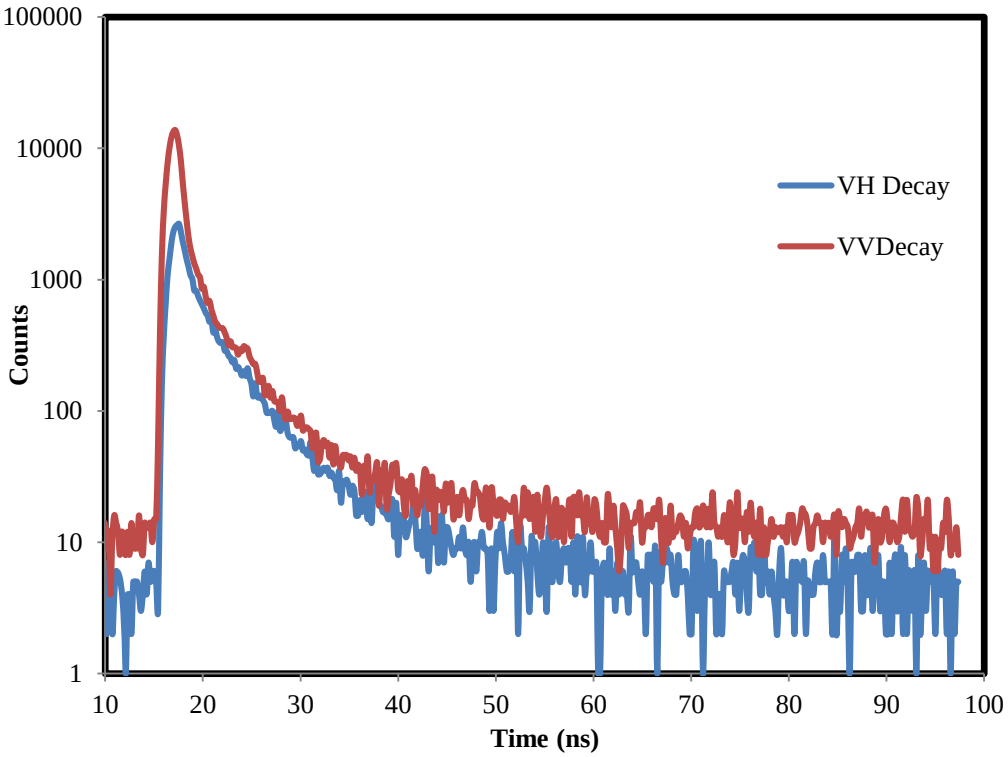

Figure 4.23 Parallel (red curve) and perpendicular (blue curve) fluorescence intensity decay curves following excitation with vertically polarized light (λ_{ex}= 370 nm) analysed at 450 nm from 10^{-1} wt% AmNS-labelled alginate aqueous solution in 10w% silica at pH = 2.

Figure 4.24 compares the fluorescence anisotropy decays of AmNS-labelled-alginate in water in the absence and presence of silica and shows that the anisotropy decays rapidly to zero in the absence of silica. Conversely, in the presence of silica, the anisotropy does not decay to zero for a longer time. This photophysical behaviour can be clarified as follows. Since the AmNS label was randomly attached to the biopolymer backbone. As chains require physical contact with the solid surface, and the control experiments proved that AmNS alone did not adsorb onto silica (see Figure 4.5 and Figure 4.6), this indicates that the biopolymer chain attaches to silica suspension. This in turn, leads to the restriction

of the segmental motion of fluorescently labelled biopolymer and longer anisotropy decay is observed accordingly.

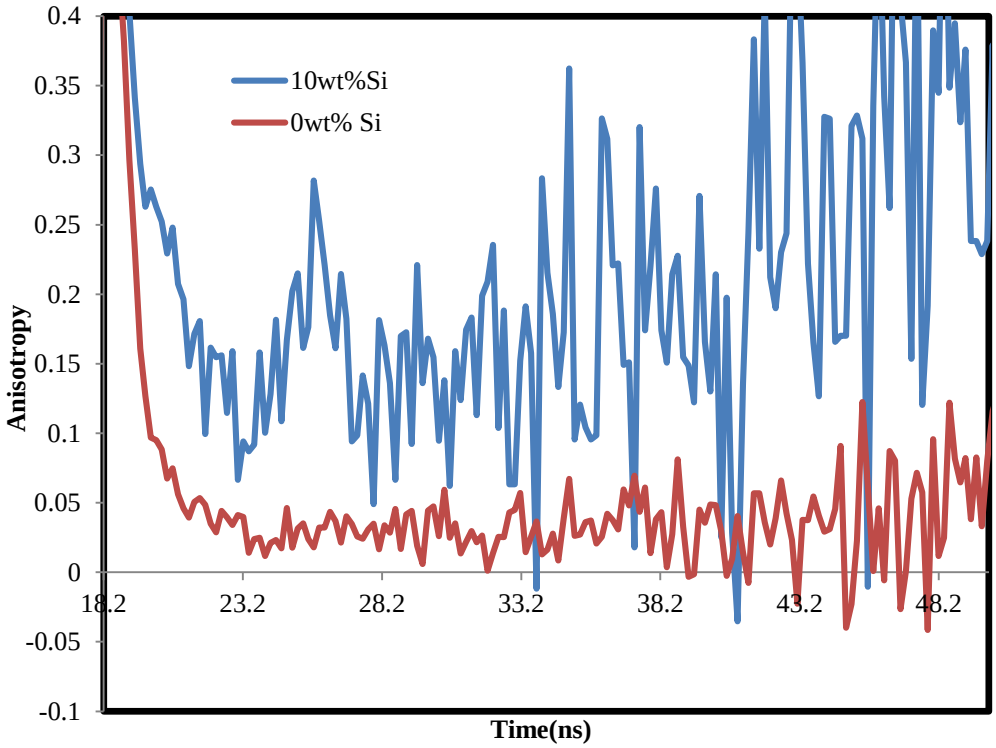

Figure 4.24 Fluorescence time resolved anisotropy data of aqueous AmNS-labelled alginate solution (10^{-1} wt %) in the absence of silica(red curve) and at the silica concentration of 10wt%(blue curve). λ_{ex}= 370 nm and λ_{em}= 450 nm.

Likewise, the anisotropy decay of the biopolymer in the presence of silica was found to be pH dependent. Figure 4.25 displays the anisotropy decays of alginate in the presence of 10 wt % silica at pH 2 and 11, respectively. It was found that the anisotropy decays rapidly to zero at pH11, whereas at pH 2 the anisotropy stays relatively higher than zero for a longer period.

The correlation times derived from mathematical analysis of anisotropy decays of AmNS-labelled-alginate (10^{-1} wt%) were plotted against the silica content at different pH values, as presented in Figure 4.26. When the concentration of added silica is low (10^{-4}, 10^{-3} and 10^{-2} wt%) no important adsorption occurs and the AmNS label exists in a homogeneous environment. In these cases, a single exponential function (Equation 1.21) could be used to calculate the correlation

times in nanoseconds. When the concentration of colloid is increased to 10 wt%, absorption begins while some of polymer remains in the bulk solution. In this complex situation a double exponential fit (Equation 1.22) presented the best results which indicates that different environments around the polymer chain might exist (adsorbed vs. free) affecting the motion of the polymer backbone.

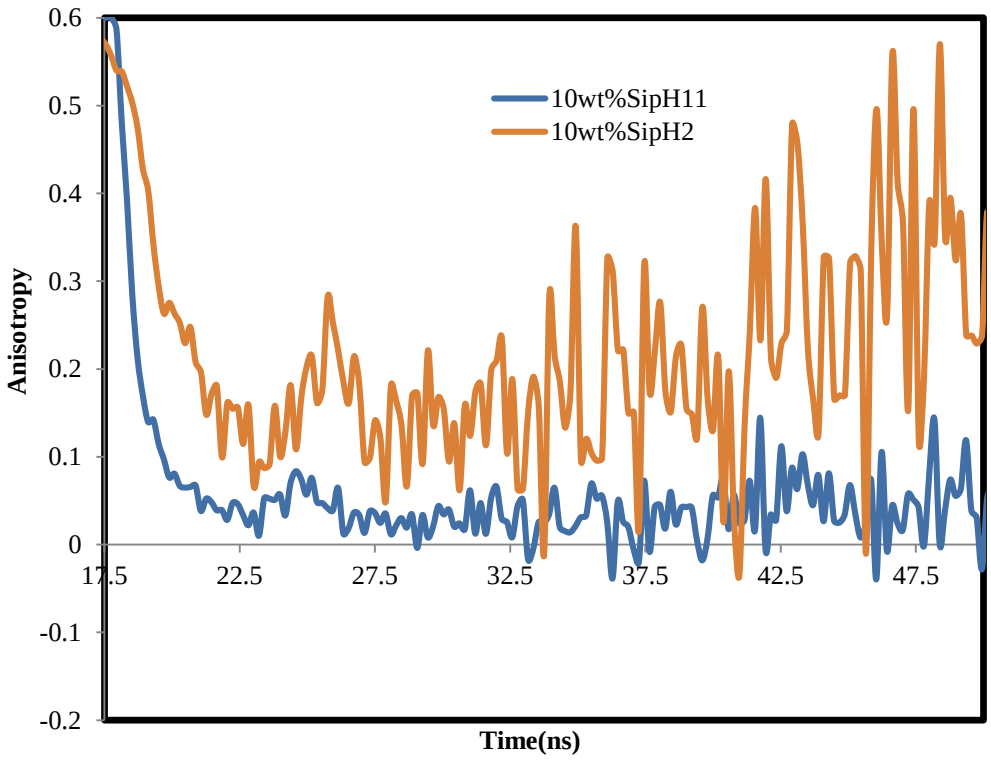

Figure 4.25 Fluorescence time resolved anisotropy data of aqueous AmNS-labelled alginate solution (10^{-1} wt%) at the silica concentration of 10wt%, pH 11(blue curve) and pH2(orange curve). (λ_{ex}= 370 nm and λ_{em}= 450 nm).

Generally, the correlation time increased with decreasing pH from 11 to 2, but increasing the amount of silica led to an increase in the τ_c values. Definitely at a low concentration of silica, from 10^{-4} to 10^{-2} wt%, there was a gradual increase in the correlation time values at pH 2 and 3, but no important change was recorded at pH values 5,7,9 and 11. Then again, an obvious rise was identified when the silica content increased to 1 wt% at pH 2 and 3. At 10 wt% of silica the correlation time remained approximately constant, this can be explained with saturation between the natural polyelectrolyte chain and the silica. However, a small increase

was recorded at pH values, 5,7,9 and 11 for silica concentration range from 10^{-1} to 10 wt%.

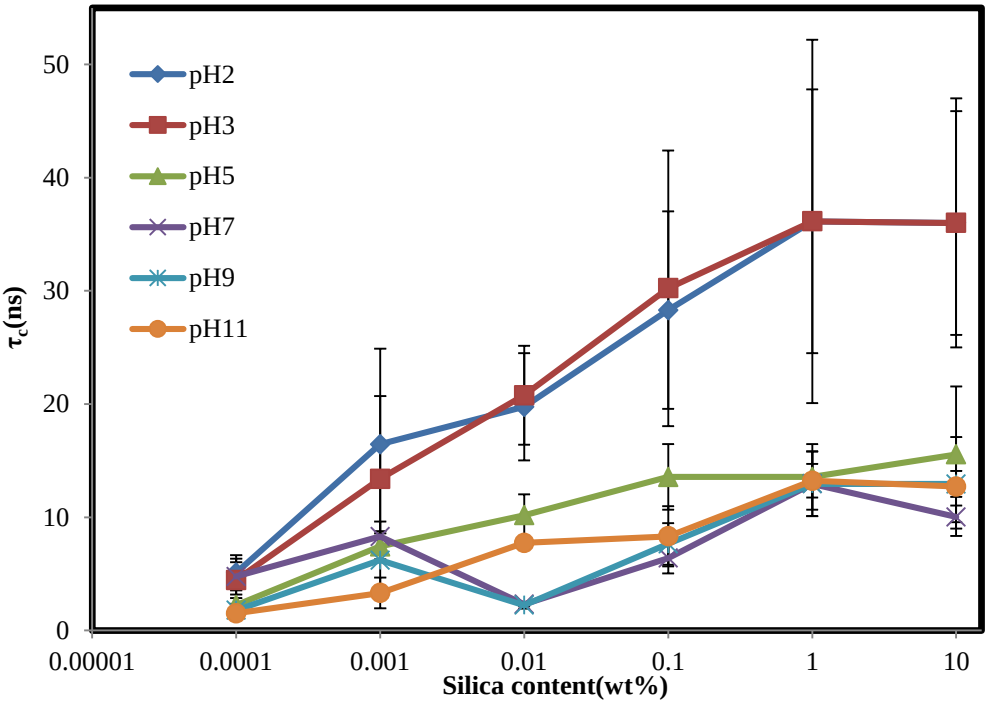

Figure 4.26 Correlation times of AmNS-labelled alginate as a function of silica concentration at various pH values.

4.10. **Adsorption of AmNS -Alginate at Alumina Surface as a Function of pH**

Fluorescence steady state and anisotropy techniques were used to study the adsorption of AmNS-alginate alumina particles after ensuring that the free AmNS fluorophore did not to attach at the alumina surface (section 4.5.).

4.10.1. **Fluorescence steady state spectra of AmNS-alginate at alumina surface as a function of pH**

The fluorescence emission spectra of 0.1 wt % of AmNS-alginate at pH 3 and 11 in 10 wt% alumina are displayed in Figure 4.27 and Figure 4.28. As mentioned before in the experimental part of the adsorption experiment the fluorescence intensities were recorded before and after separation (section 2.9.). The results showed that the fluorescence intensity of the supernatant is importantly reduced at pH 3 compared to a minor reduction at pH11, suggesting that, a large

quantity of biopolymer attaches to alumina at pH3 while a smaller quantity is adsorbed at pH 11.

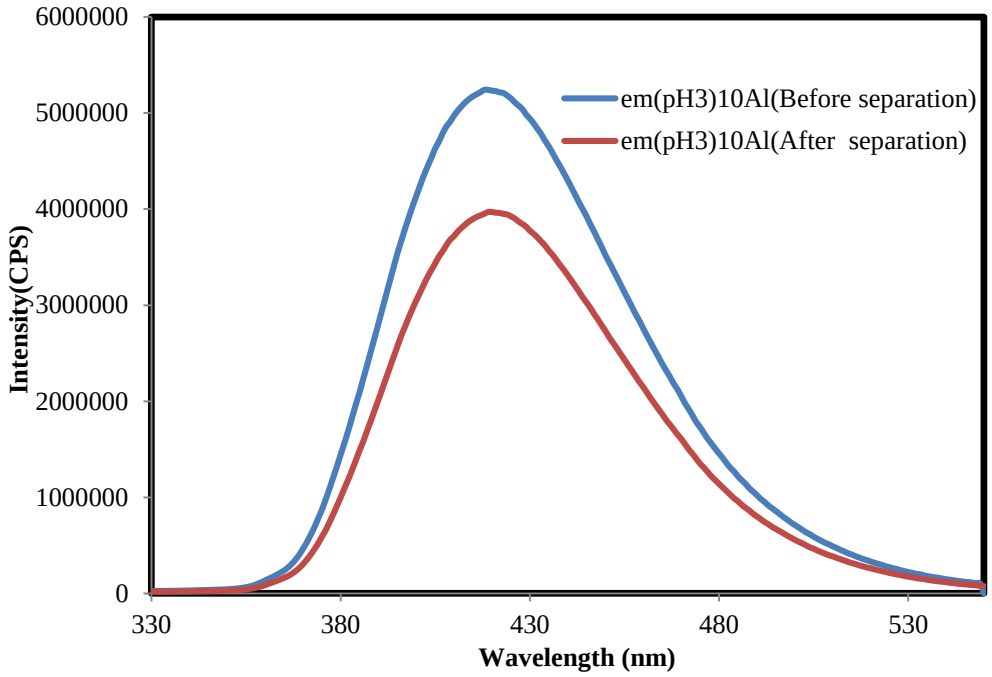

Figure 4.27 Steady state fluorescence emission spectra of aqueous AmNS-labelled alginate (10^{-1} wt%) and alumina (10 wt%) solutions before and after the separation at pH3, λ_{ex}= 320 nm.

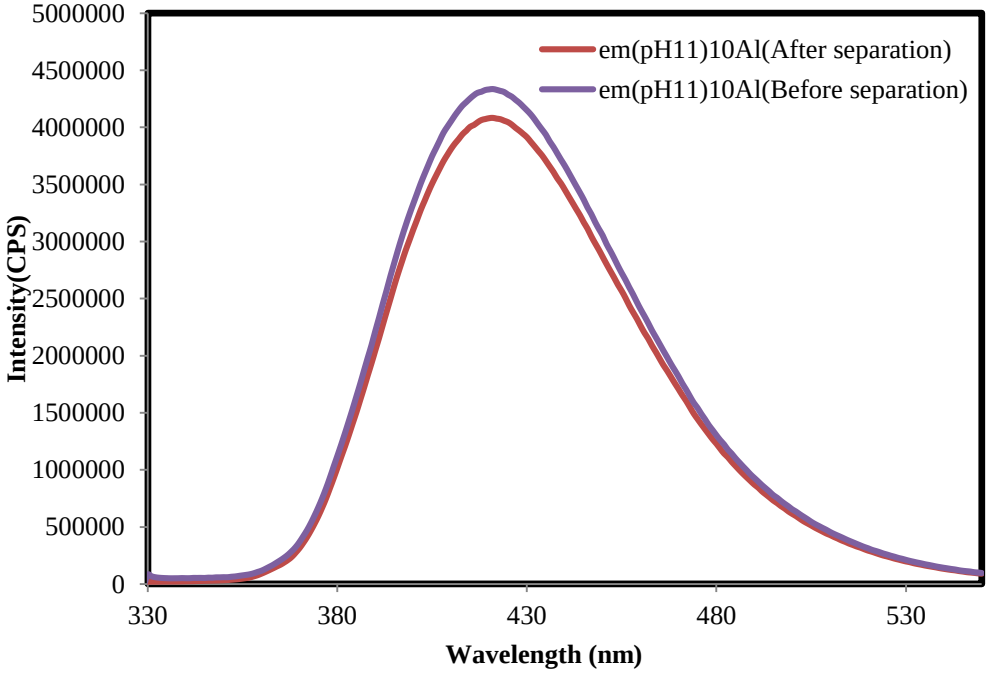

Figure 4.28 Steady state fluorescence emission spectra of aqueous AmNS-labelled alginate (10^{-1} wt %) and alumina (10 wt %) solutions before and after the separation at pH11, λ_{ex}= 320 nm.

Figure 4.29 presents the percentage amount of adsorbed alginate as a function of pH and alumina concentration. In general, the amount of adsorbed biopolymer increases when the pH drops from 11 to 2. The pH dependence of the adsorption could be attributed to the biopolymer and mineral pHzpc values, which are 2.83 [85] and ~ 9 [79], respectively. It means that apart from pH 9 and 11 the surface of alumina is positively charged, while the alginate is negatively charged in the pH range from 3 to 11. As a result, the electrostatic attraction between alginate chains and the alumina particles takes place at the pH values 7, 5 and 3. pH decrease causes the increase of biopolymer adsorption due to electrostatic attraction between the COO^- groups in alginate and the positively charged alumina groups is becoming strong. When both the biopolymer and alumina have the same kind of charge (i.e. at pH 9 and 11). The adsorption of alginate on the alumina surface could be attributed to that non-electrostatic forces appear between biopolymer and the mineral surface. Otherwise, the interaction of similarly charged materials should not occur [80]. At pH 2 besides the non-electrostatic forces, the hydrogen bonding could be responsible for adsorption.

The effect of pH on the adsorption of PAA (a typical model for alginate) to alumina was reported elsewhere [109]. It was found that a higher adsorption at the lower pH. This means that the surface of alumina is positively charged, while polyelectrolyte is negatively charged. Moreover, electrostatic interactions between the polyelectrolyte and the alumina surface play a key role in the adsorption of polymer. However, the role of the zero point of charge in the adsorption behaviour of biopolymer will be discussed further in the section 4.11. On contrary, the biopolymer adsorption increases by increasing the quantity of added mineral (from 10^{-4} to 10 wt %). Specifically, a gradual increase in the adsorbed alginate at pH values of 5, 7, 9 and11. Whereas, a marked increase was observed at pH 2 and 3, as the percentage of adsorbed alginate reaches the maximum value (~26%). Under such conditions only ~11 % of biopolymer was adsorbed on silica. This could be attributed to that at acidic media the alginate becomes relatively neutral and the biopolymer chain is more collapsed in an adsorbed state. Thus, unionised carboxylic acid (COOH) and hydroxyl (C-OH) groups adsorb via hydrogen bonding between the biopolymer carbonyl group and hydroxyls on alumina

surface [16]. Hence, at lower pH values the adsorption mechanism is predominantly hydrogen bonding in nature, whereas alginate does not adsorb significantly onto silica due to electrostatic repulsion.

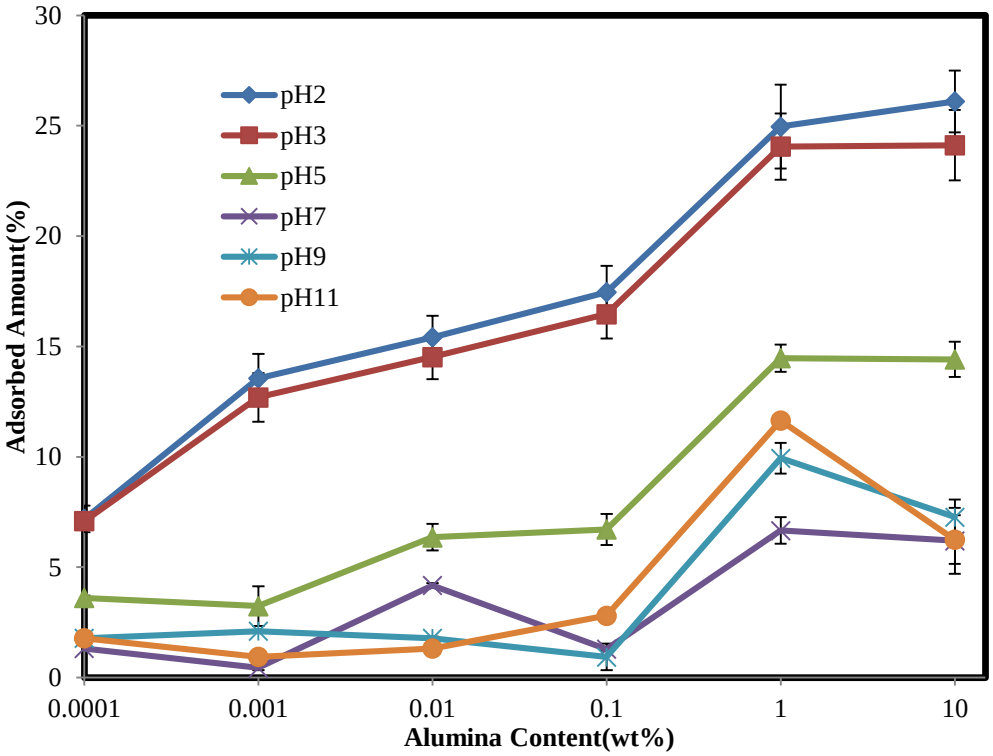

Figure 4.29 Adsorption of AmNS-labelled alginate on the alumina as a function of alumina concentration at various pH values. Concentration of biopolymer in the solution is 10^{-1} wt%.

4.10.2. Fluorescence time-resolved anisotropy measurements (TRAMS) of AmNS-alginate at alumina surface as a function of pH

Figure 4.30 matches the fluorescence anisotropy decays of AmNS-labelled-alginate in 0.0001 and 10 wt% of alumina, respectively. It was found that the anisotropy quickly drops to zero in the presence of 0.0001 wt% alumina, this proposes that an extremely dilute concentration from Al_2O_3 particles is not enough to be attached with alginate chain, accordingly cannot alter the macromolecule dynamic. When 10 wt% of alumina was added, the anisotropy did not decay entirely to zero. This result suggets that the macromolecule chain adsorbs onto the alumina particles, which in turn slows down the segmental motion of fluorescently

labelled biopolymer; hence a long anisotropy decay is observed in the presence of high concentration from alumina.

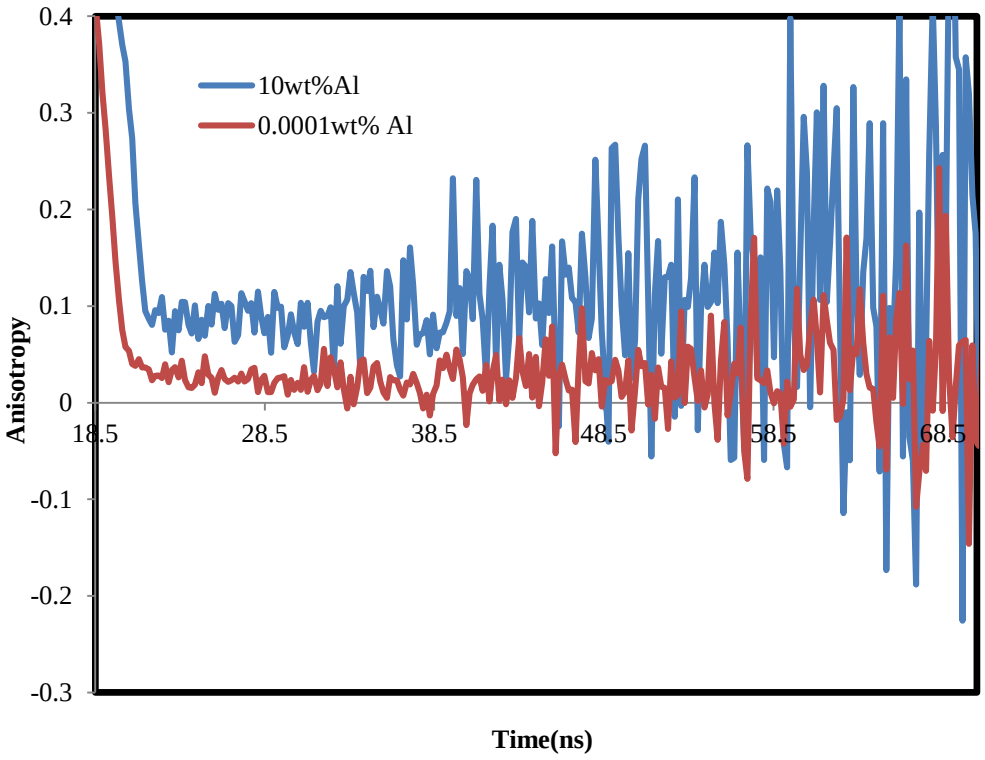

Figure 4.30 Fluorescence time resolved anisotropy data of aqueous AmNS-labelled alginate solution (10^{-1} wt%) at the alumina concentration of 0.0001wt%(red curve) and at the alumina concentration of 10wt%(blue curve). (λ_{ex}= 370 nm and λem= 450 nm).

Similarly, the anisotropy decay of the biopolymer in the presence of alumina was found to be pH dependent. Figure 4.31 displays the anisotropy decays of alginate in the presence of 10 wt % alumina at pH 2 and pH11, respectively. It was found that the anisotropy decays rapidly to zero at pH11, whereas at pH 2 the anisotropy stays for a longer period. This confirms the suggestion that the collapsed alginate chains adsorb more than the expanded coils.

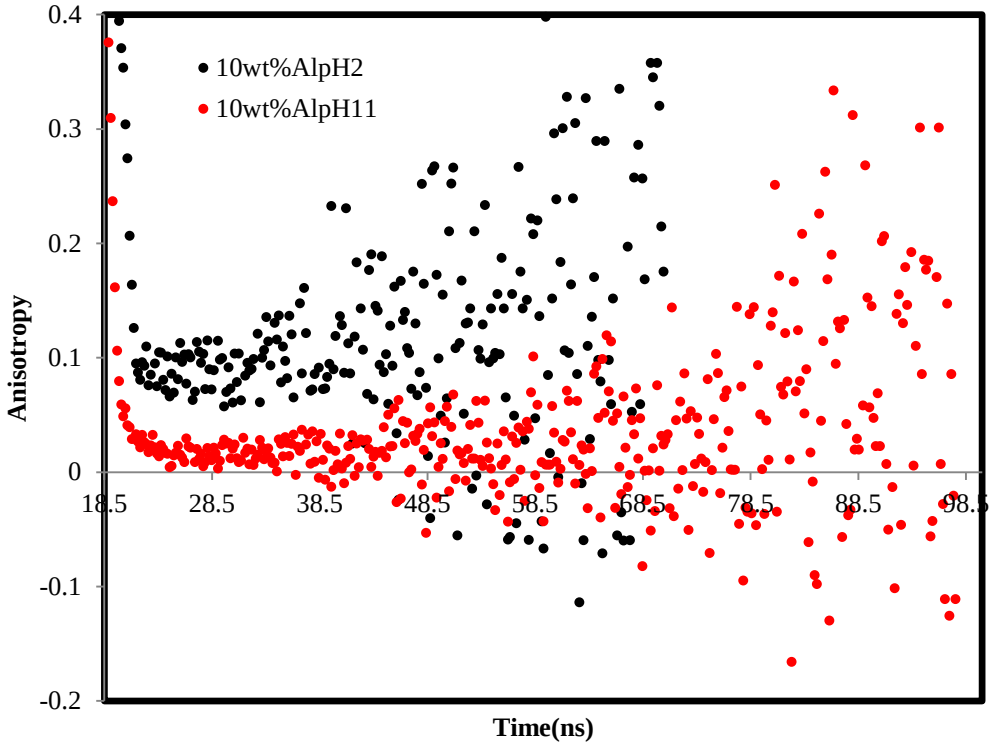

Figure 4.31 Fluorescence time resolved anisotropy decays of aqueous AmNS-labelled alginate solution (10^{-1} wt%) at the alumina concentration of 10wt%, pH 11(red curve) and pH2(black curve). (λ_{ex}= 370 nm and λ_{em}= 450 nm).

Figure 4.32 displays the correlation times (τ_c) of AmNS-labelled-alginate (10^{-1} wt %) as a function of alumina concentration at different pH values. It can be observed that from 10^{-4} to 10^{-2} wt% of alumina concentration there is a slight increase in the τ_c values over the whole pH range, this suggests a weak adsorption where the AmNS label exists in a semi homogeneous environment, since the vast majority of alginate chains are not adsorbed. In such cases, a single exponential fit is suitable to calculate the correlation time values in nanoseconds. A double exponential fit was selected to analyse the anisotropy decays at a concentration of alumina content equal to 0.1 wt % at pH 2 and 3, where the biopolymer partially adsorbs onto alumina, which means that the AmNS label is dispersed in two phases, solid and bulk solution. When the alumina concentration is increased to 10 wt %, an increase is recorded at pH 2 and pH 3, which means a strong adsorption occurs. In this case, a single exponential function was also believed to be suited to fit such anisotropy decays.

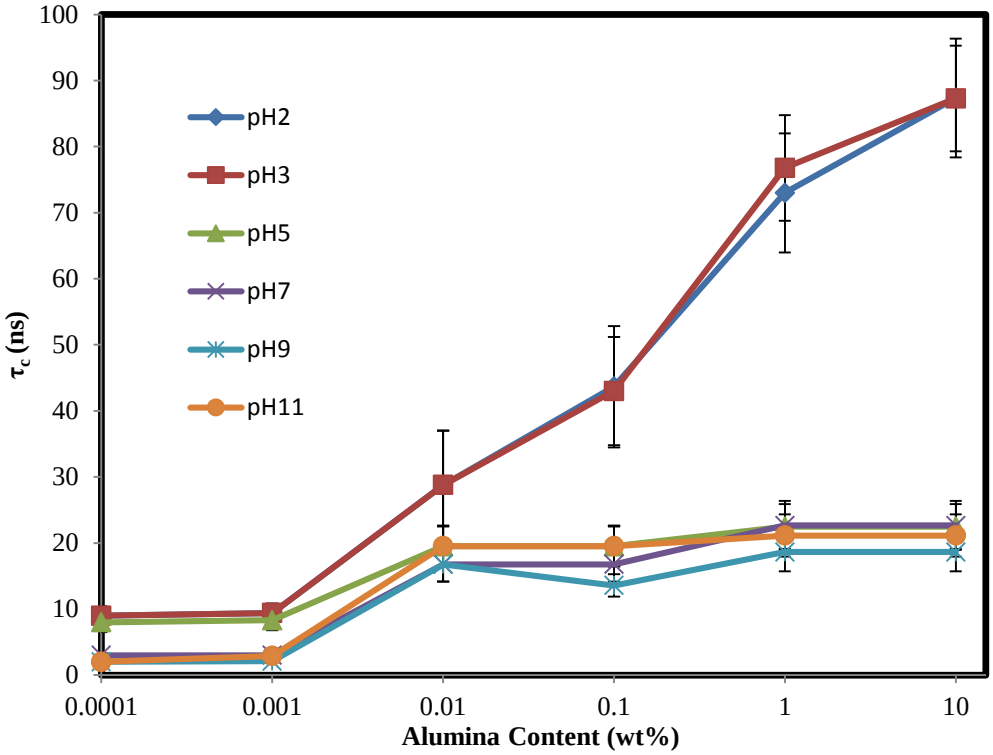

Figure 4.32 Correlation times of AmNS-labelled alginate as a function of alumina concentration at various pH values.

4.11. **Potentiometric Titration of Alginates**

The fluorescence experiments showed that the conformation of the biopolymer chain is changed from the expanded form to a collapsed coil under the influence of several factors such as pH and ionic strength. Additionally, coiled alginate chain adsorbs to a greater extent than open chains. It also showed that the polysaccharide chain is expanded at high pH values, while mostly collapsed in acid media. In this section, potentiometric titration technique is applied to study the acid-base behaviour of biopolymer as well as the effect of pH and ionic strength on the conformational behaviour of the semi-diluted aqueous solution of unlabelled alginic acid.

As shown in Figure 4.1 alginic acid chain composed of mannuronic acid and guluronic acid repeating units, which bears a carboxylic acid (COOH) group. In this work about 220 available carboxylic acid groups exist per macromolecule (M_n = 38782 g/mol). As a polymeric weak acid [110] a fraction of COOH groups for alginate dissociates to COO^- when the pH of the solution is changed. The

fraction of dissociated COOH groups for alginic acid *(α)* as a function of pH and at different NaCl concentration is illustrated in Figure 4.33. As it can be noted, *α* and, consequently, the negative charge of the alginate increase by increasing the pH and NaCl concentration. Exclusively, at pH 11 the polysaccharide bears a global negative charge and the COOH groups are totally ionized with *α* approaching one**.** In such condition, the fluorescence experiments proposed that the alginic acid chain is in the form of relatively expanded coil. This expanding is because of the electrostatic repulsion between the negatively charged COO^- moieties. The anion carboxylate are neutralized to COOH by adding acid until pH 2 and *α* approaches zero. In this case, the alginic acid chains become more hydrophobic and form a partially coiled chain, as suggested, using the fluorescence analysis.

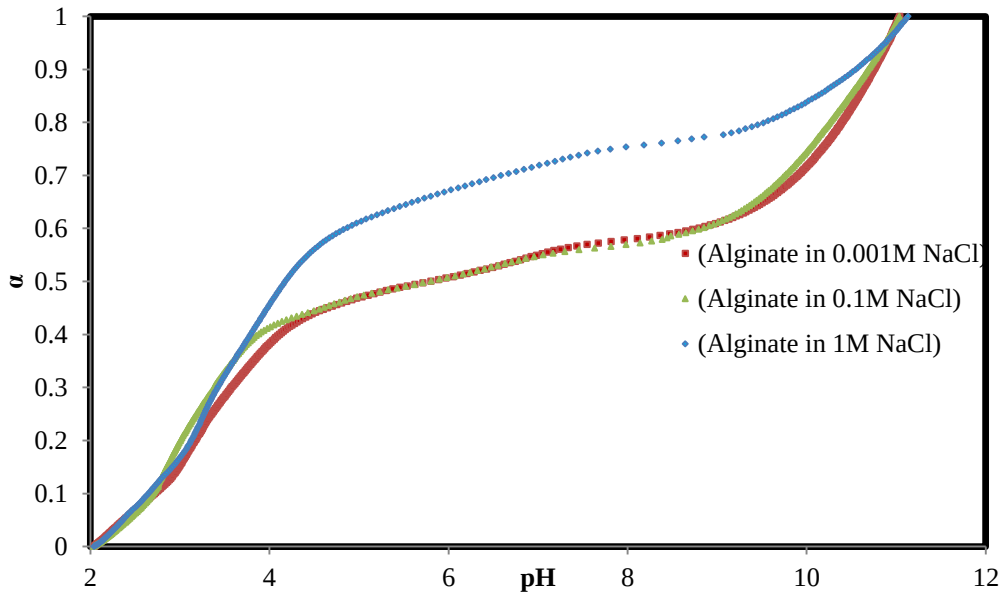

Figure 4.33 Fraction of acid groups ionized versus pH as a function of NaCl concentration for alginic acid.

Table 4.1 displays the *pKa* values of unlabelled and labelled alginic acid, calculated from the first derivative of titration curves. The numbers presented suggest the presence of hydroxyl and amine groups beside the carboxyl groups of alginic acid, where no important difference has been reported in the *pKa* values of labelled and unlabelled biopolymers. This confirms the fluorescence results,

which showed that the physicochemical behaviour for the labelled alginate is similar to that unlabelled biopolymer, and the fluorescent label does not disturb the biopolymer system.

Table 4.1 pKa Constants and pHzpc of labelled and unlabelled alginates as determined by titration curves.

System	NaCl (M)	$pKa_{(COOH)}$	$pKa_{(C\text{-}OH)}$	$pKa_{(C\text{-}NH_2)}$	pHzpc
Alginate	0.1	3.38	7.00	10.00	2.35
AmNS-alginate	0.1	3.40	7.06	9.60	2.38

Table 4.1 also displays the zero point of charge (pHzpc) for alginate and AmNS-alginate. The results show that the pHzpc value of labelled and unlabelled biopolymer is almost equivalent. This means that any conformational change in the alginate chains may occur due to the change in external conditions, such as pH. The AmNS label does not significantly affect the physicochemical behaviour of the polysaccharide backbone. However, the role of the pHzpc for alginates and minerals in the adsorption behaviour of polyelectrolytes will be discussed further in the following section.

The variation in the relative charge density of silica and alumina particles in the absence and presence of adsorbed alginate is illustrated in Figure 4.34. As it can be concluded clearly, the adsorption of the anionic polysaccharide decreases the positive charge considerably and lowers the pHzpc of the alumina from ~ 9 to 8.4, whereas no effect on the relative charge behaviour of silica suspension is recorded, since the pHzpc of the silica remains non shifted at ~3. These results propose that electrostatic interactions are predominantly responsible for the adsorption of alginic acid on Al_2O_3 molecules, whereas weak forces, such as Van der Waals assumed to control the interference between alginate and SiO_2 suspension. Since in acidic condition, the fluorescence experiment showed that the percentage of adsorbed natural polyelectrolyte reaches the value (~26%) on alumina, while only ~11% on silica. This is because at low pH levels (i.e. pH = 3)

the net charge on alumina is positive and alginate is negatively charged, whereas the silica particles are neutral.

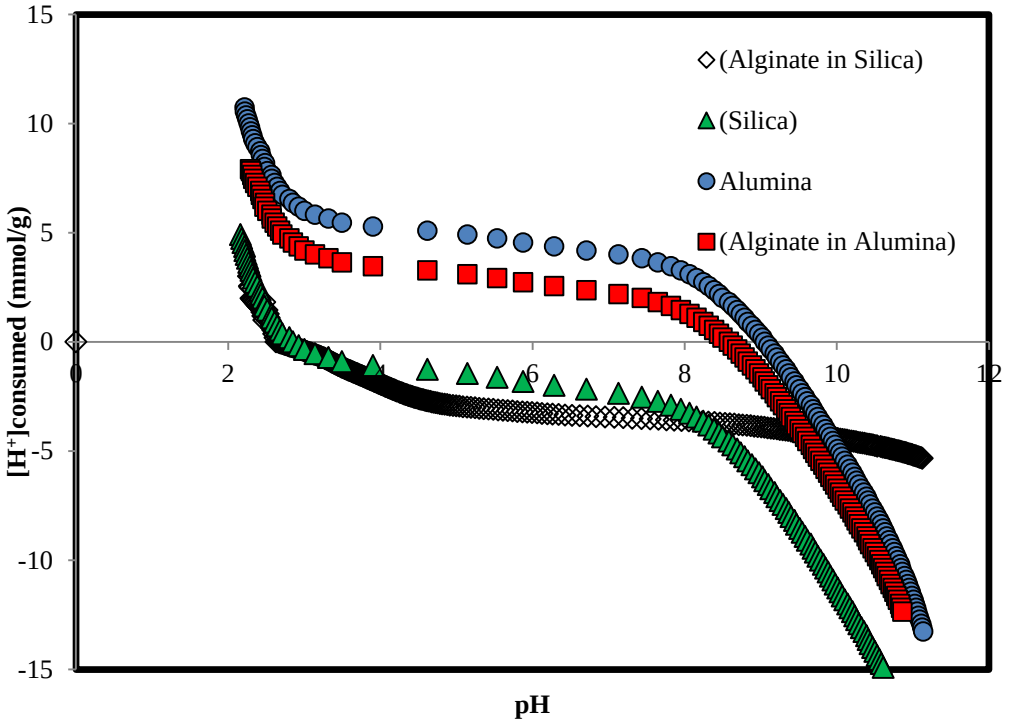

Figure 4.34 Relative surface charge versus pH for silica, alumina, alginate in alumina and alginate in silica.

4.12. **Inductively Coupled Plasma Mass Spectrometry Measurements (ICP-MS) of Silica and Alumina Adsorption on Alginate**

The results obtained from the fluorescence spectroscopy showed that a reasonable amount of fluorescently labelled biopolymer adsorbs on the surface of alumina in acidic media, but fewer adsorbs on silica suspension under the same conditions. Moreover, the increase in the quantity of solid added leads to an increase in the alginate adsorption. However, in this section, the ICP-MS is applied to quantify the adsorbed minerals on unlabelled alginic acid according to the procedure, outlined in the experimental part (section 2.9.).

Figure 3.35 shows the pH dependence for the adsorption of Al_2O_3 and SiO_2 on unlabelled alginate. As it can be observed, for the two examined minerals, the adsorption of alumina and silica on alginate increase when the pH of the solution is reduced from 11 to 2. However, the rate of increment in these amounts for silica

is less than in those for alumina. The effect of pH on the adsorbed amounts can be explained based on the type of the interaction of charged mineral with the polyelectrolyte chain. At pH lower than pHzpc of alumina (~9), the alumina is positively charged and the net charge on the alginate chain is negative. Because of that, the increase of alumina adsorption (from pH 7 to pH 3) could be attributed to that electrostatic attraction between the oppositely charged materials. A decline in the adsorption of alumina at pH higher 9 occurs because of the electrostatic repulsion between the negatively charged alumina and anionic polysaccharide. This adsorption behaviour coincides with the recent polyelectrolyte adsorption theory established by Van der Schee and Lyklema [32], which can be summarized as follows: adsorption of a negatively or partly negatively charged macromolecule on a positively charged mineral is influenced by electrostatic forces.

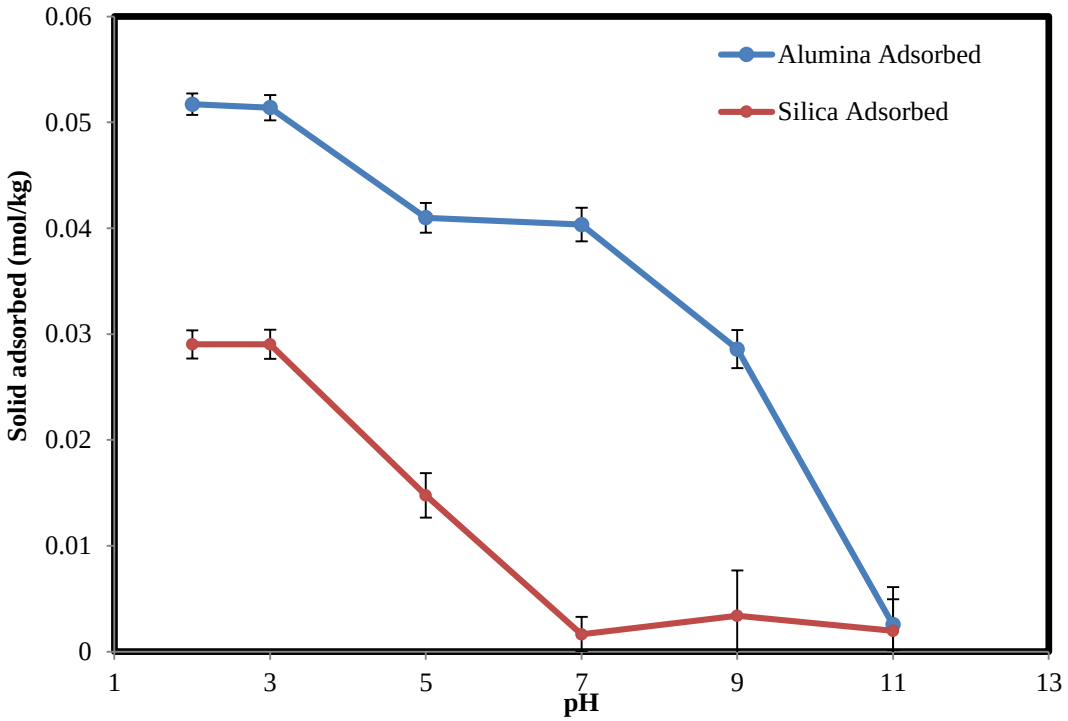

Figure 4.35 Effect of pH on the adsorption of alumina and silica on alginate (solid added 0.1M).

Interestingly, the alginate chain can adsorb on the alumina, as well as the silica particles over the entire studied pH range, even at pH values where which both the biopolymer and the solid have the same kind of charge. This could be attributed to the fact that non-electrostatic forces, such as Van der Waals, also play

a role in the adsorption between mineral and polyelectrolyte [86]. Otherwise, the adsorption of an anionic polysaccharide chain on the negatively charged mineral surface is not possible. Figure 4.36 shows the possible electrostatic interactions between alginate and minerals

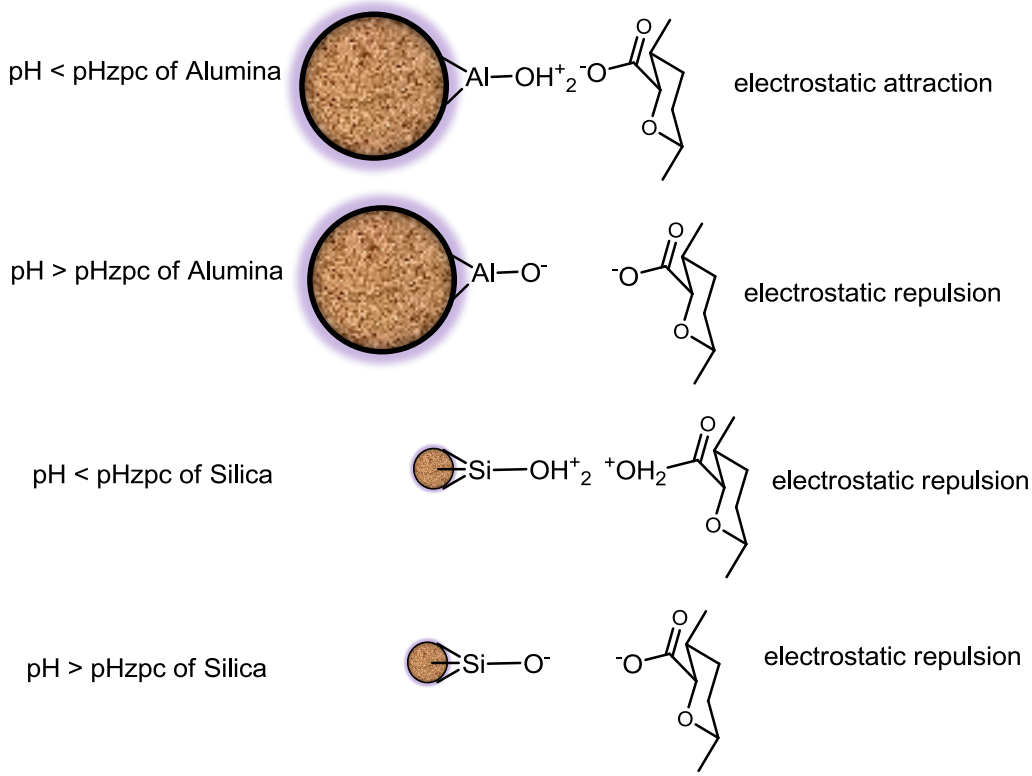

Figure 4.36 Schematic representation of the interaction between alginate and minerals.

In addition to particle charge, mineral concentration influences the adsorption process of minerals on natural polyelectrolyte. The alumina and silica isotherms plots representing the adsorbed amounts of minerals on the alginate were obtained (Figure 4.37) at pH 7 by varying the added concentration of minerals (~10^{-5} to 1 M). These adsorption measurements were carried out at the same concentration of biopolymer (10^{-1} wt %). It is evident from Figure 4.37 that the adsorbed amount of alumina on alginate increases markedly with increasing adding concentration of alumina in the liquid phase at pH 7. On the other hand, the shape of the isotherm suggests a weak affinity of alginate for silica (the adsorbed amounts are lower than alumina over the entire concentration range). This means that at pH 7 the electrostatic attraction (see Figure 4.36) enhanced the

adsorption of alumina. For example, at added concentration of ~1 *M*, the adsorbed amount of alumina on alginate is ~0.3 moll/kg, which is about 50 times greater than the adsorbed amount of silica on alginate.

The obtained isotherms are fitted to the Henry adsorption model according to Equation 3.12. These linear dependencies enable calculation of the affinity constant (K_h) of minerals adsorption from the slope of the Henry's equation. The obtained K_h and goodness of fit (R^2) values are given in Table 4.2. Considering the values of R^2 the Henry model is good to describe such isotherms. The K_h of the Henry model represents a measure of adsorption affinity. A large value of K_h reflects stronger adsorption. It can be noted that, over the complete pH range the affinity of minerals to adsorb on the polysaccharide chain increases by decreasing the pH of solution. This could also attribute to the attraction of oppositely charged materials. However, under the identical condition Al_2O_3 particles have a greater affinity for the alginate than SiO_2 suspensions. This is due to the effects of the zero point of charge for minerals. The most efficient adsorption occurred at lower pH values, under these conditions, where the alumina particles hold a positive charge, so that they are strongly attracted to negatively charged alginate, and generate larger Henry's constant values. Silica suspensions have a weak affinity for biopolymer because of the electrostatic repulsion of negative silica molecules with anionic polyelectrolytes.

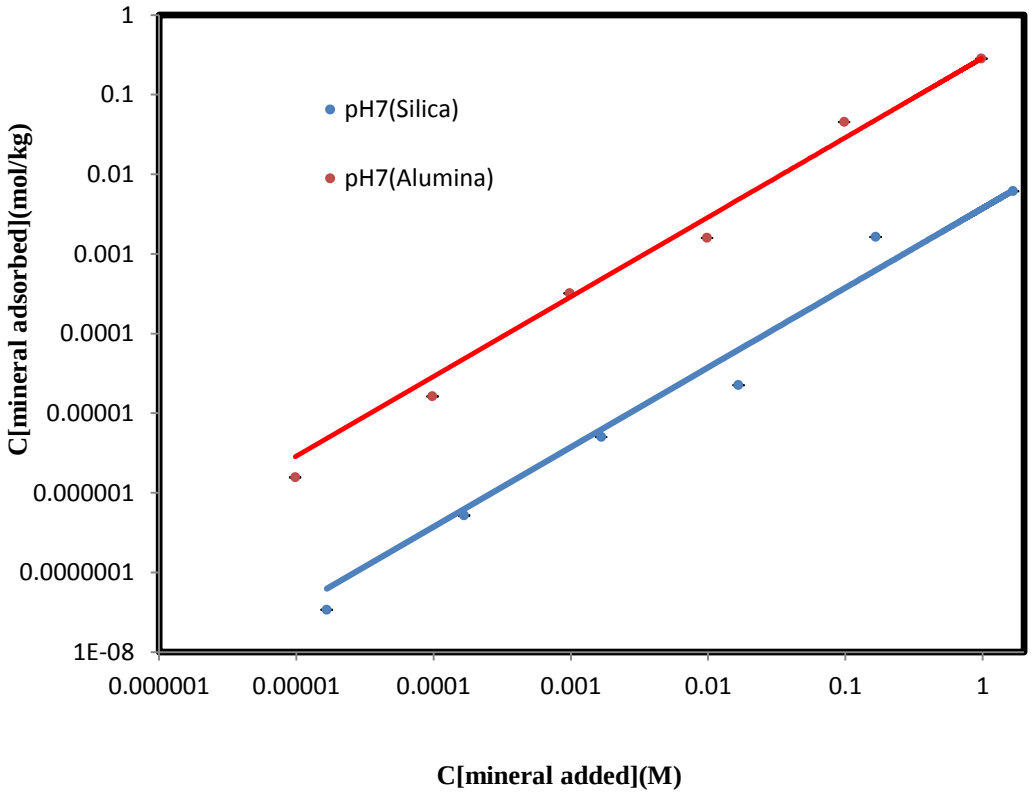

Figure 4.37 Henry adsorption isotherms of alumina and silica on alginate, at pH 7.

Table 4.2 Henry (affinity) constants of alumina and silica adsorbed on alginate and the goodness of fit values, at different pH values.

pH	K_h (L/kg) (Alumina)	R^2 (Alumina)	K_h (L/kg) (Silica)	R^2 (Silica)
2	0.5751	0.9999	0.1367	0.9868
3	0.5898	0.9998	0.1004	0.9598
5	0.2934	0.9977	0.0818	0.9485
7	0.2896	0.9954	0.0039	0.9659
9	0.0027	0.9999	0.0037	0.9706
11	0.0041	0.9993	0.0033	0.9909

4.13. **Conclusions**

- This chapter has revealed that fluorescence time resolved anisotropy is a powerful technique for the study of the conformational behaviour of dilute alginate solutions, and when attached to solid surfaces. In comparison, fluorescence steady state and lifetime measurements were less informative due to quenching of the AmNS label under acid conditions.
- From pH 5 to 10 (> *pKa* of AmNS) the fluorescence intensity and lifetime of the label are quenched. Consequently, the observed dependence of the fluorescence intensity and lifetime with pH was attributed to a change in conformation of the alginate chain.
- Fluorescence steady-state experiments showed that a greater amount of the fluorescently labelled alginate adsorbs onto the surface of alumina (~26%) in acidic media, in contrast to that onto silica (~11%) at the same pH.
- Fluorescence steady-state experiments also revealed that under the same situation, the adsorbed amount of alginate on either mineral is less than that of poly (acrylic acid). This could be attributed to the fact that the COO^- group of a simple synthetic polymer (PAA) can easily interact with the mineral particle, in contrast to the COO^- groups of an alginate, which suffer from steric hindrance caused by the bulkier sugar units reducing the effective interaction with the mineral surface.
- The correlation time, τ_c, of the labelled alginate increases as the amount of solid increases and the pH decreases: this suggests that more sites on the biopolymer chain is occupied by solid, which leads to restricted fluorophore and consequently macromolecular mobility.
- The results obtained from potentiometric analysis suggested that electrostatic interactions were predominantly responsible for the adsorption of alginate on Al_2O_3 particles, whereas weak forces, such as Van der Waals are assumed to control the interference between the polysaccharide chain and SiO_2 suspension.
- The adsorption affinity of alginate for alumina is due to electrostatic attraction between the positively charged alumina and the negatively charged alginate. In contrast, an electrostatic repulsion is responsible for

the adsorption of alginate. The Henry model can adequately describe the alginate adsorption isotherms on alumina and silica respectively.

- Collectively, these results demonstrate that a combination of fluorescence, ICP-MS and potentiometric techniques can be used to elucidate the conformational behaviour of a biopolymer. The use of these techniques can now be applied, with confidence, to investigate the adsorption behaviour of more complicated biologically produced material onto mineral surfaces, which could be used as model systems for the bacterial cell wall. This will be discussed in the following chapter.

Chapter 5. CONFORMATIONAL BEHAVIOUR OF LIPOPOLYSACCHARIDE IN BOTH BULK SOLUTION AND AT SOLID/LIQUID INTERFACES

5.1. **The Contribution of Lipopolysaccharide (LPS) to Cell Adhesion**

A Lipopolysaccharide (LPS) is an amphiphilic macromolecule with a hydrophobic lipid unit embedded in the outer membrane of Gram-negative bacteria [111, 112], as shown in Figure 1.3 (Chapter 1). This biologically produced polymeric substance is of important interest for the investigation of bacterial dynamics and adsorption, as it is the major component for outer membrane of Gram-negative bacteria [2, 10, 11], which consist of the majority of culturable cells that exist in aquatic systems [11]. The LPS chain can be extremely anionic and expands outside the outer membrane; this negatively charged chain is the major source of metal binding in gram-negative bacteria [113]. Bacteria attachment onto solids is a complex function of many factors like nature of bacterial cell wall components (e.g. LPS, surface proteins, flagella), surface charge, and aqueous environmental pH [111, 114]. LPS is known to be primarily responsible for attachment at the cell-mineral interface [11, 115]. Although functional groups of free LPS, such as hydroxyl and carboxyl moieties play a key role in LPS-solid interference [111, 116, 117]. The phosphoryl groups in this macromolecule are the probable binding sites for metal cations [118].

Jucker et al. [119] measured the adsorption of O-antigen part of LPS chains to TiO_2, Al_2O_3, and SiO_2 surfaces and they found greater adhesion to titanium oxide and alumina surfaces. They showed that by using the infrared spectroscopy all bacterial O-antigens formed hydrogen bonds with hydroxyl groups of TiO_2, $A1_2O_3$, and SiO_2 surface.

Toward the aim of establishing a molecular-level understanding of initial bacterial cell adhesion at mineral surfaces, the current work involves a synthesis of fluorescently labelled lipopolysaccharide (LPS) from *Escherichia coli 0111:B4*, and using time-resolved fluorescence anisotropy measurements to monitor the conformational behaviour of this biopolymer in aqueous media and adsorbed to mineral surfaces. This novel work is vital to bacterial growth since cell mineral

interactions are considered to play a key role in the growth and stability of biofilms. The fluorescence and potentiometric techniques are applied to study the effect of pH and ionic strength on the conformational behaviour of the LPS chain. The adsorption isotherms of LPS on minerals are determined by the inductively coupled plasma mass-spectroscopy (ICP-MS) technique.

5.2. **Conformational Behaviour of AmNS–labelled lipopolysaccharide as a Function of pH**

5.2.1. **Fluorescence steady state spectra of AmNS–labelled lipopolysaccharide as a function of pH**

Figure 5.1 presents the fluorescence emission spectra of 10^{-2} wt% unlabelled LPS and AmNS-labelled-LPS over a pH range of 5-10. Because of the acid quenching effect discussed in Chapter 4, fluorescence steady state analysis at pH below 5 is not valid. Of immediate note on fluorescence intensity is that the LPS is non-fluorescent and the emission intensity at around 420 nm is due to the AmNS label. The maximum emission peak position is dependent of the pH of the LPS solution. As it is shown in the figure below, there is a little appreciable increase in the fluorescence intensity as the pH of the solution is increased. The enhance in the fluorescence intensity from pH 5 to 10 could be attributed to the existence of the hydrophilic fluorophore in an aqueous environment, since the alginate chain becomes partly expanded in basic media, due to the electrostatic repulsion of the ionized phosphate (pKa_1 between pH 1 an d 3) and carboxyl groups [120] (pKa is ~4.5)[121].

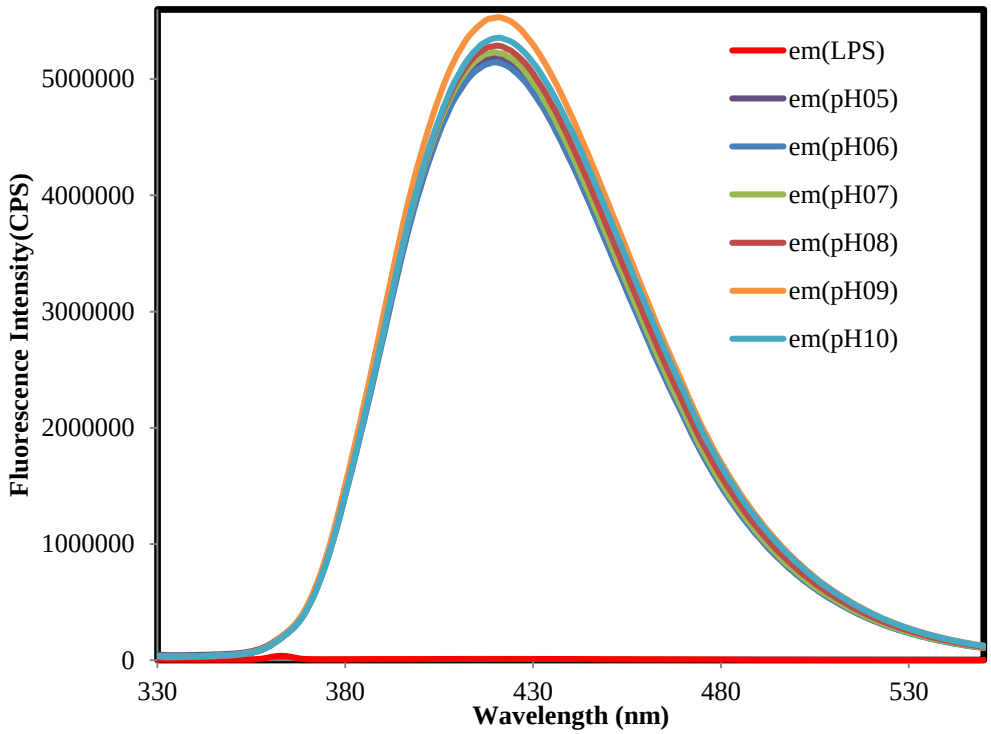

Figure 5.1 Fluorescence emission spectra for 10^{-2} w% AmNS-LPS in water as a function of pH at λ_{ex} = 320 nm.

5.2.2. **Fluorescence exited state lifetimes of AmNS–labelled lipopolysaccharide as a function of pH**

The fluorescnce liftime of the AmNS fluorophore is a measure of the micropolarity sensed by the label. The fluorescence intensity decays for 10^{-2} wt % AmNS-labelled-lipopolysaccharide have been generated over a pH range of 5-10. Because the complexity of LPS system decays, all the fluorescence decay curves could be satisfactory fitted by a double exponential function, hence the average lifetime was calculated. Figure 5.2 shows the average fluorescence excited state lifetimes of AmNs-LPS in water as a function of pH.

When the pH of the solution is increased the average life time increases. At high pH, the longer decay time corresponds to the behaviour of the AmNS probe in a hydrophilic envioronment, in contrast at low pH, the shorter decay time corresponds to the AmNS probe behaviour in a hydrophobic envioronment. These results suggest that the LPS chain conformation adopts an expanded coil in basic conditions. By decreasing pH of solution the coil is partially collapsed. This is in agreement with the

DLS analysis [122], which demonstrated that a decrease in the hydrodynamic radius of LPS aggregates with decreasing pH of solution from ~400 nm(at pH9) to ~200 nm (at pH3).

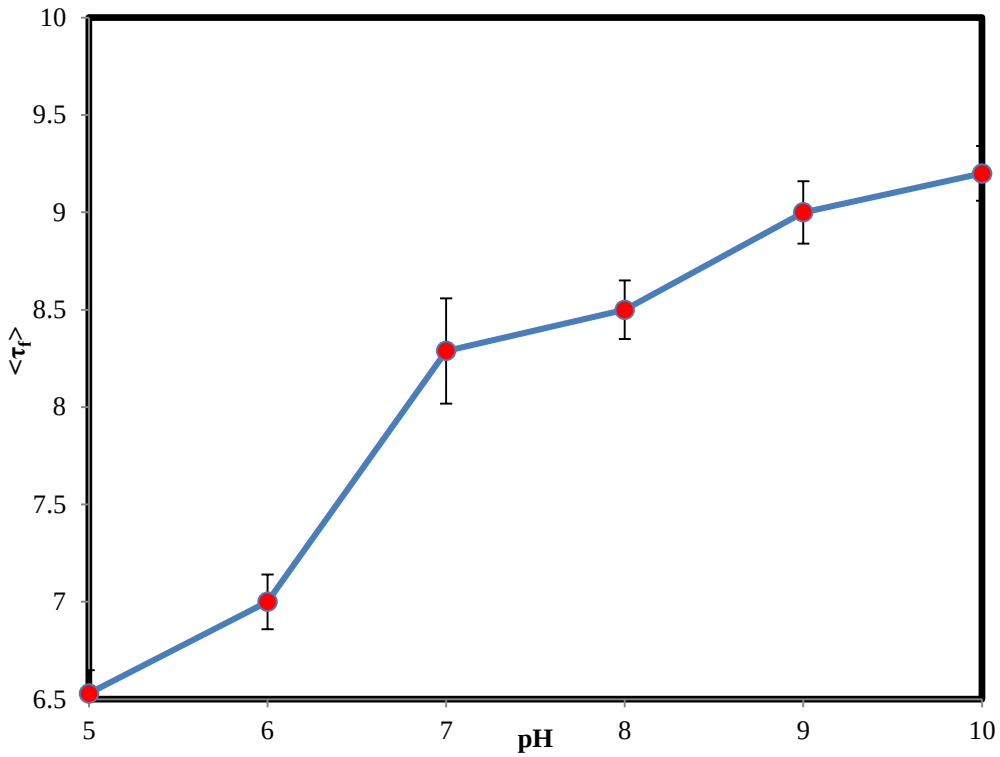

Figure 5.2 Fluorescence excited state lifetimes of 10^{-2}w % AmNS-LPS in water as a function of pH.

5.2.3. Fluorescence time-resolved anisotropy measurements of AmNS–labelled lipopolysaccharide as a function of pH

In order to monitor the change in the mobility of AmNS label attached to the LPS chain, the fluorescence time-resolved anisotropy measurements were carried out, and the rotational time of the probe was estimated as the measure of the motion of the biologically produced LPS chain.

Figure 5.3 shows the fluorescence time-resolved decays of AmNS-labelled lipopolysaccharide in dilute aqueous solution (10^{-2} wt %) at pH 12. Parallel and perpendicular fluorescence intensities are plotted logarithmically against time on the nanosecond time range. Since the expanded LPS chains rotated without restrictions overall, shortly after excitation the two polarized fluorescence decays were

superimposed on each other. Contrarily, once the pH decreased to 2, rotational motion of AmNS label was hindered by the aggregation of LPS chain, and a tramline gap was generated between the two polarized decays for a longer time, as depicted in Figure 5.4.

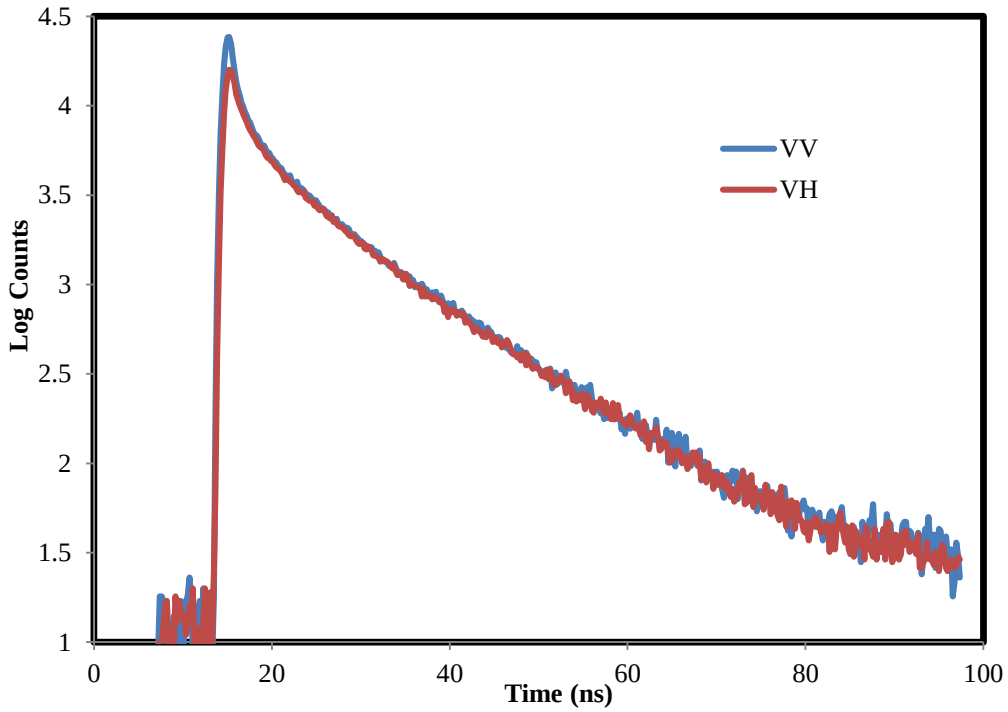

Figure 5.3 Parallel (blue curve) and perpendicular (red curve) fluorescence intensity decay curves following excitation with vertically polarized light (λ_{ex}= 370 nm) analysed at 450 nm from 10^{-2} wt% AmNS-labelled LPS in aqueous solution at pH = 12.

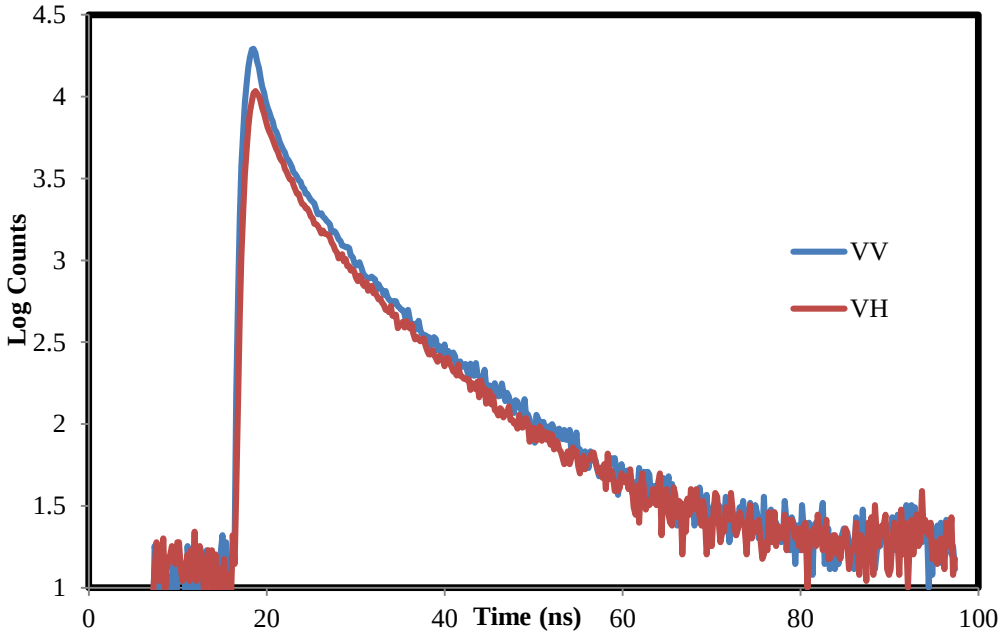

Figure 5.4 Parallel (blue curve) and perpendicular (red curve) fluorescence intensity decay curves following excitation with vertically polarized light (λ_{ex}= 370 nm) analysed at 450 nm from 10^{-2} wt% AmNS-labelled LPS in aqueous solution at pH = 2.

The anisotropy decays of the AmNS-LPS generated from the parallel and perpendicular fluorescence intensity decays are shown in Figure 5.5. It can be noted that the anisotropy is rather small at pH 12, whereas at pH 2, an obvious increase can be observed. It is worthy to note that at pH 2 the anisotropy decay does not reach zero for long time, which indicates that the AmNS label impeded in a collapsed LPS chain experiences a mobility restriction, but it is still to undergo some rotational motion as we will see from the τ_c values.

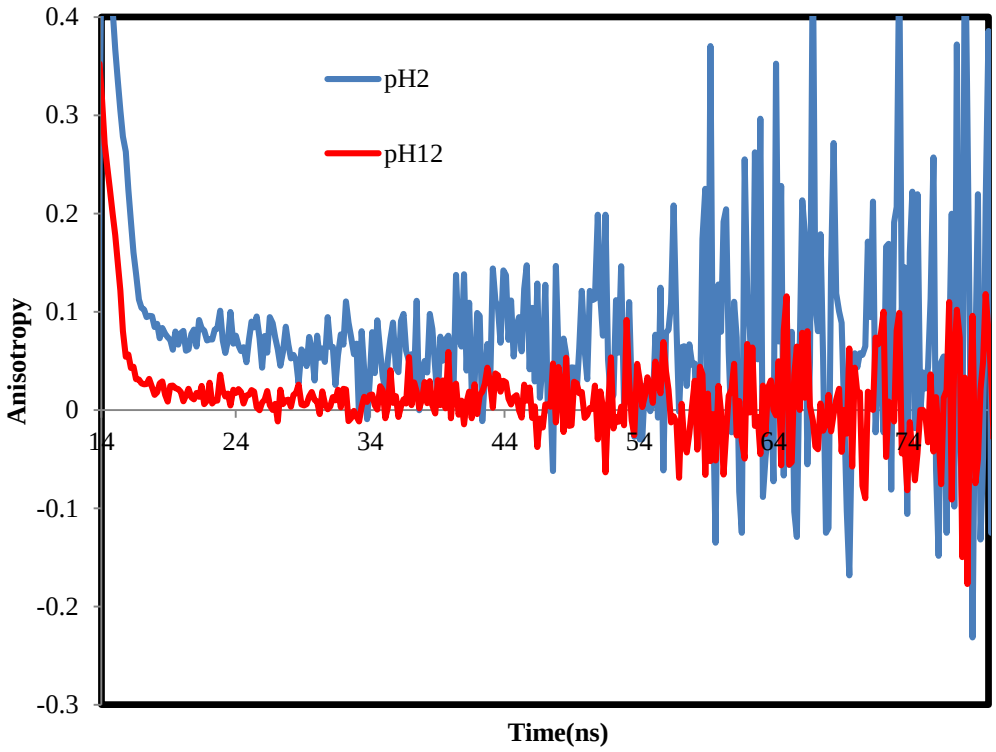

Figure 5.5 Decay of anisotropies, r(t), of 10^{-2} wt% AmNS-labelled LPS in aqueous solution at pH 2(blue curve) and pH 12(red curve). (λ_{ex}=370nm and λ_{em}=450nm).

Figure 5.6 shows the rotational correlation time of AmNS-LPS as a function of pH. The anisotropy decays of AmNS-LPS sample across a low pH values were best fitted with single exponential fits (Equation 1.21) fixing B (r_∞) to 0 to produce a physically meaningful value of τ_c representive of the dynamic behaviour of the biologically produced LPS. At high pH values, a single exponential fit is proper to analyse the anisotropy decays. The figure shows the pH dependence of τ_c for LPS in aqueous solutions. This pH dependence is similar to the results of steady-state and lifetime measurement described in sections 5.2.1. and 5.2.2. which showed that the AmNS label is surrounded by a hydrophobic environment at low pH and a hydrophilic environment at high pH.

As it can be seen, between pH 3 and 6 the τ_c decreases from ~10 ns to ~2 ns, suggesting that within this scale, there is a transition in LPS chain conformation from a coiled (high τ_c value) to an expanded form (low τ_c value) as the pH is increased. This could be attributed to the global negative charges on the LPS chains which result

from the first ionization of phosphate groups (pKa_1~ 1-3) besides ionization of the carboxyl moieties (pKa~3-5), causing an electrostatic repulsion making the LPS coil expanded at pH >5 [120], see Figure 5.15. As a result, an increase in the macromolecule dynamic motion is observed by decreasing the correlation time values at high pH values.

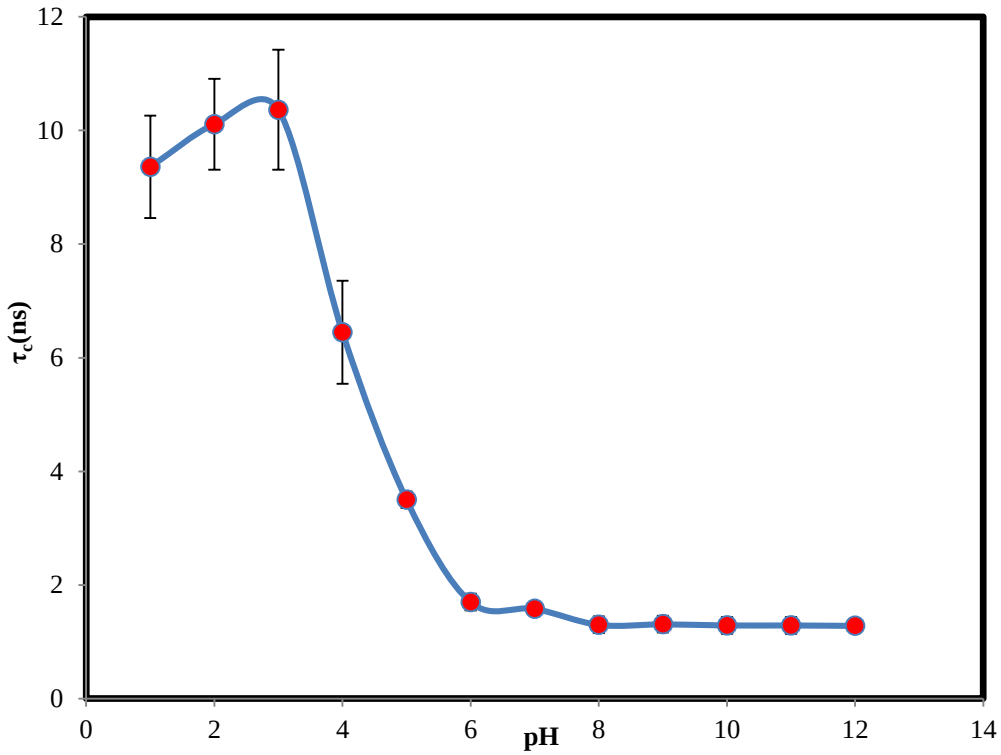

Figure 5.6 Correlation times(τ_c) for molecular segmental motion of 10^{-2} wt% AmNS- labelled LPS in aqueous solution at different pH values. (λ_{ex}=370nm and λ_{em}=450nm).

5.3. Conformational Behaviour of AmNS-Labelled Lipopolysaccharide and its Interaction with Sodium Ions

The interaction of ionisable groups within the lipopolysaccharide chain, such as carboxyl and phosphate moieties with monovalent cations as Na^+ was examined in order to evaluate their effect on the natural polyelectrolyte conformations. The fluorescence steady state and TRAMS data was collected for the AmNS-LPS compound at different NaCl concentration. Fluorescence studies enabled the

observation of changes in the LPS conformation in basic solutions at variable salt concentration. The results of TRAMS contribute to a better understanding of conformational changes of the LPS macromolecule in the presence of cations in acidic and basic media.

5.3.1. **Fluorescence steady state spectra of AmNS-labelled lipopolysaccharide as a function of NaCl concentration**

The dependence of the fluorescence intensity of aqueous AmNS-LPS on the NaCl concentration at pH 9, is plotted in Figure 5.7. It is obvious that considerable decrease in the fluorescence spectra when the NaCl concentration is increased up to 5 M. The observation proposes that the quench in the fluorescence spectra for high salt concentrations results from the collapse of the natural macromolecule chain. Possibly, the anionic carboxylate and phosphate groups of LPS with its expanded chain are neutralized by Na^+ cations [120]. The collapse of the LPS chains creates pockets of the macromolecule that entrap the AmNS label, resulting in a localised hydrophobic environment. This may result then in a quenching of the fluorescent intensity of the AmNS and a reduction of high of the peak in the spectra. Possible conformation models for the LPS structure under influence the sodium chloride salt is depicted in Figure 5.15.

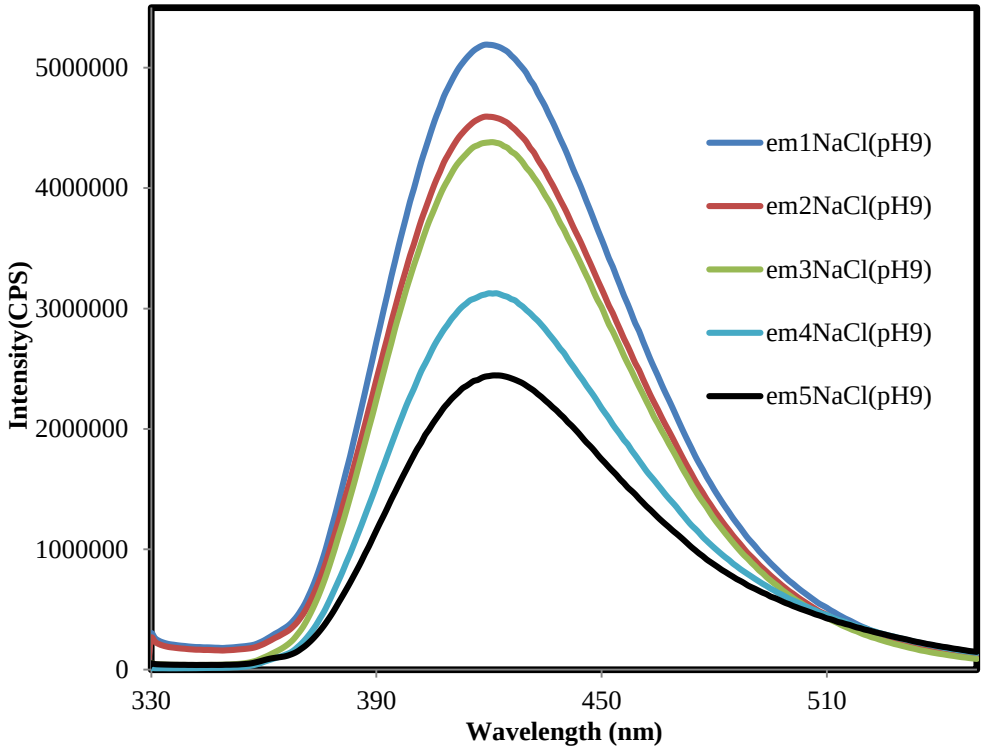

Figure 5.7 Fluorescence emission spectra for 10^{-2}w% AmNS-LPS in water as a function of NaCl concentration (M) at pH = 9, λ_{ex}= 320nm.

5.3.2. **Fluorescence time-resolved anisotropy measurements of AmNS-labelled lipopolysaccharide as a function of NaCl concentration**

The anisotropy decays of the AmNS-LPS at 1 and 5 M NaCl solutions at pH 3 and 9 are presented in Figure 5.8 and Figure 5.9, respectively. It can be seen that the anisotropy decays interfere with each other over the entire time range, when the concentration of salt is increased to 5 M at pH 3 (Figure 5.8). However, the anisotropy is rather greater at 5 M NaCl than at 1 M NaCl when the pH is increased to 9 (Figure 5.9). This is perhaps due to fact that the motion of AmNS label is restricted by the collapsing of neutralized LPS chain at high salt concentration because of its interaction with sodium ions. It is known that the addition of salt screens the polymeric charges and reduces the repulsion so that the stretching influence is lower at higher salt concentrations [123].

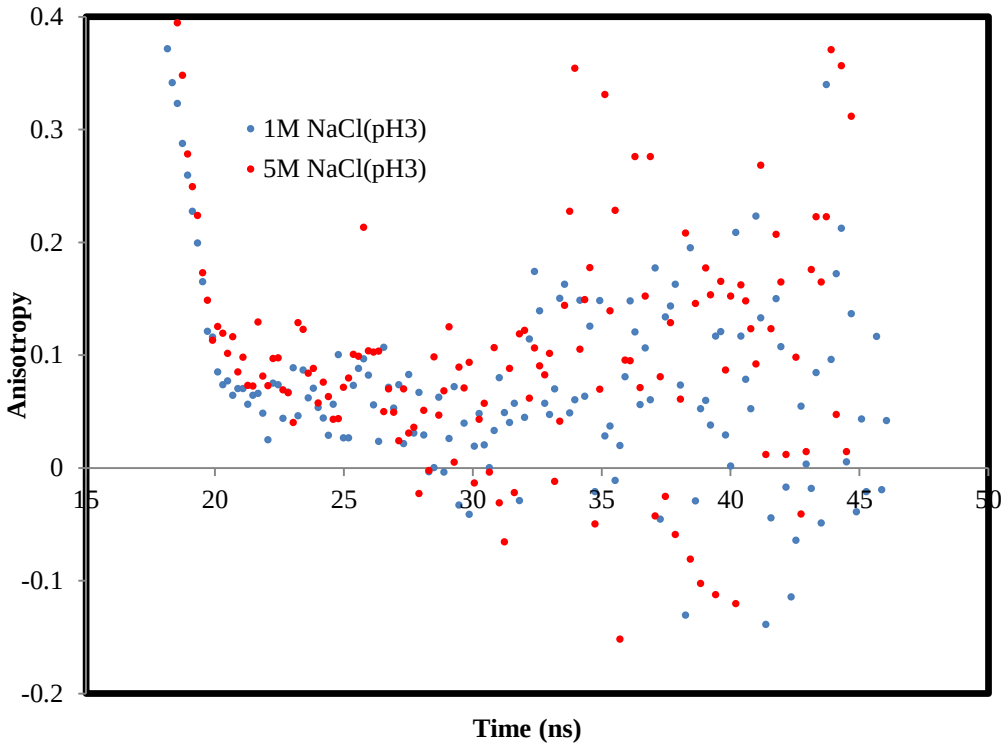

Figure 5.8 Decay of anisotropy, r(t), of 10^{-2} wt% AmNS-labelled LPS in aqueous solution in 1M NaCl (blue dots) and 5M NaCl (red dots) at pH3. (λ_{ex}= 370nm and λ_{em}=450nm).

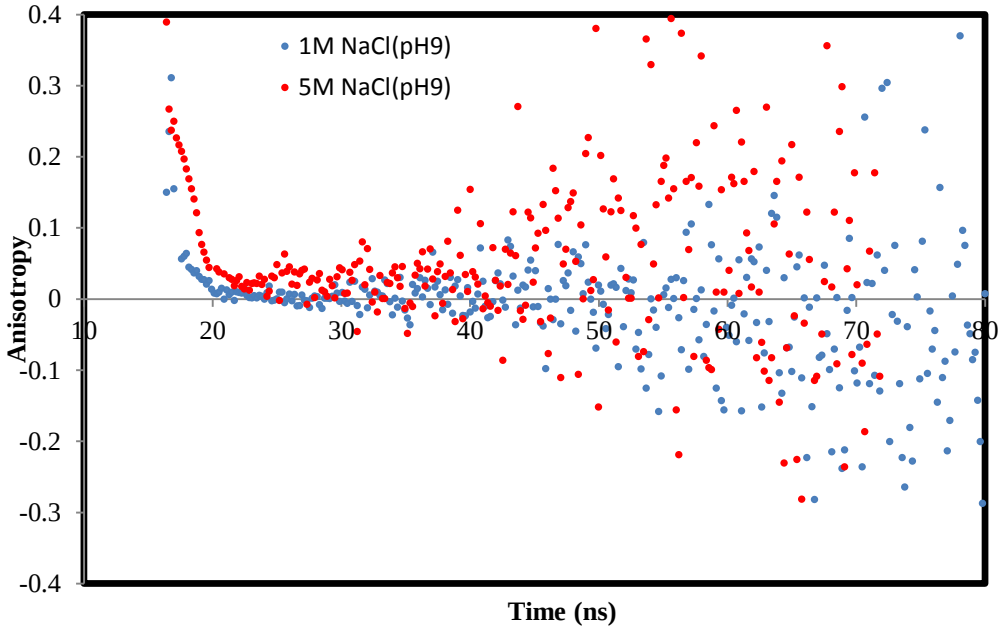

Figure 5.9 Decay of anisotropy, r(t), of 10^{-2} wt% AmNS-labelled LPS in aqueous solution in 1M NaCl (blue dots) and 5M NaCl (red dots) at pH9. (λ_{ex}= 370nm and λ_{em}=450nm).

Figure 5.10 shows the distribution of τ_c with respect to the concentration of NaCl added to the AmNS-LPS solutions at pH 3 and 9. The anisotropy decays of all AmNS-LPS sample were best fitted with single exponential fits (Equation 1.21) fixing B (r_∞) = 0 to produce a physically meaningful value of τ_c representive of the dynamic behaviour of LPS in presence of electrolytes.

However, an obvious increase of correlation times with increasing concentration of NaCl is noted at pH 9, whereas a small increase was recorded at pH 3. Moreover, the rate of increment in τ_c values at pH 9 is more than in those at pH 3 over the entire concentration range. The figure also shows that τ_c is independent of the NaCl concentration up to 2 M. The possible effect of Na^+ cations is the electrostatic interactions between the anionic COO^- and HPO_4^- groups in LPS at high pH values [120]. This binding may lead to the aggregation of LPS chain, which in turn inhibits the chain dynamics. A DLS study [122] demonstrated decreasing hydrodynamic radius of LPS chains with increasing NaCl concentration at pH 9.

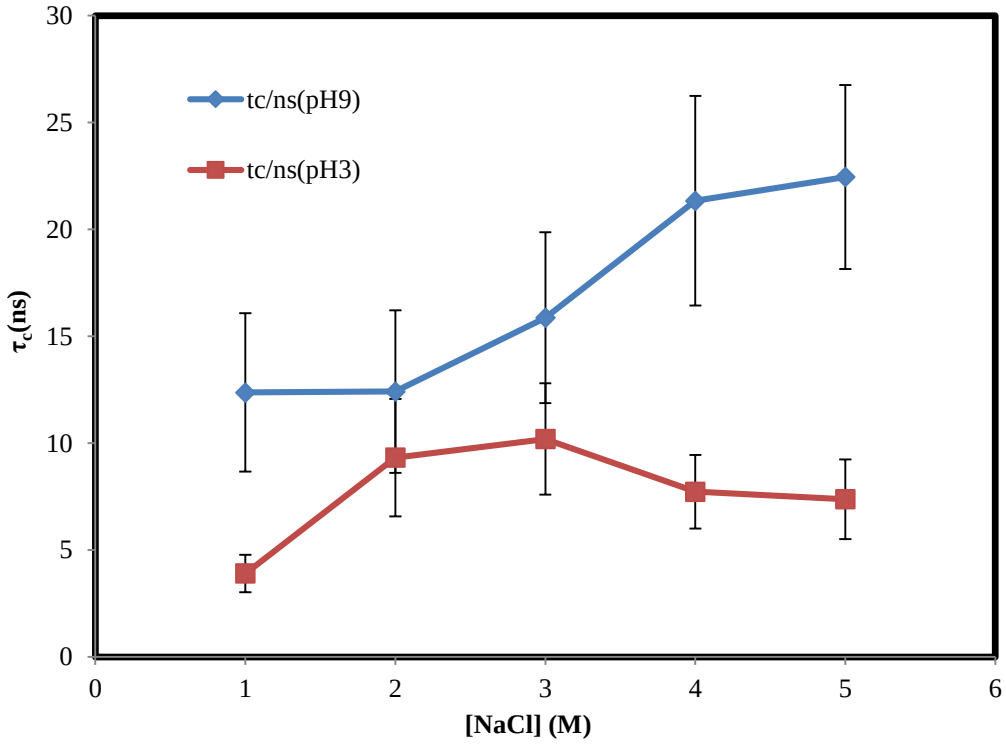

Figure 5.10 Correlation times of AmNS-labelled LPS (10^{-2} wt %) as a function of NaCl concentration at pH 3 (red curve) and pH 9 (blue curve).

5.4. **Conformational Behaviour of AmNS-Labelled Lipopolysaccharide and Its Interaction with Calcium Ions**

Similarly to the studies on the presence of Na^+, the aggregation of lipopolysaccharide chains in presence of Ca^{2+} ions was examined. The fluorescence intensity and TRAMS data were collected for the AmNS-LPS as a function of calcium chloride concentration.

5.4.1. **Fluorescence steady state spectra of AmNS-labelled lipopolysaccharide as a function of $CaCl_2$ concentration**

The fluorescence spectra of AmNS-LPS (10^{-2} wt %) as a function of calcium chloride concentration at pH 9 are presented in Figure 5.11. It is observable that a quenching in the fluorescence intensity occurs when the $CaCl_2$ concentration is increased up to 1.5 M. The observation proposes that the decrease in the fluorescence spectra for high Ca^{2+} concentrations results from the collapse of the LPS chain. The collapse of the LPS chains creates pockets of the macromolecule that entrap the AmNS label, resulting in a localised hydrophobic environment. This may result then in a quenching of the fluorescent intensity of the AmNS and a reduction in the intensity of the peak in the spectra. Perhaps, the anionic carboxylate and phosphate groups of LPS chain are bridged by Ca^{2+} ions [120]. Possible conformation models for the LPS structure under influence the calcium chloride salt is illustrated in Figure 5.15.

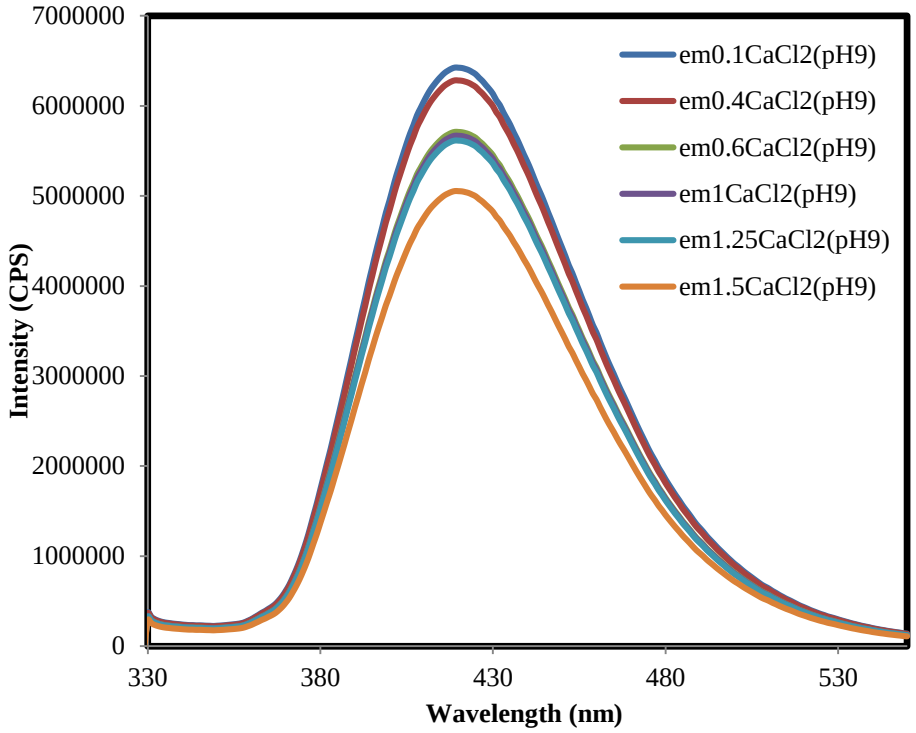

Figure 5.11 Fluorescence emission spectra for 10^{-2}w% AmNS-LPS in water as a function of $CaCl_2$ concentration (M) at pH= 9, λ_{ex}= 320nm.

5.4.2. Fluorescence time-resolved anisotropy measurements of AmNS-labelled lipopolysaccharide as a function of $CaCl_2$ concentration

TRAMS was also applied to examine the effect of Ca^{2+} ions on the LPS chain conformation. The anisotropy decays of the AmNS-LPS (10^{-2} wt %) in 0.1 and 1.5 M $CaCl_2$ solutions at pH 3 and 9 are shown in Figure 5.12 and

Figure 5.13. It can be observed that the anisotropy decays are exactly similar for both 0.1 and 1.5 M CaCl2 at pH 3 (Figure 5.12), which means Ca2+ ions do not affect the LPS conformation at pH 3. On the contrary, increasing the pH to 9 letting the anisotropy is rather higher at 1.5 M CaCl2 than at 0.1 M CaCl2 (Figure 5.13). This confirms that anionic groups, such as carboxylate and phosphate groups of LPS chain are interacting with Ca2+ ions. This causes an aggregation of LPS chain and hence restricts the mobility of AmNS fluorophore and a higher anisotropy decay is generated.

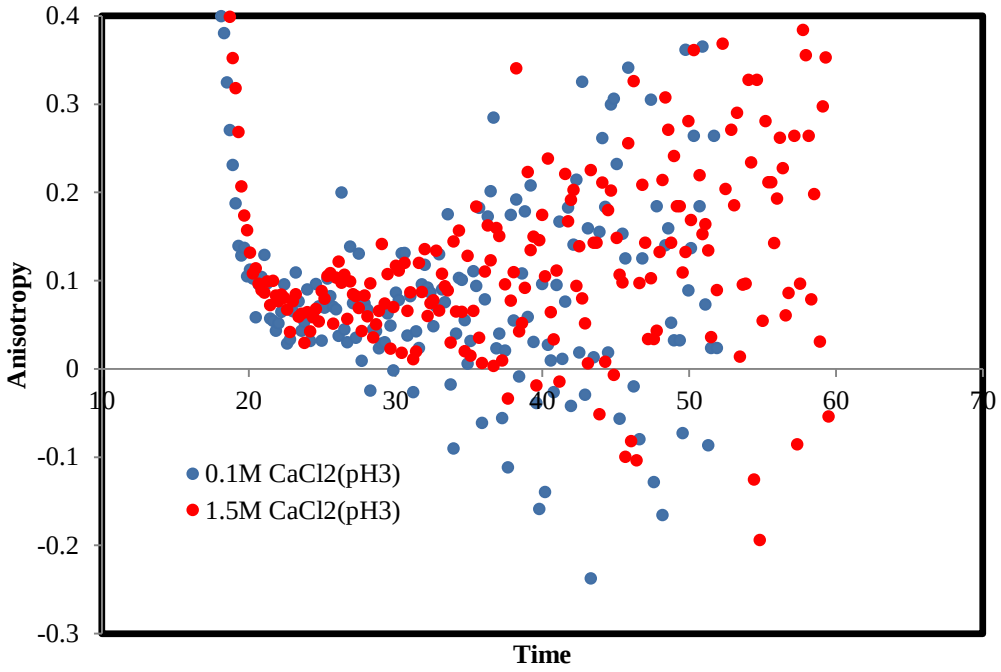

Figure 5.12 Decay of anisotropy, r(t), of 10^{-2} wt% AmNS- labelled LPS in aqueous solution in 0.1M $CaCl_2$ (blue dots) and 1.5M $CaCl_2$ (red dots) at pH3. (λ_{ex}=370nm and λ_{em}=450nm).

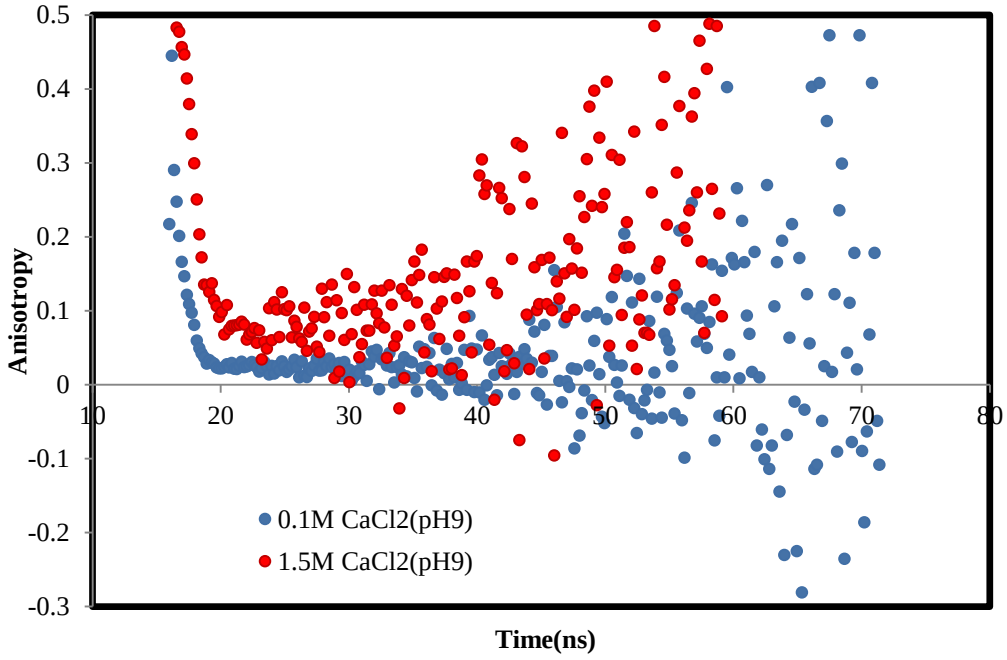

Figure 5.13 Decay of anisotropy, r(t), of 10^{-2} wt% AmNS- labelled LPS in aqueous solution in 0.1M $CaCl_2$ (blue dots) and 1.5M $CaCl_2$ (red dots) at pH9. (λ_{ex}=370nm and λ_{em}=450nm).

The relationship between the correlation times and the concentrations of $CaCl_2$ added to the AmNS-LPS solutions at pH 3 and 9 are shown in Figure 5.14. The τ_c values were calculated by using single exponential fits (Equation 1.21) fixing B (r_∞) = 0, which is believed to be suitable to analyse such difficult anisotropy decays.

Increasing calcium chloride concentration in the LPS solution showed an increase in the correlation times at pH 9, but no important effect were recorded at pH 3. Furthermore, the rate of increment in τ_c values at pH 9 is more than in those at pH 3 over the entire concentration range. The plots also display that τ_c is independent of the calcium chloride concentration up to 0.6 M after that a marked increase in τ_c values at pH 9 is recorded (~55ns at 1.5M). The probable effect of Ca^{2+} ions is the bridging of the anionic COO^- and HPO_4^- groups in LPS chain [120]. This binding may lead to the aggregation of LPS chain, which in turn restricts the chain dynamics, high correlation time is produced. It is worthy to note that at pH9, the τ_c increases from ~12 to ~22 ns by increasing Na^+ concentration (Figure 5.10), while τ_c increases from ~22 to ~55 ns by increasing Ca^{2+} concentration (Figure 5.14). This indicates that Na^+ ions have less effect on LPS aggregation compared to the case for Ca^{2+} ions. This in agreement with the DLS analysis, which showed that at 100 mM from the salt concentration, the particle size of LPS, is ~400nm (in presence of Na^+) and reduces to ~250nm (in presence of Ca^{2+}) [122].

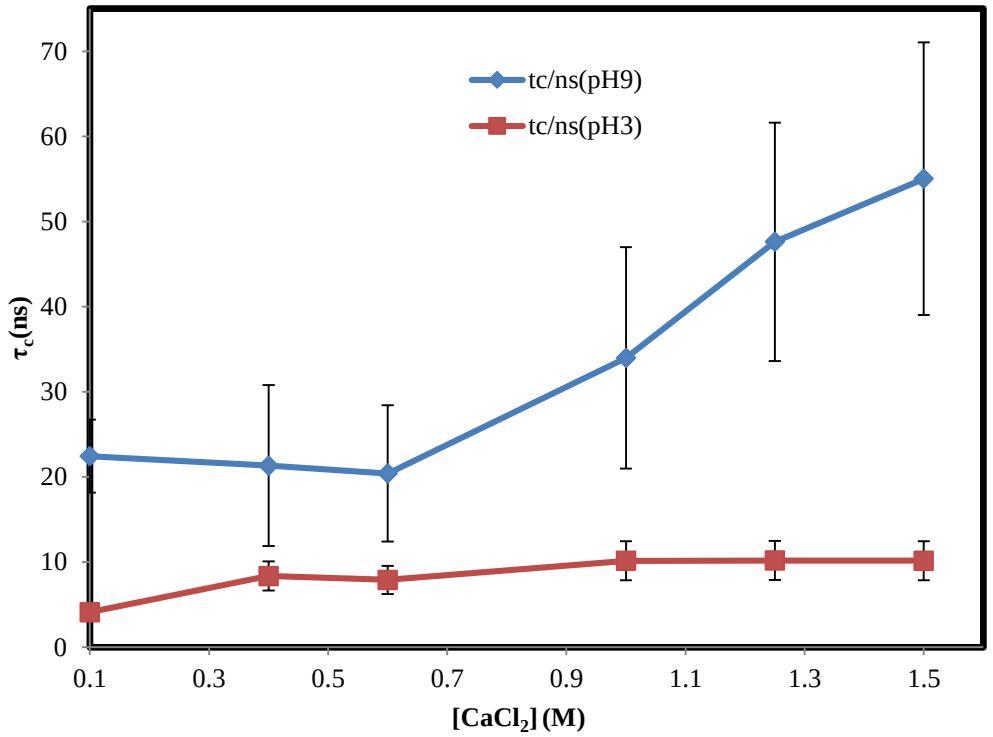

Figure 5.14 Correlation times of AmNS-labelled LPS (10^{-2}wt%)as a function of $CaCl_2$ concentration at pH 3 (red curve) and pH 9 (blue curve).

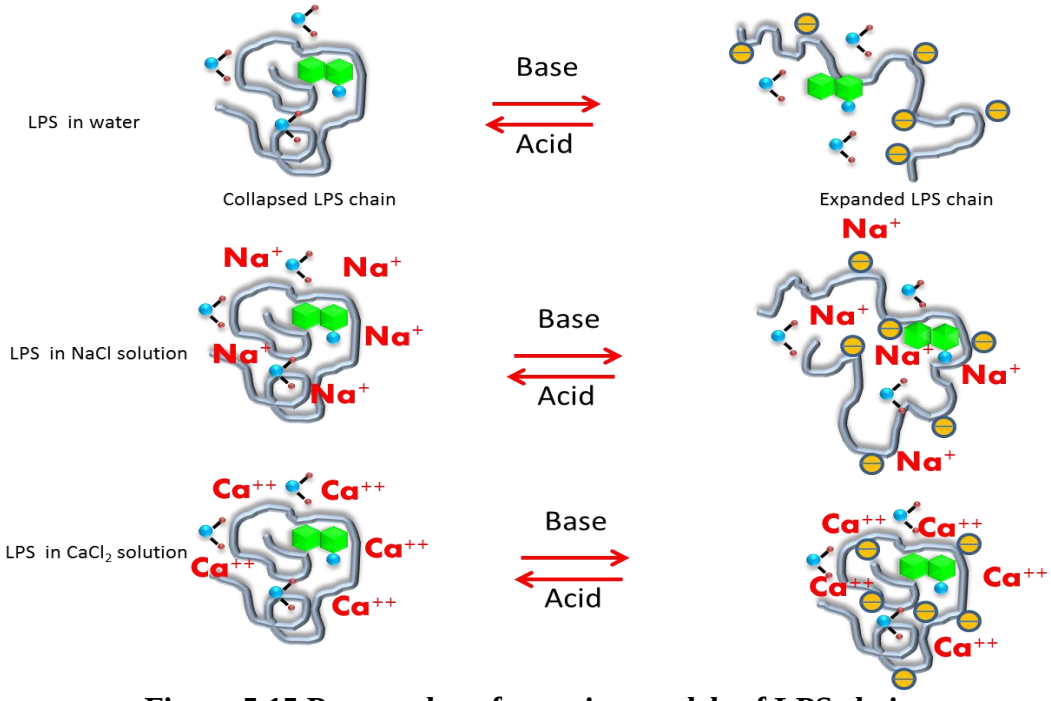

Figure 5.15 Proposed conformation models of LPS chain.

5.5. **Adsorption of AmNS-Labelled Lipopolysaccharide on Silica Surface as a Function of pH**

The adsorption of biologically produced biopolymers from dilute solutions on the surfaces of solids has been characterized by the fluorescence steady-state and anisotropy measurements.

5.5.1. **Fluorescence steady state spectra of AmNS-labelled lipopolysaccharide on silica surface as a function of pH**

Figure 5.16 shows the amount of adsorbed lipopolysaccharide (percentage) onto silica suspension as a function of pH. The amount of labelled LPS adsorbed on the silica suspension was quantified by the fluorescence intensity values. The percentage value was calculated by subtracting the fluorescence intensity of the supernatant solution, separated by centrifugation (at 50000 rpm), from the fluorescence intensity of equilibrated AmNS-LPS/ colloidal silica. It was assumed that any LPS remaining in the supernatant solution was representative of the LPS not adsorbed to the silica surface. By mass balance, the sorbed LPS was calculated as the difference between free LPS in the supernatant solution compared to the total initial concentration of LPS in solution. This was presented in Equation 3.5.

It can be observed that the amount of adsorbed LPS increases by decreasing the pH from 11 to 2. This pH dependence can be explained in terms of zero points of charge for LPS and silica. The pHzpc of LPS is ~2.5 [124], whereas it is ~3 of silica [16, 79, 80]. It indicates that except for pH 2 the relative charges of SiO_2 and LPS are negative in the pH range from 2 to 11. In this condition, the electrostatic repulsion between LPS chains and the suspension occurs. pH increase causes the decrease of LPS adsorption because of electrostatic repulsion between the HPO_4^- and/or COO^- groups in LPS and the negatively charged silica particle is becoming strong. The adsorption of LPS on the silica suspension could be attributed to that non-electrostatic forces occur between LPS and the silica surface. Otherwise, the interaction of similarly charged materials should not occur [80]. Similar results were obtained for adsorption of E. *coli* on zeolites (SiO_2 and Al_2O_3 particles) [125]. The effect of pH on bacterial cell adsorption was investigated by measuring the optical density under

various pH conditions (pH 5 to 9). It was found that the maximum amount for adsorption of cell was at acidic pH (~20% *E. coli* adsorbed). Based on the measurement of zeta-potentials and the range of pH conditions from 5 to 9, both *E. coli* and zeolites were negatively charged and interacted with each other. At pH 5, the repulsion between cell and zeolites was decreased. Therefore, the amount of cells adsorbed reached the maximum at pH5.

On the other hand, increasing the amount of silica led to an enhancement in the amount of adsorbed LPS. Particularly, from 10^{-4} to 10^{-2} wt% of added SiO_2, there is a small increase in the adsorbed amount of LPS at pH 2 and 3, while no important adsorption was recorded at pH levels 5, 7, 9 and 11. When the concentration of added SiO_2 was increased further to 1wt% and 10 wt% the adsorbed amount of LPS reached the maximum (~10% of LPS was adsorbed). We can therefore say that some of LPS chain attached to the silica surface. Also it should be noted that, at the same conditions, a double amount from poly (acrylic acid) is adsorbed (Figure 3.33) (Chapter 3). This could be attributed to the steric effect of O-antigen chains in LPS reducing bacterial adsorption upon various solids [126].

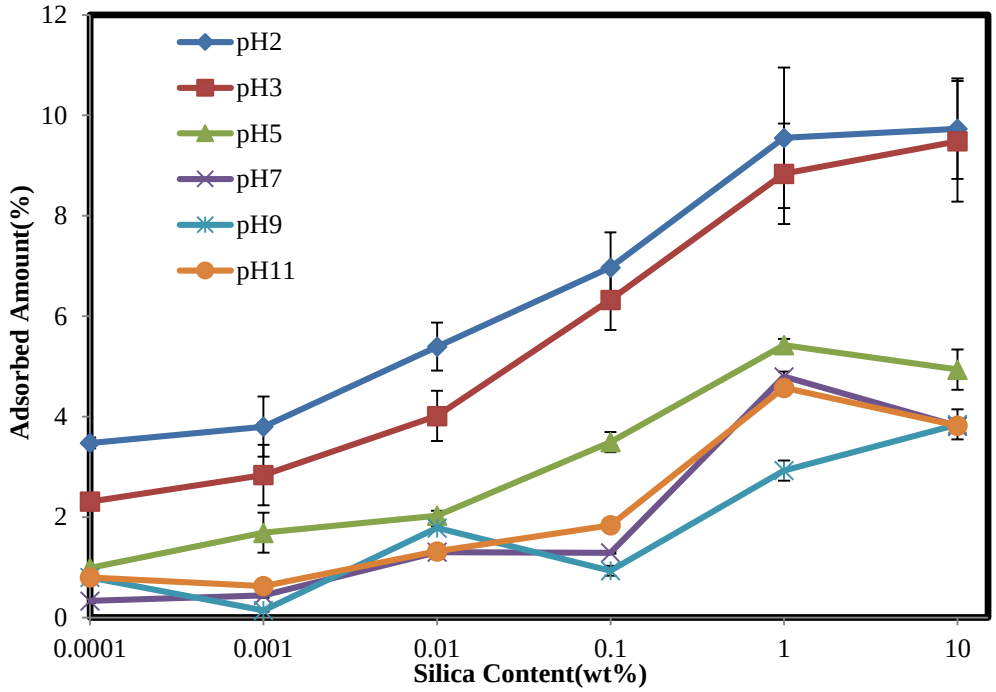

Figure 5.16 Adsorption of AmNS-labelled LPS (10^{-2} wt %) on the silica at various pH values.

5.5.2. **Fluorescence time-resolved anisotropy measurements of AmNS-labelled lipopolysaccharide at silica surface as a function of pH**

In this section, we describe novel work intends to assess the applicability of TRAMS) to monitor the dynamics of fluorescently labelled biologically produced LPS onto solid particle.

The anisotropy decay of 10^{-2} wt% AmNS-LPS in water quickly reaches zero in the absence of silica, reflecting the freedom of AmNS molecule motion in solution. However, by adding silica to the labelled-LPS system, the anisotropy value takes a longer time to decay to zero, as is shown in Figure 5.17**.** This behaviour can be explained as follows: Since the AmNS label was covalently labelled to the LPS, so that it can exist only within the adsorbed LPS chains, which contact with the solid surface, and my control experiments proved that AmNS alone did not adsorb onto silica, this indicates that the LPS chains adsorb to silica suspension. This leads to the

limit of the segmental motion of fluorescently labelled biopolymer. Long anisotropy decay is generated accordingly.

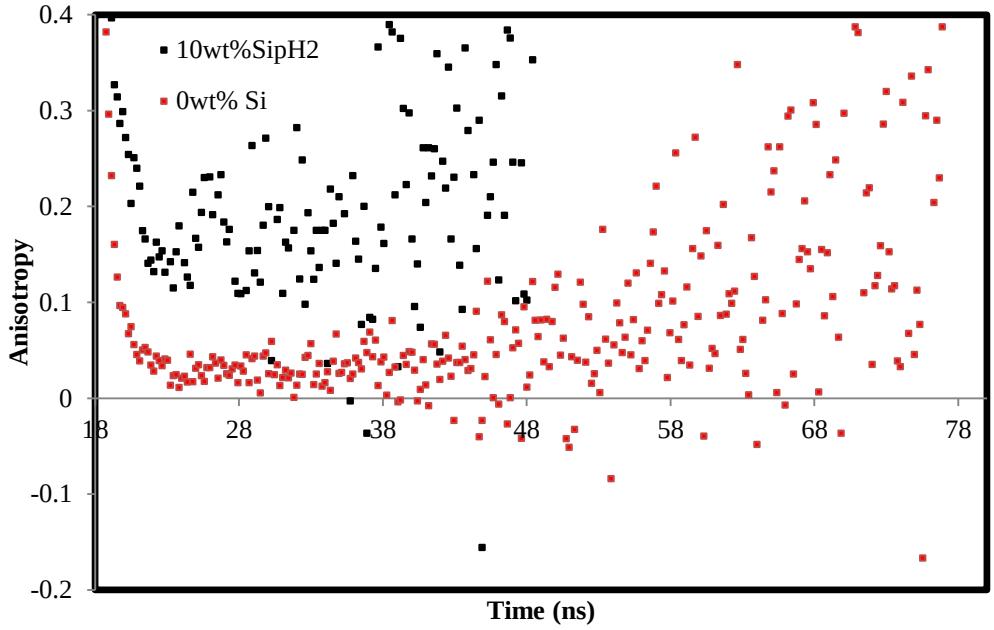

Figure 5.17 Fluorescence time resolved anisotropy decays of aqueous AmNS-labelled LPS solution (10^{-2} wt%) in the absence of silica(red dots) and at the silica concentration of 10wt%(black dots). (λ_{ex}= 370 nm and λ_{em}= 450 nm).

It is worthy to note that the anisotropy decay of the LPS in the presence of silica is pH dependent. Figure 5.18 displays the anisotropy decays of AmNS-LPS in the presence of 10 wt % silica at pH 2 and pH11, respectively. It can be clearly seen that the pH 2 anisotropy remains un-decayed to zero for longer time compared to the pH11 anisotropy curve. Probably, the aggregated adsorbed LPS chain at acidic pH moves slower than the expanded one.

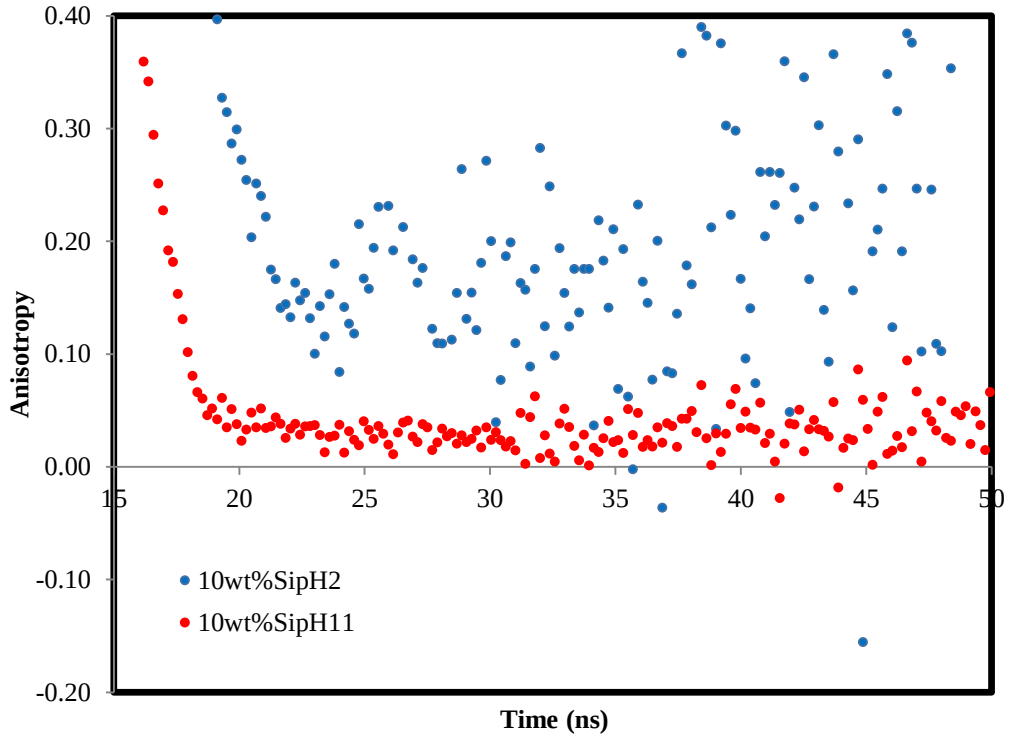

Figure 5.18 Fluorescence time resolved anisotropy data of aqueous AmNS-labelled LPS solution (10^{-2} wt%) at the silica concentration of 10wt%, pH 11(red dots) and pH 2(blue dots). (λ_{ex}= 370 nm and λ_{em}= 450 nm).

The correlation times of AmNS-labelled-LPS are plotted against the silica concentration at different pH values, as shown in Figure 5.19. It can be assumed that at low silica content (eg. 10^{-4}-10^{-2} wt%) no important adsorption occurs and the AmNS fluorophore exists in a homogeneous environment. So that the τ_c vales are produced by using single exponential fits (Equation 1.21) fixing B (r∞) = 0, which is believed to be suitable to analyse such complex anisotropy decays. When the concentration of silica is increased to 10 wt%, absorption begins and some of LPS remains in the bulk solution. Therefore, a double exponential fit (Equation 1.22) is suited to such anisotropy decays.

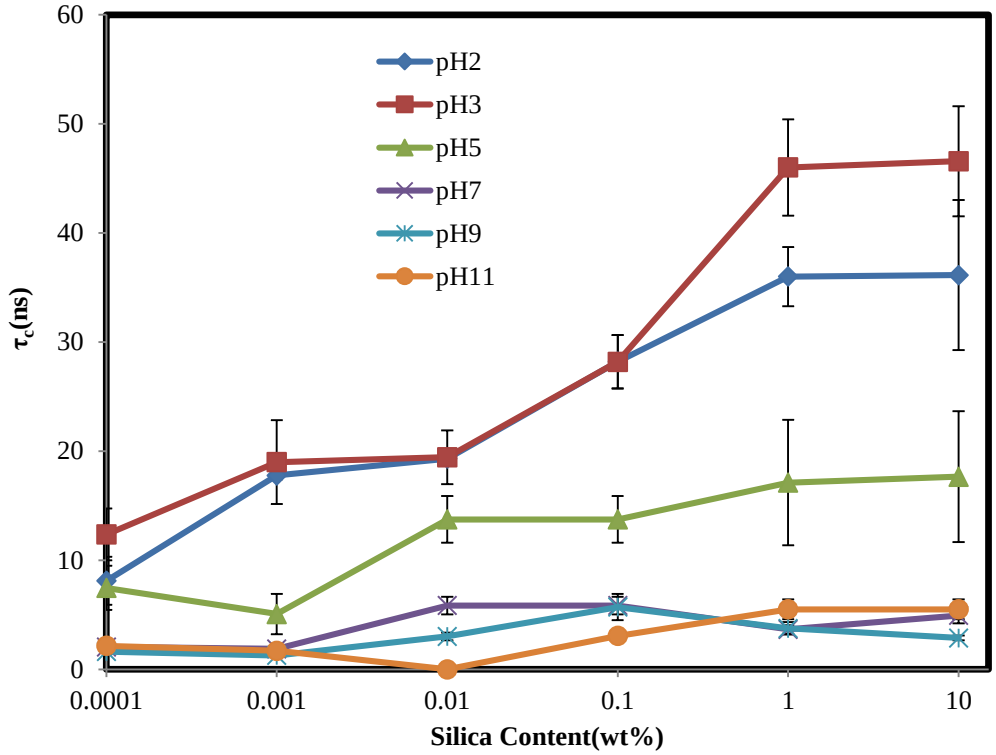

Figure 5.19 Correlation times of AmNS-labelled LPS (10^{-2} wt %) as a function of silica concentration at various pH values.

Over the entire pH scale studied, the τ_c value increases by decreasing the pH, but the correlation times are increasing when increasing the amount of silica. At a low concentration of silica a slight increase in the correlation time values are recorded at pH values 2, 3 and 5, but no important change was recorded at higher pH values. When the silica content is increased to 10 wt % a noticeable rise in τ_c value is recognized at pH 2 and 3. This can be explained with strong adsorption between the collapsed LPS chain and the silica particle. However, a small increase is recorded at pH 5 and negligible change in the correlation time values are gained at higher pH values.

5.6. **Adsorption of AmNS-Labelled Lipopolysaccharide on Alumina Surface as a Function of pH**

Fluorescence intensity and TRAMS techniques were used to quantify the adsorption of biologically produced LPS to large particles, such as alumina.

5.6.1. **Fluorescence steady state spectra of AmNS-labelled lipopolysaccharide at alumina surface as a function of pH**

Figure 5.20 presents the amount of adsorbed lipopolysaccharide (percentage) at alumina surface over a wide range of pH values. The amount of labelled LPS adsorbed on the alumina particles is determined by using Equation 3.5.

The results show an increase in the percentage of adsorbed LPS chains with a decrease in pH. This could be attributed to the LPS and alumina pHzpc values, which are ~2.5 [124] and ~ 9[79], respectively. It means that apart from pH 9 and 11 the surface of alumina is positively charged, while the LPS is negatively charged in the pH range from 3 to 11. Therefore, the increase of LPS adsorption by decreasing the pH is because of electrostatic attraction between the negatively charged groups in LPS and the positively charged alumina groups is becoming strong (from pH 7-3). At pH 9 and 11, the adsorption of LPS on the alumina could be attributed to that non-electrostatic forces appear between LPS and the mineral. Otherwise, the interaction of similarly charged materials should not occur [80]. At pH 2 besides the non-electrostatic force, hydrogen bonding could be responsible for adsorption. However, ATR-FTIR spectra demonstrated [111] that the pH-dependent charge controls Ca-LPS adsorption to hydrophilic surfaces, such as Al_2O_3. A strong adsorption was observed at lower pH values, where alumina surface is generally positively charged.

On the other hand, the LPS adsorption increases by increasing the amount of added alumina (from 10^{-4} to 10 wt %). Specially, a small increase in the adsorbed LPS at pH values of 5, 7, 9 and11. While, a marked increase is observed at pH 2 and 3, as the percentage of adsorbed LPS reaches the maximum value (~24%). In such a condition only ~10 % of biopolymer is adsorbed on silica. This could be attributed to that at acidic media the LPS becomes relatively neutral and the biopolymer chain is more collapsed in an adsorbed state. Thus, unionised carboxylic acid (COOH) [16] or phosphate (H_2PO_4) groups adsorb via hydrogen bonding between the biopolymer carbonyl or phosphoryl groups and hydroxyls on alumina surface. Therefore, at lower pH values the adsorption mechanism is predominantly hydrogen bonding in nature, whereas LPS does not adsorb significantly onto silica due to electrostatic repulsion.

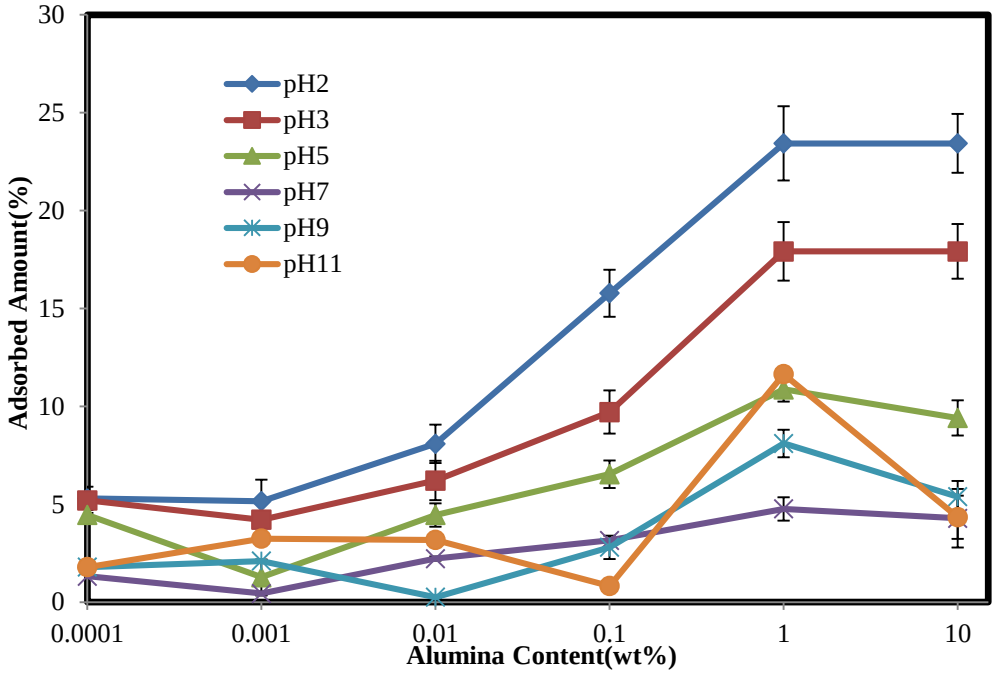

Figure 5.20 The percentage of adsorbed amount for 10^{-2} wt % AmNS-labelled LPS on alumina at various pH.

5.6.2. Fluorescence time-resolved anisotropy measurements of AmNS-labelled lipopolysaccharide at alumina surface as a function of pH

The dynamic motion of biologically produced LPS on alumina has been investigate by running the anisotropy decays of AmNS-labelled-LPS (10^{-2} wt %) over a wide range of pH. Once the anisotropies are generated, the corresponding correlation times of labelled-LPS samples are plotted against the alumina concentration at different pH values, as shown in Figure 5.22. This indicates that at low mineral content (eg. 10^{-4}-10^{-2} wt%) no important adsorption arises and the AmNS label exists in a homogeneous surrounding, since the vast majority of AmNS-labelled-LPS chains are moving away from the solid surface. So that the τ_c vales are determined by applying single exponential fits (Equation 1.21) fixing B (r∞) = 0, which is believed to be suitable to analyse such complex anisotropy decays. When the concentration of alumina is increased to 10 wt %, a quantifiable attachment occurs but some of LPS remains in the bulk solution. Therefore, a double exponential fit (Equation 1.22) is suited to such anisotropy decays. Accordingly, two values of correlation time are gained, τ_{c1} represents the motion of free LPS, which is expected

to be faster than the mobility of adsorbed LPS chain (τ_{c2}). Figure 5.21 shows a selected sample of anisotropy decay with its fit and residuals data of adsorbed AmNS-LPS.

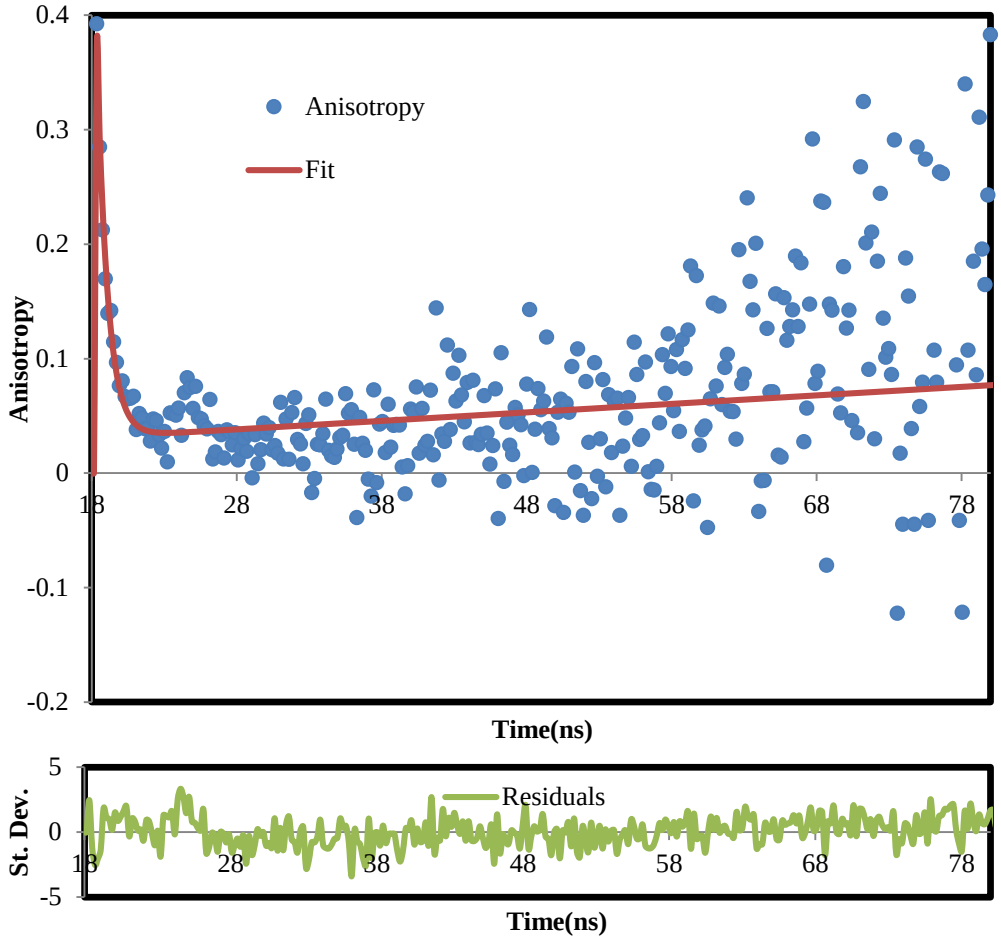

Figure 5.21 Fluorescence anisotropy decay of 10^{-2} wt % AmNS- labelled LPS in alumina solution at pH 7, and the associated double-exponential fit with the distribution of residuals. (λ_{ex} = 370 nm and λ_{em}=450nm).

The τ_c values are increasing by adding more acid and alumina. Specifically, at a low concentration of alumina a gradual increase in the correlation time values are recorded over the whole pH range. When the alumina content is increased to 10 wt % a dramatic increase in τ_c value is recorded at pH 2. This can be explained with strong adsorption between the collapsed LPS chain and the alumina particle and a considerable quantity of chains are attached. However, a marked increase is recorded at pH 3 and 5 and slight change in the correlation time values is gained at higher pH values. This suggests that a decreasing in the LPS affinity for alumina by increasing the pH.

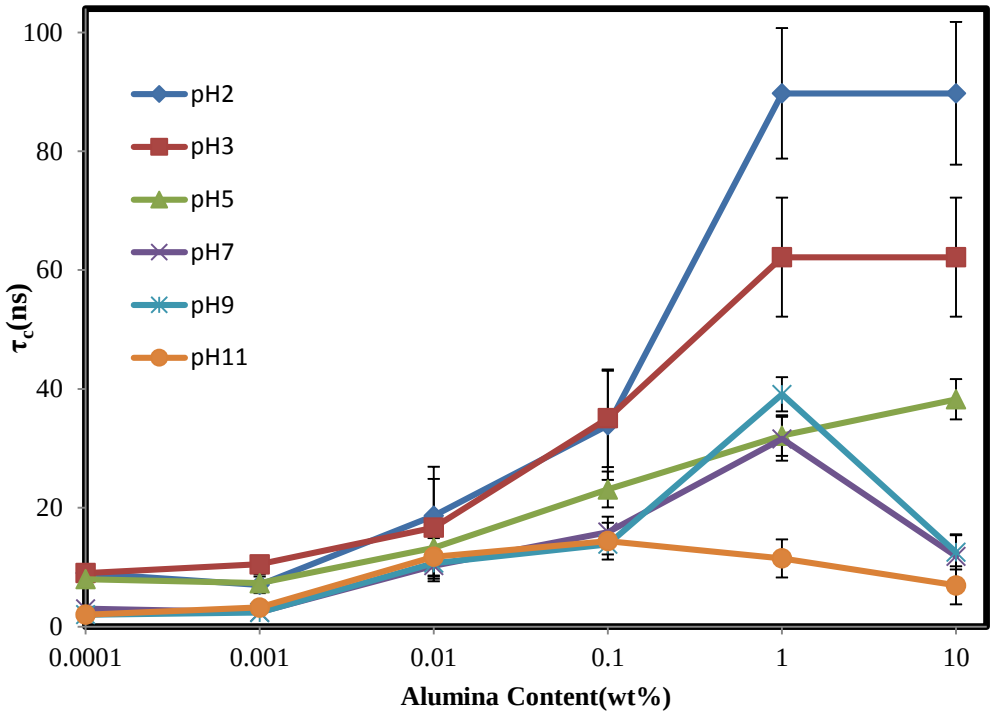

Figure 5.22 Rotational correlation times (τ_c) as a function in pH and Alumina concentration for 10^{-2}wt% AmNS-labelled LPS.

5.7. **Potentiometric Titration of Lipopolysaccharide**

The LPS chain can be existed in an expanded form or a collapsed coil under the influence of pH and ionic strength as has been revealed by the fluorescence analysis of labelled-LPS. However, the fluorescence data also demonstrated that the LPS chain is expanded and has low affinity for solids at high pH values, while almost collapsing and has high affinity for solids in acid media. In this section, the potentiometric titration technique is used to study the acid-base behaviour of LPS as well as the effect of pH and ionic strength on the conformational behaviour of the diluted aqueous solution of unlabelled LPS.

As shown in Figure 2.5 the LPS chain contains different ionisable groups, such as carboxylic acid (COOH), phosphate (H_2PO_4), amine (NH_2) and hydroxyl (OH). These groups ionize to COO^-, HPO_4^-, NH_3^+, and O^- , respectively to produce a net negative charge on the outer surface of the bacterium when the pH of the solution is changed [120]. However, the fraction of dissociated groups for LPS (α) as a

function of pH and at different NaCl concentration is showing in Figure 5.23. As it can be seen, α and, consequently, the negative charge of the LPS increase by increasing the pH and NaCl concentration. Exclusively, at pH 11 the LPS bears a global negative charge and the functional groups are totally ionized with α approaching one**.** At similar condition, the fluorescence experiments proposed that the LPS chain is in the form of relatively expanded coil. This can be interpreted now to that the electrostatic repulsion between the similarly charged moieties. The acidic groups are neutralized to H_2PO_4 and COOH by adding acid until pH 2 and α approaches zero. In this case, the LPS chains become more hydrophobic and form a partially coiled chain, as suggested, using the fluorescence analysis.

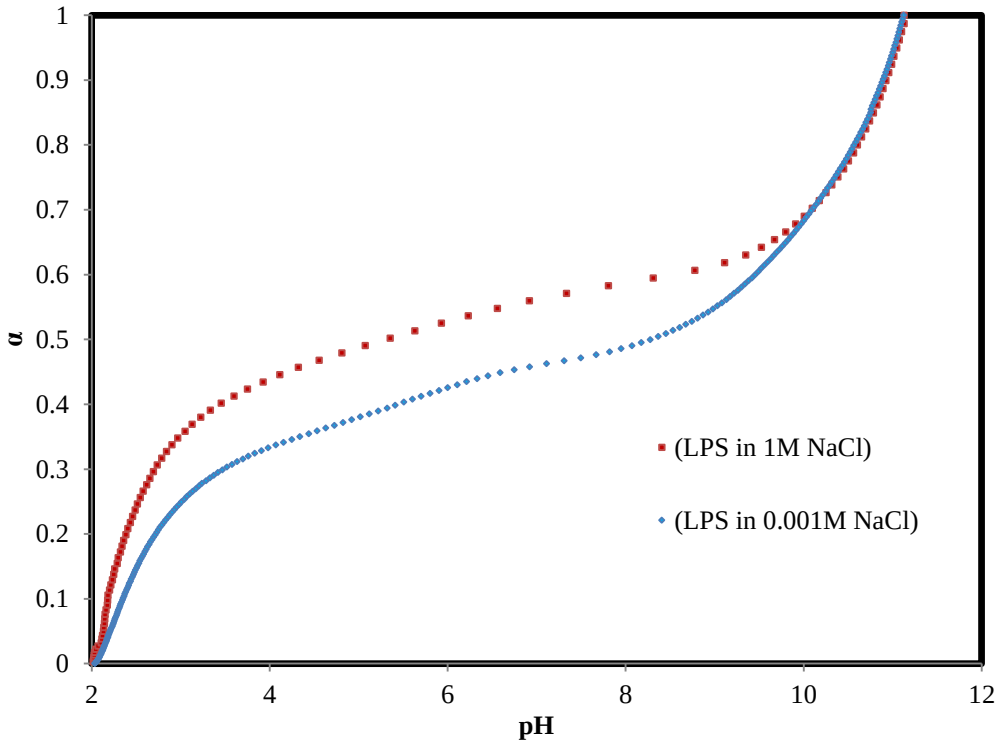

Figure 5.23 Fraction of functional groups ionized versus pH as a function of NaCl concentration for lipopolysaccharide.

Table 5.1 is listing the *pKa* values of unlabelled and labelled LPS, calculated from the first derivative of titration curves. The records presented propose the presence of phosphate, hydroxyl and/or amine groups beside the carboxyl groups of LPS. However, it is worthy to note that the *pKa* values of labelled and unlabelled LPS are similar. This means that fluorescently labelled LPS behaves like unlabelled

lipopolysaccharide, when the external stimuli such as pH and ionic strength are variable, and the AmNS label does not disturb the natural macromolecule system.

Table 5.1 pKa Constants and pHzpc of labelled and unlabelled LPS as determined by titration curves.

System	NaCl (M)	pKa (H_2PO_4)	pKa (COOH)	pKa (C-NH_2) or (C-OH)	pHzpc
LPS	0.1	2.50	4.96	9.50	2.39
AmNS-LPS	0.1	2.78	5.02	9.50	2.40

Table 5.1 also exhibits the zero point of charge (pHzpc) for LPS and AmNS-LPS. The results show that the pHzpc value of labelled and unlabelled LPS is almost equal. This means that any conformational change in the alginate chains may occur due to the change in external conditions, such as pH. The AmNS label cannot affect the physicochemical behaviour of the polysaccharide backbone.

The variation in relative charge density of silica and alumina solutions in the absence and presence of adsorbed lipopolysaccharide is showing in Figure 5.24. As it can be seen, the adsorption of the multi ionisable LPS chain decreases the positive charge considerably and lowers the pHzpc of the alumina from ~ 9 to ~ 8.5, but no considerable effect on the relative charge behaviour of silica suspension is noted, since the pHzpc of the silica remains unchanged at ~3 by adding LPS. These results suggest that electrostatic interactions are mainly responsible for the adsorption of LPS on Al_2O_3 particles, whereas weak forces, such as Van der Waals are assumed to control the interference between lipopolysaccharide and SiO_2 suspension.

However, in acidic condition, the fluorescence experiment exhibited that the percentage of adsorbed LPS reaches the value (~23%) on alumina, while only ~10% on silica. This is because at low pH levels (i.e. pH = 3) the net charge on alumina is positive and LPS is negatively charged, whereas the silica particles are neutral.

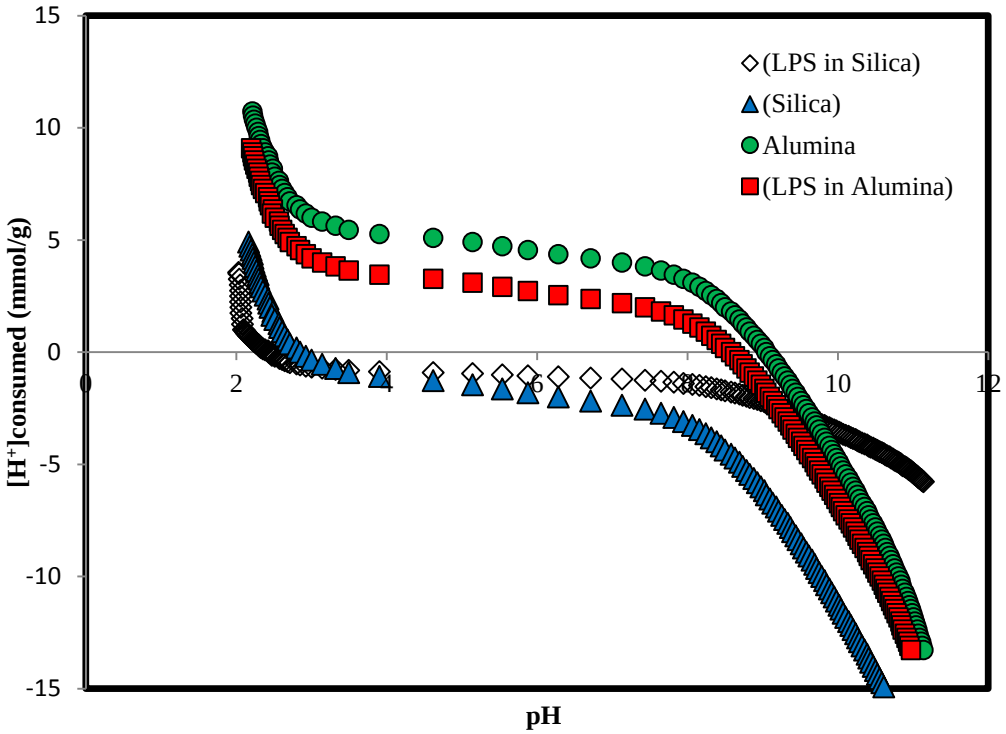

Figure 5.24 Relative surface charge versus pH for lipopolysaccharide in silica, silica, alumina and lipopolysaccharide in alumina.

5.8. **Inductively Coupled Plasma Mass Spectrometry Measurements (ICP-MS) of Silica and Alumina Adsorption on LPS**

The fluorescence experiments revealed that a considerable amount of fluorescently labelled LPS adsorbs on the surface of alumina in acidic media, but smaller amount adsorbs on silica suspension under the same conditions. Furthermore, the increase in the quantity of mineral added leads to an increase in the LPS adsorption. However, in this section, the ICP-MS is applied to quantify the attached mineral to unlabelled LPS according to the procedure, outlined in the experimental part (section 2.9.).

Figure 5.25 displays the pH dependency for the interference of Al_2O_3 and SiO_2 on unlabelled LPS. As it can be seen, for the two examined minerals, the adsorption of both minerals increases when the pH of the solution is decreased. However, the rate of increment in these amounts for alumina is more than in those for silica at low pH values. The effect of pH on the adsorbed amounts can be clarified based on the kind of the interaction of charged mineral with the LPS chain. Under the pHzpc of

alumina, the adsorption behaviour is of the high-affinity type, this supposes that the alumina strongly adsorbs to the LPS. Nevertheless, at pH > 9 the electrostatic repulsion between the LPS chain and the alumina surface causes the decrease of mineral adsorption. This adsorption behaviour coincides with the recent polyelectrolyte adsorption theory introduced by Van der Schee and Lyklema [32], which can be summarized as follows: adsorption of a negatively or partly negatively charged macromolecule on a positively charged mineral is influenced by electrostatic forces. Figure 5.26 shows the possible electrostatic interactions between LPS and minerals.

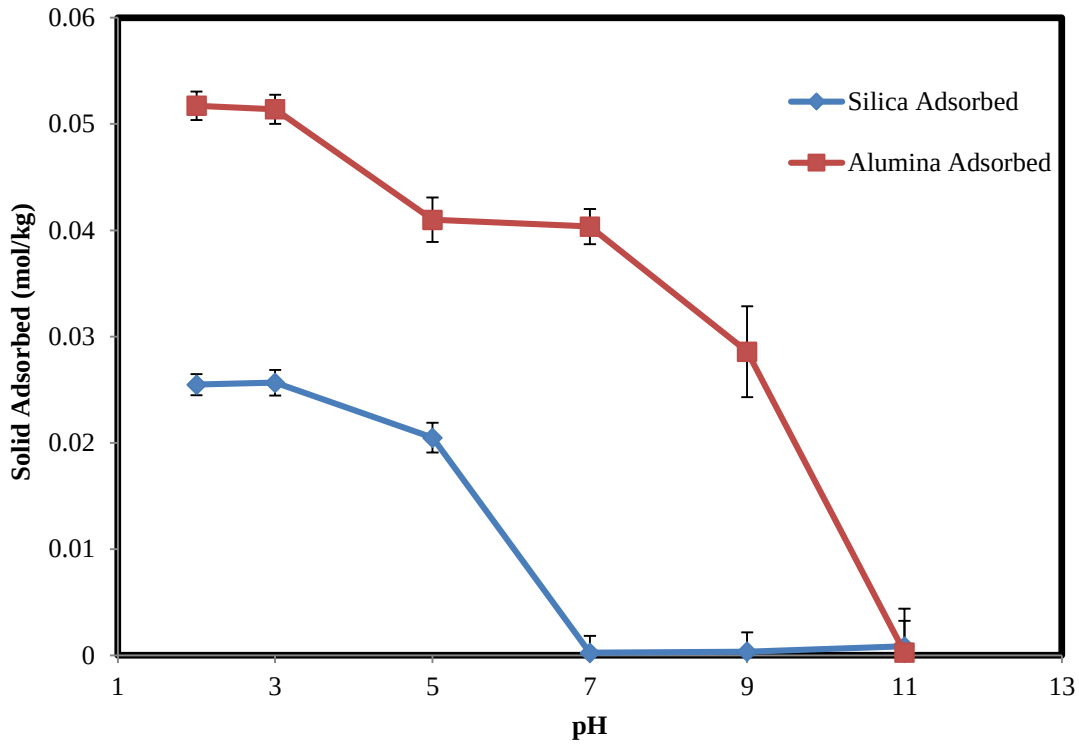

Figure 5.25 Effect of pH on the adsorption of alumina and silica on LPS (solid added 0.1M).

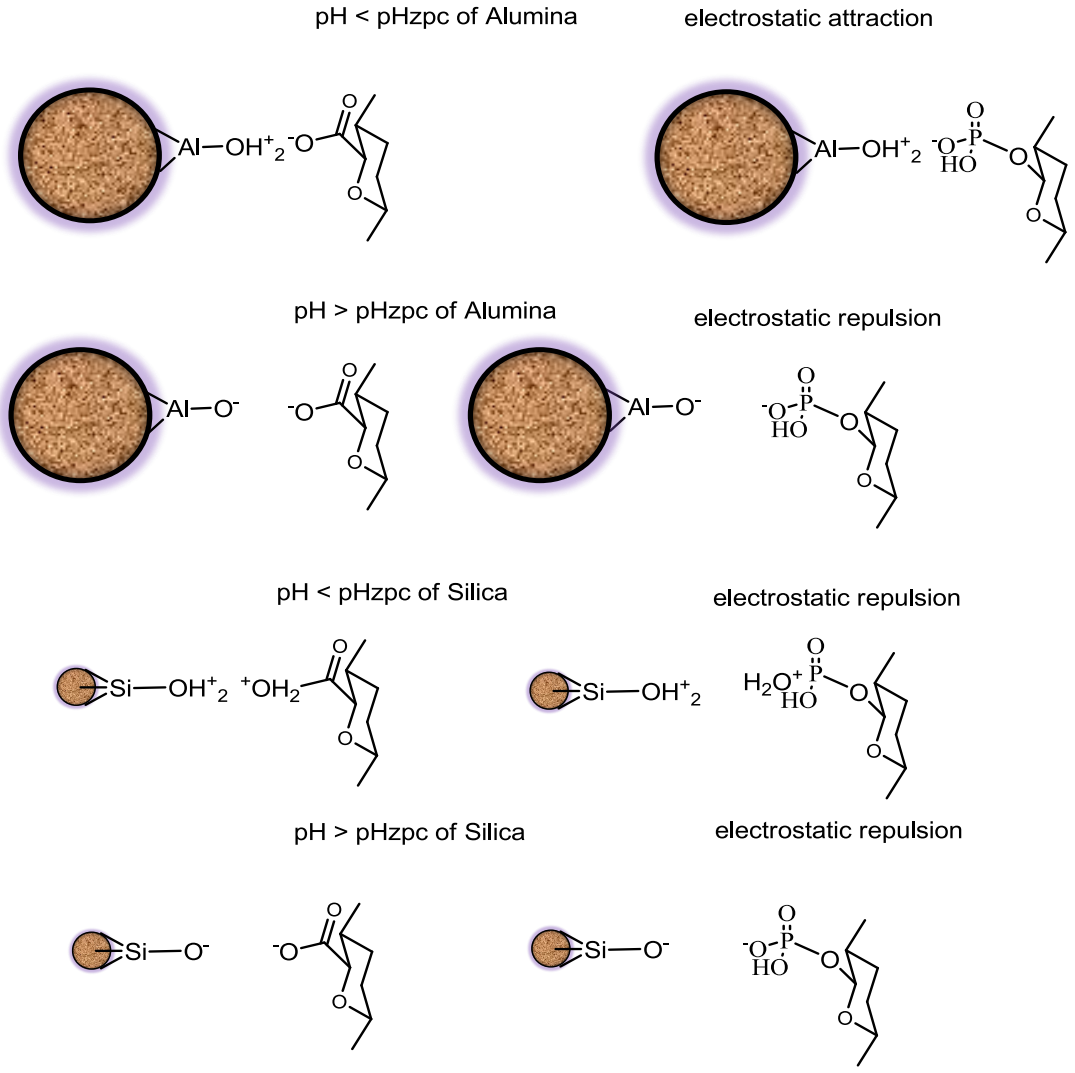

Figure 5.26 Schematic representation of the interaction between LPS and minerals.

Interestingly, the LPS chain can adsorb on the alumina, as well as the silica surfaces over the entire studied pH range, even when the pH, at which both LPS and solid have the same kind of charge. This could be attributed to the fact that non-electrostatic forces, such as van der Waals attraction dominates over the electrostatic repulsion between adsorbed polyelectrolyte coils and the similarly charged surface

[86]. Otherwise, the adsorption of an ionisable lipopolysaccharide chain on the negatively charged mineral surface is not possible to happen.

Besides particle charge, mineral concentration affects the adsorption process of minerals on LPS. Figure 5.27 shows the alumina and silica adsorption isotherms on the LPS at pH 7. These adsorption measurements were carried out at the same concentration of LPS (10^{-2} wt %). It can be observed that the adsorbed amount of alumina on LPS increases obviously with increasing adding concentration of alumina in the liquid phase at pH 7. Alternatively, the shape of the isotherm suggests a weak affinity of LPS for silica. This supposes that at pH 7 the electrostatic attraction (see Figure 5.26) increased the adsorption of alumina. For example, at added concentration of ~1 M, the adsorbed amount of alumina on alginate is ~0.028 moll/kg, which is approximately 18 times more than the adsorbed amount of silica on LPS.

The obtained isotherms are fitted to the Henry adsorption model according to Equation 3.12. These linear dependencies enable calculation of the affinity constant (K_h) of minerals adsorption from the slope of the Henry's equation. The obtained K_h and goodness of fit (R^2) values are given in Table 5.2. Considering the values of R^2 the Henry model is good to describe such isotherms. The K_h of the Henry model represents a measure of adsorption affinity. A large value of K_h reflects stronger adsorption. It can be noted that, over the complete pH range the affinity of minerals to adsorb on the LPS increases by decreasing the pH of solution. This could also attribute to the attraction of oppositely charged materials. However, under the identical condition Al_2O_3 particles have a greater affinity for the LPS than SiO_2 suspensions. This is due to the effects of the zero point of charge for minerals. The most efficient adsorption occurred at lower pH values, under these conditions, where the alumina particles hold a positive charge, so that they are strongly attracted to negatively charged LPS, and produce larger Henry's constant values. Silica suspensions have a weak affinity for LPS because of the electrostatic repulsion of negative silica molecules with anionic polyelectrolytes.

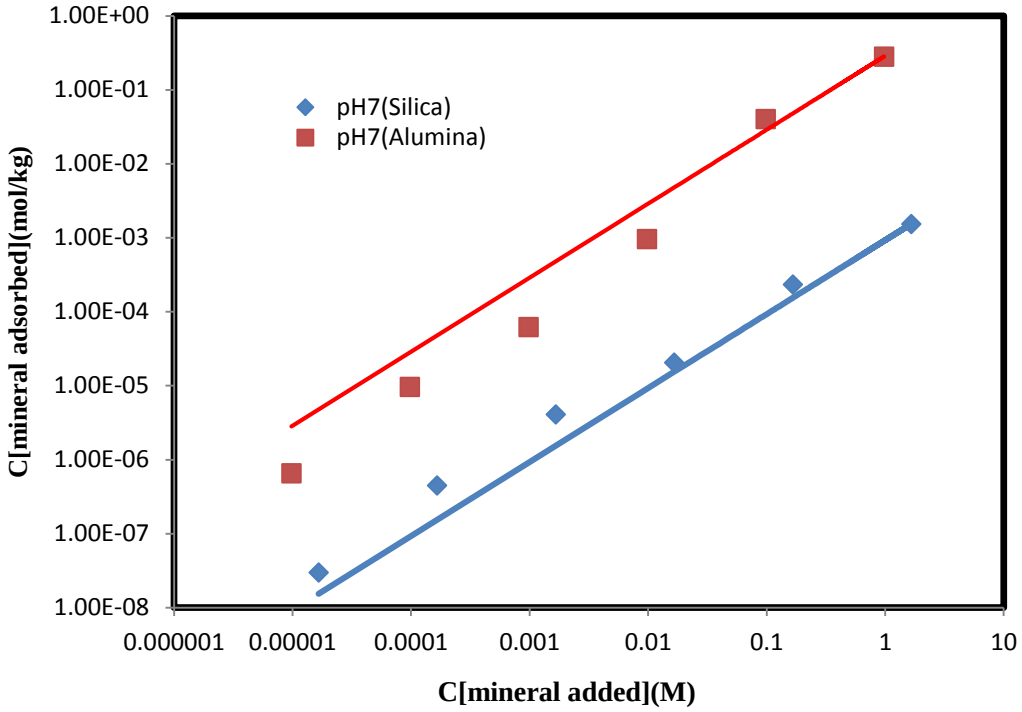

Figure 5.27 Henry adsorption isotherms of alumina and silica on LPS, at pH 7.

Table 5.2 Henry (affinity) constants of alumina and silica adsorbed on LPS and the goodness of fit values, at different pH values.

pH	**K_h** (L/kg) (Alumina)	**R^2** (Alumina)	**K_h** (L/kg) (Silica)	**R^2** (Silica)
2	0.5751	0.9999	0.0869	0.9571
3	0.5898	0.9998	0.0902	0.9613
5	0.2934	0.9977	0.0618	0.9601
7	0.2891	0.9977	0.0009	0.9967
9	0.0027	0.9999	0.0010	0.9969
11	0.0041	0.9993	0.0011	0.9968

5.9. **Conclusions**

- Fluorescence steady-state techniques have revealed that a greater amount of the fluorescently labelled LPS adsorbs onto the surface of alumina (~23%) in acidic media, than that on a silica suspension (~10 %) under the same condition.
- Fluorescence experiments have confirmed that the LPS coil behaves in a similar manner to that of a poly (acrylic acid) chain: the LPS expands at high pH while partially contracting at low pH.
- TRAMS have demonstrated to be an extremely powerful fluorescence technique in revealing the conformational behaviour of natural biologically produced substance, such as LPS in dilute solution, and when attached to solid surfaces.
- The correlation time, τ_c, of labelled LPS increases as the amount of mineral surface increases and the pH decreases: this suggests that more sites on the LPS chain is occupied by solid, which leads to restricted fluorophore macromolecular mobility.
- These results, obtained from potentiometric analysis suggested that electrostatic interactions were predominantly responsible for the adsorption of LPS on Al_2O_3 particles, whereas weak forces, such as Van der Waals are assumed to control the interference between lipopolysaccharide chain and SiO_2 suspension.
- ICP-MS demonstrated that LPS had a high adsorption affinity for Al_2O_3, but adsorbed weakly on the SiO_2 surface. Stronger adsorption was observed at low pH for both minerals than at high pH. The dependence of adsorption on the mineral concentration was also examined under different pH conditions: the adsorption amount was seen to increase by increasing the solid concentration. Adsorption isotherms obtained at low and high solid concentrations were found to be Hennery in type.
- The pH dependant solution behaviour of LPS is very similar to that of the synthetic polyelectrolyte.

- The Al_2O_3 particles have a greater affinity for the biologically produced LPS than SiO_2 suspensions: (This behaviour is similar to that of poly (acrylic acid)). Nevertheless, both minerals have stronger affinity for poly (acrylic acid) than for the lipopolysaccharide, which suggests that the LPS ionisable groups do not easily attract and interact with the mineral surface due to the steric hindrance as a consequence of the complex structure of biopolymer.

Chapter 6. A COMPARATIVE SUMMARY

6.1. Conformational Behaviour of Synthetic and Bacterial Polymers

Fluorescence techniques have shown that the singly labelled poly (acrylic acid) forms an expanded structure at high pH values, whereas partially collapses in acidic media. This is in agreement with the doubly labelled PAA results: an increase in energy transfer occurred at low pH which in consistent with a partially collapsed conformation. An increase in increase in the correlation time was also observed below pH 5, from TRAMS. Similarly, the fluorescence data have revealed that the biopolymer (alginate) and biologically produced (lipopolysaccharide) coils behave in a similar manner to that of poly (acrylic acid): both sample expand at high pH (low *τc* value) and partially collapse at low pH (high τc value), as shown in Figure 6.1.

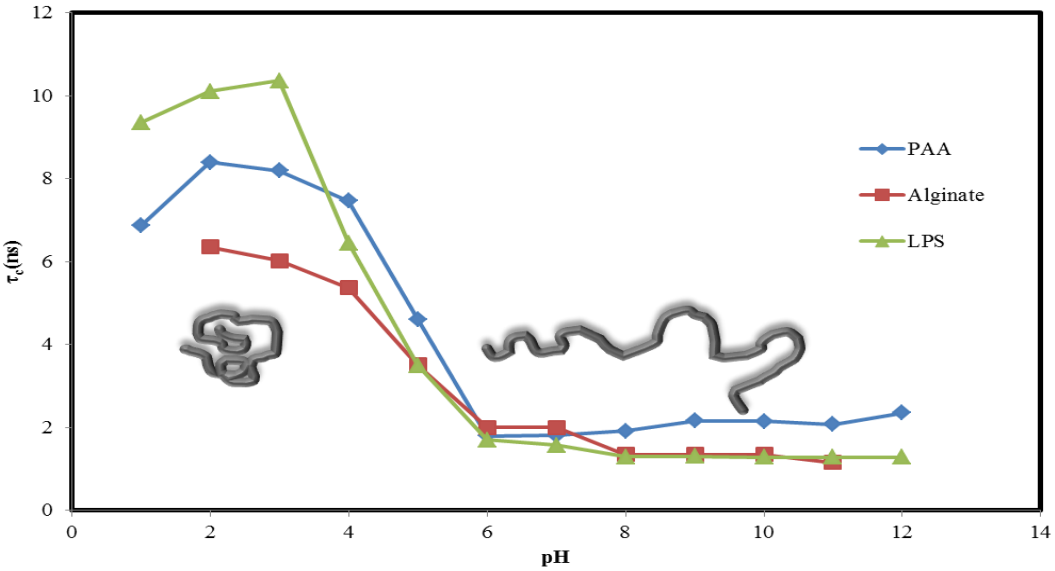

Figure 6.1 Conformational change of PAA and bacterial polymers as a function of pH.

6.2. Effect of Ionic Strength on the Synthetic and Bacterial Polymers Conformations

The addition of simple electrolytes to the charged PAA, alginate and LPS systems shows that there is an influence at high salt concentrations where coiling of the macromolecules chains is increased. This suggests that the ionisable groups of the

macromolecules are neutralised by interaction with Na^+ and Ca^{2+} ions encouraging chain collapse as the hydrophobic interactions dominate, and hence restrict the mobility of the fluorescent label and macromolecular chain; a higher τ_c value is generated, as shown in Figure 6.2. However, all macromolecules display increased coiling upon addition of $CaC1_2$ than NaCl.

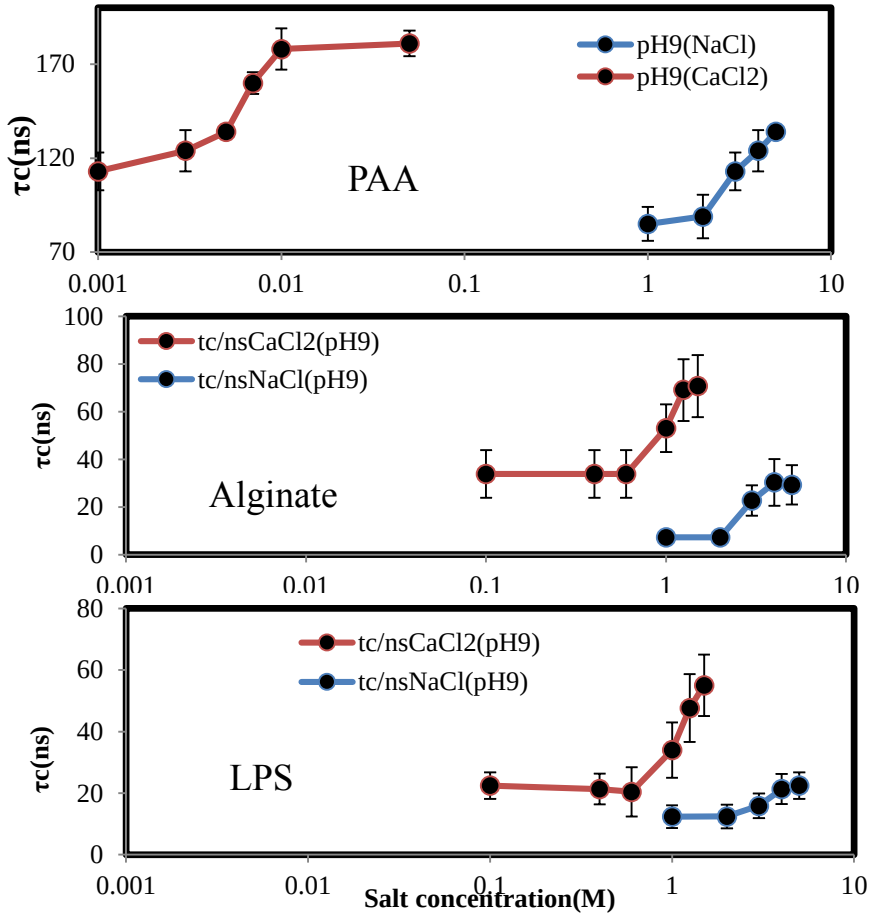

Figure 6.2 Correlation times of PAA and bacterial polymers as a function of ionic strength.

6.3. **Synthetic and Bacterial Polymers at Mineral Interfaces**

Fluorescence steady-state experiments showed that in general, a greater amount of the fluorescently labelled macromolecule adsorbs onto the surface of alumina in acidic media (~100% of PAA), (~26% of alginate) and (~23% of LPS). In contrast, less adsorbs onto the silica suspension under the same pH conditions (~20% of PAA), (~11% of alginate) and (~10 % of LPS). The results obtained from

potentiometric analyses suggested that electrostatic interactions were predominantly responsible for the adsorption of macromolecules onto Al_2O_3 particles, whereas weak forces, such as Van der Waals are assumed to control the interference between the macromolecular chains and SiO_2. ICP-MS demonstrated that both PAA and the biopolymers had a high adsorption affinity for Al_2O_3, but adsorbed weakly onto the SiO_2 surface. Stronger adsorption was observed at low pH for both mineral surfaces than at high pH. The dependence of adsorption on the mineral concentration was also examined under different pH conditions: the adsorption amount was observed to increase by increasing the solid concentration. Adsorption isotherms obtained at low and high solid concentrations were found to be Hennery in type. Nevertheless, both minerals have a stronger affinity for poly (acrylic acid) than for either the alginate or the lipopolysaccharide. This suggests that the biopolymers ionisable groups do not interact sufficiently with the mineral surface due to the complex structure of the naturally occurring macromolecules. Figure 6.3 summarises the interaction of poly (acrylic acid) and the biopolymers with the two types of mineral surface:

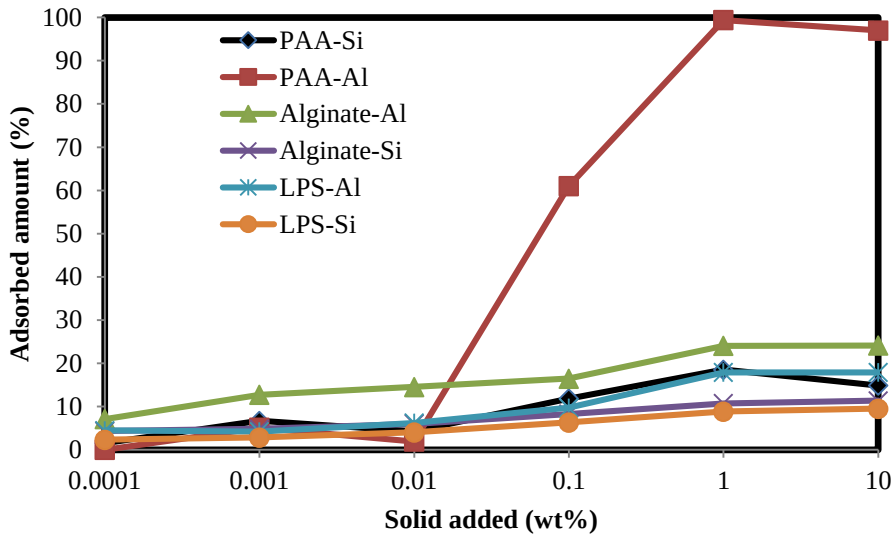

Figure 6.3 The percentage of macromolecules-minerals interference at pH 3.

Chapter 7. SUGGESIONS FOR FURTHER WORK

Building on the work presented in this thesis there are several potential areas for further research:

The behaviour of donor (ACE)-acceptor (AMMA) labelled synthetic polymer was discussed. This type of study provides us with more information about distance distribution of a polymer chain, since we used ACE and AMMA labels covalently bound to the poly (acrylic acid) backbone. Doubly labelling the biopolymer chains with a donor and acceptor fluorophore could provide further information and insights into the conformational transition.

Ionic strength is one of the most important external conditions controlling the conformational behaviour of an adsorbed polyelectrolyte onto a surface in an aqueous system. Since variations in ionic strength can lead to enhance the adsorption amount of the macromolecule onto a solid surface. It would be interesting to study the effect of ionic strength in addition to the pH on the conformational behaviour of the adsorbed macromolecules.

It would be interesting to extend this work and examine more complex systems like extracellular polymeric substance (EPS) produced by a live bacterium. The influence of surface hydrophobicity of the EPS at the solid–water interface could be investigated by fluorescence spectroscopy. This should provide information regarding the conformation of the biopolymer at the mineral surface, which could then be correlated with dispersion stability. These are key questions that, if answered, could enhance our understanding of the efficiency and stability of bacterial growth in real systems.

Chapter 8. REFERENCES

1. Lennox, J. and J. Ashe, *Biofilms as biobarriers.* American Biology Teacher, 2009. **71**(1): p. 20-26.
2. Horia, K. and S. Matsumotob, *Bacterial adhesion: From mechanism to control.* Biochemical Engineering Journal 2010. **48**: p. 424–434.
3. Zobell, C.E. and E.C. Allen, *The significance of marine bacteria in the fouling of submerged surfaces.* Journal of Bacteriology, 1935. **29**(3): p. 239-251.
4. Rijnaarts, H., et al., *Reversibility and mechanism of bacterial adhesion.* Colloids and Surfaces B: Biointerfaces, 1995. **4**: p. 5-22.
5. Donlan, R.M., *Biofilms: Microbial life on surfaces.* Emerging Infectious Diseases, 2002. **8**(9): p. 881-890.
6. Sutherland, I.W., *Biofilm exopolysaccharides: a strong and sticky framework.* Microbiology-Uk, 2001. **147**: p. 3-9.
7. Katsikogianni, M. and Y.F. Missirlis, *Concise review of mechanisms of bacterial adhesion to biomaterials and of techniques used in estimating bacteria-material interactions.* European cells & materials, 2004. **8**: p. 37-57.
8. Hong, Z., et al., *Initial adhesion of Bacillus subtilis on soil minerals as related to their surface properties.* European Journal of Soil Science. **63**(4): p. 457-466.
9. Busscher, H. and A. Weerkamp, *Specific and nonspecific interactions in bacterial adhesion to solid substrata.* Fems Microbiology Reviews, 1987. **46**(2): p. 165-173.
10. Atabek, A. and T.A. Camesano, *Atomic force microscopy study of the effect of lipopolysaccharides and extracellular polymers on adhesion of Pseudomonas aeruginosa.* Journal of Bacteriology, 2007. **189**(23): p. 8503-8509.
11. Walker, S.L., J.A. Redman, and M. Elimelech, *Role of cell surface lipopolysaccharides in Escherichia coli K12 adhesion and transport.* Langmuir, 2004. **20**(18): p. 7736-7746.

12. Marshall, K.C. and Cruicksh.Rh, *Cell-surface hydrophobicity and orientation of certain bacteria at interfaces.* Archiv Fur Mikrobiologie, 1973. **91**(1): p. 29-40.
13. Mayer, C., et al., *The role of intermolecular interactions: studies on model systems for bacterial biofilms.* International Journal of Biological Macromolecules, 1999. **26**(1): p. 3-16.
14. Schwarzenbach, R.P., P.M. Gschwend, and D.M. Imboden, *Environmental Organic Chemistry*. Second Edition ed. 2003, New Jersey: John Wiley & Sons, Inc.
15. Stamm, M., ed. *Polymer Surfaces and Interfaces Characterization, Modification and Applications*. First edition ed. Surface Modification by Adsorption of Polymers and Surfactants, ed. C. Bellmann. 2008 Springer-Verlag Berlin Heidelberg: Berlin Heidelberg.
16. Zaman, A.A., R. Tsuchiya, and B.M. Moudgil, *Adsorption of a Low-Molecular-Weight Polyacrylic Acid on Silica, Alumina, and Kaolin.* Journal of Colloid and Interface Science, 2002. **256**(1): p. 73-78.
17. Pereira, M.O., M.J. Vieira, and L.F. Melo, *The effect of clay particles on the efficacy of a biocide.* Water Science and Technology, 2000. **41**(4-5): p. 61-64.
18. Morawetz, H., *Polyelectrolyte solutions: Phenomena and interpretation*, in *Polyelectrolytes and Polyzwitterions: Synthesis, Properties, and Applications*, A.B.M.C.L. Lowe, Editor. 2006. p. 1-18.
19. Swanson, L., *Optical Properties of Polyelectrolytes*, in *Photochemistry and Photophysics of Polymer Materials*

N.S. Allen, Editor. 2010, John Wiley & Sons, Inc.: New Jersey. p. 41-91.

20. Zhao, Y., et al., *Preparation of calcium alginate microgel beads in an electrodispersion reactor using an internal source of calcium carbonate nanoparticles.* Langmuir, 2007. **23**(25): p. 12489-12496.
21. Radeva, T., ed. *Physical Chemistry of Polyelrctrolytes*. Surfactant Science, ed. T. Radeva. Vol. 99. 2001, Marcel Dekker, Inc.: New York,. 896.
22. Li, K., et al., *Conformational transition of poly (acrylic acid) detected by microcantilever sensing.* Chinese Physics Letters, 2007. **24**(6): p. 1502-1504.

23. Currie, E.P.K., et al., *Polyacrylic acid brushes: Surface pressure and salt-induced swelling.* Langmuir, 2000. **16**(22): p. 8324-8333.
24. Zhang, H.J. and Y. Ito, *pH control of transport through a porous membrane self-assembled with a poly(acrylic acid) loop brush.* Langmuir, 2001. **17**(26): p. 8336-8340.
25. Sarkar, D. and P. Somasundaran, *Conformational dynamics of poly(acrylic acid). A study using surface plasmon resonance spectroscopy.* Langmuir, 2004. **20**(11): p. 4657-4664.
26. Benegas, J.C., F.M.J. Cleven, and M. van den Hoop, *Potentiometric titration of poly(acrylic acid) in mixed counterion systems: Chemical binding of Cd ions.* Analytica Chimica Acta, 1998. **369**(1-2): p. 109-114.
27. Crescenzi, V., *Some recent studies of polyelectrolyte solutions.* Advances in Polymer Science, 1968. **5**: p. 358--386.
28. Zhuang, D.Q., et al., *Rheological properties of semidilute solutions of poly(acrylic acid) modified with hydrocarbon and fluorocarbon end-capped poly(ethylene glycol) macromonomer.* Journal of Applied Polymer Science, 2003. **88**(12): p. 2777-2783.
29. Crisci, A., et al., *pH- and ionic-strength-induced structural changes in poly(acrylic acid)-lipid-based self-assembled materials.* Macromolecular Symposia, 2009. **281**: p. 126-134.
30. Olea, A.F. and J.K. Thomas, *Fluorescence studies of the conformational-changes of poly(methacrylic acid) with pH.* Macromolecules, 1989. **22**(3): p. 1165-1169.
31. Khousakoun, E., J.F. Gohy, and R. Jerome, *Self-association of double-hydrophilic copolymers of acrylic acid and poly(ethylene oxide) macromonomer.* Polymer, 2004. **45**(25): p. 8303-8310.
32. Van der Schee, H.A. and J. Lyklema, *A lattice theory of polyelectrolyte adsorption.* The Journal of Physical Chemistry, 1984. **88**(26): p. 6661-6667.
33. Somasundaran, P. and S. Krishnakumar, *Adsorption of surfactants and polymers at the solid-liquid interface.* Colloids and Surfaces A: Physicochemical and Engineering Aspects, 1997. **123–124**(0): p. 491-513.
34. Ian Soutar, L.S., S. J. L. Wallace, K. P. Ghiggino, D. J. Haines, and T. A. Smith, *Fluorescence Studies of the Behaviour of Poly(dimethylacrylamide)*

in Dilute Aqueous Solution and at the Solid-Liquid Interface, in *Multidimensional Spectroscopy of Polymers Vibrational, NMR, and Fluorescence Techniques*, T.P. Marek W. Urban, Editor. 1995, American Chemical Society: Washington, DC. p. 363-378.

35. Notley, S.M., et al., *Adsorbed layer structure of a weak polyelectrolyte studied by colloidal probe microscopy and QCM-D as a function of pH and ionic strength.* Physical Chemistry Chemical Physics, 2004. **6**(9): p. 2379-2386.
36. Gao, H.F., et al., *Preparation of a water-soluble fluorescent polymer.* Journal of Macromolecular Science-Pure and Applied Chemistry, 2004. **A41**(4): p. 357-371.
37. Arora, N.J.T.a.K.S., *Pyrene as a photophysical probe for internolecular interactions of water-soluble polymers in dilute solution* Polymer, 1986. **27**: p. 783-796.
38. Lakowicz, J.R., *Principles of Fluorescence Spectroscopy*. 3th ed. 2006, New York: (SpringerScience+Business Media, LLC, 233 Spring Street, New York, NY 10013, USA). 960.
39. Tanaka, H., et al., *Homogeneous fluorescent Labeling of cationic polyacrylamides.* Journal of Applied Polymer Science, 2002. **86**(3): p. 672-675.
40. Winnik, M.A., et al., *Synthesis and characterization of pyrene-labeled poly(ethylenimine).* Macromolecules, 1998. **31**(20): p. 6855-6864.
41. Soutar, I. and L. Swanson, *Luminescence studies of polyelectrolyte behavior in solution .3. Time-resolved fluorescence anisotropy measurements of the conformational behavior of poly(methacrylic acid) in dilute aqueous-solutions.* Macromolecules, 1994. **27**(15): p. 4304-4311.
42. Strauss, U.P. and G. Vesnaver, *Optical probes in polyelectrolyte studies .1. Acid-base equilibria of dansylated copolymers of maleic-anhydride and alkyl vinyl ethers.* Journal of Physical Chemistry, 1975. **79**(15): p. 1558-1561.
43. Anghel, D.F., et al., *Fluorescent dyes as model 'hydrophobic modifiers' of polyelectrolytes: a study of poly(acrylic acid)s labelled with pyrenyl and naphthyl groups.* Polymer, 1998. **39**(14): p. 3035-3044.

44. Bergbreiter, D.E., et al., *Polyvalent hydrogen-bonding functionalization of ultrathin hyperbranched films on polyethylene and gold.* Macromolecules, 2001. **34**(9): p. 3018-3023.
45. Bunyakan, C., L. Armanet, and D. Hunkeler, *Precipitation polymerization of acrylic acid in toluene. II: mechanism and kinetic modeling.* Polymer, 1999. **40**(23): p. 6225-6234.
46. Amao, Y., *Probes and polymers for optical sensing of oxygen.* Microchimica Acta, 2003. **143**(1): p. 1-12.
47. Banu Mansuroğlu, Z.M., *Characterization of water-soluble conjugates of polyacrylic acid and antigenic peptide of FMDV by size exclusion chromatography with quadruple detection.* Materials Science and Engineering C 2012. **32** (2): p. 112–118.
48. Balzani, V., *Supramolecular photochemistry.* Tetrahedron, 1992. **48**(48): p. 10443-10514.
49. Croney, J.C., D.M. Jameson, and R.P. Learmonth, *Fluorescence spectroscopy in biochemistry: teaching basic principles with visual demonstrations.* Biochemistry and Molecular Biology Education, 2001. **29**(2): p. 60-65.
50. Behera, G.B., et al., *Fluorescent probes for structural and distance effect studies in micelles, reversed micelles and microemulsions.* Advances in Colloid and Interface Science, 1999. **82**(1-3): p. 1-42.
51. Michl, M.K.a.J., *Excited States and Photochemistry of Organic Molecules*. 1995, New York,: VCH Publishers, Inc.
52. Forster, T., *10Th spiers memorial lecture - transfer mechanisms of electronic excitation.* Discussions of the Faraday Society, 1959(27): p. 7-17.
53. Forster, T., *Energiewanderung und fluoreszenz.* Naturwissenschaften, 1946. **33**(6): p. 166-175.
54. Soutar, I., et al., *Fluorescence studies of the dynamic behavior of poly(dimethylacrylamide) and its complex with poly(methacrylic acid) in dilute solution.* Macromolecules, 1996. **29**(3): p. 918-924.
55. Ming Chen, K.P.G., Albert W. H. Mau, Wolfgang H. F. Sasse, and a.G.J.W. San H. Thang, *Amphiphilic acenaphthylene-maleic acid light-harvesting alternating copolymers: Reversible addition-fragmentation*

chain transfer synthesis and fluorescence. Macromolecules 2005. **38**: p. 3475-3481.

56. Ruiz-Perez, L., et al., *Conformation of poly(methacrylic acid) chains in dilute aqueous solution.* Macromolecules, 2008. **41**(6): p. 2203-2211.
57. Zinsli, P.E., *Inhomogeneous interior of aerosol ot microemulsions probed by fluorescence and polarization decay.* Journal of Physical Chemistry, 1979. **83**(25): p. 3223-3231.
58. Rimmer, S., I. Soutar, and L. Swanson, *Switching the conformational behaviour of poly(N-isopropyl acrylamide).* Polymer International, 2009. **58**(3): p. 273-278.
59. Soutar, I., et al., *Synchrotron-generated time-resolved fluorescence anisotropy studies of the segmental relaxation of poly(acrylic acid) and poly(methacrylic acid) in dilute methanolic solutions.* Macromolecules, 1992. **25**(17): p. 4399-4405.
60. Swanson, L., *Unpublished lecture*. 2004: Sheffield.
61. Kosmella, J.K.a.S., *Polyelectrolytes and Nanoparticles*. 2007, Berlin Heidelberg Springer
62. Boyer, R., *Modern Experimental Biochemistry*. third ed. 2000, San Francisco: Addison Wesely Longman.
63. Chee, C.K., et al., *Fluorescence investigations of the thermally induced conformational transition of poly(N-isopropylacrylamide).* Polymer, 2001. **42**(12): p. 5079-5087.
64. Huh, G., et al., *Synthesis of a photo-patternable cross-linked epoxy system containing photodegradable carbonate units for deep UV lithography.* Journal of Applied Polymer Science, 2009. **114**(4): p. 2093-2100.
65. Blonk, J.C.G., et al., *A new CSLM-based method for determination of the phase behaviour of aqueous mixtures of biopolymers.* Carbohydrate Polymers, 1995. **28**(4): p. 287-295.
66. Yuki, N., et al., *A bacterium lipopolysaccharide that elicits guillain-barre-syndrome has a gm1 ganglioside-like structure.* Journal of Experimental Medicine, 1993. **178**(5): p. 1771-1775.
67. Magalhaes, P.O., et al., *Methods of endotoxin removal from biological preparations: a review.* Journal of Pharmacy and Pharmaceutical Sciences, 2007. **10**(3): p. 388-404.

68. Fontanille, Y.G.a.M., *Organic and Physical Chemistry of Polymers*. 2008, John Wiley & Sons, Inc.
69. Ojeda, J.J., et al., *Characterization of the cell surface and cell wall chemistry of drinking water bacteria by combining XPS, FTIR spectroscopy, modeling, and potentiometric titrations.* Langmuir, 2008. **24**(8): p. 4032-4040.
70. Cumming, G., F. Fidler, and D.L. Vaux, *Error bars in experimental biology.* Journal of Cell Biology, 2007. **177**(1): p. 7-11.
71. Ebdon, J.R., et al., *Luminescence studies of hydrophobically modified, water-soluble polymers .1. Fluorescence anisotropy and spectroscopic investigations of the conformational behaviour of copolymers of acrylic acid and styrene or methyl methacrylate.* Canadian Journal of Chemistry-Revue Canadienne De Chimie, 1995. **73**(11): p. 1982-1994.
72. Smith, T.A., et al., *Time-resolved fluorescence anisotropy measurements of the adsorption of Rhodamine-B and a labelled polyelectrolyte onto colloidal silica.* Colloid and Polymer Science, 1998. **276**(11): p. 1032-1037.
73. Smith, T.A., D.J. Haines, and K.P. Ghiggino, *Steady-state and time-resolved fluorescence polarization behavior of acenaphthene.* Journal of Fluorescence, 2000. **10**(4): p. 365-373.
74. Hao, J., et al., *Interchain hydrogen-bonding-induced association of poly(acrylic acid)-graft-poly(ethylene oxide) in water.* Macromolecules. **43**(4): p. 2002-2008.
75. Tsukida, N., et al., *Effect of neutralization of poly(acrylic acid) on the structure of water examined by Raman spectroscopy.* Journal of Physical Chemistry B, 1997. **101**(34): p. 6676-6679.
76. Schweins, R., J. Hollmann, and K. Huber, *Dilute solution behaviour of sodium polyacrylate chains in aqueous NaCl solutions.* Polymer, 2003. **44**(23): p. 7131-7141.
77. Schweins, R. and K. Huber, *Collapse of sodium polyacrylate chains in calcium salt solutions.* European Physical Journal E, 2001. **5**(1): p. 117-126.

78. Bonapasta, A.A., F. Buda, and P. Colombet, *Interaction between Ca ions and poly(acrylic acid) chains in macro-defect-free cements: A theoretical study.* Chemistry of Materials, 2001. **13**(1): p. 64-70.
79. Carty, W.M. and U. Senapati, *Porcelain—raw materials, processing, phase evolution, and mechanical behavior.* Journal of the American Ceramic Society, 1998. **81**(1): p. 3-20.
80. Wisniewska, M., *Temperature effect on adsorption properties of silica-polyacrylic acid interface.* Journal of Thermal Analysis and Calorimetry. **101**(2): p. 753-760.
81. Foissy, A., A. El Attar, and J.M. Lamarche, *Adsorption of polyacrylic acid on titanium dioxide.* Journal of Colloid and Interface Science, 1983. **96**(1): p. 275-287.
82. Somasundaran, P. and S. Krishnakumar, *Adsorption of surfactants and polymers at the solid-liquid interface.* Colloids and Surfaces a-Physicochemical and Engineering Aspects, 1997. **123**: p. 491-513.
83. Reith, D., et al., *How does the chain extension of poly (acrylic acid) scale in aqueous solution? A combined study with light scattering and computer simulation.* Journal of Chemical Physics, 2002. **116**(20): p. 9100-9106.
84. Cesarano, J., I.A. Aksay, and A. Bleier, *Stability of aqueous alpha-Al_2O_3 suspensions with poly(methacrylic acid) poly-electrolyte.* Journal of the American Ceramic Society, 1988. **71**(4): p. 250-255.
85. Jeon, C., J.Y. Park, and Y.J. Yoo, *Characteristics of metal removal using carboxylated alginic acid.* Water Research, 2002. **36**(7): p. 1814-1824.
86. Dobrynin, A.V. and M. Rubinstein, *Effect of short-range interactions on polyelectrolyte adsorption at charged surfaces.* Journal of Physical Chemistry B, 2003. **107**(32): p. 8260-8269.
87. Sist, P., et al., *Macromolecular and solution properties of Cepacian: the exopolysaccharide produced by a strain of Burkholderia cepacia isolated from a cystic fibrosis patient.* Carbohydrate Research, 2003. **338**(18): p. 1861-1867.
88. Lin, Y., H. Zhang, and A. Adin, *Characterization of bacterial alginate extracted from biofilm matrix.* Desalination and Water Treatment, 2009. **8**(1-3): p. 250-255.

89. Li, L., et al., *Reexamining the egg-box model in calcium-alginate gels with X-ray diffraction.* Biomacromolecules, 2007. **8**(2): p. 464-468.
90. Yang, J., S. Chen, and Y. Fang, *Viscosity study of interactions between sodium alginate and CTAB in dilute solutions at different pH values.* Carbohydrate Polymers, 2009. **75**(2): p. 333-337.
91. Zhang, H.C., et al., *The interaction of sodium alginate with univalent cations.* Biopolymers, 1998. **46**(6): p. 395-402.
92. Draget, K.I., et al., *Swelling and partial solubilization of alginic acid gel beads in acidic buffer.* Carbohydrate Polymers, 1996. **29**(3): p. 209-215.
93. Draget, K.I., et al., *Small-angle x-ray scattering and rheological characterization of alginate gels. 3. Alginic acid gels.* Biomacromolecules, 2003. **4**(6): p. 1661-1668.
94. Coradin, T., N. Nassif, and J. Livage, *Silica-alginate composites for microencapsulation.* Applied Microbiology and Biotechnology, 2003. **61**(5-6): p. 429-434.
95. Cao, Y., et al., *pH-induced self-assembly and capsules of sodium alginate.* Biomacromolecules, 2005. **6**(4): p. 2189-2196.
96. Oberyukhtina, I.A., K.G. Bogolitsyn, and N.P. Popova, *Physicochemical properties of solutions of sodium alginate extracted from brown algae Laminaria digitata.* Russian Journal of Applied Chemistry, 2001. **74**(10): p. 1645-1649.
97. Smidsrød, O., *Solution properties of alginate.* Carbohydrate Research, 1970. **13**(3): p. 359-372.
98. West, E.R., et al., *Physical properties of alginate hydrogels and their effects on in vitro follicle development.* Biomaterials, 2007. **28**(30): p. 4439-4448.
99. Brizzolara, R.A., *Adsorption of alginic acid to titanium investigated using x-ray photoelectron spectroscopy and atomic force microscopy.* Surface and Interface Analysis, 2002. **33**(4): p. 351-360.
100. de Kerchove, A.J. and M. Elimelech, *Structural growth and viscoelastic properties of adsorbed alginate layers in monovalent and divalent salts.* Macromolecules, 2006. **39**(19): p. 6558-6564.

101. Dhar, G. and A. Bhaduri, *Synthesis and characterization of stacked and quenched uridine nucleotide fluorophores.* The Journal of biological chemistry, 1999. **274**(21): p. 14568-14572.
102. Fick, J., R. Lawaczeck, and F.W. Schneider, *Fluorescence of intramolecular and intermolecular interactions of aminonaphthyl-sulfonate with nucleotides.* European Journal of Biochemistry, 1982. **126**(2): p. 367-372.
103. Cao, Y., et al., *pH-Induced self-assembly and capsules of sodium alginate.* Biomacromolecules, 2005. **6**(4): p. 2189-2196.
104. Chen, K.L., S.E. Mylon, and M. Elimelech, *Aggregation kinetics of alginate-coated hematite nanoparticles in monovalent and divalent electrolytes.* Environmental Science & Technology, 2006. **40**(5): p. 1516-1523.
105. Kim, K.-P., et al., *Adsorption of aluminum ion from water on alginate-modified polyurethane.* Journal of Chemical Engineering of Japan. **44**(4): p. 247-255.
106. Tsutsumi, K. and T. Norisuye, *Excluded-volume effects in sodium hyaluronate solutions revisited.* Polymer Journal, 1998. **30**(4): p. 345-349.
107. Torres, E., et al., *Gold and silver uptake and nanoprecipitation on calcium alginate beads.* Langmuir, 2005. **21**(17): p. 7951-7958.
108. Decho, A.W., *Imaging an alginate polymer gel matrix using atomic force microscopy.* Carbohydrate Research, 1999. **315**(3-4): p. 330-333.
109. Pan, Z.H., A. Campbell, and P. Somasundaran, *Polyacrylic acid adsorption and conformation in concentrated alumina suspensions.* Colloids and Surfaces a-Physicochemical and Engineering Aspects, 2001. **191**(1-2): p. 71-78.
110. Qin, Y., B. Shi, and J. Liu, *Application of chitosan and alginate in treating waste water containing heavy metal ions.* Indian Journal of Chemical Technology, 2006. **13**(5): p. 464-469.
111. Parikh, S.J. and J. Chorover, *ATR-FTIR study of lipopolysaccharides at mineral surfaces.* Colloids and Surfaces B-Biointerfaces, 2008. **62**(2): p. 188-198.
112. Meredith, T.C., et al., *Redefining the requisite lipopolysaccharide structure in Escherichia coli.* Acs Chemical Biology, 2006. **1**(1): p. 33-42.

113. Langley, S. and T.J. Beveridge, *Effect of O-side-chain-lipopolysaccharide chemistry on metal binding.* Applied and Environmental Microbiology, 1999. **65**(2): p. 489-498.
114. Makin, S.A. and T.J. Beveridge, *The influence of A-band and B-band lipopolysaccharide on the surface characteristics and adhesion of Pseudomonas aeruginosa to surfaces.* Microbiology-Uk, 1996. **142**: p. 299-307.
115. Flemming, C.A., et al., *Cell surface physicochemistry alters biofilm development of pseudomonas aeruginosa lipopolysaccharide mutants.* Biofouling, 1998. **13**(3): p. 213-231.
116. Bergstrand, A., et al., *Aggregation behavior and size of lipopolysaccharide from Escherichia coli O55 : B5.* Colloids and Surfaces B-Biointerfaces, 2006. **53**(1): p. 9-14.
117. Santos, N.C., et al., *Evaluation of lipopolysaccharide aggregation by light scattering spectroscopy.* ChemBioChem, 2003. **4**(1): p. 96-100.
118. Ferris, F.G. and T.J. Beveridge, *Site specificity of metallic ion binding in escherichia-coli k-12 lipopolysaccharide.* Canadian Journal of Microbiology, 1986. **32**(1): p. 52-55.
119. Jucker, B.A., et al., *Adsorption of bacterial surface polysaccharides on mineral oxides is mediated by hydrogen bonds.* Colloids and Surfaces B-Biointerfaces, 1997. **9**(6): p. 331-343.
120. Coughlin, R.T., et al., *A Ph titration study on the ionic bridging within lipopolysaccharide aggregates.* Biochimica Et Biophysica Acta, 1985. **821**(3): p. 404-412.
121. Shephard, J., A.J. McQuillan, and P.J. Bremer, *Mechanisms of cation exchange by pseudomonas aeruginosa PAO1 and PAO1 wbpL, a strain with a truncated lipopolysaccharide.* Applied and Environmental Microbiology, 2008. **74**(22): p. 6980-6986.
122. Parikh, S.J., *A spectroscopic Study Of Bacterial Polymers Mediating Cell Adhesion and Mineral Transformations*, in *Department of Soil, Water And Environmental Science*. 2006, The University of Arizona.
123. Katchalsky, A., *Polyelectrolytes and their biological interactions.* Biophysical Journal, 1964. **4**(1SP): p. 9-&.

124. Fowle, D.A., Kulczycki, E., and Roberts, J.A., *Linking bacteria-metal interactions to mineral attachment: A role for outer sphere complexation of cations?*, in *Water-Rock Interaction. Proceedings of the Eleventh International Symposium on Water-Rock Interaction WRI-11* R.B.a.S. Wanty, R.R., , Editor. 2004: Saratoga Springs, NY, USA p. 1113-1117
125. Kubota, M., et al., *Selective adsorption of bacterial cells onto zeolites.* Colloids and Surfaces B-Biointerfaces, 2008. **64**(1): p. 88-97.
126. Lu, Q., et al., *Understanding the molecular interactions of lipopolysaccharides during E. coli initial adhesion with a surface forces apparatus.* Soft Matter. **7**(19): p. 9366-9379.